

UNIVERSITY OF SOUTHERN QUEENSLAND

**Better Characterisation
of the Underwater Solar
Ultraviolet Environment Using a
High – Exposure Dosimeter**

A Dissertation submitted by

Peter Schouten, B Sc(Hons)

For the award of

Doctor of Philosophy

2009

Abstract

This dissertation presents the development, testing and application of a chemical film UV dosimeter based on the polymer Poly (2, 6-dimethyl-1, 4-phenylene oxide) (PPO) prepared especially for long – term high – exposure underwater use. Initial testing of the dosimeter was performed in a water tank within a controlled laboratory environment with an artificial UV source in which various optical and physical properties of the film were rigorously tested such as UV dose and depth response, cosine response, interdosimeter variation, dose rate independence, dark reaction, watermarking effect, exposure additivity and visible and UVA wavelength response. In each of these tests the PPO dosimeter displayed results proving that it could be reliably used in aquatic environments at a level of accuracy only slightly lower than what could be expected for in – air dosimetric measurements. The use of a polyethylene derived neutral density filter (NDF) was then employed with the PPO dosimeter in order to extend exposure time. Results from this investigation showed that the polyethylene NDF could extend the effective life time of the PPO dosimeter by as much as five days in early autumn. Following this the PPO dosimeter was calibrated in the field to the solar erythemal action spectrum in – air and to the solar UVB spectrum in clear water, creek water, sea water and dam water over the duration of a year. In both the in – air and underwater calibrations it was found that the response of the PPO dosimeter lasted over a much greater amount of time when compared to the more commonly used polysulphone dosimeter and also varied with the modulation of the incident solar spectrum brought on by changing SZA and fluctuations in atmospheric column ozone. Additionally, it was discovered that in – air and underwater calibration regimes could not be interchanged and that the PPO dosimeter response underwater is dependent upon water type, but only when

transmission spectra differed between two water types by a difference on average of more than 5% across the UVB waveband. As a final test, the PPO dosimeter was deployed over a year to take UVB exposure measurements with the use of a custom built submersible float in three different real – world field environments that included a creek, a sea water tank and a stagnant dam. Exposures could be measured reliably up to a depth of 5 cm in the creek water and the dam water and up to and possibly beyond a depth of 35 cm in the sea water. From the sea water PPO dosimeter measurements a series of attenuation coefficients were estimated for each season. These coefficients showed reasonable agreement when compared to attenuation coefficient calculations made using a calibrated spectrometer in the same sea water, further proving the usefulness of the PPO dosimeter.

Table of Contents

<i>Section</i>	<i>Page Number</i>
Abstract.....	II
Table of Contents.....	IV
List of Figures.....	IX
List of Tables.....	XVIII
Certification of Dissertation.....	XIX
Acknowledgements.....	XX
Chapter 1 – Introduction.....	1
1.1 Introduction.....	2
1.2 Objectives.....	5
1.3 Dissertation Outline.....	6
Chapter 2 – Properties of Solar Ultraviolet Radiation on Earth.....	8
2.1 Introduction.....	9
2.2 Solar UV Radiation.....	9
2.3 The Propagation of Solar UV in the Earth’s Atmosphere.....	12
2.3.1 Cloud Cover.....	12
2.3.2 Ozone.....	14
2.3.3 Aerosol and Molecular Scattering.....	18
2.3.4 Solar Zenith Angle.....	21
2.3.5 Altitude.....	22
2.3.6 Albedo.....	24
2.3.7 Earth Orbit.....	24
2.4 Chapter Discussion.....	25

Chapter 3 – Properties of Solar Ultraviolet Radiation in the Underwater Environment and its Effect upon Aquatic Ecosystems.....	26
3.1 Introduction.....	27
3.2 Penetration and Propagation of Solar UV Underwater.....	29
3.2.1 Solar UV at the Water Surface.....	29
3.2.2 Behaviour and Distribution of Solar UV Underwater.....	30
3.2.3 Effect of Dissolved Organic Matter.....	38
3.3 Influence of Solar UV on the Aquatic Ecosystem.....	43
3.3.1 Plankton Varieties.....	44
3.3.2 Cyanobacteria.....	48
3.3.3 Seagrass and Macroalgae.....	49
3.3.4 Coral Communities.....	50
3.3.5 Large Scale Organisms.....	51
3.4 Chapter Discussion.....	54
Chapter 4 – Calibration and Measurement of Solar UV Radiation Underwater with Optical Instrumentation and Dosimeters.....	55
4.1 Introduction.....	56
4.2 Underwater Solar UV Radiation Measurement.....	57
4.2.1 Spectral and Broadband Measurements.....	57
4.2.2 Biological and Chemical Dosimeters.....	59
4.3 Optical Instrumentation Employed for this Research.....	61
4.3.1 IL1400 Broadband Meter.....	61
4.3.2 Mobile Scanning Spectroradiometer.....	64
4.3.3 EPP2000 Spectrometer.....	69
4.3.4 Bentham Spectroradiometer and Solar Light UV Broadband Meter.....	72
4.4 The Immersion Effect.....	79

4.4.1 Mobile Scanning Spectroradiometer Immersion Effect Correction and Calibration to the IL1400.....	84
4.4.2 EPP2000 Spectrometer Immersion Effect Correction and Calibration to the IL1400.....	87
4.5 Chapter Discussion.....	92
Chapter 5 – Development of the PPO Dosimeter.....	93
5.1 Introduction.....	94
5.2 The PPO Dosimeter.....	95
5.2.1 Fabrication and Physical Properties.....	95
5.2.2 PPO Dosimeter Optical Measurement.....	96
5.3 Optical Properties of the PPO Dosimeter in Air.....	99
5.3.1 Applications as an Erythemat and a UVA Dosimeter.....	99
5.4 Analysis of the PPO Dosimeter in a Controlled Clear Water Environment.....	101
5.4.1 Water Tank, Irradiation Source Description and Water Analysis.....	101
5.4.1.1 Dose – Response.....	102
5.4.1.2 Cosine Response.....	106
5.4.1.3 Independence of Dose Rate.....	108
5.4.1.4 Dark Reaction.....	109
5.4.1.5 Reaction to UVA and Visible Wavelengths.....	111
5.4.1.6 Watermarking Effects.....	113
5.4.1.7 Additivity of Exposures.....	115
5.5 Chapter Discussion.....	116
Chapter 6 –Testing of a Neutral Density Filter and Seasonal Calibrations with the PPO Dosimeter.....	117
6.1 Introduction.....	118
6.2 Neutral Density Filter Testing with the PPO Dosimeter.....	119

6.2.1 Neutral Density Filter Properties.....	119
6.2.2 PPO Dosimeter and Neutral Density Filter Calibrations.....	122
6.3 Seasonal In – Air Erythemal Calibrations of the PPO Dosimeter.....	126
6.3.1 Comparison of Complete Calibration Equations.....	133
6.4 Chapter Discussion.....	135
Chapter 7 – Calibration of the PPO Dosimeter in an Underwater Semi – Controlled Environment.....	140
7.1 Introduction.....	141
7.2 PPO Dosimeter Solar Calibration Campaign.....	141
7.2.1 Water Tank Description.....	144
7.2.2 Optical Properties of Each Water Type.....	145
7.2.2.1 UV Transmission and Absorption Distributions.....	145
7.2.2.2 Attenuation Coefficients.....	148
7.2.3 PPO Dosimeter Solar Calibration Campaign Results.....	150
7.2.3.1 Comparison of Complete Calibration Equations.....	156
7.3 Chapter Discussion.....	157
Chapter 8 – Deployment of the PPO Dosimeter in Real – World Aquatic Environments.....	162
8.1 Introduction.....	163
8.2 Dosimeter Submersible Float Specifications.....	163
8.3 Underwater UV Exposures at Different Aquatic Locales.....	166
8.3.1 Japanese Gardens Creek.....	166
8.3.2 University of Southern Queensland Research Dam.....	168
8.3.3 Simulated Sea Water Environment.....	170
8.3.4 PPO Dosimeter Calibrations for Each Location.....	173

8.4 Measurement Campaign Results.....	178
8.4.1 Creek Water.....	178
8.4.2 Sea Water.....	182
8.4.3 Dam Water.....	185
8.4.4 Attenuation Coefficient Calculation for the PPO Dosimeters.....	186
8.4.5 Attenuation Coefficient Calculation for the Calibrated EPP2000 Spectrometer.....	186
8.4.6 Comparison of the Attenuation Coefficients Calculated in the Sea Water with the EPP2000 Spectrometer and the Dosimeters.....	187
8.5 Chapter Discussion.....	188
Chapter 9 – Conclusions.....	193
9.1 Conclusions.....	194
9.2 Future Work.....	197
References.....	200
Appendices.....	223

List of Figures

Figure 2.1: Example atmospheric column ozone output chart as measured by OMI on 7 December 2008.....	18
Figure 4.1: The International Light IL1400 broadband UVB meter with the waterproof detector.....	63
Figure 4.2: The total UV, visible and infrared transmittance of the UVB1 filter.....	64
Figure 4.3: The mobile scanning spectroradiometer where A) is the computer which acts as the measurement control unit and data logger by means of specialist software, B) is the diffuser connected to the fibre optic link, C) is the system controller which sends messages to the spectroradiometer from the computer and vice versa, D) is the Peltier temperature control unit and E) is the housing that contains the monochromator.	65
Figure 4.4: The spectral irradiance of the SSL originally obtained by the CSIRO National Standards Laboratory ($SS(\lambda)$).....	67
Figure 4.5: A spectral counts scan of the SSL measured by the mobile scanning spectroradiometer ($CSS(\lambda)$).....	68
Figure 4.6: An example of a spectral responsivity distribution ($R(\lambda)$) calculated for the UV waveband.....	68

Figure 4.7: The EPP2000 spectrometer with a laptop computer used for data acquisition and the diffuser connected via a fibre optic link.....70

Figure 4.8: Comparisons between UVB measurements integrated from 298 nm to 320 nm for the Bentham spectroradiometer and the EPP2000 spectrometer taken over March, April, July and August in 2007.....72

Figure 4.9: The Bentham spectroradiometer on the roof inside the Envirobox. The diffuser can be seen on the right hand side of the unit.....74

Figure 4.10: The Solar Light UV broadband meter.....75

Figure 4.11: Calibration charts linking the Solar Light UV broadband meter to the Bentham spectroradiometer for (A) autumn, (B) winter, (C) spring and (D) summer.....78

Figure 4.12: Flowchart of the outdoors PPO dosimeter calibration scheme for both in – air and underwater measurements.....79

Figure 4.13: The immersion effect scenario where n_{WATER} is the refractive index of the water in which the optical meter is submerged, n_{DIFFUSER} is the refractive index of the diffuser/collector employed by the optical meter, I_{O} is the irradiance incoming from a source, I_{R} is the reflected irradiance off the diffuser/collector, I_{S} is the backscattered irradiance from within the diffuser/collector and I_{D} is the irradiance intercepted by the detector (Zibordi *et al*, 2004).....80

Figure 4.14: The refractive index distribution across the 295 nm to 320 nm waveband at an average temperature of 23 ° C.....83

Figure 4.15: Immersion effect factors as calculated for the mobile spectroradiometer for the waveband running from 298 nm to 320 nm.....85

Figure 4.16: Profile of immersion effect corrected spectral irradiances from 298 nm through to 320 nm in the water tank at $Z_{1\text{CM}}$ and $Z_{16\text{CM}}$ in comparison with a spectrum measured at the water surface.....86

Figure 4.17: Mobile spectroradiometer, UV in the 298 nm to 320 nm waveband, versus IL1400 calibration for in – air (A) and underwater (B) applications.....87

Figure 4.18: Immersion effect factors as calculated for the EPP2000 spectrometer over the 298 nm to 320 nm waveband.....90

Figure 4.19: Profile of immersion effect corrected spectral irradiances from 298 nm through to 320 nm in the water tank measured with the EPP2000 spectrometer at Z_{4CM} and Z_{25CM} in comparison with a spectrum measured at the water surface.....91

Figure 4.20: EPP2000 spectrometer to IL1400 radiometer calibration transfer data for low SZA conditions (A) and high SZA conditions (B).....92

Figure 5.1: A typical PPO dosimeter.....96

Figure 5.2: Change in optical transmission and absorbance across the entire terrestrial UV waveband for PPO film after an underwater UVB exposure of 18.4 kJ m^{-2}98

Figure 5.3: Spectrophotometer unit connected to the data acquisition computer.....98

Figure 5.4: Dosimeter holder apparatus employed for the measurement of each PPO dosimeter.....99

Figure 5.5: An example horizontal plane PPO film dose – response calibration made in autumn to the erythemally active wavelengths.....100

Figure 5.6: An example horizontal plane PPO film dose – response calibration made in autumn to the UVA.....101

Figure 5.7: Horizontal plane PPO film calibrations of the dose – response at the water surface and at Z_{1CM} and Z_{16CM} . The error bars represent 1δ for each of the calibrations.....104

Figure 5.8: PPO dosimeter cosine response underwater at an arbitrary depth. The y – error bars represent the cumulative $\pm 9\%$ in – water interdosimeter variation following normalisation.....107

Figure 5.9: Overnight dark reaction data shown as a percentage of the cumulative ΔA_{320} value measured as the accumulation of the increase in optical absorbency within the PPO film after each daily exposure. The y – error bars represent the cumulative $\pm 9\%$ for the in-water interdosimeter variation.....111

Figure 5.10: PPO film reaction to UVA and visible wavelengths on a horizontal plane after 60 hours total exposure to sunlight given as a percentage ratio. The y – error bars represent a predicted cumulative $\pm 7\%$ in – air interdosimeter variation.....113

Figure 5.11: Percentage ratio of the daily watermark effect measurement to the average daily ΔA_{320} value. The y – error bars represent the cumulative $\pm 9\%$ for the in-water interdosimeter variation.....115

Figure 6.1: Transmission and absorption spectra across the waveband running from 300 nm to 340 nm for the Multix, Coles Reliance and Savings waste bags.....121

Figure 6.2: Transmission and absorption spectra across the waveband running from 300 nm to 340 nm for the Savings waste bag after a solar erythemal exposure of 45 kJ m⁻².....122

Figure 6.3: The variation of the erythemal UV exposures received by the NDF and PPO dosimeters during autumn.....124

Figure 6.4: Ozone levels detected by the OMI satellite above Toowoomba during the NDF trial period (March to May 2008).....124

Figure 6.5: Erythemal calibrations for the filtered and unfiltered PPO dosimeters over the months of autumn.....126

Figure 6.6: A time series of the in – air erythemal UV exposures measured over each day during the PPO dosimeter calibration measurement campaign.....127

Figure 6.7: The erythemal action spectrum in the waveband running from 280 nm to 400 nm.....129

Figure 6.8: Ozone over the Toowoomba region from March 2007 to February 2008.....130

Figure 6.9: Solar erythemal exposure calibration regimes measured for the PPO dosimeter over the months of autumn, winter, spring and summer.....133

Figure 6.10: Complete solar erythemal exposure calibration equations for the PPO dosimeter for autumn, winter, spring and summer.....134

Figure 7.1: Transmission and absorption distributions for clear water, creek water, sea water and dam water.....146

Figure 7.2: Transmission (A) and absorption (B) spectrophotometry data at 315 nm for the clear, creek, dam and sea water.....147

Figure 7.3: The K_d values calculated using the EPP2000 spectrometer in the clear, creek, sea and dam water for high SZA conditions (A) and the K_d values calculated using the EPP2000 spectrometer in the clear, creek, sea and dam water for low SZA conditions (B).....149

Figure 7.4: (A) Calibration curves against the solar UVB exposures over autumn for tap water, creek water, sea water and dam water at Z_{1CM} . The surface (in – air) calibration curve acts as the control. (B) Calibration curves against the solar UVB exposures over autumn for tap water, creek water, sea water and dam water at Z_{20CM}152

Figure 7.5: (A) Calibration curves against the solar UVB exposures over winter for tap water, creek water, sea water and dam water at Z_{1CM} . (B) Calibration curves against the solar UVB exposures over winter for tap water, creek water, sea water and dam water at Z_{20CM}153

Figure 7.6: (A) Calibration curves against the solar UVB exposures over spring for tap water, creek water, sea water and dam water at Z_{1CM} . (B) Calibration curves against the solar UVB exposures over spring for tap water, creek water, sea water and dam water at Z_{20CM}154

Figure 7.7: (A) Calibration curves against the solar UVB exposures over summer for tap water, creek water, sea water and dam water at Z_{1CM} . (B) Calibration curves against the solar UVB exposures over summer for tap water, creek water, sea water and dam water at Z_{20CM}155

Figure 7.8: Comparison between underwater complete calibrations obtained over the months of autumn, winter, spring and summer.....157

Figure 8.1: (A) North side view of the DSF and (B) the top – down view of the DSF.....166

Figure 8.2: The Japanese Gardens Lake located on the University of Southern Queensland campus grounds.....168

Figure 8.3: Positioning of the DSF in the Japanese Gardens Lake.....168

Figure 8.4: The agricultural dam located on the University of Southern Queensland campus grounds.....170

Figure 8.5: Positioning of the DSF in the agricultural dam.....170

Figure 8.6: The simulated sea water environment located on the University of Southern Queensland campus grounds.....172

Figure 8.7: Positioning of the DSF in the simulated sea water environment.....173

Figure 8.8: Creek (A), sea (B) and dam (C) underwater calibrations used to obtain field UVB exposures for each season.....177

Figure 8.9: In – air UVB calibrations employed for the water surface field measurements made in each season.....178

Figure 8.10: UVB exposure distributions in the creek, sea and dam water in autumn (A), winter (B), spring (C) and summer (D).....181

Figure 8.11: Averaged UVB exposure depth regimes as extracted from horizontally aligned sea water exposure distribution data for each season of the year.....186

Figure 8.12: K_d values calculated from the sea water UVB exposure depth regimes compared to the K_d value calculated using the EPP2000 spectrometer for sea water.....189

List of Tables

Table 4.1: The slope, y – intercept and R^2 values as calculated for the Bentham spectroradiometer comparison to the EPP2000 spectrometer.....	72
Table 4.2: Values for all ε and ρ parameters as measured for clear, creek, sea and dam water in both low SZA and high SZA conditions.....	90
Table 6.1: ν , κ and R^2 values obtained for all calibrations produced over autumn, winter, spring and summer.....	131
Table 7.1: α , β and R^2 values obtained for each particular calibration over autumn, winter, spring and summer.....	151
Table 8.1: α , β and R^2 values obtained for the combined creek water, sea water, dam water UVB underwater calibrations measured over autumn, winter, spring and summer.....	175
Table 8.2: α , β and R^2 values obtained for the in – air UVB calibrations measured over autumn, winter, spring and summer.....	176
Table 8.3: ψ , ω and R^2 values calculated for the sea water UVB depth distributions for autumn, winter, spring and summer.....	185

Certification of Dissertation

I certify that the ideas, experimental work, results, analyses, software and conclusions reported in this dissertation are entirely my own effort, except where otherwise acknowledged. I also certify that the work is original and has not been previously submitted for any other award, except where otherwise acknowledged.

Signature of Candidate

Date

ENDORSEMENT

Signature of Supervisor/s

Date

Acknowledgements

The author of this dissertation would like to thank the following: Associate Professor Alfio Parisi for developing the original idea for the research and providing countless hours of supervision, guidance, enthusiasm and proof – reading over the course of the project, Dr David Turnbull for providing several ideas for the initial development of the PPO dosimeter and for stepping in as the associate supervisor of this project, Mr Graham Holmes for his helpful and quick assistance with any technical issues, Mr Oliver Kinder for his excellent construction of the DSF, the University of Southern Queensland for providing me with an Australian Postgraduate Awards scholarship and my family and friends who have given me great amounts of support and encouragement over the duration of my PhD candidature.

Chapter 1

Introduction

1.1 Introduction

The measurement and modelling of solar ultraviolet radiation (UV) in underwater environments has been a subject of major interest for both physicists and marine biologists for several decades. Researchers such as Davies – Colley & Smith (1995), Smith *et al* (1973), Neale *et al* (2001), Hargreaves (2003) and Dunne (1999) have primarily investigated how the UV along with other wavebands in the electromagnetic spectrum (predominantly the visible spectrum) penetrate and propagate by employing various types of optical instrumentation such as spectroradiometers, broadband sensors and a limited range of dosimetric systems within various types of underwater environments, such as oceans, lakes and creek beds.

Chemical UV actinometers based upon the photolysis of nitrite and nitrate have been developed to measure underwater solar UV by means of scalar photon exposure with very high levels of sensitivity at an accuracy exceptionally close to spectroradiometric measurements (Jankowski *et al*, 2000). However, considerable knowledge relating to their chemical composition is required in order to prepare and deploy them properly and specialised equipment is needed for degradation analysis in order to obtain any meaningful data from them.

Underwater UV irradiance calculations have been made in the past by using numerical radiation transfer models such as Hydrolight (<http://www.sequoiasci.com/products/Hydrolight.aspx>) combined with atmospheric ozone and aerosol data taken directly from the TOMS and OMI instrumentation on board the Aura remote sensing satellite (Vasilkov *et al*, 2005). These calculations are useful as they do not require any real – world field work to be carried out, hence

saving the researcher a great deal of time, effort and possibly money. Unfortunately, they do require a substantial level of numerical modelling experience to perform, which may be a prohibitive factor for scientists not familiar with computer programming or modelling software.

UV chemical dosimeters, such as polysulphone (CIE, 1992), provide a readily deployable and cost effective method of measuring UV exposures in comparison to more expensive and unwieldy spectrometer and radiometer systems. In underwater conditions, the usage of radiometers and spectrometers becomes difficult with routine specialised calibration techniques, such as calibrating for the immersion effect, power requirements and maintenance becoming necessary, more so than when they are in operation on land.

Several UV chemical dosimeters, such as o – nitrobenzaldehyde and polysulphone (Fleischmann, 1989; Dunne, 1999, Frost *et al*, 2006) have been used in real marine environments. However, these dosimeters only have the capability to record a cumulative UV exposure over small temporal increments, usually no greater than two days. This small amount of time spent in the underwater field environment greatly reduces the amount of exposure data available for analysis. The ability to record high levels of exposure is very important, as the biological damage caused by solar UV radiation to marine biota can be a long-term cumulative process. So there is a definite need for a chemical dosimeter that can be easily employed for marine usage and which is capable of measuring large amounts of exposure over a substantial amount of time. The only real disadvantage of using UV chemical dosimeters over extended intervals is that due to the loss of all temporal resolution during deployment only the

total UV exposure over the measurement period can be determined. This means that the pattern of UV exposure delivery can not be evaluated. However, simple average irradiance estimations can still be made by dividing exposure data by the amount of time the dosimeters were operational in the field. In spite of this, most studies investigating long – term solar UV exposures do not require exposure delivery information and are only interested in total dosages.

Biological dosimeters, based on DNA samples, viral strains and bacteria have also been employed for underwater use with success, such as the study performed by Wilhelm *et al* (2002). However, these types of dosimeters are more difficult to calibrate and measure using conventional equipment, and require a far greater amount of time and exactness to prepare for use and analyse in comparison to their chemical counterparts.

Early research performed by Davis *et al* (1976) and Lala (1984) showed that Poly (2, 6-dimethyl-1, 4-phenylene oxide) (PPO) film can be successfully used in air to measure high amounts of UV exposure over extended periods of time. Lester *et al* (2003) followed this work and detailed various optical properties of PPO film in – air. These optical properties included the cosine response, temperature effect on optical absorbance, spectral responsivity and exposure reproducibility. From this analysis, Lester *et al* (2003) found that PPO film is capable of a dynamic range extending to 2 MJ m⁻² of biologically damaging UV exposure before total optical saturation, which is approximately equivalent to four days unshaded exposure to the Sun in summer at subtropical locales. This is a four – fold increase of the dynamic range in comparison to polysulphone. Also, in-air studies performed by Berre and Lala (1989) have shown

that PPO film dosimeters have accuracy equal to or better than 20% when compared to UV data collected by a radiometer.

Therefore, from this work it is a logical progression to test the optical properties and operational limitations of the PPO film in underwater environments in order to develop a dosimetric system capable of measuring long – term UV exposures in marine environments. This, in turn, will greatly increase the amount of exposure time over which exposures can be measured by the researcher and more importantly, will help to better quantify the distribution of solar UV radiation underwater and its influence upon different aquatic life forms, such as the various forms of plankton, algae and coral amongst others.

1.2 Objectives

The objectives of this research project are the following:

1. To verify the suitability of the PPO dosimeter for measuring underwater solar UV exposures by testing its optical properties in water within a controlled laboratory environment using solar simulation techniques;
2. To calibrate the PPO dosimeter to the erythemal action spectrum in – air and to the UVB spectrum underwater in the field environment in autumn, winter, spring and summer and to deduce its operational limitations in three different water types commonly found in water bodies around South – East Queensland;
3. To deploy the PPO dosimeter in three different water bodies in the field, each with their own characteristic turbidity and dissolved organic matter (DOM) level to measure the distribution of the solar UV in these water bodies at varying depths

and orientations and to then compare these measurements to data collected from a spectrometric system. This will be carried out again over the months of summer, autumn, winter and spring.

1.3 Dissertation Outline

This dissertation has been written in the following sequence:

- Chapter 2 details an overview of the properties of solar UV and also reviews the various types of natural attenuation factors that influence the solar UV incident on the surface of the Earth;
- Chapter 3 provides a brief primer on the behaviour of solar UV on both the water surface and in the aquatic environment and how various constituents such as natural turbidity and DOM influence the solar UV distribution underwater. Chapter 3 also describes both the positive and negative effect that solar UV has upon the organisms living within the intricate aquatic ecosystem and how it all relates back to the human population;
- Chapter 4 gives a description of how solar UV is currently measured underwater using a wide variety of scientific instrumentation and methodologies. Together with this, detailed descriptions of the radiometer, spectroradiometer and spectrometer equipment employed in this research are given. This chapter also reviews the techniques used to properly maintain and calibrate radiometers, spectroradiometers and spectrometers for use underwater. The theory and application of the immersion effect is also discussed;

- The initial development and testing of the optical properties characteristic to the PPO dosimeter as measured in a controlled underwater environment is described in Chapter 5;
- Extended solar UV exposure measurements made by the PPO dosimeter combined with a unique neutral density filter are detailed in Chapter 6. Along with this long – term calibrations made with the PPO dosimeter for erythemal exposures in – air are also presented for each season and directly compared;
- Chapter 7 extends the work displayed in Chapter 5 and Chapter 6 by showing how the PPO dosimeter can be calibrated effectively for accurate underwater solar UV measurements in the field. The influence of atmospheric column ozone and solar zenith angle upon the underwater calibrations is also investigated;
- Chapter 8 gives a summary of a year – long measurement campaign using the PPO dosimeter in combination with a custom built submersible float to measure underwater solar UV exposures in a creek, a dam and a simulated sea water environment. The data from the campaign is compared directly to data measured with a spectrometer in order to fully deduce the operational precision of the PPO dosimeter.

Chapter 2

Properties of Solar Ultraviolet Radiation on Earth

2.1 Introduction

Before solar UV enters an underwater environment it passes through the Earth's complex evolving atmosphere where it can be subject to a number of different wavelength dependent scattering, absorption and enhancement processes instigated by various constituents such as aerosols, airborne molecules, clouds and ozone. Solar UV intensity as measured on the surface of the Earth can also be moderated by other geophysical factors like altitude, albedo and reflectivity along with geometric properties of the Sun such as the solar position most commonly defined by calculation of the solar zenith angle and the Earth – Sun distance. Therefore, before complete knowledge of the distribution of the underwater light field can be obtained, an understanding of the atmosphere's role in solar UV modulation must be initially acquired. This chapter will briefly introduce the mechanics behind these various important influencing parameters and will discuss some important selected case studies in which the quantitative and qualitative effects of these parameters on the solar UV have been investigated.

2.2 Solar UV Radiation

The World Health Organisation (WHO) defines ultraviolet (UV) radiation as the spectrum of electromagnetic radiation that exists within the wavelength range running from 100 nm to 400 nm (WHO, 2004). Here on earth, UV radiation is sourced from the Sun, which is essentially a giant thermonuclear reactor working with a surface temperature of approximately 6000 Kelvin. The Sun, which is approximated as a hot blackbody, emits electromagnetic radiation over a wide spectral range characteristic of its temperature, given by Planck's Law (Freedman & Kaufmann, 2002; Serway *et al*, 2005). The types of electromagnetic radiation emitted by the Sun vary from highly

energetic gamma and x – rays capable of causing excessive biological damage and mutation to relatively weak and biologically ineffective radio waves. The majority of electromagnetic radiation emitted from the Sun is in the visible waveband ranging from 400 nm in the violet region up to 700 nm in the red region, which is what human vision has adapted to see over time. The UV spectrum output by the Sun is most commonly divided into three different wavebands with respect to wavelength as defined by the International Commission on Illumination (CIE):

UVA (315 – 400 nm)

UVB (280 – 315 nm)

UVC (200 – 280 nm)

Many scientists, especially those working in the field of photobiology, define the limit between the UVB and the UVA wavebands as being 320 nm due to the considerable energetic potential of the wavelengths in the 315 nm to 320 nm region (Wong & Parisi, 1999; Turnbull, 2005). Water accounts for 0.33% of the total atmospheric mass and is responsible for approximately 70% of all atmospheric radiation absorption. This absorption takes place predominantly in the infrared waveband (Chaplin, 2009). However, water molecules also combine with air to completely absorb the UV wavelengths below about 200 nm before they have any opportunity to make it to the Earth's surface. Atmospheric ozone practically absorbs the majority of incoming solar UV radiation within the Hartley waveband, which runs from 200 nm to 290 nm. In the Hartley waveband, ozone absorption reaches a maximum at about 250 nm with UV absorption gradually reducing through the wavelengths past the Hartley end limit until becoming almost completely negligible at 320 nm (Pickett, 1994). As a result of this,

UVA photons are unaffected by ozone during their time spent in the atmosphere (Urbach, 1997). At altitudes below 70 km all UV radiation absorbed by ozone is converted into molecular kinetic energy, resulting in an increase of local atmospheric temperature (Houghton, 2002). Fortunately for all living species here on Earth, UVC radiation will continue to be completely blocked out even if the ozone layer thickness decreases substantially (Parisi & Kimlin, 1997a). UVB and UVA radiation constitutes only 8% to 9% of the Sun's total electromagnetic energy output (Feister *et al*, 1992; Lenoble, 1993; Simon, 1997). From this, solar UV radiation represents about 3% of the total solar radiation incident on the Earth's surface during cloud – free conditions (Grant & Heisler, 1997), with the UVB component equating to less than 1% of this amount (Blumthaler, 1993; Grant *et al*, 1997a).

Terrestrial solar UV (UV radiation propagating inside the Earth's atmosphere) contains a reflected, a direct and a diffuse component with the diffuse component being the hardest to measure and predict (Coombes & Harrison, 1988). This diffuse component represents at least 50% of the terrestrial solar UV irradiance under zero cloud conditions and is the most prevalent component in overcast conditions as the direct component is blocked out by cloud coverage (Grant *et al*, 1997b). The diffuse portion of terrestrial solar UV increases towards the shorter UV wavelengths due to the propensity of these wavelengths to be influenced by Rayleigh and aerosol scattering processes (discussed further in Section 2.3.3). As scattering does not eliminate these wavelengths from the atmosphere, a large proportion of this radiation reaches the Earth's surface (Parisi & Kimlin, 1997b). The ratio of diffuse to total terrestrial solar radiation increases with solar zenith angle (Basher, 1989; Frederick, 1993; Ireland & Sacher, 1996). As UVB is scattered more readily than UVA, the

diffuse UVB radiation present in the sky exceeds the direct UVB from the sun, except for a few hours around solar noon. However, the direct component of UVA is more prevalent than the diffuse for the majority of the day, with the exception of a few hours in the early morning and evening.

2.3 The Propagation of Solar UV in the Earth's Atmosphere

2.3.1 Cloud Cover

The most influential atmospheric parameter on the distribution and propagation of terrestrial UV irradiance levels is cloud cover. Numerous investigations in recent years have been made looking into the direct effect of cloud cover on solar UV at sites all over the world using various types of measurement and monitoring equipment, most commonly radiometers, spectroradiometers, spectrophotometers and sky cameras along with some assorted methods of radiative transfer modeling (Sabburg & Wong, 2000; Sabburg *et al*, 2001; Cede *et al*, 2002; Grant & Gao, 2003; Piacentini *et al*, 2003; Crawford *et al*, 2003; Parisi & Downs, 2004; Kuchinke *et al*, 2004; Calbo *et al*, 2005; Kylling *et al*, 2005; Sabburg and Parisi, 2006). Scattered cloud cover has been shown to reduce solar UV, most especially the UVB by 50% or more, with this value increasing to an even greater percentage on totally overcast days (Bais *et al*, 1993). However, recent studies detailed by Den Outer *et al* (2005) have shown that clouds attenuate solar UV radiation by 15% to 45% less than visible radiation due to the tendency of the Rayleigh scattering process to interfere more with the solar UV wavelengths. In addition to this, Winiecki and Frederick (2005) have established that UV cloud transmission is wavelength dependent and as a result shorter wavelengths are less affected by cloud attenuation. The amount by which a certain type of cloud

will attenuate UV radiation changes with respect to various macrophysical properties, for instance three – dimensional geometry, spatial homogeneity, sky coverage and altitude along with their microphysical properties, like optical density and constituent composition and distribution, with optical density assumed to be the primary influencing attribute on the transfer of UV radiation through a cloud mass (Károly, 1997; Pfister *et al*, 2003; Kerr, 2003). Additionally, Nichol *et al* (2003) have found that increasing SZA can amplify the effect of UV modulation by cloud coverage.

Broken cloud can enhance UV irradiance levels measured on ground level (WMO, 2007). Many recent studies have evaluated this phenomenon. Weihs *et al* (2000) presented research showing that UV radiance measured under broken cloud conditions could be up to 2.5 times higher than measurements made under clear sky conditions. Sabburg and Wong (2000) showed that at a sub – tropical location up to 3% of all terrestrial solar UVB measurements made over a year – long time period are enhanced above clear sky values to some degree. Piacentini *et al* (2003) has reported that UV irradiances can increase with unevenly distributed cloud coverage by up to 6% at a high altitude location in the deserts of Argentina. Also, Sabburg *et al* (2001) have employed sky cameras in unison with broadband UV sensors to measure cloud enhancement effects. In this research it was discovered that the influence of cloud on solar UVA could result in sizeable enhancements of approximately $25 \pm 23\%$. Crawford *et al* (2003) has also delivered a study with similar significant results, showing that cloud can enhance actinic UV flux by as much as 40%. Additional research detailed by Sabburg *et al* (2003) found that enhancement in the UV waveband could be a wavelength dependent factor below a threshold wavelength at 306 nm. However, this work was updated by Sabburg and Parisi (2006), in which

various measurement regimes produced for the UVB and UVA wavebands showed that increasing, decreasing and zero levels of wavelength dependence were possible for both shorter and longer wavelengths, with wavelength dependency trends appearing to be correlated to overall cloud fraction. From these studies it is now certain that cloud not only reduces the intensity of incoming solar UV radiation, but in some certain circumstances cloud can increase it for short periods of time.

2.3.2 Ozone

Ozone (O₃) is located predominantly in the stratosphere at an altitude of between 10 to 30 kilometres above the surface of the earth at concentrations of no more than 10 parts per million by volume (Plumb, 1989; McKenzie & Bodeker, 1996). Atmospheric ozone is usually measured in Dobson units (DU), which are defined as the actual thickness of the ozone layer in centimetres to the negative third power if it were sampled on the Earth's surface at standard measures of temperature and pressure which are respectively 0°C and 1013 hPa. The precise value of 1 DU is given as 2.69×10^{16} molecules cm⁻² (Madronich *et al*, 1998; Parisi *et al*, 2004).

The genesis of ozone within the stratosphere begins with the photodissociation of an oxygen molecule (O₂) by a UV photon with a wavelength of no more than 240 nm, which results in the production of atomic oxygen. The free atomic oxygen units can then go on and join with unperturbed O₂ molecules to form new molecules of ozone. The atomic oxygen can also join up with a free nitrogen molecule (N₂) to form nitrogen oxide. The nitrogen oxide can then be dissimilated back down into its constituents by visible radiation, once again allowing the atomic oxygen to merge with another O₂ molecule. Additionally, solar UV can break ozone down into its

original atomic oxygen and O₂ components, allowing them to be free for other molecular interactions. The development cycle of ozone can be negatively affected by the introduction of several catalytic elements such as Br, NO, Cl, H and OH into the atmosphere, usually by anthropogenic means such as the release of chlorofluorocarbon compounds (CFC's) by households and industry. (Frazer, 1996; Mason & Pathak, 1997; Karoly, 1997).

Solar UV radiation within the range of 200 nm to 320 nm can be effectively absorbed by stratospheric ozone (Meloni *et al*, 2000). Over recent years it has become clear that even small reductions in stratospheric ozone amounts will lead to an increase in solar UVB irradiance levels coinciding with a shift of the short wavelength UVB cut – off for radiation reaching the Earth's surface to shorter wavelengths, increasing the effectiveness of biologically damaging irradiance incident to humans and animals living on Earth (Nunez *et al*, 1994; Turnbull, 2005).

A large number of studies have been carried out within the last few decades looking into the depletion of stratospheric ozone over sites such as the United States (Komhyr *et al*, 1994), South America (Rousseaux *et al*, 1999) and Antarctica (Bernhard *et al*, 2004; Bernhard *et al*, 2006). Several other investigations have quantified exact increases in solar UVB irradiances brought on by stratospheric ozone reduction. For example, Roy *et al* (1990) have measured an 11.9% increase in UVB in Melbourne, Australia during the months of summer correlating to a 10.5% decrease in ozone at the same time. Jokela *et al* (1995) working at a location in Finland discovered an increase in biologically effective UV of 10% on average in relation to a 40% decrease in total ozone. McKenzie *et al* (1999) reported that a substantial drop in ozone over

New Zealand coincided with an amplification of erythemal UV levels by as much as 12%. Kimlin *et al* (2000) found that only a relatively short – term decrease in stratospheric ozone of about 5% in a subtropical location resulted in an increase of clear sky UV of 14%. Also, a long – term report made by the NIWA research group based in Lauder, New Zealand described how damaging UV levels have increased by 15% since the 1970's, when stratospheric ozone was first found to be decreasing (McKenzie *et al*, 1999). Additionally, O'Toole (1994) has concluded that for every 1% decrease in total ozone, a 1.1% to 1.4% increase in UVB should be expected.

Ozone can be monitored directly using various types of instrumentation deployed and operated from the ground, in the atmosphere or in space. Most ground – based atmospheric ozone research projects have made use of radiometer, spectroradiometer or spectrophotometer (usually the Brewer or Dobson spectrophotometers) solar UV measurements in combination with shadow band systems, special regression methods and computer algorithms to estimate and/or model levels of atmospheric column ozone. Some examples of how well these techniques have worked over time include Stamnes *et al* (1991), Bojkov *et al* (1995), Huber *et al* (1995), Fioletov *et al* (1997), Slusser *et al* (1999) and Bernhard *et al* (2003). Data products delivered from the numerous implementations of the TOMS satellite program were once the choice resource of atmospheric column ozone information for atmospheric scientists across the globe. Example case studies such as McPeters *et al* (1996) and McPeters and Labow (1996) have mapped trends in TOMS ozone measurements in conjunction with Dobson spectrophotometer derived ozone values over long time intervals. Unfortunately, the most recent iteration of the TOMS platform has been rendered inoperable and is no longer used. Now, daily updated atmospheric column ozone data

obtained from the Ozone Monitoring Instrument (OMI) currently in Earth orbit on board the Aura satellite is the most commonly used source employed by atmospheric scientists for reliable ozone information.

The OMI optical system uses hyper spectral imaging by means of a wide – field telescope delivering input to two imaging grating CCD – based spectrometers to sample backscattered solar radiation in both the UV and visible wavebands. The hyper spectral capability of this setup increases precision levels of atmospheric column ozone measurements in comparison to what TOMS could produce. The system also features onboard automated wavelength and radiometric calibration (NASA, 2008). The wide – field telescope works at a viewing angle of 114° which provides a 2600 km wide swath on the Earth’s surface, enabling the measurement of daily ozone amounts across the entire planet (KNMI, 2008). In Figure 2.1 an example atmospheric column ozone output chart as measured by OMI on 7 December 2008 is presented. By using the coloured legend in this chart it can be seen that on that particular day atmospheric column ozone levels over South – East Queensland were in the vicinity of 250 to 275 DU, which is an ozone range typical for the region at that time. All daily ozone measurements mentioned in this research dissertation were obtained directly from the NASA OMI source.

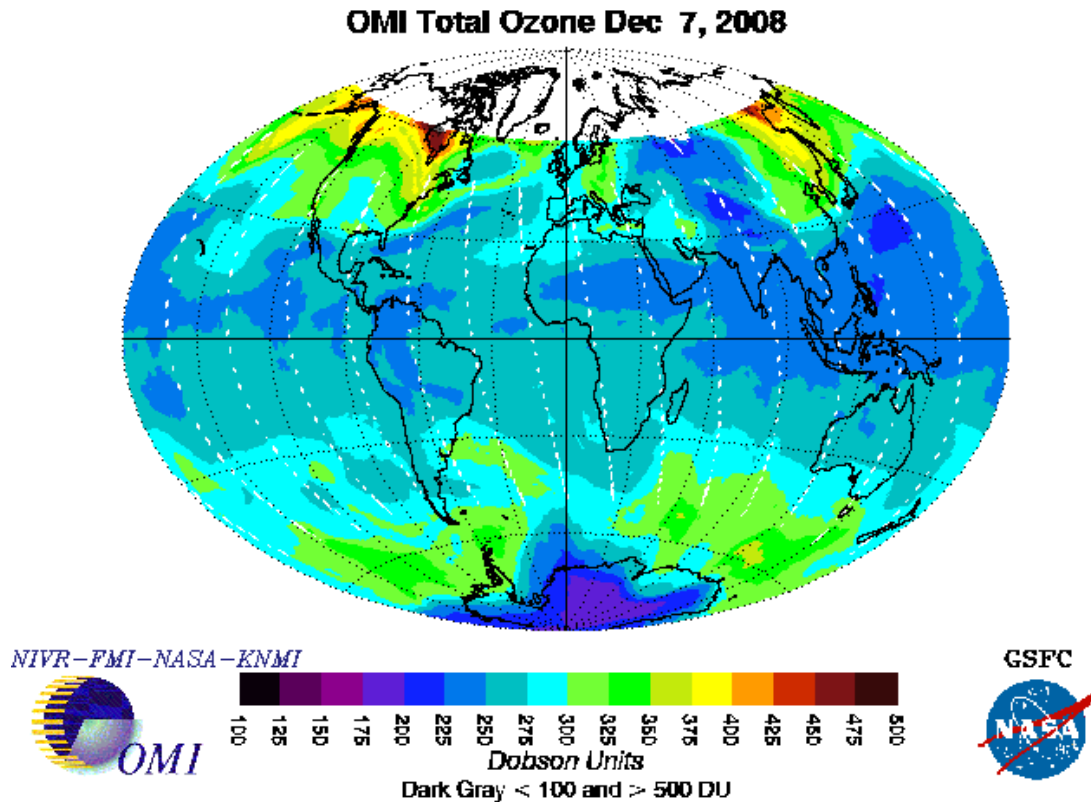


Figure 2.1: Example atmospheric column ozone output chart as measured by OMI on 7 December 2008.

(Source: ftp://toms.gsfc.nasa.gov/pub/omi/images/global/FULLDAY_GLOB.PNG)

2.3.3 Aerosol and Molecular Scattering

Aerosols are relatively small solid or liquid particles suspended in the atmosphere such as airborne soil, dust, water vapour, sea salts, soot and smoke. Aerosols can be launched into the atmosphere by natural means such as forest fires and volcanoes or by anthropogenic means such as pollution resulting from mining and manufacturing operations (Iribarne & Cho, 1980; Sturman & Tapper, 1997). Aerosols possess two different optical properties that can directly affect incoming solar UV radiation, these being scattering and absorption (Jacovides *et al*, 1993) and in combination with this they can also instigate and influence the formation and life cycle of clouds which can lead to further solar UV attenuation (Chowdhary *et al*, 2005). The magnitude of

aerosol scattering is inversely proportional to wavelength, a process sometimes also referred to as Mie scattering (Goyot, 1998). Due to this inverse relationship, UVB is more vulnerable to scattering by aerosols in comparison to wavelengths in the visible waveband (Parsons *et al*, 1998). Numerous studies have been carried out in recent years measuring atmospheric aerosol content at various locations around the world using a wide range of techniques and hardware including LIDAR systems (di Sarra, 2002), spectrophotometers (Meleti & Cappellani, 2000) radiometers and spectroradiometers (Wenny *et al*, 2001; Bais *et al*, 2002; Kim *et al*, 2003; Gianelli *et al*, 2005) and also remote sensing satellites and airplanes working in synergy with computer algorithms and software (Smith *et al*, 2005; Chowdhary *et al*, 2005; Kahn *et al*, 2005; Redemann *et al*, 2005; Levy *et al*, 2005; Remer *et al*, 2005; Ignatov *et al*, 2005).

The general methodology used to find the total atmospheric optical depth and from that the aerosol optical depth is usually done from Earth level by employing the Langley regression methodology in tandem with the Beer – Lambert – Bouguer Law, as modified for the analysis of the attenuation of radiation through an atmospheric column (Ingle & Crouch, 1988):

$$I = I_0 e^{-\tau_{TOTAL}m}$$

where I is the direct solar irradiance at the Earth's surface, I_0 is the solar irradiance present at the very top of the Earth's atmosphere, τ_{TOTAL} is the total column optical depth for all atmospheric constituents in the zenith direction and m is the total air mass in the zenith direction. The value for m is calculated by using an equation derived by Kasten and Young (1989) which is given as follows:

$$m = \frac{1}{\sin(\phi) + 0.50572(6.07995 + \phi)^{-1.6364}}$$

with ϕ being the solar elevation angle in degrees. By applying natural logarithms to both sides of the Beer – Lambert – Bouguer Law, it takes on the following form:

$$\ln(I) = \ln(I_0) - m\tau_{TOTAL}$$

This equation can be corrected for fluctuations in the distance between the Sun and the Earth by employing a correction factor that is dependant on ordinal day number. By plotting I against m on a completely cloud free day, the calculation of the magnitude of the slope by means of linear regression gives τ_{TOTAL} with the y – intercept being I_0 . After τ_{TOTAL} has been calculated, the various extinction components within τ_{TOTAL} can be extracted with (Bigelow *et al*, 1998):

$$\tau_{TOTAL} = \tau_{O_3} + \tau_A + \tau_{RAYLEIGH}$$

where $\tau_{RAYLEIGH}$ is the total Rayleigh column optical depth, τ_{O_3} is the total ozone column optical depth and τ_A is the total aerosol column optical depth. Many equations have been derived over the years to calculate localized values of $\tau_{RAYLEIGH}$, with $\tau_{RAYLEIGH}$ being evaluated either directly as a function of site pressure, or indirectly as a function of site altitude. A review of the most accurate equations to derive $\tau_{RAYLEIGH}$ is detailed in Bodhaine *et al* (1999). Following the calculation of $\tau_{RAYLEIGH}$, τ_{O_3} can be extracted from τ_A by using the methodology suggested by Rosales *et al* (2006).

Rayleigh scattering is a process not unlike aerosol scattering. While aerosol scattering occurs due to the stochastic dislocation of solar wavelengths due to the Brownian motion of large airborne particulates, the Rayleigh scattering process takes place when solar wavelengths are displaced in the atmosphere by much smaller molecular units such as nitrogen, oxygen and carbon dioxide (Webb, 1998). The total amount of Rayleigh scattering is proportional to the inverse of the wavelength to the fourth power (Caldwell, 1981; Turnbull & Parisi, 2005). As a consequence, UV is the most scattered waveband by molecules in the atmosphere with UVB wavelengths more likely to undergo scattering than their UVA counterparts (Caldwell, 1981; Parisi *et al*, 2004). In ideal clear sky conditions, the total amount of Rayleigh scattering has a substantial impact on the ratio of diffuse to direct radiation incident on the Earth's surface and as a consequence of this, the effect of another atmospheric parameter (such as aerosol scattering or ozone absorption) on the incoming UV wavelengths can be analysed and defined in terms of its influence on the direct to diffuse ratio (Rikus, 1996). The mechanism of Rayleigh scattering has been well defined in a previous study by Bates (1984). From this knowledge, radiative transfer models using SZA and atmospheric pressure as primary variables can be generated in order to accurately estimate the direct effect of Rayleigh scattering upon UV wavelengths in the atmosphere (Stamnes, 2002a; Kerr, 2003).

2.3.4 Solar Zenith Angle

The solar zenith angle (SZA) is defined as the angle between the zenith and the solar disk position as seen in the sky (Madronich, 1993). Hence, the SZA at any given time can be calculated as 90° minus the altitude of the sun. This SZA value will vary with respect to the geographical location, time of day and also with changes in season

(Madronich, 1993). The minimum SZA measured at midday in a sub – tropical location (Toowoomba, Queensland) can differ from a value as low as 5° in summer to as high as 53° in winter. With decreasing SZA, incoming solar UV wavelengths have a shorter atmospheric path to travel through on their way down to the Earth’s surface. Therefore, in low SZA conditions, solar UV is subject to less scattering and absorption, which means that incoming UV has higher irradiances than they do during high SZA conditions. In addition to this, within low SZA ranges, the cut – off for solar UV moves down to more energetic wavelengths that have greater potential to deliver biological damage to both terrestrial and aquatic organisms (Parisi & Turner, 2006).

2.3.5 Altitude

The intensity of incoming solar UV irradiance is known to increase with altitude (McKenzie *et al*, 2001). Due to decreases in the amount of atmospheric pollutant and molecular constituents with altitude, wavelengths of solar UV incident at higher altitude locations are influenced by a fewer number of absorption and scattering processes. The resulting increase of solar UV irradiance with altitude is called the altitude effect (AE) and is calculated by the following formula first presented in the literature by Blumthaler *et al* (1997):

$$AE = \left(\frac{I_H}{I_L} - 1 \right) \times \frac{\Delta A}{1000} \times 100\%$$

where *AE* is a measure of the increase in irradiance per kilometre relative to a low altitude reference site (as a percentage), *I_H* is the irradiance measured at the high altitude site, *I_L* is the irradiance at the low altitude site and ΔA is the change in altitude between the high altitude site and the low altitude site. The magnitude of the altitude

effect can depend upon changes in albedo (discussed further in Section 2.3.6). In colder regions snow is generally present at higher altitudes, for instance at the top of a mountain. At a high location like this the albedo and in turn the total irradiance would be greater when compared to the albedo and total irradiance at a lower location at which no snow is present. As a result, this discrepancy leads to an overall increase in the altitude effect calculated between the two sites.

After taking several years worth of measurements in the Alps, Schmucki and Philipona (2002) showed that under clear skies mean yearly values of the direct UV irradiance could increase by 17.4% per 1000 metres and that the global and diffuse components could also increase by 10.7% per 1000 metres and 8.5% per 1000 metres respectively. Also, from UV measurements taken in the Chilean Andes for solar elevation angles of between 20° and 90°, Piazena (1996) depicted how an increase in global UVB irradiance of 8% to 10% could occur for every 1000 metre increase in altitude. A study made by Barton and Paltridge (1979) discovered that an increase in altitude as small as 1 kilometre above sea level could result in a 15% increase in biologically damaging UV availability. Additionally, McKenzie (1991) found a 10% increase in UV irradiance at an altitude of 2 kilometres brought on by a decrease in the number of molecular constituents available for Rayleigh scattering processes. Another example of how altitude can affect UV levels has been presented by Blumthaler *et al* (1994). In this investigation, solar UV was measured simultaneously at two locations with different ozone and aerosol levels separated by a vertical distance of 1 kilometre. It was found that the measurements made at the higher site were greater than the lower site with irradiance increases of 24% at 300 nm, 11% at 320 nm and 9% at 370 nm seen in the trial.

2.3.6 Albedo

Albedo is the term used to define the ability of a material to reflect any form of radiation. The UV albedo, ρ of a given surface is wavelength dependent (Blumthaler, 1993) and is found by finding the ratio between the upward diffuse irradiance (UV_{UP}), resulting from surface reflection, and downward global irradiance (UV_{DOWN}), that is the summation of both incoming direct and diffuse radiation (Feister & Grewe, 1995; McKenzie *et al*, 1996; Kerr, 2003; Turner *et al*, 2008):

$$\rho = \frac{UV_{UP}}{UV_{DOWN}}$$

This equation for albedo only produces results of between $\rho = 0$ and $\rho = 1$. If $\rho = 1$ the material under analysis can be regarded as a perfect reflector for the given waveband as all downward global irradiance is reflected back into the atmosphere off its surface. On the other hand, if $\rho = 0$ all downward global irradiance is completely absorbed by the material itself. In this case the material can be regarded as a perfect absorber for the given waveband or wavelength. Natural materials like water, dirt and grass reflect less than 10% of incident UV radiation, while high albedo surfaces, such as sand can reflect as much as 25% and also fresh snow, which has been shown to intensify the downward irradiance by at least 20% up to as much as 80% in some scenarios (Blumthaler & Ambach, 1988; McKenzie *et al*, 1996).

2.3.7 Earth Orbit

The Earth moves about the Sun in an elliptical orbit at an average distance of 149,597,893 kilometres (Moore, 1995). The 23.5° tilt of the Earth's axis with respect to the orbital direction affects the angle at which solar radiation is incident on the Earth's surface and also causes seasonal and latitudinal variations in day length. A

variation in distance of approximately 5×10^6 kilometres or 3.4% has been measured to occur from when the Sun is closest to the Earth in early January to when it is furthest away in early July (Madronich, 1993; Moore, 1995; Stamnes, 2002b; Kerr, 2003). As a result, the difference in magnitude of the terrestrial solar irradiance between the peak in January and the low point in July can be as great as 6.9% (Madronich, 1993; Stamnes, 2002b).

2.4 Chapter Discussion

The next chapter will describe how solar UV, after making it through the atmosphere, behaves once it reaches and propagates within the underwater environment, in which it can encounter an even greater number of complex attenuative factors and cause substantial amounts of physiological damage and stress to aquatic animal and plant life, that in turn, has a direct influence upon all of the life forms living here on Earth, including humans.

Chapter 3

Properties of Solar Ultraviolet Radiation in the Underwater Environment and its Effect upon Aquatic Ecosystems

3.1 Introduction

Some marine species have evolved over time to either avoid or adapt to solar UV using a number of methods such as refuge and depth migration (Vinebrooke & Leavitt, 1999; Boeing *et al*, 2004; Leech *et al*, 2005) along with various DNA related photoprotective and photorepairing adaptations (Shick & Dunlap, 2002; Moeller *et al*, 2005). It is a well known fact that terrestrial solar UV still has a detrimental impact upon marine organisms with reported reductions in reproduction, growth and development rates and an increase in DNA damage in species such as phytoplankton, zooplankton, bacterioplankton, picoplankton, fish eggs, fish larvae, seagrasses and also macroalgae (Hader *et al*, 2003).

Increases in the amount of incoming solar UV into a marine ecosystem, such as those caused by widespread decreases of atmospheric ozone levels for instance, can lead to decreases in biomass productivity, which can go on to affect each level of the food chain, working all the way to the top with reduced food production available for human consumption (Hader, 1998). In addition to this serious scenario, there would also be a noticeable reduction in the global sink capacity for carbon dioxide alongside wide scale changes in marine species composition (Hader, 1998; Ducklow *et al*, 1995).

The pronounced influence of UVB upon marine biochemistry along with the suspected global climate change are allowing for substantial changes to occur in the distribution of solar UV underwater and in turn the marine trace gas exchange. A vast number of investigations including Thomas and Lara (1995), Reitner *et al* (1997) and Tranvik and Kokalj (1998) have analysed the complex biochemical balance between

solar UVB, DOM and other trace marine chemicals. From these studies it has become clear that microbial activity is enhanced by the decomposition of polymeric components of DOM down to biologically available organic compounds and other types of mineral nutrients after intensive solar UV exposure. Additionally, the photodegradation of DOM into carbon dioxide by means of solar UV exposure is known to be a highly important source of decomposition in numerous types of marine locations (UNEP, 1998).

As a consequence of its extreme influence upon aquatic ecosystems, solar UV radiation must be measured and monitored in underwater locations using a wide variety of optical instrumentation and measurement techniques in order to better understand the damage it causes on both a macro and micro scale and perhaps provide solutions as to how this damage can be adequately managed. However, before the various types of instrumentation and methodologies can be employed properly and efficiently an understanding of the penetrative and behavioural properties of UV radiation in aquatic media must be achieved. The first half of this chapter presents a brief overview into how the distribution of UV light on both the water surface and underwater is described mathematically and how this distribution can be disturbed by the presence of dissolved organic matter and other assorted constituents. Subsequently, the second half of this chapter details how UV can affect various types of marine life forms by summarising some of the most relevant and prevalent scientific case studies carried out in the discipline of marine photochemistry and photobiology over the last half century.

3.2 Penetration and Propagation of Solar UV Underwater

3.2.1 Solar UV at the Water Surface

Not all solar UV energy that reaches the water surface penetrates through to the deeper depths. A variable proportion of the energy hits the water and is immediately reflected back into the atmosphere. The amount of albedo at the water surface is dependent primarily upon the SZA, which varies with the time of day, the season and the latitude. However, the SZA becomes less of a factor in surface reflection when cloudy skies are prominent over the water body as the ratio of diffuse to direct solar UV increases in these conditions (Cole, 1975).

The amount of incoming UV light that is reflected at the water interface varies from 2% for vertically incident UV all the way up to 100% for UV wavelengths that approach the critical angle. The reflectance r for unpolarised light can be modelled as a function of the angle of the incident light in air θ_a and the angle of light propagation in the water θ_w using a modified version of Fresnel's equation (Kirk, 1994):

$$r = \frac{1 \sin^2(\theta_a - \theta_w)}{2 \sin^2(\theta_a + \theta_w)} + \frac{1 \tan^2(\theta_a - \theta_w)}{2 \tan^2(\theta_a + \theta_w)}$$

The angle θ_w can be calculated directly from knowledge of θ_a and the refractive indices of air n_a and the water type under analysis n_w by using Snell's Law:

$$\frac{\sin \theta_a}{\sin \theta_w} = \frac{n_w}{n_a}$$

The refractive index for air is usually always approximated to be 1 while the refractive index value for a particular water type can vary dependent upon its composition. A refractive index value of 1.33 can be used for either fresh or sea water (Kirk, 1994). However, a more accurate system of equations have been developed by

the International Association for the Properties of Water and Steam (1997) to evaluate refractive indices for any given type of water. These equations are discussed further in Section 4.4.

Another factor that can affect water surface reflection and also the underwater UV light regime is wave motion. Waves have the capability of refracting incoming solar UV rays into an intensified collimated beam lasting only for a short amount of time. To date, very little analysis has been completed that directly evaluates the lensing effect of waves upon solar UV. One recent study produced by Deckert and Michael (2006) has used a three – dimensional Monte Carlo simulation to quantify flashes of UV radiation brought upon by different kinds of water surface conditions including undisturbed surface water, sinusoidal surface wave motion along with other more complicated wave formations. It was found that the wave enhanced UV light flashes were intensified to extreme levels with one example case at 350 nm exceeding the collimated surface UV irradiance by greater than 100% and another example at 300 nm exceeding the reference beam by more than 60%. In general, UV light flashes modelled at 300 nm dissipated at a much more rapid rate than those at 350 nm and were found to be insignificant at depths below 3.7 metres.

3.2.2 Behaviour and Distribution of Solar UV Underwater

Electromagnetic radiation moving within a natural body of water is subject to both absorption and scattering processes initiated by the constituent materials held within the water body. These absorption and scattering processes have the potential to change the original distribution of irradiance existing above the surface of the water.

The extent of this change is of course limited by the type and amount of materials propagating inside the water body.

The mathematical description of the behaviour of photon flux in a water body element has been detailed by Bukata *et al* (1995). Consider an incident photon flux Φ_I travelling through a single element of water with a thickness Δx . This incoming flux will lose energy during its journey through the water element and is consequently reduced to a transmitted flux, Φ_T . The difference between Φ_I and Φ_T must be directly proportional to the product between Φ_I and Δx and can be presented as the following equation:

$$\Phi_T - \Phi_I = -\sigma\Phi_I\Delta x$$

that can be simplified as:

$$\Delta\Phi = -\sigma\Phi_I\Delta x$$

where the σ value seen in the equations is simply a constant of proportionality, which is most commonly called the absorption coefficient and is measured in units of either m^{-1} or cm^{-1} .

As the limits of both $\Delta\Phi$ and Δx approach zero a new expression emerges:

$$\frac{d\Phi}{\Phi} = -\sigma dx$$

which is the Beer – Lambert – Bouguer Law. This expression can be integrated from $x = 0$ to an arbitrary position x within the water element in order to obtain the exponential function (Bukata *et al*, 1995):

$$\Phi(x) = \Phi_0 e^{-\sigma x}$$

For these derivations it has been assumed that the σ value associated with the water body under analysis does not vary at all with any changes of the x variable. The Beer – Lambert – Bouger Law can be further defined in terms of radiant flux which is defined as the temporal flow of radiant energy through a medium, which is in this case a water body. This time considering an incident beam of radiant flux consisting of an unmeasurably large number of photons propagating through a water column, the loss of beam energy via absorption processes from an original subsurface radiant flux value of J_I to a final radiant flux value of J_T after moving over a distance Δx is calculated as:

$$J_T - J_I = -aJ_I \Delta x$$

or alternatively:

$$\Delta J = -aJ_I \Delta x$$

where a is defined as the absorption coefficient given in units of either m^{-1} or cm^{-1} .

After the limits of both ΔJ and Δx approach zero the following equation is obtained:

$$\frac{dJ}{J} = -a dx$$

After integrating the above equation from $x = 0$ to an arbitrary location x and factoring in the fact that the beam attenuation coefficient changes with wavelength λ this formula is given (Bukata *et al*, 1995):

$$J(x, \lambda) = J(0, \lambda) e^{-a(\lambda)x}$$

From this exponential function a solution for $a(\lambda)$ can be determined explicitly with the following partial differential equation (Bukata *et al*, 1995):

$$a(\lambda) = -\frac{1}{J(x, \lambda)} \frac{[\partial J(x, \lambda)]_{ABSORPTION}}{\partial x}$$

This equation is the general definition of the absorption coefficient $a(\lambda)$ which is defined as the fraction of radiant energy removed from a beam $[\partial J(x, \lambda)]_{ABSORPTION}$ as it propagates through a distance ∂x in a water body divided by ∂x .

The radiant flux travelling through a water body is also attenuated by scattering processes characteristic to the particular water type. The scattering coefficient $b(\lambda)$ is derived and defined in the same manner as the absorption coefficient $a(\lambda)$ and is calculated as such (Bukata *et al*, 1995):

$$b(\lambda) = -\frac{1}{J(x, \lambda)} \frac{[\partial J(x, \lambda)]_{SCATTERING}}{\partial x}$$

where as was the case with $a(\lambda)$, $b(\lambda)$ is measured in units of either m^{-1} or cm^{-1} .

In any natural body of water incoming radiant flux is both absorbed and scattered by waterborne constituents. So a parameter combining both the $a(\lambda)$ and $b(\lambda)$ characteristics of the water must be introduced. This parameter is known as the beam attenuation coefficient $c(\lambda)$ and it is defined as the measurement of the fractional amount of energy extracted from a beam of radiant flux by the amalgamation of the absorption and scattering processes over an infinitesimally small length within a given water body. The general equation describing the beam attenuation coefficient is presented as:

$$c(\lambda) = a(\lambda) + b(\lambda)$$

and by introducing the explicit solutions for $a(\lambda)$ and $b(\lambda)$ it becomes this expanded form (Bukata *et al*, 1995):

$$c(\lambda) = -\frac{1}{J(x, \lambda)} \left[\frac{[\partial J(x, \lambda)]_{ABSORPTION} + [\partial J(x, \lambda)]_{SCATTERING}}{\partial x} \right]$$

where $c(\lambda)$ is provided in units of m^{-1} or cm^{-1} .

Irradiance E is mathematically defined as the radiant flux per unit area dJ on a given infinitesimal surface area dA :

$$E = \frac{dJ}{dA}$$

where E is traditionally measured in W m^{-2} . By substituting this identity into the original equations given for radiant flux the subsequent formula appears after simplification (Bukata *et al*, 1995):

$$E(z, \lambda) = E(0, \lambda)e^{-K(z, \lambda)z}$$

where z is the depth below the water surface, $E(z, \lambda)$ is the spectral irradiance at depth z , $E(0, \lambda)$ is the spectral irradiance measured at a depth just below the water line and $K(z, \lambda)$ is a total attenuation coefficient. $K(z, \lambda)$ can be extracted from the formula for $E(z, \lambda)$ by using:

$$K(z, \lambda) = -\frac{1}{E(z, \lambda)} \frac{\partial E(z, \lambda)}{\partial z}$$

It is important to note that irradiance can be measured in two different parts as either a downwelling component E_d or an upwelling component E_u which are defined as the irradiance received at a surface from a beam of downwards travelling radiation or upwards travelling radiation respectively. The equation shown above used to determine the total $K(z, \lambda)$ can be rewritten in terms of the downwelling and upwelling components of irradiance, with the downwelling component provided as:

$$K_d(z, \lambda) = -\frac{1}{E_d(z, \lambda)} \frac{\partial E_d(z, \lambda)}{\partial z}$$

and for the upwelling component:

$$K_u(z, \lambda) = -\frac{1}{E_u(z, \lambda)} \frac{\partial E_u(z, \lambda)}{\partial z}$$

In the applicable sections of this research, only the K_d value has been evaluated as the downwelling irradiance was the only component of irradiance evaluated in all of the UV light measurements performed. In general, clear waters with minimal levels of turbidity caused by buoyant particulate materials, such as glacial streams, have smaller characteristic K_d values in comparison to turbid waters such as stagnant dams inhabited by various forms of animal and plant life where the K_d approximations can be increased by the existence of numerous forms of particulate and dissolved matter floating in the water, for example DOM or phytoplankton (Williamson, 2005).

The exponential formula describing the decay of irradiance with depth in water can be converted into the following logarithmic form:

$$\ln\left(\frac{E(z, \lambda)}{E(0, \lambda)}\right) = -K_d z$$

From this equation K_d can be found graphically by plotting $\ln\left(\frac{E(z, \lambda)}{E(0, \lambda)}\right)$ data obtained from a real – world aquatic environment using UV measurements against z and subsequently calculating the absolute of the gradient of the resulting straight line of best fit.

K_d values can also be determined for real world marine locales by using what is known as a Secchi disk. The Secchi disk was invented by an Italian scientist of the same name in order to make rapid estimations of the transparency of water to light. It works by simply attaching a white disk 20 cm in diameter to a long rope and lowering it until it can no longer be seen (Wetzel, 2001). The length of rope present underwater

at the time when the disk becomes invisible is referred to as the Secchi depth (z_s). With the Secchi depth a crude estimation of the K_d value of the water type under investigation can be found with:

$$K_d = \frac{f}{z_s}$$

where f is a dimensionless parameter characteristic to the particular water type. It has been estimated to be 1.7 in clear ocean or sea water and 1.4 in turbid coastal water (Tett, 2005). It is important to note that this equation assumes the K_d value for the water type under analysis remains constant with depth.

The difficulties of making spectral solar UV irradiance measurements in real – world underwater environments brought on as a result of cumbersome spectroradiometric measurement equipment, poor spectroradiometric response with changes in depth, unpredictable changes in water quality and transparency as a result of both natural and anthropogenic activity, shading caused by nearby plant life along with the presence of surface waves have made recording reliable K_d estimates an extremely taxing operation (Morrow & Booth, 1997). Additionally, Morrow and Booth (1997) have made the point that underwater UV measurements can also be complicated by the fact that the UV flux becomes a very small signal that has to be measured alongside the much more intensive visible waveband coupled with unpredictable features at the surface of the water including wave focusing effects like those reported by Deckert & Michael (2006) and also changes in water line elevation caused by evaporation and tidal changes.

Belmont *et al* (2007) has recently presented a laboratory and microcosm based technique aiming to remedy these problems. The methodology involved suspending

sediment concentrations obtained from creek and river sources and manipulating them inside a custom – built microcosm, which was then employed to find direct measurements of the K_d in combination with a standard light meter sampling five separate wavelengths throughout the UV waveband. Dissolved and particulate absorption measurements of samples taken from the different water types used in the microcosm tests were then used in the laboratory method by using a spectrophotometer in order to derive several optical parameters required for an approximation of another K_d value. These K_d estimates were then directly compared to *in situ* K_d estimations made at various points along the Lehigh River in eastern Pennsylvania. Comparisons between the K_d values obtained via the two methodologies and the field measurements showed promising levels of agreement.

After calculating the K_d for a particular water type using either a UV meter, the Secchi disc method or in a laboratory, a useful parameter known as the 1% attenuation depth can be determined as:

$$z_{1\%} = 4.605K_d$$

where $z_{1\%}$ is the depth at which 1% of the incident surface light penetrates through the water column (Bukata *et al*, 1995). When an approximation is made for $z_{1\%}$, only water types where the K_d value is known to be relatively constant over a large depth range can be analysed in order to minimise the uncertainties resulting from extrapolation into depths where attenuation properties become variable (Williamson, 2005). Interestingly, the $z_{1\%}$ for any water type can not be regarded as an annual constant value. One example study carried out by Kuwahara *et al* (2000) has shown that the $z_{1\%}$ for relatively optically clear coastal waters off the shores of Japan can

vary by as much as 5.7 m at a wavelength of 305 nm and 17.6 m at a wavelength of 380 nm over the space of a year.

3.2.3 Effect of Dissolved Organic Matter

Many investigations have found that the attenuation of solar UV in marine locations such as streams and lakes can be attributed to fluctuations in the concentration of DOM constituents in the water column (Rautio & Korhola, 2002; Rae *et al*, 2001; Conde *et al*, 2000; Laurion *et al*, 1997). DOM is extracted from decaying plant material, such as leaves, bark and twigs, located in and around water bodies. High amounts of DOM in a sample of water will make it look dark brown in colour. Commonly, stagnant water bodies located in heavily vegetated areas contain water rich in DOM content. Conversely, water bodies found in regions like tundra, where there is little vegetation, have water relatively low in DOM content. These low DOM water bodies tend to be more transparent to solar UV, and therefore provide less protection from UV radiation for any inhabitant life forms (Rae *et al*, 2001).

The interaction between the solar UV and DOM constituents in water bodies is not at all dissimilar to the interaction between solar UV and column ozone in the atmosphere, with short solar UV wavelengths being more vulnerable to absorption by DOM in the water column in comparison to the longer solar UV wavelengths (Xenopoulos *et al*, 2000). In waters with average amounts of DOM, it is common for UVB wavelengths to be blocked up to three times more than UVA wavelengths and ten times more than wavelengths in the visible spectrum (Brooks *et al*, 2005). In addition, the intensity of the solar UV attenuated by DOM in a given water sample is

dependent upon the DOM particle size distribution as well as the number of DOM particles present (Pan *et al*, 2008).

While DOM does provide a good shield against solar UV in marine environments, it is susceptible to varying degrees of photochemical degradation. This degradation can lead to changes in the optical properties of the DOM. This process is most commonly referred to as photobleaching (Morris & Hargreaves, 1997). Photobleaching has been studied experimentally, and it has been shown that it is the primary cause in the reduction of the UV absorption capability in DOM samples (Lindell *et al*, 1995). Photobleaching can also directly lead to the decay of DOM into its mineral constituents or indirectly by breaking the DOM down to such a low molecular weight that it can be consequently mineralized by microbes (Lindell *et al*, 1995). These two processes also contribute to the reduction of DOM attributed UV absorption.

The main component of DOM that is believed to be completely responsible for aquatic UV absorption is chromophoric (coloured) DOM, which is usually referred to as CDOM. Like regular DOM, CDOM occurs naturally from the microbial and enzymatic decomposition of organic matter from terrestrial sources into smaller molecules, such as humic and fulvic acids. These acids are generally very difficult to break down any further. The effect of CDOM on the underwater UV light regime and in turn the biologically effective UV exposure is known to be even more substantial than attenuation caused by atmospheric column ozone (Gibson *et al*, 2000).

The quantification of the loss of colour and in turn the decrease in UV absorbance efficiency for CDOM after an exposure to UV radiation is not a simple task. For every

single UV photon absorbed by a given sample of CDOM, colour loss is not only seen at the absorbed wavelength, but is also seen across the whole absorbance spectrum, which is a physical process most commonly called polychromatic photobleaching. The relationship between CDOM fading and photonic energy can be described to a certain extent using straightforward two – dimensional functions. Simplified spectral weighting functions for photobleaching previously developed by Tzortziou *et al* (2007) is proof of this. However, it is believed that highly complicated three – dimensional models are a necessity in order to completely evaluate the spectral responsivity of CDOM to UV induced colour fading (Bissett *et al*, 2001).

On the other hand, several investigations have successfully attempted to generate relatively simplistic analytical models relating DOM and CDOM composition to characteristic K_d values in different water types. Some of the earliest models were transcribed in investigations delivered by Smith and Baker (1981) and again by Baker and Smith (1982). In these two studies a simple model was developed and employed to calculate what was called the spectral diffuse attenuation coefficient K_T , an optical parameter equivalent to the K_d value for natural waters as follows:

$$K_T(\lambda) = K_w(\lambda) + K_C(\lambda) + K_{DOM}(\lambda)$$

where $K_w(\lambda)$ is a clear water attenuation coefficient obtained from field measurements, K_C represents an optical measure of the chlorophyll component of the water body under analysis and its effect on propagating waterborne UV and K_{DOM} describes the UV attenuation caused completely by CDOM. From this model K_{DOM} could be calculated directly using this exponential expression:

$$K_{DOM}(\lambda) = K_{DOM}^A(\lambda^A)De^{-K_{DOM}^B(\lambda-\lambda^A)}$$

with $K_{DOM}^A(\lambda^A)$ provided as $0.565 \text{ m}^{-1} (\text{mg DOM litre}^{-1})^{-1}$ and K_{DOM}^B given as 0.014 nm^{-1} as estimated in an earlier campaign completed by Hojerslev (1980), D is a DOM concentration coefficient measured in units of mg DOM litre^{-1} and λ^A is a reference wavelength at 380 nm. The chlorophyll component K_C was estimated in a similar manner to K_{DOM} as such:

$$K_C(\lambda) = K_C^A(\lambda)C_K e^{-K_C^B(\lambda)^2(\log C_K - \log C_0)^2} + 0.001C_K^2$$

having $K_C^A(\lambda)$ and $K_C^B(\lambda)$ presented in lookup tables in units of $\text{m}^{-1} (\text{mg Chlorophyll litre}^{-3})^{-1}$ and C_0 given as a chlorophyll concentration coefficient set to 0.50 in units of $\text{mg Chlorophyll litre}^{-3}$. The C_K variable could be approximated by finding the average chlorophyll concentration in the given water column:

$$C_K = \frac{1}{K_{PAR}} \int_0^{K_{PAR}^{-1}} C(z) dz$$

in which K_{PAR}^{-1} is one attenuation length for photosynthetically active solar radiation, K_{PAR} is the total attenuation coefficient for photosynthetically active solar radiation measured with an optical meter with an appropriate response and $C(z)$ is the chlorophyll concentration in $\text{mg Chlorophyll litre}^{-3}$ at depth z in metres. This chlorophyll concentration has been measured in numerous studies by using fluorometrical techniques after extraction in 90% acetone (Baker & Smith, 1982).

Apart from Smith and Baker (1981) and Baker and Smith (1982), another notable investigative example analysing the correlation between K_d and CDOM has been presented by Laurion *et al* (1997) who gave an equation specifically for sub – arctic lakes in the forest – tundra region of northern Quebec linking fluorometrically measured CDOM (F_{CDOM}) and the K_d value estimated for the lake water at a wavelength of 380 nm ($K_{d(\lambda=380)}$), shown here as simplified by Gibson *et al* (2000):

$$K_{d(\lambda=380)} = 10^{1.153+0.973\log F_{CDOM}}$$

For wavelengths other than 380 nm Laurion *et al* (1997) also provided another formula as follows as derived by Gibson *et al* (2000):

$$K_{d\lambda} = 10^{1.153+0.973\log F_{CDOM}} e^{-s(\lambda-380)}$$

where S is calculated as the gradient of a log – linear plot between water absorbance against wavelength.

Another series of equations exploring the relationship between DOC (dissolved organic carbon, the carbon only component of DOM) and K_d values for Arctic and Antarctic freshwater locales specifically for wavelengths of 305 nm, 320 nm, 340 nm and 380 nm were formulated by Vincent *et al* (1998) and presented by Gibson *et al* (2000):

$$K_{d(\lambda=305)} = 10^{-0.12+1.68\log[DOC]}$$

$$K_{d(\lambda=320)} = 10^{-0.42+1.98\log[DOC]}$$

$$K_{d(\lambda=340)} = 10^{-0.58+2.04\log[DOC]}$$

$$K_{d(\lambda=380)} = 10^{-0.75+1.91\log[DOC]}$$

where $[DOC]$ is the concentration of DOC in units of g DOC m⁻³. By plotting the outcomes from these equations on a log – linear graph, K_d approximations for all other UV wavelengths can be found. However, the accuracy that these equations hold is limited by the fact that they assume that the optical parameters associated with all types of DOM is very similar in all marine environments, which is not the case in the real world.

Willamson *et al* (1996) and Williamson (1996) have plotted the relationship between $z_{1\%}$ values and DOC concentrations for a sizeable number of lakes across North America. Over the research campaign, a pronounced hyperbolic relationship was found to exist between the two parameters with an extremely rapid decrease in attenuation depth occurring in correspondence to DOC concentrations of beyond 2 mg litre⁻¹ for both solar UVA and UVB wavelengths. The authors suggest from this outcome that even the smallest decreases in DOC concentration could lead to substantial increases in the $z_{1\%}$ for solar UV, and hence extend the effective region in which aquatic life forms could sustain damage.

3.3 Influence of Solar UV on the Aquatic Ecosystem

Some studies have sought to ascertain a general idea of how biologically weighted UVB radiation is distributed with depth to give a general prediction on how solar UVB could affect certain aquatic organisms. The most commonly employed action spectrum in these investigations is the DNA damaging action spectrum as initially presented by Setlow (1974). One such study looking at the basic depth distribution for DNA damaging UV was executed by Dunne and Brown (1996) in which DNA damaging irradiances were measured at different depths at an atoll, an inshore reef and a coastal island within the Indian Ocean and the Andaman Sea using a spectroradiometer. It was discovered that the measured UVB irradiance when weighted against the DNA damage action spectrum showed increased levels of attenuation with $z_{1\%}$ values calculated as 9 metres for the ocean atoll, 2.6 metres for the inshore reef and 4.7 metres for the coastal island compared to $z_{1\%}$ values estimated for the unweighted UVB irradiance measurements of 11 metres for the ocean atoll, 3 metres for the inshore reef and 6 metres for the coastal island.

Most studies have taken a different approach to the study by Dunne and Brown (1996) in measuring and quantifying the actual damage caused by biologically effective UVB radiation to marine life forms by using various types of biological sampling procedures performed either in the field or in the laboratory in combination with the measurement of UV radiation by the usual systems such as radiometers, spectrometers and spectroradiometers. These kinds of investigations are now more important than ever with current global warming conditions modulating an increased level of stratification in natural waters leading to conditions in which UVB can penetrate to deeper depths and thus cause more biological harm (Siegel & Michaels, 1996). Sections 3.3.1 to 3.3.5 will provide a brief review on these kinds of investigations over recent years made for various varieties of plankton, cyanobacteria, seagrasses, macroalgae, coral communities and also larger scale organisms like fish respectively.

3.3.1 Plankton Varieties

Life forms that live in either fresh water locales or in the sea can be divided into three distinct classifications, which are the bottom – dwellers (benthos), the drifters (plankton) or the swimmers (nekton). Plankton is then further divided into two more groups that are known as animal plankton (zooplankton) or plant plankton (phytoplankton). Within the zooplankton group a further sub – species exists called ichthyoplankton which encompasses fish and amphibian eggs and larvae. All types of phytoplankton depend upon sunlight as their primary energy source, which means that they must reside in a region no deeper than 100 metres below the water surface. This particular region where large enough amounts of sunlight penetrate to sustain life is called the euphotic zone. Zooplankton depends almost entirely on phytoplankton as a

food source, so as a consequence of this they also exclusively inhabit the euphotic zone (Diffey, 1991).

Phytoplankton play an extremely important role in the Earth's ecosystem. Phytoplankton have evolved over time to use the green and blue wavelengths available in the ocean. From this, aquatic photosynthesis performed by phytoplankton generates approximately half of the oxygen available in our air supply. Additionally, phytoplankton also play a significant role in the regulation of the Earth's climate. On a day to day basis, phytoplankton removes massive amounts of carbon dioxide from the atmosphere by converting it into organic matter through photosynthesis. A great deal of this organic carbon is consumed by other animals living in the euphotic regions of the ocean. The organic carbon that is not eaten usually falls to the ocean floor where it is gradually converted into natural oil and gas deposits in a process taking thousands of years to complete (Johnsen & Sosik, 2004).

More specifically, it has been predicted by Hader and Worrest (1997) that any major loss in primary biomass productivity due to increasing UVB will have staggering consequences for the life cycle in the marine ecosystem and will lead to a decrease in food productivity and quality for humans. Furthermore, again in the findings of Hader and Worrest (1997) it was estimated that a 16% reduction in atmospheric column ozone would lead to a 5% decrease in total phytoplankton productivity causing a drop in total worldwide aquaculture yield of 7 million tonnes of fish per annum.

Banaszak and Neale (2001) have completed a study showing that natural phytoplankton assemblages living within a shallow estuary of the Chesapeake Bay region along the east coast of the United States were extremely sensitive to solar UV,

most specifically wavelengths from the UVB waveband. It was concluded that the high levels of volatility seen in healthiness of the phytoplankton assemblages could be most directly related to short – term fluctuations in the optical parameters and in turn chemical composition in the estuary itself.

Conde *et al* (2002) has followed the work of Banaszak & Neale (2001) by analysing the influence of solar UVB and also UVA on phytoplankton photosynthesis in the Laguna de Rocha, a shallow coastal lagoon located on the south – eastern coast of South America in direct contact with the Atlantic Ocean. Results showed that on average that near – surface primary production rates were decreased by a substantial margin, with UVA causing on average twice as much inhibition as UVB. Alongside this discovery, it was also found that compositional changes brought upon by river discharge and periodical exchange with the Atlantic Ocean seemed to be a more important factor in the modulation of the UV underwater climate and hence phytoplankton primary production rates than increases in incident UVB irradiance brought on as a result of diminishing amounts of atmospheric column ozone.

Recently several studies have started to detail the effect of a process known as mixing upon phytoplankton photosynthesis. Mixing is a physical underwater process that can directly change the damaging influence produced exclusively by UV, as phytoplanktonic cells are moved up and down within a water column and are exposed to varying amounts of irradiance ranging from relatively high irradiances near the water surface to lower irradiance values at the bottom of the mixing layer (Helbling *et al*, 2003).

Further investigations delivered by Helbling *et al* (1994) and Neale *et al* (1998) have shown that shallow depth mixing can profoundly increase UV related phytoplankton photosynthesis inhibition as compared to samples measured within deep mixing regions. Neale *et al* (1998) also predicted that the effect of mixing could deliver an even more pronounced negative impact upon phytoplankton communities in comparison to fluctuations in atmospheric column ozone levels. In addition, Barbieri *et al* (2002) described how the influence of UV could change from negative to positive according to the region and amount of the euphotic zone undergoing the mixing process. These authors simulated mixing over 90% of the euphotic zone and observed a net enhancement of integrated primary productivity.

Excessive UV exposure also poses a significant threat to the propagation of zooplankton. The use of transparency as a vital camouflage technique for zooplankton can be negated with the adaptive development of UV sensitive protective pigments that are not transparent to UV wavelengths and hence may reveal zooplankton to both predators and also prey equipped with UV vision (Johnsen & Widder, 2001).

Planktonic bacteria play an important role within aquatic ecosystems by cycling elements like nitrogen and carbon along with other essential nutrients (Karl *et al*, 1997; Fenchel *et al*, 1998). The estimated productivity rates for bacterioplankton have been found to vary between 14% and to as much as 76% of the total primary productivity within a given ecosystem depending upon the location and the time of year (Jeffery *et al*, 1996).

Bacterioplankton lack any form of pigmentation to defend it against UV exposure, unlike some phytoplankton that can produce their own protective UV absorbing amino acid based compounds (Herndl, 1997; Karentz *et al*, 1994). It has also been discovered that bacterioplankton may be too small to develop the pigments that are necessary to protect the organism against biologically damaging UV (Garcia – Pichel, 1994). From this it has been suggested that bacterioplankton are potentially more susceptible to UV induced DNA damage in comparison to phytoplankton and other larger aquatic organisms (Herndl, 1997).

An investigation made by Huot *et al* (2000) used a combination of mathematical models along with field measurements carried out offshore at the Gulf of Mexico and in the Gerlache Strait near Antarctica in order to directly quantify the effect of UV radiation upon the DNA structure of bacterioplankton along with the effect of water column mixing. Mixed layer depth coupled with atmospheric column ozone thickness were evaluated as being the two most influential variables related to total DNA damage in a given water body. The models in good agreement with the measurements estimated that the total amplification factor (a parameter usually referred to as the TAF which gives a relative measurement of changes in levels of biologically effective UV associated with variations in the total amount of column ozone thickness) specifically for DNA damage to bacterioplankton in the euphotic zone was 1.7 in contrast to approximately 2.2 at the water surface.

3.3. 2 Cyanobacteria

Cyanobacteria are important constituents of marine ecosystems as they deliver a sizeable percentage of primary productivity in a wide variety of aquatic locations

ranging from hot springs to Arctic and Antarctic water bodies (Hader *et al*, 2003). One example of how cyanobacteria play an important role in the global ecosystem is its nitrogen – fixing capability which helps to aid in the improvement of soil fertility, such as the soil in rice paddy fields as reported by Vaishampayan *et al* (2002).

Roos and Vincent (1998) have found that growth rates for cyanobacteria sourced from a pond on the McMurdo ice shelf in Antarctica were inhibited by accumulated UVB exposure. More specifically other researchers including Newton *et al* (1979), Tyagi *et al* (1992), Vincent and Roy (1993), Sinha *et al* (1995), Sinha *et al* (1996), Sinha *et al* (1997), Sinha and Hader (1997) and Sinha *et al* (2002) have shown experimentally that UVB can have a direct influence upon important proteins and the permeability of the cellular membrane structure, which once compromised can lead to death.

3.3.3 Seagrass and Macroalgae

Macroalgae, more commonly known as seaweed, and macrophytes, commonly known as seagrasses play a highly critical part in marine ecological systems, in both inter – tidal and sub – tidal regions. Their leaves provide a support network for an extensive variety of marine organisms by providing a food source, a shelter that can be used for protection against rough mixing conditions, undercurrents and camouflage from predatory animals. Macroalgae is also used as a natural nursery for the young of several marine species (Roleda *et al*, 2007).

Some macroalgae have adapted to live in the region just above the water line which is only affected by high tides or spray water. Their positioning means that they are under constant solar exposure throughout the day as well as highly variable amounts of

salinity alongside drastic changes in temperature. However, the majority of the macroalgae population exist in either the eulittoral (intertidal) or the sublittoral (far offshore) zone. These macroalgae are far better protected against solar UVB radiation in comparison to their counterparts on the water surface. The downside to this is that if the natural ratio between UVB and photosynthetic radiation undergoes an increase brought on by a fluctuating environmental parameter such as atmospheric column ozone, these macroalgae may become exposed to UVB wavelengths for which they have no innate protective mechanism (Hader & Worrest, 1997).

3.3.4 Coral Communities

Corals obtain their necessary nutrients from the ocean via two different mechanisms, the first being the capture of plankton using small tentacles existent on their outer tissue. The second mechanism utilises microscopic single cell algae known as zooxanthellae that live within coral tissue itself. Zooxanthellae share a symbiotic relationship with coral by primarily providing carbon as an energy source and improving calcification within the coral structure in exchange for protective shelter and a source of carbon dioxide to aid with photosynthetic processes. Zooxanthellae are also responsible for providing the coral with their colour (Buchheim, 1998).

Coral bleaching and mortality, is thought to be directly related to the decrease of available zooxanthellae communities caused by a number of different factors including increases in oceanic temperatures as a result of global warming and increases in solar light levels brought on by a reduction in atmospheric column ozone (Birkeland, 1997). Numerous investigations and theses over the last thirty years such as Jokiel (1980), Harriott (1985), Siebeck (1988), Lesser *et al* (1990), Gleason and

Wellington (1993), Warner *et al* (1996), Schick *et al* (1996), and Brown *et al* (2000) have highlighted how solar UV possibly has a detrimental effect on coral health and their appearance.

Despite the compelling evidence provided by these investigations, several counter studies have given results that have hinted at the fact that mass bleaching events may not have any exact correlation with high levels of underwater UV intensity (Hoegh – Guldberg, 1999). It is now thought that coral bleaching is only caused by high water temperatures with increases in solar UV playing either a very small but still important role in the process (Lesser, 1996) or absolutely no role whatsoever (D’Croz *et al*, 2001). Nevertheless, at this point in time no action spectrum and hence no definitive measure have been derived unequivocally linking the response effect of UV, visible and infrared wavelengths to zooxanthellae mortality and in turn coral damage and bleaching.

3.3.5 Large Scale Organisms

One prime example of the negative impact that solar UV can have upon a large scale marine species occurs with the amphibians in the *Bufo* genus, known most commonly as toads. Solar UV has been found to inhibit the development of the toad’s embryos, which makes them far more susceptible to an aggressive fungal disease known as *Saprolegnia ferax*, which is a worldwide amphibian killer. In water bodies less than 50 cm deep, up to 12% of a given tadpole cluster will die from the fungus, while in water bodies less than 20 cm deep, with more solar UV reaching the tadpoles, as much as 80% of a cluster will be killed (Flannery, 2005; Pounds, 2001). Blaustein and Kiesecker (1997) have also found that embryo hatching rate of the mountain –

dwelling Cascades frog can decrease after being irradiated by solar UVB radiation over an extended amount of time.

A study delivered by Lesser *et al* (2004) has found that shortwave UVB can effectively penetrate through the Austral spring annual ice of McMurdo ice shelf and cause damage to the embryonic DNA of the sea urchin species *Sterechinus neumayeri*. In this research it was discovered that the rate of DNA damage and mortality was depth dependent, with higher levels of DNA damage and mortality measured at 1 metre below the ice surface compared to levels recorded at 3 metres deep and 5 metres deep. Interestingly, more DNA damage was estimated to take place over 2003 compared to 2002 when a thicker ice shelf was existent. However, smaller amounts of atmospheric column ozone were in effect at the measurement site during 2002 due to an increase in the size of the Antarctic ozone hole.

Investigations performed by Kouwenberg *et al* (1999a) have detailed how Atlantic cod egg mortality can be directly affected by UVB irradiance by illuminating several samples with two filtered xenon light sources in a laboratory environment. After making calculations based upon a cod egg mortality biological weighting function, it was discovered that under regular noon surface UVB irradiance as calculated for the research site at the Gulf of St. Lawrence, Canada, approximately 50% of all Atlantic cod eggs found near the ocean surface would be killed off after a total dose of only 42 hours. Simulating a 20% decrease in atmospheric column ozone, the time required for 50% mortality time decreased by 10 hours.

A second study was performed by Kouwenberg *et al* (1999b) using similar techniques as in the first study, this time showing how mortality rates for *Calanus finmarchicus* (Copepoda) eggs were exclusively modulated by UVB. The results that were discovered were even more drastic than in the original study with the Atlantic cod eggs. Calculations based again from a modified biological weighting function showed that, under expected levels of noon surface UVB irradiance, 50% of all Copepoda eggs found within a close vicinity to the oceanic water line would die following an exposure of only 2.5 hours. Again, with a 20% decrease in ozone layer thickness that predicted extermination time decreased to only 2.2 hours. In the two studies, UVA irradiance was found to not have any effect on the Atlantic cod eggs or on the Copepoda eggs in any way.

Experiments using either natural solar UV or artificial UV have provided conclusive evidence that both the embryos and larvae of numerous species of fish are highly susceptible to internal damage caused by incident UV. Initial research performed by Bell and Hoar (1950) using artificial UVB radiation detailed how increasing mortality in sockeye salmon eggs coincided with increasing amounts of exposure. Another investigation delivered by Hunter *et al* (1979) demonstrated that the survival of the eggs and larvae of both anchovy and mackerel were both dependent on solar UV levels and that the damage caused to the two different egg species could be linked to the DNA damaging dose derived from the DNA damaging action spectrum calculated by Setlow (Zagarese & Williamson, 2001).

3.4 Chapter Discussion

Despite the fact that the selected example studies described in this chapter have only briefly summarised some of the investigations performed in recent history, it can clearly be seen that there is certainly no doubt that the solar UV, most specifically the solar UVB, in synergy with declining atmospheric column ozone levels and possible global warming, does inflict a sizeable amount of damage and distress upon aquatic organisms across the entirety of the food chain that not only results either directly or indirectly in the death of different life forms yearly but also contributes to significant financial loss for people involved in the primary industries, such as fishers and farmers. There is a necessity to further this previous research by monitoring the solar UV received within water bodies and by aquatic species using new and simpler measurement methods and equipment so that UV data can be gathered over increased periods of time and in a wider amount of underwater environments with less effort required by the researcher. This is where the PPO dosimeter can come into play with long term underwater UV measurements in order to better understand the underwater UV. The following chapter will begin to discuss the process of calibrating the PPO dosimeter for underwater use by detailing the necessary equipment along with the measurement and calibration techniques required for reliable underwater dosimetric measurements.

Chapter 4

Calibration and Measurement of Solar UV Radiation Underwater with Optical Instrumentation and Dosimeters

4.1 Introduction

As was mentioned in Section 3.2.2, the measurement of solar UV on the surface of the Earth is not a simple process. Instruments such as spectroradiometers, spectrometers and radiometers must be adequately calibrated to appropriate standards, maintained fastidiously and employed correctly within their operational limitations in order to obtain accurate data that is of the quality necessary for scientific research. Other factors such as atmospheric parameters like column ozone, trace gases and aerosols and their influence upon instrument response must also be taken into account during measurements or else critical errors may become apparent in the measured data. These issues are also in effect with solar UV measurements made underwater, except that in the underwater environment the difficulty of obtaining useable data becomes greatly amplified due to the optically complex and at times unpredictable nature of water itself. The instrumentation employed to take the solar UV measurements must not only be calibrated to proper standards and prepared for changes in the dynamic atmosphere, but they also must be completely sealed and waterproofed in readiness for the harsh surrounds of the underwater environment and also corrected for the optical phenomenon known as the immersion effect.

The following chapter details a brief history of underwater solar UV measurements made using various forms of electronic optical instrumentation. In addition, a summary of the usage of various biological and chemical dosimeters that have been deployed as both an alternative and complementary method for the measurement of solar UV in aquatic locations over the last few decades will be provided. Following this, specifications, operating procedures, calibration techniques and immersion factor corrections relating to the spectroradiometer, spectrometer and radiometer systems

employed throughout this research are presented. It was of utmost importance that each instrument was suitably calibrated and corrected as the accuracy and validity of the calibrations and measurements made with the PPO dosimeter to be given in Chapters 5, 6, 7 and 8 were inextricably linked to the solar UV data obtained by the spectroradiometer, spectrometer and radiometer.

4.2 Underwater Solar UV Radiation Measurement

4.2.1 Spectral and Broadband Measurements

Several studies over the last few decades have analysed the behaviour of both the spectral and broadband solar UV underwater using radiometers, spectroradiometers and spectrometers with varying degrees of success. Radiometers measure underwater radiation by absorbing radiation with an internal bolometer. The temperature of the bolometer increases following radiation absorption. This temperature increase is measured and converted into a meaningful expression for radiation. Spectroradiometers work by collecting incoming underwater radiation over a certain field of view using an entrance optics detector (such as a diffuser). This radiation is split into its constituent wavelengths via a monochromator driven by a computer-controlled stepper motor. The measurement of radiation intensity per wavelength increment is done by means of a photomultiplier tube. Commonly, a computer system is used as a data acquisition unit. Spectrometers acquire underwater radiation by means of a diffuser. The radiation is then sent via a fibre optic to a CCD array detector and is filtered and converted into a spectrum for display on a computer screen.

One recent notable underwater radiation investigation was made by Frost *et al* (2005) where spectral data was obtained over a range of different depths in order to calculate K_d values in the UV waveband for a variety of different streams, each with their own particular DOM levels. Some other notable similar investigations detailing underwater solar UV irradiance and exposure and its relationship with DOM and other marine constituents have been delivered by: Conde, Aubriot and Sommaruga (2000) in lagoon waters within the Southern Atlantic Ocean; Crump *et al* (1999) in shallow pond water; Vincent *et al* (1998) in Antarctic ice covered lakes; and Sommaruga and Psenner (1997) in a high altitude mountain lake in Austria.

There have been several more examples of underwater UV measurement work using spectroradiometers or radiometers in numerous types of water bodies located across the world since the turn of the century. Bracchini *et al* (2004) have analysed solar visible and UV radiation distributions in shallow lake water. Hanelt *et al* (2001) used a spectroradiometer system with a custom diffuser housing to measure UVB radiation distributions in an arctic fjord. Dring *et al* (2001) used an underwater light sensor to make daily UV measurements in the Helgoland region of the North Sea over a time period of six years. Frenette *et al* (2003) measured the depth profiles of both UV and photosynthetically active radiation (PAR) in Lake Saint Pierre, Quebec with a spectroradiometer. Reinhart *et al* (2005) also employed a spectroradiometer to measure both spectral UV and PAR at set depth increments in order to estimate various optical properties of Lake Verevi, Estonia. Also, again with the use of a spectroradiometer, Schubert *et al* (2001) investigated variations in UV and PAR spectral irradiance levels in a shallow estuary on the southern coastline of the Baltic Sea.

All of these measurement campaigns have been limited by the fact that the electronic measurement equipment used would have required some kind of a constant power supply, most probably a battery in most instances, a human controller and regular calibrations in order to keep the equipment operating correctly. Also, due to the high cost of spectroradiometric, radiometric and spectrometric equipment, usually in these kinds of investigations only one unit can be employed during a series of measurements. This greatly reduces the amount of measurement data available for analysis and also does not allow for precise same – time comparisons to be made with the data, for example comparisons between measurements made at different angles and at different depths.

4.2.2 Biological and Chemical Dosimeters

The problems associated with making underwater UV measurements with optical instrumentation can be alleviated with the use of a UV dosimeter prepared for use underwater. This is due to the fact that many dosimeters can be deployed at different angles and depths at the same time at a cost far less than that of a conventional spectroradiometer, radiometer or spectrometer, no human operator is required apart from their initial calibration, setting – up and collection and they require no external power source to work.

Dosimeters based on biological constituents sensitive to UV wavelengths have been used for in – air and underwater measurements by researchers in the past. A summary of all the biological dosimetry investigations performed up until the late 1990's has been presented by Horneck (1997). Since then there have been several more studies carried out with biological dosimeters in aquatic locations. Boelen *et al* (1999) has

delivered one of the most extensive underwater biological dosimeter investigations to date. Using DNA dosimeters fabricated out of calf thymus DNA, the authors developed distributions of DNA damaging UV irradiance as a function of depth. Other notable examinations have been carried out by Koussoulaki *et al* (1998) using *Euglena gracilis* cultures and Li *et al* (2002) by calibrating tobacco cells against UVB DNA damaging effects. These studies have all shown good results, however the time and skill necessary to make biologically active dosimeters appear to far outweigh their capabilities.

A multitude of different types of chemical dosimeters have been previously used for in – air solar UV measurements (Parisi, Sabburg & Kimlin, 2004). However, only two chemical dosimeter types have been deployed in the underwater environment. The first and most commonly used has been polysulphone. Dunne (1999) evaluated UVB radiation with polysulphone dosimeters in a variety of different types of seawater at tropical latitudes. The author found that polysulphone had a practical depth range of between 2.2 and 7.0 m, dependent upon seawater turbidity with a 5% error margin. However, exposures of between 1.5 to 40.0 kJ m⁻² could only be measured. Polysulphone was also successfully employed by Frost *et al* (2006) to estimate K_d values in shaded water bodies in the North-east region of the United States. The only other type of chemical dosimeter used for underwater UV measurements has been the o – nitrobenzaldehyde dosimeter, which was used in one study carried out by Fleischmann (1989) at Discovery Bay in Jamaica. This research measured UV exposures with the o – nitrobenzaldehyde dosimeter to calculate the typical depth distribution and variation of solar UV throughout a single day. However, this dosimeter could only measure UV exposures over the period of a single day.

However, despite their usefulness, it is important to note that dosimetric measurements are not a complete replacement for underwater solar UV measurements made with electronic optical instrumentation. Spectroradiometers, spectrometers and radiometers are still the most effective way of recording short term changes in underwater UV irradiance levels, such as those brought on by rapidly evolving atmospheric systems, such as cloud cover.

Additionally, even though UV dosimeters can be used in the field independently, they are still required to be calibrated to the underwater solar UV spectrum via the utilisation of standardised optical instrumentation before application in marine environments. The PPO dosimeter investigated in this research was calibrated using an IL1400 broadband meter in collaboration with a calibrated and immersion effect corrected mobile scanning spectroradiometer over the initial development phase and an EPP2000 spectrometer during the field calibration phase. For long – term in – air calibrations of the PPO dosimeter a stationary Bentham spectroradiometer was used in conjunction with a continuously operating Solar Light UV broadband meter. The following sections of this chapter will detail the operational specifications of these particular instruments and will discuss how they were employed, calibrated and corrected for the immersion effect when necessary.

4.3 Optical Instrumentation Employed for this Research

4.3.1 IL1400 Broadband Meter

The primary UV radiation measurement instrument employed throughout Chapter 5 and Chapter 7 was the IL1400 broadband meter ('A' Series, International Light,

Newburyport, MA). The reason behind this was that the IL1400 has the capability to integrate UVB exposures over time that was necessary to allow calibration of the PPO dosimeter over extended time periods. This integrating capability was something that the mobile scanning spectroradiometer and the EPP2000 spectrometer could not do. Also, the IL1400 had superior power economy when compared to the mobile scanning spectroradiometer and the EPP2000 spectrometer, only requiring four AA sized batteries to operate consistently over 35 hours working time.

Before measurements began, the meter was fitted with a waterproof detector (SUD240, International Light) with a working spectral response in the UV running from 265 nm to 332 nm (International Light, 2009). This detector was combined with a UVB filter (UVB1 phototherapy filter, International Light Inc.). In this configuration the IL1400 broadband meter gives a response only to UVB wavelengths. Figure 4.1 displays the IL1400 broadband UVB meter with the underwater capable detector and Figure 4.2 shows a graph of the total UV, visible and infrared transmittance of the UVB1 filter from 200 nm through to 1000 nm as measured by International Light. International Light (1998) states that the IL1400 has 0.2% linearity and has a level of repeatability no greater than $\pm 3\%$ when compared to the National Institute of Standards and Technology (NIST) transfer standards.



Figure 4.1: The International Light IL1400 broadband UVB meter with the waterproof detector.

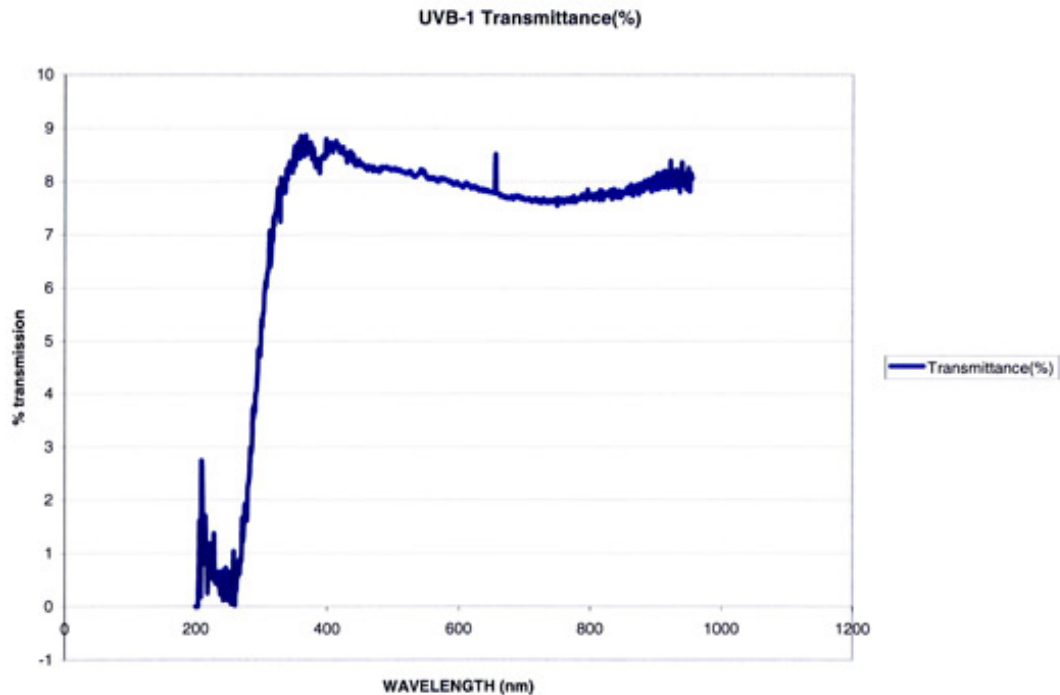


Figure 4.2: The total UV, visible and infrared transmittance of the UVB1 filter.

(Source: <http://www.intl-lighttech.com/products/filters/img/uvb-1.jpg>).

4.3.2 Mobile Scanning Spectroradiometer

A mobile scanning spectroradiometer was employed during the initial development phase (Chapter 5) of the PPO dosimeter to calibrate the IL1400 for use underwater in an indoors water tank against an artificial UV source. For this the spectroradiometer collected incoming radiation using a diffuser input optic (type D6, Bentham Instruments, Reading, UK) with a range from 200 to 800 nm with wavelength dispersal provided by a double holographic grating monochromator (model DH10, Jobin Yvon, France) ruled at $1200 \text{ lines mm}^{-1}$. The diffuser and monochromator were connected via a 2 – metre fibre optic link. Signal detection was performed by a photomultiplier tube (model R212, Hamamatsu Co., Japan) that was kept at a temperature of $15.0 \pm 0.5 \text{ }^\circ\text{C}$ by a programmed Peltier cell controller. Figure 4.3 shows a picture of the mobile scanning spectroradiometer configuration.

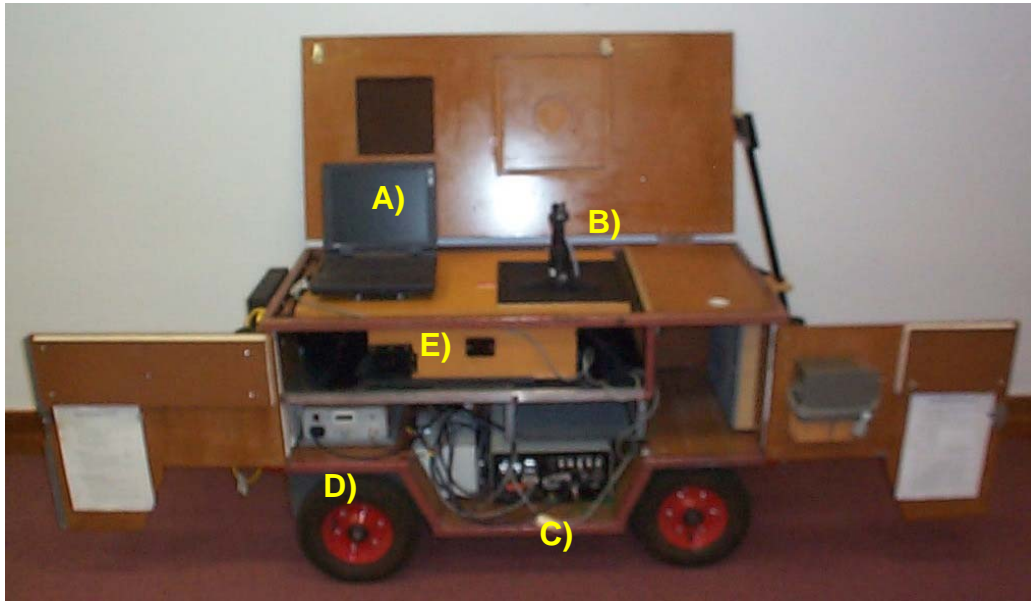


Figure 4.3: The mobile scanning spectroradiometer where A) is the computer which acts as the measurement control unit and data logger by means of specialist software, B) is the diffuser connected to the fibre optic link, C) is the system controller which sends messages to the spectroradiometer from the computer and vice versa, D) is the Peltier temperature control unit and E) is the housing that contains the monochromator.

Before the commencement of any recording session, the spectroradiometer was wavelength calibrated against the mercury UV spectral lines within a waveband running from 350 nm to 410 nm and absolute irradiance calibrated against a 250 W secondary standard quartz tungsten halogen lamp (SSL) maintained at a current of 9.500 ± 0.005 A d.c. The mercury calibration lines in the 350 nm to 410 nm waveband were chosen as they are the most intense and hence the easiest to detect. The SSL current supply was provided by a regulated power supply (Model PD36 20AD, Kenwood) that was monitored by a calibrated multimeter (MX 56 Metrix). The SSL had its calibration regime traceable to a primary standard located at the CSIRO National Standards Laboratory, Lindfield. This primary standard has a

predicted uncertainty level of $\pm 3.0\%$ at 240 nm that decreases in a linear fashion with increasing wavelength to $\pm 2.0\%$ at 350 nm and then decreases further with increasing wavelength to $\pm 1.1\%$ at 550 nm (CSIRO, 1997). An uncertainty of $\pm 3.0\%$ is also introduced during the calibration transfer from the primary to secondary standard (CSIRO, 1997). Additionally, fluctuations seen in the spectral irradiance measured by the spectroradiometer have been computed to be in the order of approximately $\pm 5\%$ (Wong *et al*, 1995).

For the absolute irradiance calibration sessions with the spectroradiometer, the SSL was supported within a closed box above the diffuser. This box was designed in order to minimise the interference of stray light and to also keep the SSL at an appropriate working temperature via an externally operated cooling device (an air blower). The responsivity of the spectroradiometer was measured by running a scan on the SSL at the necessary current, voltage and lamp to aperture distance to sustain a high level of repeatability. Following the irradiance calibration, three dark count (DK) scans were performed where DK is defined as the measurement of stochastic electronic noise present within the spectroradiometer system. The diffuser was covered up for each DK scan so that absolutely no radiation could enter it.

After the completion of the SSL and DK scans, the spectral responsivity of the spectroradiometer could then be calculated in a spreadsheet with the equation (Parisi *et al*, 2004):

$$R(\lambda) = \frac{SS(\lambda)}{CSS(\lambda) - DK}$$

where $SS(\lambda)$ is the spectral irradiance of the SSL in units of $\text{W m}^{-2} \text{nm}^{-1}$, $CSS(\lambda)$ is the counts of the SSL measured by the spectroradiometer at wavelength increments of 1 nm and DK is the averaged electronic noise signal over the chosen waveband. Figures 4.4, 4.5 and 4.6 respectively display the spectral irradiance of the SSL across the UV waveband as provided by the CSIRO National Standards Laboratory ($SS(\lambda)$), a spectral counts scan of the SSL as measured by the spectroradiometer ($CSS(\lambda)$), and an example spectral responsivity distribution ($R(\lambda)$).

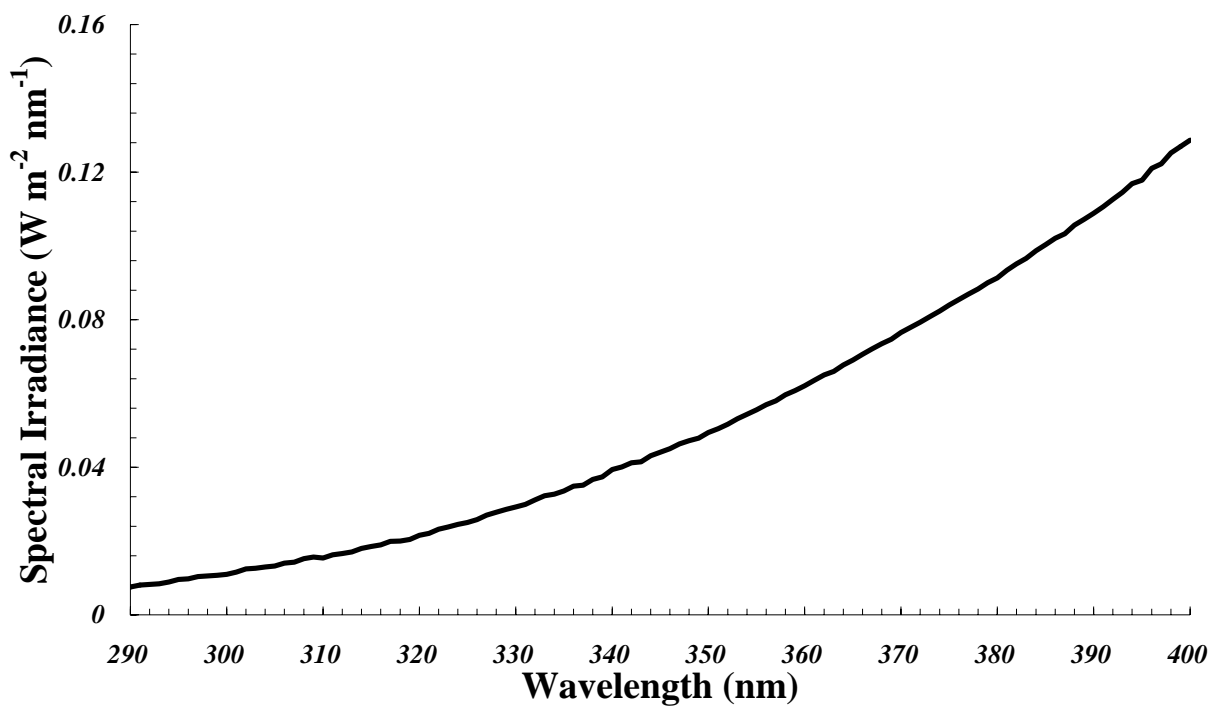


Figure 4.4: The spectral irradiance of the SSL originally obtained by the CSIRO National Standards Laboratory ($SS(\lambda)$).

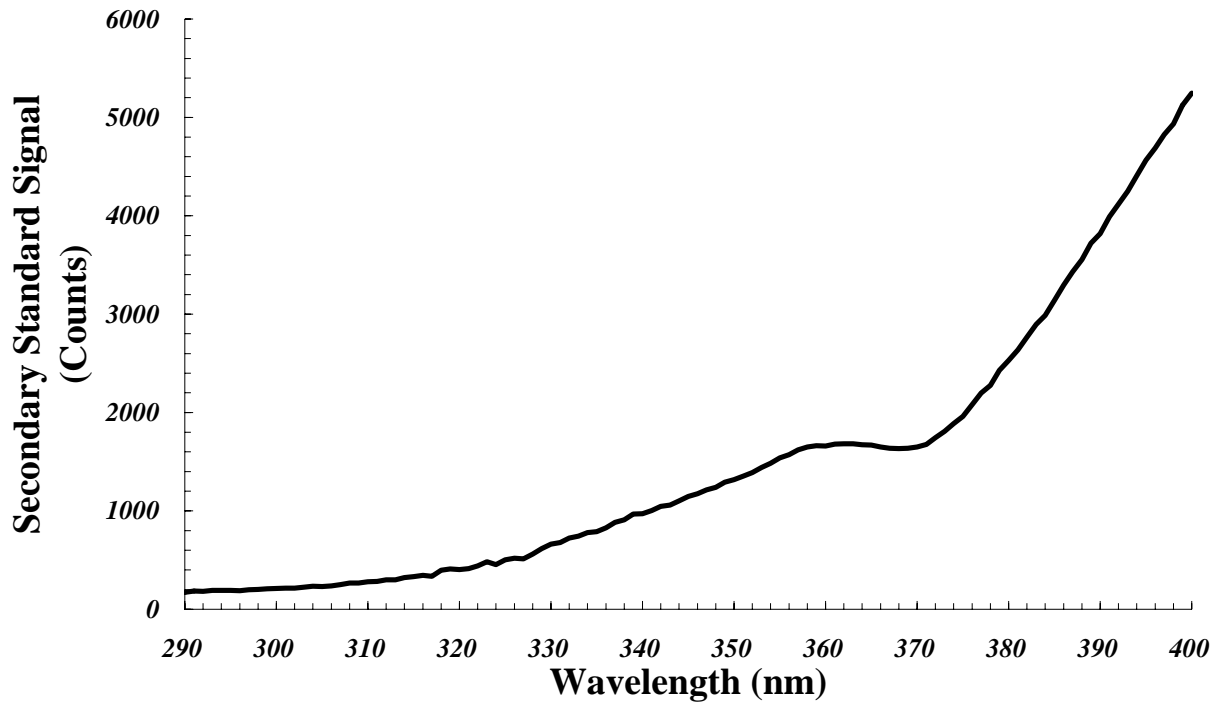


Figure 4.5: A spectral counts scan of the SSL measured by the mobile scanning spectroradiometer ($CSS(\lambda)$).

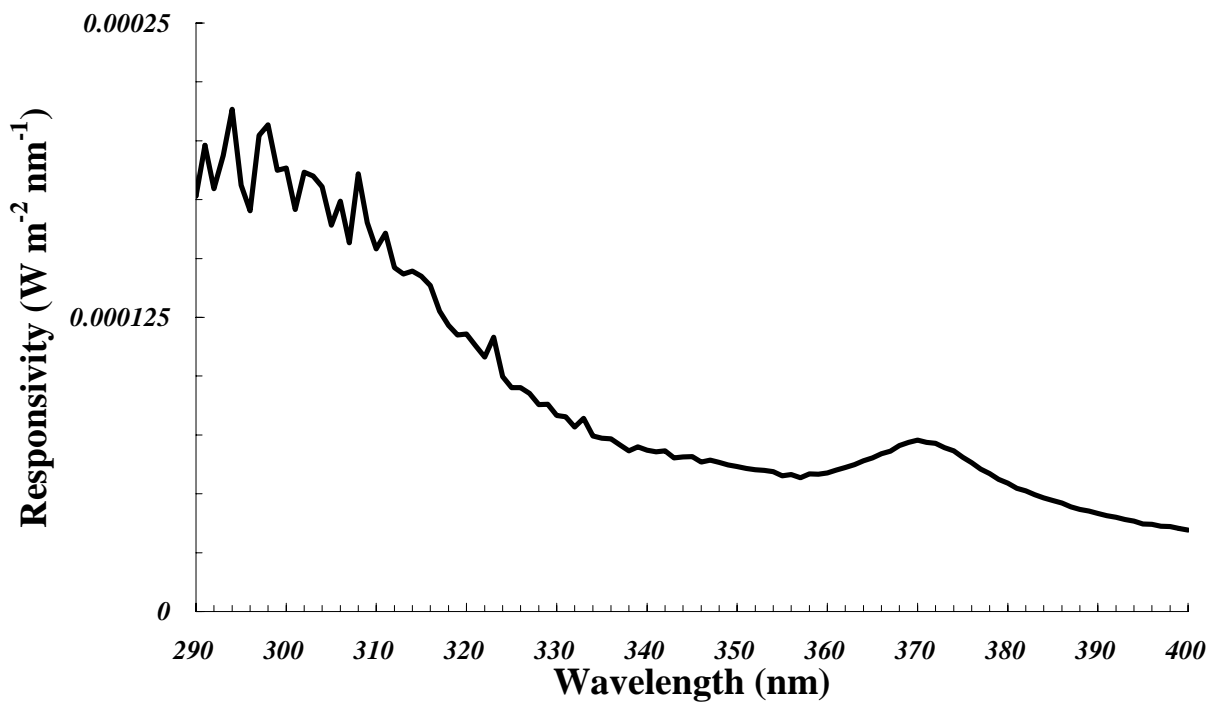


Figure 4.6: An example of a spectral responsivity distribution ($R(\lambda)$) calculated for the UV waveband.

After the calculation of the spectral responsivity, the spectral irradiance distribution was found in units of $W m^{-2} nm^{-1}$ using (Parisi *et al*, 2004):

$$S(\lambda) = R(\lambda) \times (CSO(\lambda) - DK)$$

where $CSO(\lambda)$ is the counts of the UV energy as received from the artificial UV source as measured by the spectroradiometer in single nanometre increments. The spectral irradiance distribution could then be weighted against the immersion factor distribution $I(\lambda)$ (provided for the spectroradiometer in Section 4.4.1) in order to evaluate the corrected irradiance for each distinctive underwater measurement.

Following the spectral responsivity, irradiance calculations and corrections, the total UV irradiance ($UVTOT$) was then be determined in units of $W m^{-2}$ by summing over the necessary UV spectral ranges as required:

$$UVTOT = \sum_X^Y S(\lambda) \Delta\lambda$$

where X and Y represent the limits of summation of the UV waveband and $\Delta\lambda$ is the wavelength increment in nm.

4.3.3 EPP2000 Spectrometer

A StellarNet EPP2000 spectrometer (StellarNet EPP2000 C-UV-VIS, Tampa, Florida) was employed in the underwater field calibration phase of the research (Chapter 7) to calibrate the IL1400 broadband meter as the EPP2000 spectrometer unit was several times smaller and lighter than the mobile scanning spectroradiometer, which made it much easier to use for field based measurement campaigns. Another

advantage of the EPP2000 was that it was capable of running directly off the battery power of a laptop computer for several hours, greatly increasing its portability.

The EPP2000 spectrometer consisted of a sensitive charge coupled device (CCD) working in unison with a high speed parallel digitizer interface with a large spectral scan memory. This setup allowed for almost instantaneous measurement of incoming solar spectra over a waveband of 200 nm to 1100 nm. Input was provided by a SMA 905 fibre optic connector with a small diffuser attached to the end. Control of the EPP2000 and spectral data collection was performed by a laptop computer. The EPP2000 spectrometer with the laptop computer used for control and data acquisition and the diffuser connected via a fibre optic link is shown in Figure 4.7.



Figure 4.7: The EPP2000 spectrometer with a laptop computer used for data acquisition and the diffuser connected via a fibre optic link.

The EPP2000 spectrometer has a stray light rejection of approximately 0.1% as determined by the manufacturer. This might appear to be very good, but if it is considered that long wave UVA and visible solar irradiances are measured as being

two to three orders of magnitude greater than irradiances less than 305 nm, stray light from the longer wavelengths can acutely bias the shortwave UV. This characteristic of the EPP2000 spectrometer's response should be kept in mind when interpreting the measurements made with the EPP2000 spectrometer in the following chapters.

Figure 4.8 shows a series of comparisons between integrated UVB measurements from 298 nm to 320 nm for the EPP2000 spectrometer and the Bentham spectroradiometer taken over March, April, July and August in 2007. Even though the EPP2000 spectrometer has reduced short wave sensitivity due to stray light effects it can be seen that after integration and averaging across the UVB, measurements made with the EPP2000 spectrometer do compare reasonably well to those made with the Bentham spectroradiometer. Table 4.1 displays the slope, y – intercept and R^2 associated with each of the trend lines shown in Figure 4.8

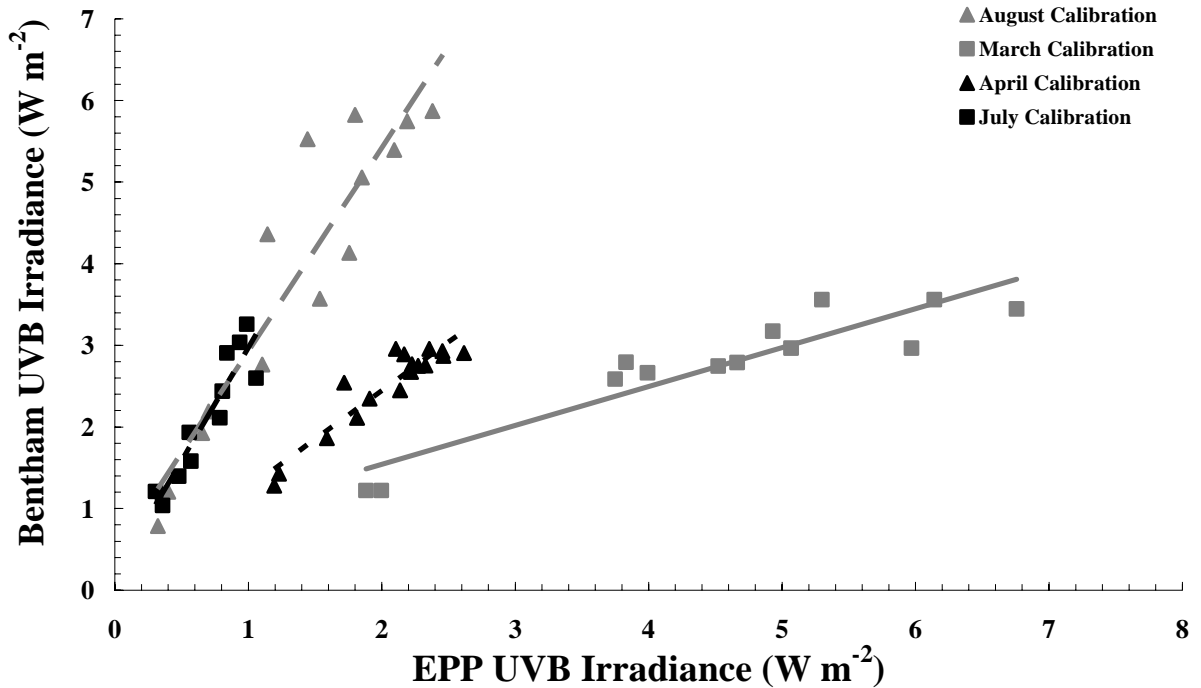


Figure 4.8: Comparisons between UVB measurements integrated from 298 nm to 320 nm for the Bentham spectroradiometer and the EPP2000 spectrometer taken over March, April, July and August in 2007.

Table 4.1: The slope, y – intercept and R^2 values as calculated for the Bentham spectroradiometer comparison to the EPP2000 spectrometer.

Comparison Month	Slope	Y – Intercept	R^2
March	0.48	0.59	0.85
April	1.19	0.06	0.87
July	2.78	0.2	0.86
August	2.49	0.44	0.86

4.3.4 Bentham Spectroradiometer and Solar Light UV Broadband Meter

In order to produce the long – term in – air solar UVB and erythemal calibrations of the PPO dosimeter presented in Chapter 6 and Chapter 7, a stationary standard calibrated Bentham spectroradiometer was used in conjunction with a continuously operating Solar Light UV broadband meter.

The Bentham spectroradiometer consisted of a double grating monochromator with twin holographic gratings with 2400 lines nm^{-1} (model DTM300, Bentham Instruments, Reading, UK). Input was provided by a diffuser (model D6, Bentham Instruments, Reading, UK) linked into the input slit of the monochromator via a 4 mm diameter fibre optic connection. A scanning resolution of 0.5 nm was delivered by input and output slit widths in the monochromator of 0.37 mm. UV detection was performed by a side window photomultiplier tube operating with a Bi-alkali photocathode (model DH10, Bentham Instruments, Reading, UK) together with an amplifier featuring software variable gain (model 267, Bentham Instruments, Reading, UK) and an integrating analogue to digital converter with a 100 ms integration period (model 228A, Bentham Instruments, Reading, UK). The spectroradiometer was controlled using the BenWin+ software package (Bentham Instruments, Reading, UK) running off a remote workstation. The software was set up so that integrations of total UV, UVB, UVA and erythemal irradiances in the appropriate units could be calculated on demand for each scan.

The Bentham spectroradiometer was calibrated regularly to the National Physical Laboratory (NPL), UK standard by using a 150 W quartz tungsten halogen lamp. Wavelength calibration was also carried out at frequent intervals by using the UV spectral lines emitted by a mercury lamp. Bentham has estimated that the cosine error of the diffuser is less than $\pm 0.8\%$ for SZA less than or equal to 70° and is approximately 3.3% at a SZA of 80° .

During the PPO dosimeter calibration campaigns the Bentham spectroradiometer was positioned on top of an unshaded roof where it measured the complete solar UV

spectrum in increments of 10 minutes taking approximately 2 minutes per scan. In order to protect against the elements, the Bentham spectroradiometer was housed in a sealed container (Envirobox, Bentham Instruments, Reading, UK). Temperature stabilisation was provided by a custom built air conditioning unit with a condenser placed several metres from the envirobox. Figure 4.9 shows the Bentham spectroradiometer on the roof inside the envirobox.



Figure 4.9: The Bentham spectroradiometer on the roof inside the Envirobox. The diffuser can be seen on the right hand side of the unit.

On the same roof, stationed in close proximity was the Solar Light UV broadband meter (model 501, Solar Light Co. PA, USA) with a working spectral response close to that of the erythemal action spectrum running between 280 nm to 320 nm (Solar Light, 2009). The Solar Light UV broadband meter was set up so that it collected erythemal integrated UV exposure data from within its response waveband of 280 nm

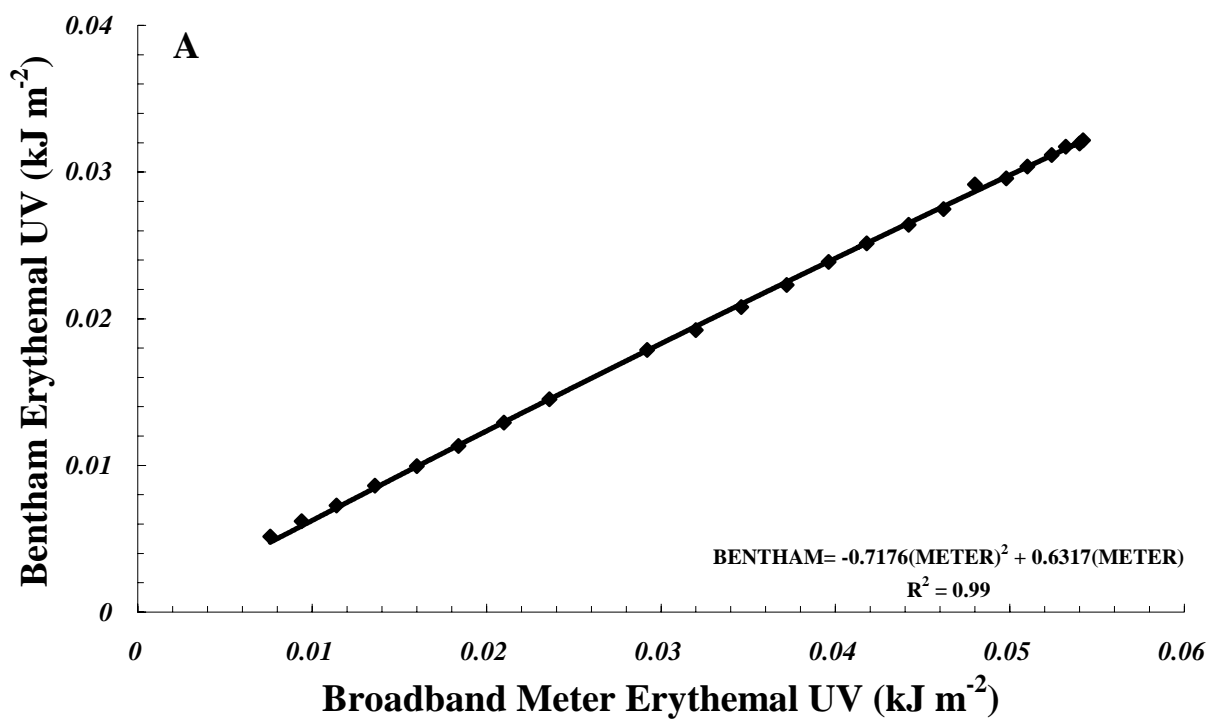
to 320 nm every five minutes. This data was then sent through to an automated data logger unit where it was then stored on a server. The manufacturer has stated that a cosine error of no more than $\pm 5\%$ exists per incident angle (Solar Light Co., n.d.). Figure 4.10 provides a picture of the Solar Light UV broadband meter.

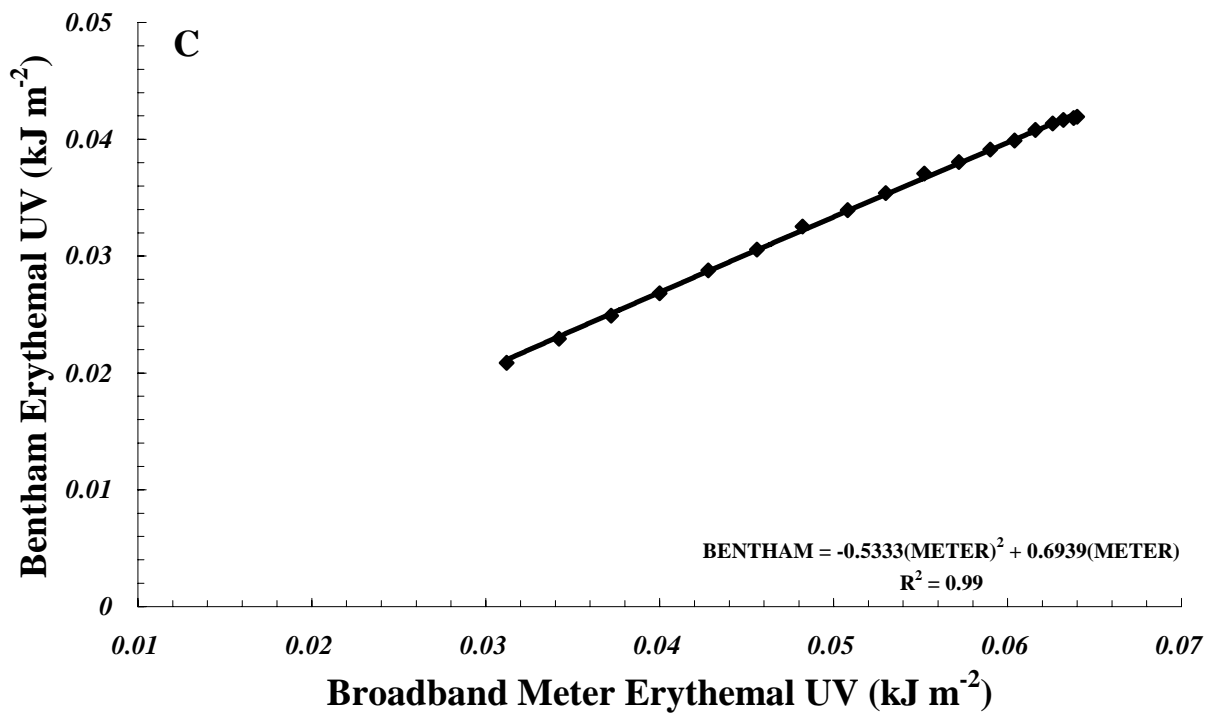
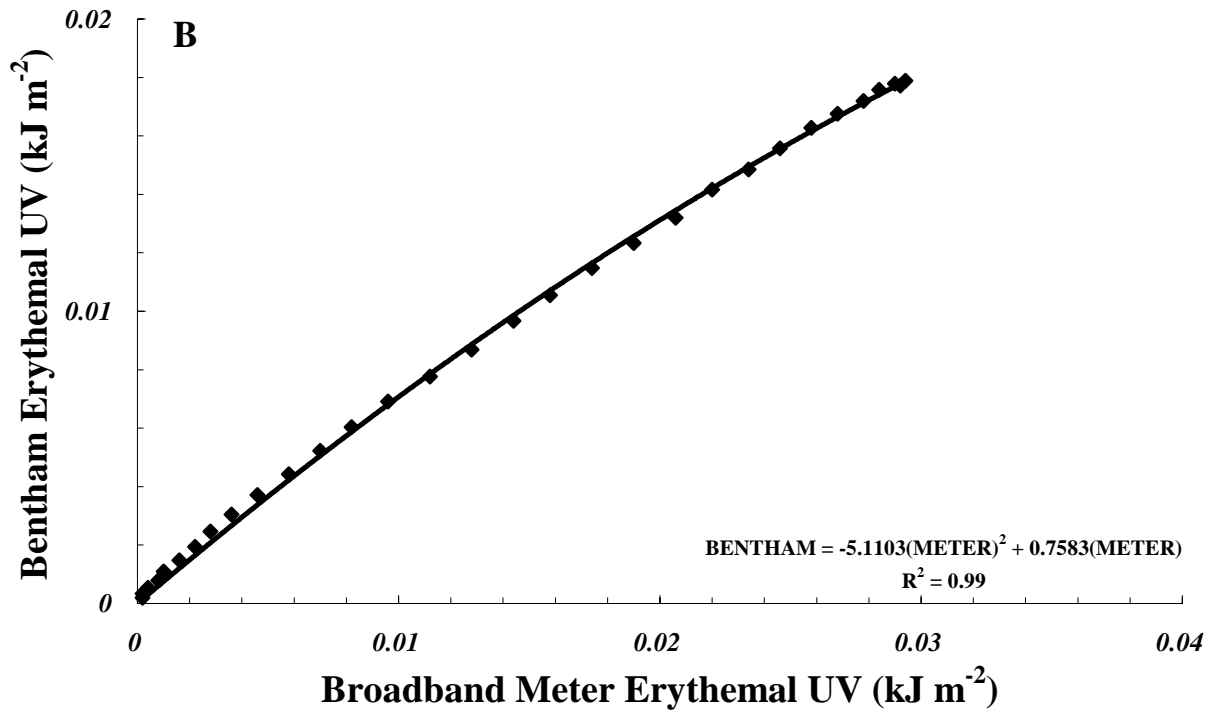


Figure 4.10: The Solar Light UV broadband meter.

For the calibrations of the PPO dosimeters to be used for in – air applications outdoors the Solar Light UV broadband meter was employed as the primary measurement instrument. The reason behind this was that it was capable of measuring integrated solar UV exposures within the wavelength range necessary and recorded at five minute time increments. This factored in fluctuations in quickly changing atmospheric parameters such as cloud cover. This was something that the Bentham spectroradiometer could not do as well due to possible changes in cloud cover between the ten minute scans and also due to the fact it was set up to measure

irradiance, not integrated exposure. The Solar Light UV broadband meter was calibrated directly to the Bentham spectroradiometer for erythemal exposures on a cloud free day in each season over the year long measurement campaign in order to standardise its measurements. Figure 4.11 (A), (B), (C) and (D) displays example calibrations for autumn, winter, spring and summer respectively. The spring calibration is missing some early morning data points due to a power outage.





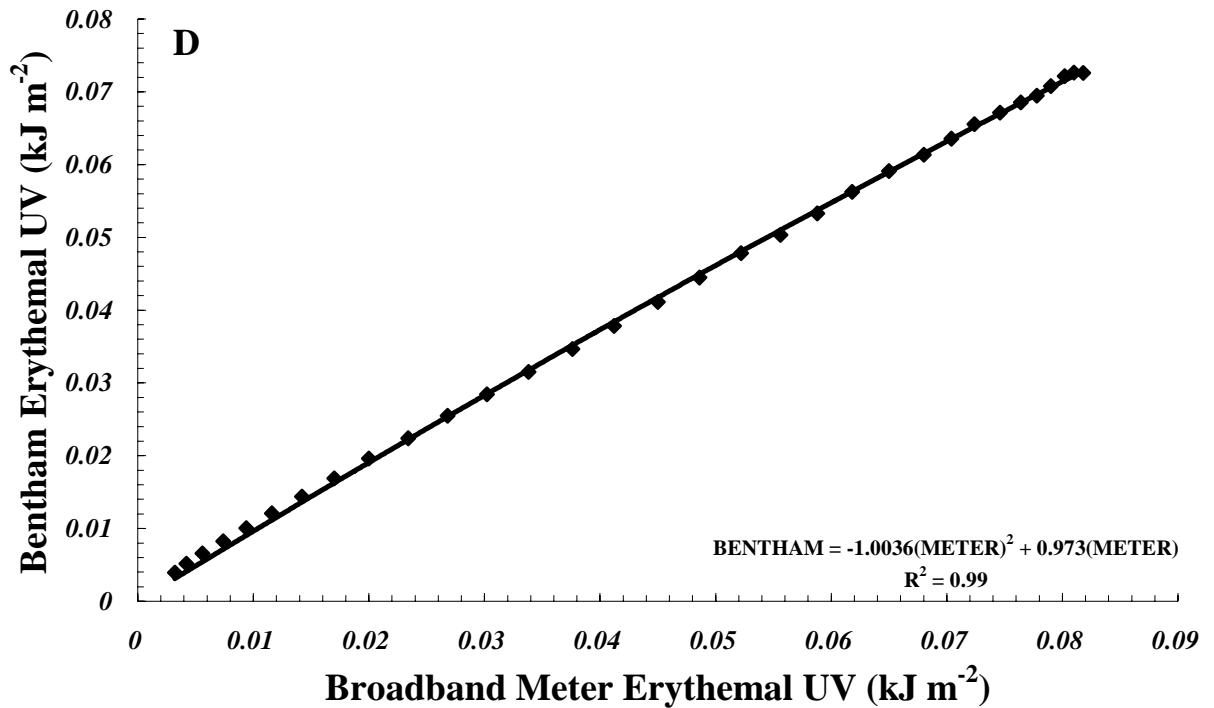


Figure 4.11: Calibration charts linking the Solar Light UV broadband meter to the Bentham spectroradiometer for (A) autumn, (B) winter, (C) spring and (D) summer.

Additionally, the measurements made with the Bentham spectroradiometer and the Solar Light UV broadband meter combination allowed the calibration of the EPP2000 spectrometer and the IL1400 broadband meter. To do this a set of transfer equations linking the Bentham spectroradiometer to the EPP2000 spectrometer were developed over a wide range of SZA from the data that was gathered over the measurement campaign described in Section 4.4.2. In order to clearly define the link between each instrument and the PPO dosimeter a flowchart of the complete outdoors PPO dosimeter calibration scheme for both in – air and underwater measurements is shown in Figure 4.12. How the links between each instrument were made for the underwater calibrations will be elaborated upon in Section 4.4.2

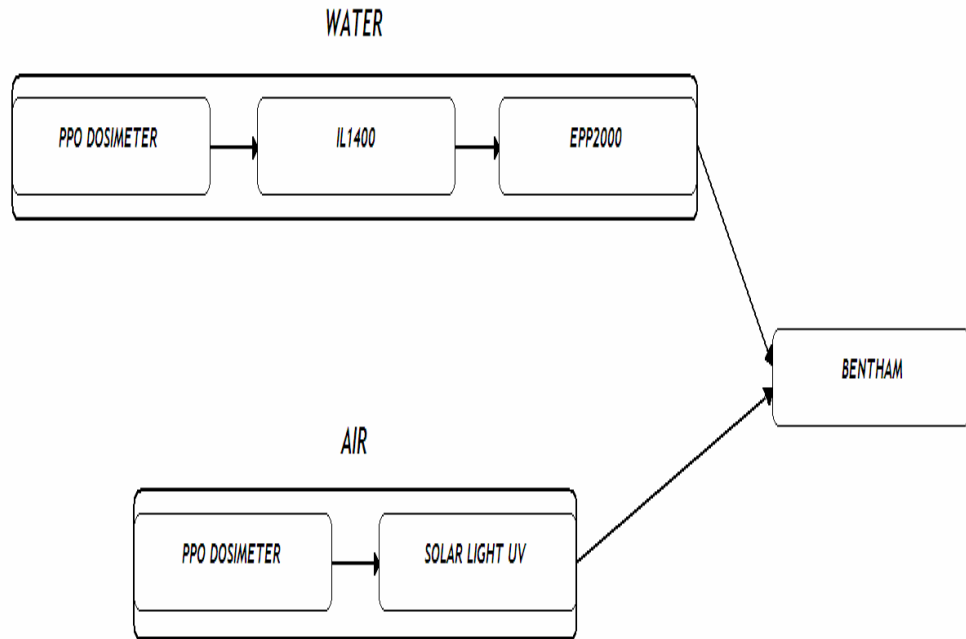


Figure 4.12: Flowchart of the outdoors PPO dosimeter calibration scheme for both in – air and underwater measurements.

4.4 The Immersion Effect

Three main factors influence underwater UV measurements made with spectrometric and radiometric instrumentation. The first being that the field of view as seen by a sensor is reduced and hence a smaller amount of radiation is intercepted by the sensor. The second being the change in the local refractive index between the open – air environment where the sensor was calibrated in comparison to the underwater environment where the sensor was employed (Ohde & Siegel, 2003). The third factor being that during a water-based measurement, a greater amount of light is backscattered out of the meter in comparison to a similar air – based measurement, which is caused by the difference between the refractive indices for air and water at the meter interface (Hooker & Zibordi, 2005; Zibordi, 2005; Zibordi *et al*, 2004).

Figure 4.13 shows a basic schematic detailing the immersion effect phenomena based on the description provided by Zibordi *et al* (2004).

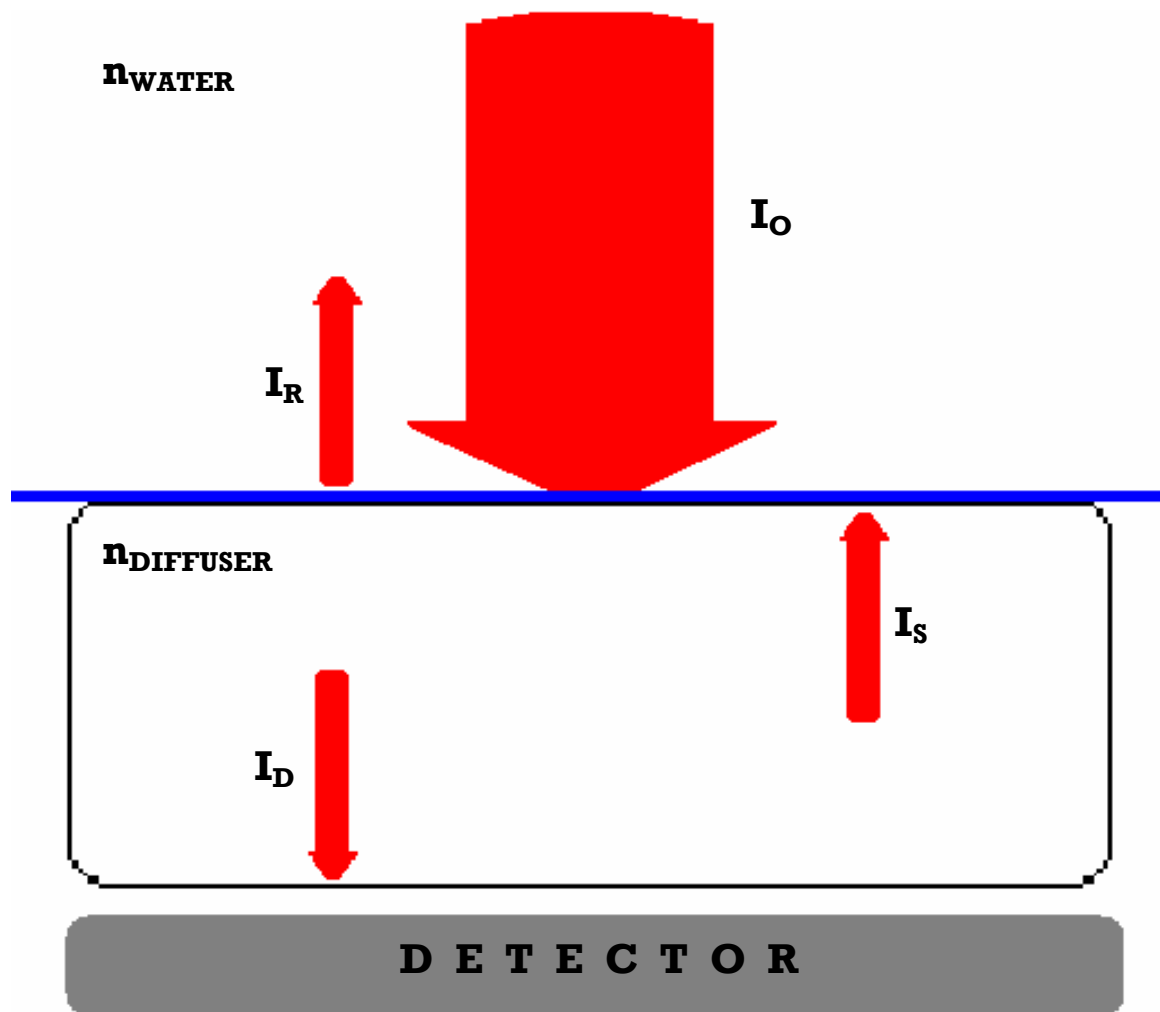


Figure 4.13: The immersion effect scenario where n_{WATER} is the refractive index of the water in which the optical meter is submerged, n_{DIFFUSER} is the refractive index of the diffuser/collector employed by the optical meter, I_O is the irradiance incoming from a source, I_R is the reflected irradiance off the diffuser/collector, I_S is the backscattered irradiance from within the diffuser/collector and I_D is the irradiance intercepted by the detector (Zibordi *et al*, 2004).

In order for reliable spectral irradiance $S(\lambda)$ measurements to be made underwater, wavelength dependent immersion factors were applied using this equation:

$$S(\lambda) = R(\lambda)I(\lambda)[CSO(\lambda) - DK]$$

where $R(\lambda)$ is the responsivity of the spectroradiometer, $I(\lambda)$ is the immersion factor, $CSO(\lambda)$ is the counts of the UV source as measured by the spectroradiometer per unit wavelength and DK is the averaged output noise over the given wavelength range.

The process for determining the immersion factors in the UV waveband for the optical instrumentation (the mobile scanning spectroradiometer and the EPP2000 spectrometer) was carried out in an indoors laboratory environment. By using a collimated UV source delivering a constant exposure level, measurements were made in a water tank (described in Section 5.4.1) holding fresh particulate and bubble free clean water over a range of different depths starting at just below the water line in order to obtain an irradiance depth regime. Clean water was used as it has been recommended as the primary water type of choice for immersion effect evaluations by Hooker and Zibordi (2005). At the beginning of the measurement series, a single measurement was made just above the surface of the water. Following this $I(\lambda)$ was evaluated with this expression (Zibordi *et al*, 2004):

$$I(\lambda) = T(\lambda) \frac{S_{AIR}(\lambda)}{S_{WATER}(\lambda)}$$

where $T(\lambda)$ is the transmittance of the water surface to downward spectral irradiance, $S_{AIR}(\lambda)$ is the irradiance measured in-air and $S_{WATER}(\lambda)$ is the irradiance measured in water. $T(\lambda)$ was estimated from the Fresnel reflectance for a vertical irradiance beam as presented by Zibordi *et al* (2004):

$$T(\lambda) = \frac{4n_{WATER}(\lambda)}{[1 + n_{WATER}(\lambda)]^2}$$

with $n_{WATER}(\lambda)$ being the wavelength dependent index of refraction for the particular water type under analysis. The $n_{WATER}(\lambda)$ values were calculated using the equation developed by the International Association for the Properties of Water and Steam (1997):

$$\frac{n^2 - 1}{n^2 + 2} \left(\frac{1}{\bar{\rho}_*} \right) = a_0 + a_1 \bar{\rho}_* + a_2 \bar{T}_* + a_3 \bar{\lambda}_*^2 \bar{T}_* + \frac{a_4}{\bar{\lambda}_*^2} + \frac{a_5}{\bar{\lambda}_*^2 + \bar{\lambda}_{UV}^2} + \frac{a_6}{\bar{\lambda}_*^2 + \bar{\lambda}_{IR}^2} + a_7 \bar{\rho}_*^2$$

where n is the refractive index of the water, $\bar{\rho}_*$ is the water dimensionless reference density, a_0 to a_7 are dimensionless coefficients supplied by the International Association for the Properties of Water and Steam, \bar{T}_* is the water dimensionless reference temperature, $\bar{\lambda}_*$ is a dimensionless wavelength reference value, $\bar{\lambda}_{UV}$ is a constant given as 0.2292020 μm and $\bar{\lambda}_{IR}$ is also a constant with a value of 5.432937 μm . For the clean water used in the immersion effect experiments in this research the refractive index distribution across the wavelengths running from 295 nm to 320 nm at an average temperature of 23 °C is shown in Figure 4.14.

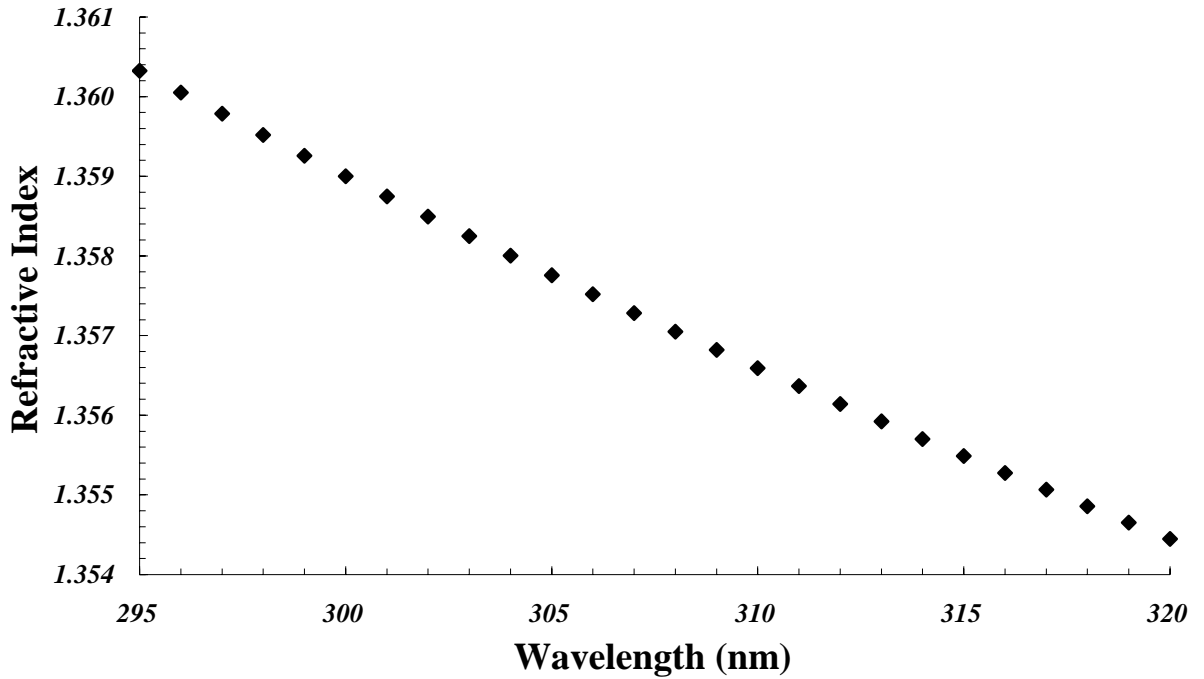


Figure 4.14: The refractive index distribution across the 295 nm to 320 nm waveband at an average temperature of 23 °C.

The precise calculation of $I(\lambda)$ was made by performing a linear regression on the natural logarithm of the irradiances measured in – water (the $S_{WATER}(\lambda)$ values as detailed previously) corrected for measurement fluctuations caused by the finite distance between an ideal collimated source and the sensor. This correction was estimated as $\ln\left[\frac{S_{WATER}(\lambda)}{C(\lambda)}\right]$ (Zibordi *et al*, 2004) where $C(\lambda)$ is known as the

geometric correction factor and was calculated by (Zibordi *et al*, 2004):

$$C(\lambda) = \frac{S_{AIR}(\lambda)}{S_{WATER}(\lambda)^{Z=0}}$$

where $S_{WATER}(\lambda)^{Z=0}$ was the spectral irradiance measured at zero depth (the irradiance measured just below the water surface).

During the immersion effect evaluations for both the mobile scanning spectroradiometer and the EPP2000 spectrometer it was discovered that due to their rapidly increasing attenuation, measurements for UVB wavelengths below a cut – off point of 298 nm could not be made without substantial amounts of noise entering the spectral signal, hence reducing the reliability of the scan. As a result of this, it was decided that the UVB waveband running from 298 nm to 320 nm was to be used for all PPO film calibrations both in the laboratory and in the field. The 320 nm UVB waveband cut – off was chosen instead of the usual 315 nm cut – off as it has been previously used by photobiologists and is more applicable to the response of the PPO film.

4.4.1 Mobile Scanning Spectroradiometer Immersion Effect Correction and Calibration to the IL1400

The immersion effect factors for the spectroradiometer were evaluated using the same methodology as specified in Section 4.4. A fluorescent UV light was used as the UV source for each specific measurement. It was estimated that a variation of less than 1% would exist between the immersion effect factors calculated over the range of temperatures recorded during each underwater experiment described in Chapter 5. Hence, only one set of immersion effect factor values, calculated at 23 °C was used in the calibrations.

The immersion effect factors in the UVB waveband from 298 nm to 320 nm for the scanning spectroradiometer are presented in Figure 4.15. The $\pm 10\%$ error margin shown with respect to the y – axis was estimated to have arisen during the measurement and calculation of the immersion effect factors. From Figure 4.13, it can be seen that the immersion effect factors fluctuate across the UVB waveband, tending

to decrease in magnitude slightly with increasing wavelength. Example immersion effect corrected spectral irradiances in the UVB waveband are depicted in Figure 4.16 at a depth of 1 cm and at a depth of 16 cm in comparison with a spectrum measured just above the water surface. For each scan a peak can be seen at 313 nm, which is due to the spectral emission from mercury constituents in the UV source lamp. For the scan taken at $Z_{16\text{CM}}$, the two irregular troughs at 300 nm and at 317 nm can be attributed to photon noise, occurring due to lower UV signal levels at this depth.

The calibrations of the IL1400 against the spectroradiometer for both underwater and in – air conditions applicable for the fluorescent UV source can be seen in Figure 4.17 (A) and 4.17 (B) respectively. These calibrations took into account the different cosine response and in the case of the underwater calibration, immersion effect properties of the IL1400 in comparison to the spectroradiometer and hence, empirically adjust for the combined effect of all of these optical factors.

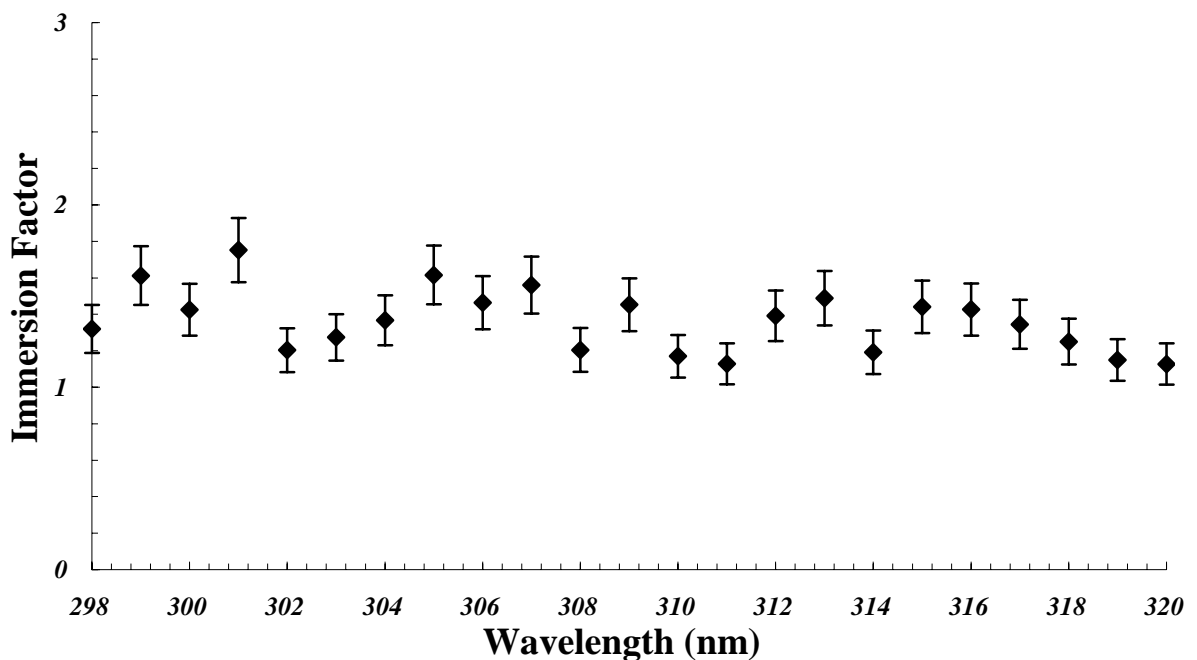


Figure 4.15: Immersion effect factors as calculated for the mobile spectroradiometer for the waveband running from 298 nm to 320 nm.

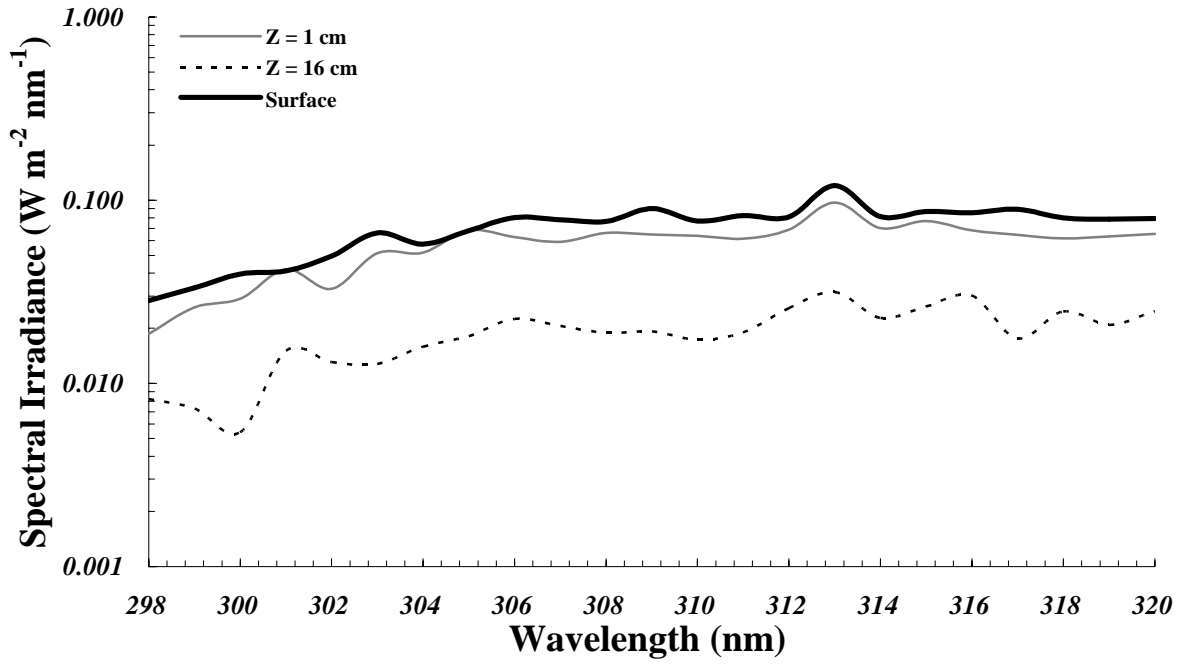
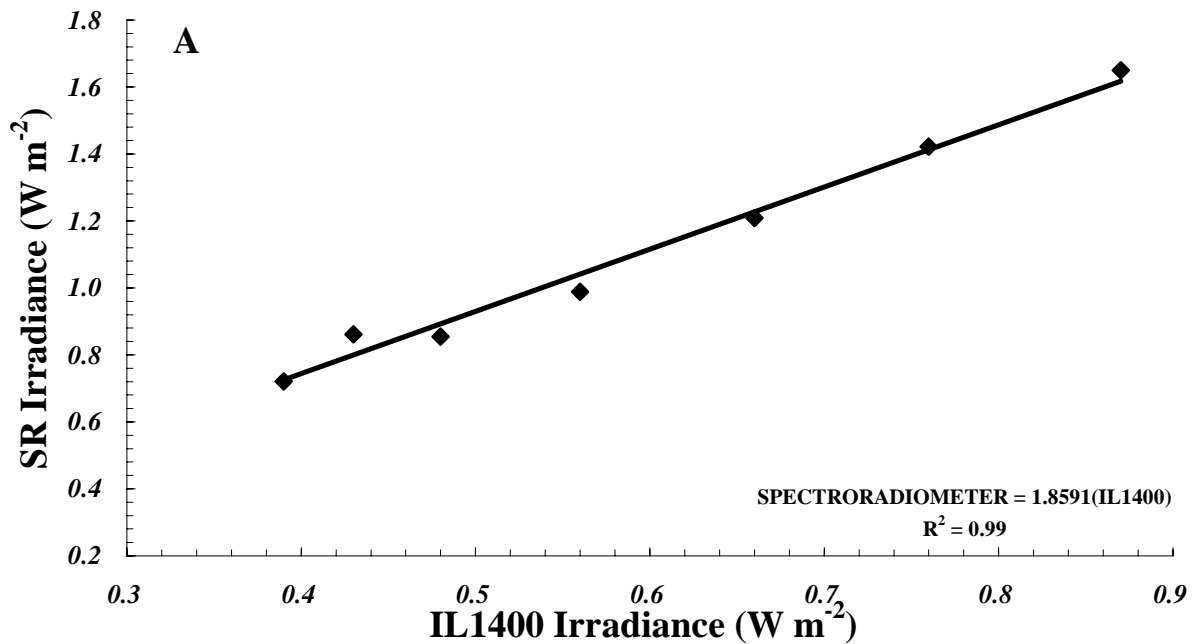


Figure 4.16: Profile of immersion effect corrected spectral irradiances from 298 nm through to 320 nm in the water tank at $Z_{1\text{CM}}$ and $Z_{16\text{CM}}$ in comparison with a spectrum measured at the water surface.



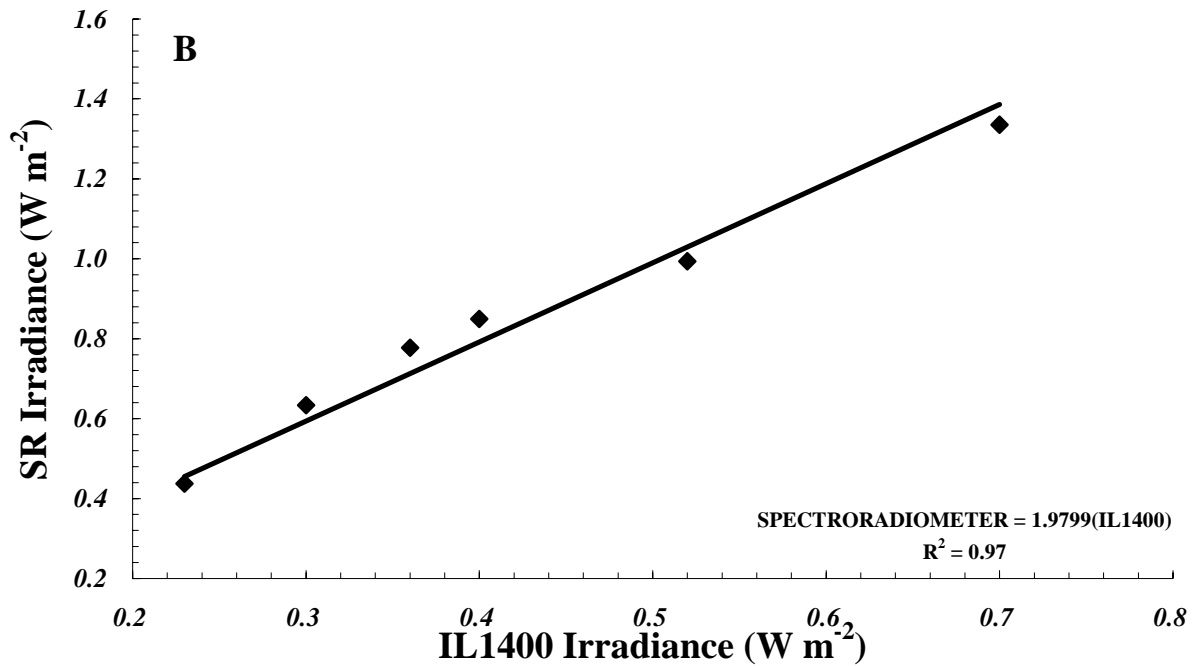


Figure 4.17: Mobile spectroradiometer, UV in the 298 nm to 320 nm waveband, versus IL1400 calibration for in – air (A) and underwater (B) applications.

4.4.2 EPP2000 Spectrometer Immersion Effect Correction and Calibration to the IL1400

The immersion effect factors in the UVB waveband for the EPP2000 spectrometer are displayed in Figure 4.18. The y – error bars are a representation of the $\pm 10\%$ uncertainty accumulated throughout the immersion effect factor measurement and calculation process. A solar simulator source was the UV source employed for each irradiance measurement. It can be seen in the graph that the immersion effect factors do not deviate a great deal from an average value of approximately 1.09 over the waveband running from 298 to 320 nm. There are minor variations from the average immersion effect factor value from 298 nm to 305 nm. This results from the reduced UV signal within this particular region. As was the case with the mobile scanning spectroradiometer, it was estimated that fluctuations in ambient temperatures during outdoors calibration measurements would not change the immersion effect factors

initially calculated for use with the EPP2000. Figure 4.19 displays a regime of immersion effect corrected spectral irradiances from 298 nm through to 320 nm in a water tank used in the immersion effect factor calculation trial at the depths of Z_{4CM} and Z_{25CM} compared to a spectrum obtained at the water surface.

Before any accurate underwater UVB measurements could be made with the PPO dosimeter, a calibration transfer methodology had to be applied between the IL1400 and the EPP2000. The UVB data calculated for the EPP2000 in these calibrations was defined as the integral of the irradiance running from 298 nm to 320 nm. The IL1400 broadband meter was used to measure UVB irradiance with respect to its response spectrum during the calibration process. This was calibrated underwater for each water type against the immersion effect corrected EPP spectrometer (calibrated with respect to the NPL standard irradiance). In order to do this a calibration campaign was run over two cloud free days in early autumn and two additional cloud free days in mid winter to gather two sets of horizontal plane irradiance calibration data under two distinct ranges of SZA to transfer the EPP2000 spectrometer calibration to the IL1400 broadband meter in the underwater environment. The two days in autumn had SZA ranges of between 20° to 61° and 21° to 61° respectively (defined in this research as low SZA conditions), while the two days in winter had SZA ranges of between 49° to 75° and 39° to 68° respectively (defined in this research as high SZA conditions). These measurements were performed at the University of Southern Queensland Toowoomba Campus ($27^{\circ} 33' S$, $151^{\circ} 57' E$, 691 m elevation). Each day measurements were made in clear tap water, creek water, sea water and dam water (these water types will be discussed in more detail in Chapter 7). From this data a

complete set of calibration equations for all four water types were formulated using the following base equation:

$$EPP_{IRRADIANCE} = \varepsilon(IL1400_{IRRADIANCE}) + \rho$$

where $EPP_{IRRADIANCE}$ is the solar UVB irradiance as measured by the EPP spectrometer in units of $W\ m^{-2}$ and $IL1400_{IRRADIANCE}$ is the solar UVB irradiance as measured by the IL1400 broadband meter in units of $W\ m^{-2}$. EPP2000 irradiance versus IL1400 broadband meter irradiance calibration charts are presented for both low and high SZA conditions in Figure 4.20 (A) and Figure 4.20 (B) respectively. Table 4.2 shows the calibration factors relating to each of the calibrations displayed in Figure 4.20 (A) and Figure 4.20 (B).

In Figure 4.20 (A) and Figure 4.20 (B) it can be seen that relatively small negative and positive calibration regime offsets were found to exist between the EPP2000 spectrometer and IL1400 broadband meter. The offsets came into play primarily due to the fact that the EPP2000 spectrometer is based off a CCD detector. This means that it is susceptible at times to fixed stray light and temperature fluctuation effects that are very hard to prevent. These stray light and temperature fluctuation effects can manipulate measurement output by amounts significant enough to provide the positive and negative offsets seen in the creek water low SZA, clear water high SZA and creek water high SZA calibration regimes. It is important to note that both the stray light and temperature fluctuation effects on the EPP2000 spectrometer were in play all throughout the calibration series, with their relative influence consistently changing in accordance with atmospheric conditions.

Table 4.2: Values for all ε and ρ parameters as measured for clear, creek, sea and dam water in both low SZA and high SZA conditions.

Calibration Type	ε	ρ	R^2
Clear Water Low SZA	1.5	-0.42	0.88
Creek Water Low SZA	1.19	0.37	0.9
Sea Water Low SZA	0.73	-0.11	0.97
Dam Water Low SZA	0.87	-0.17	0.99
Clear Water High SZA	0.55	0.05	0.9
Creek Water High SZA	0.62	0.03	0.85
Sea Water High SZA	0.82	-0.12	0.98
Dam Water High SZA	0.92	-0.17	0.99

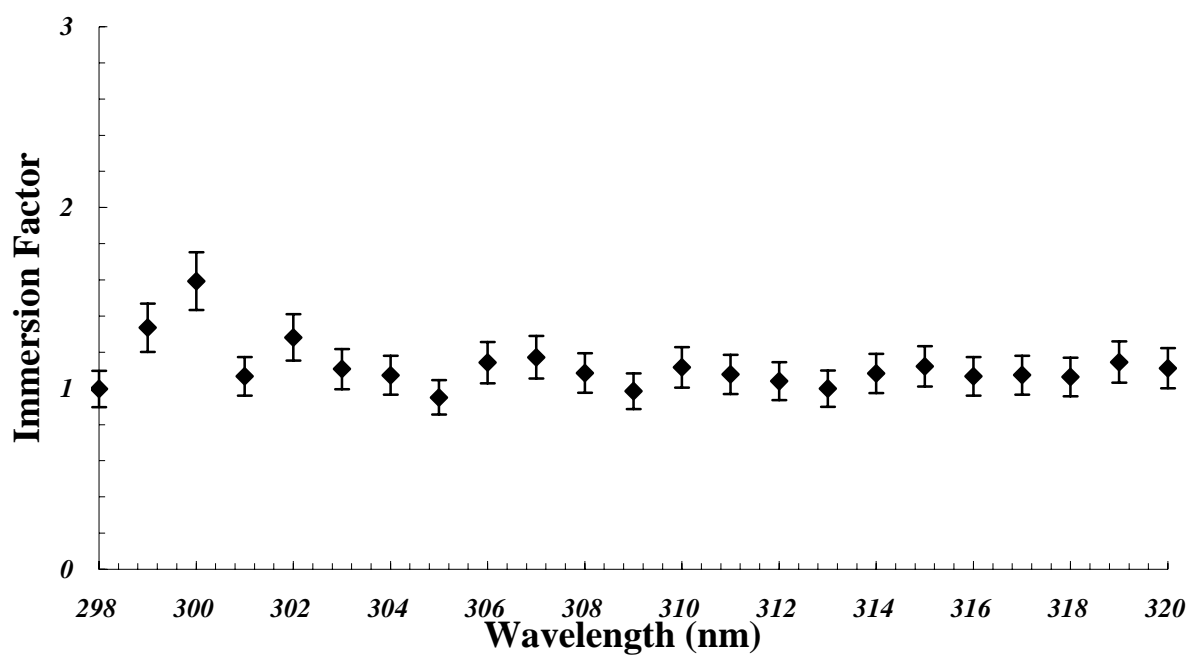


Figure 4.18: Immersion effect factors as calculated for the EPP2000 spectrometer over the 298 nm to 320 nm waveband.

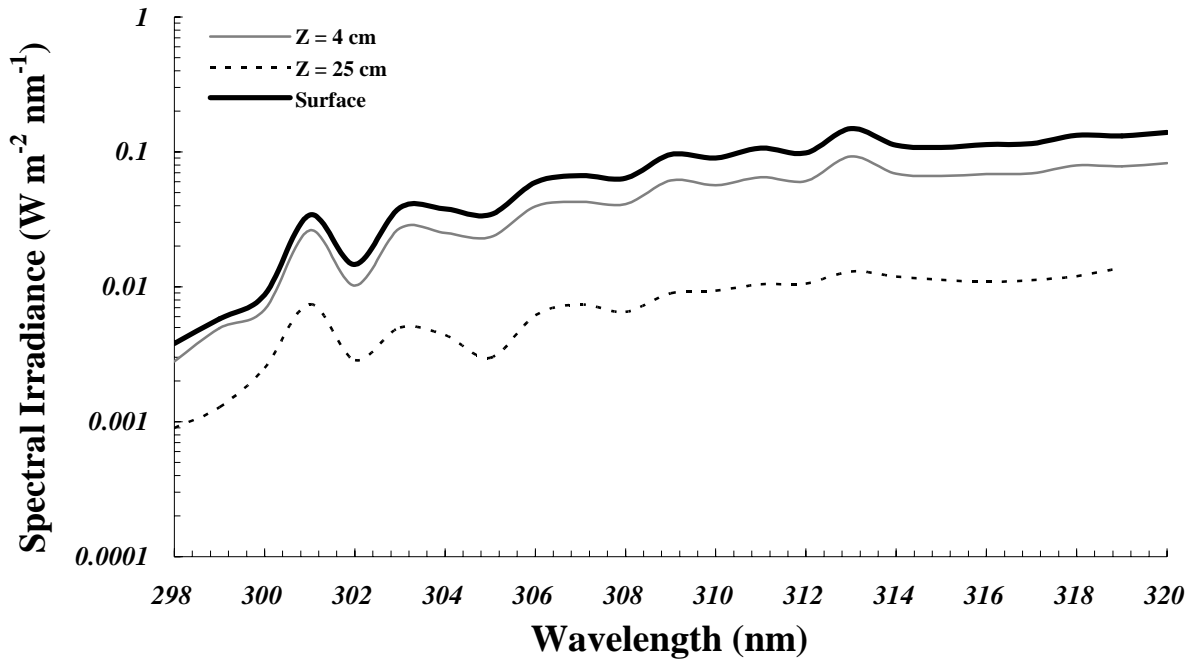
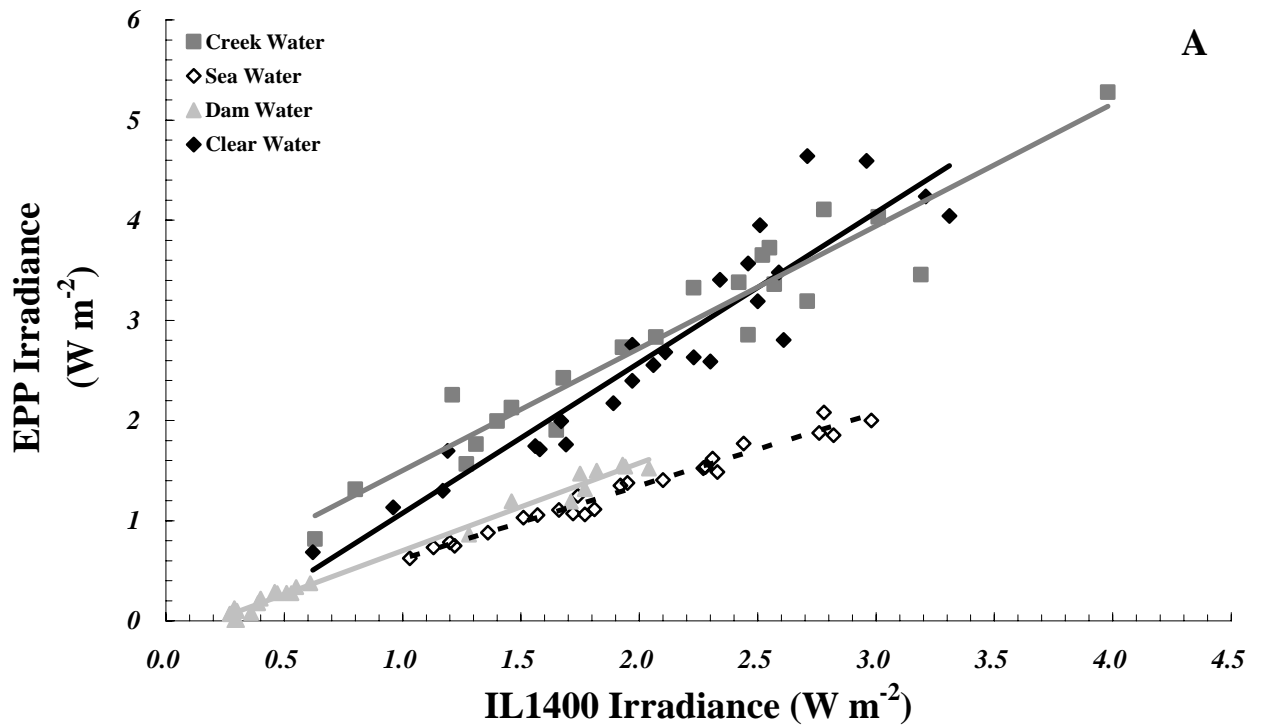


Figure 4.19: Profile of immersion effect corrected spectral irradiances from 298 nm through to 320 nm in the water tank measured with the EPP2000 spectrometer at $Z_{4\text{CM}}$ and $Z_{25\text{CM}}$ in comparison with a spectrum measured at the water surface.



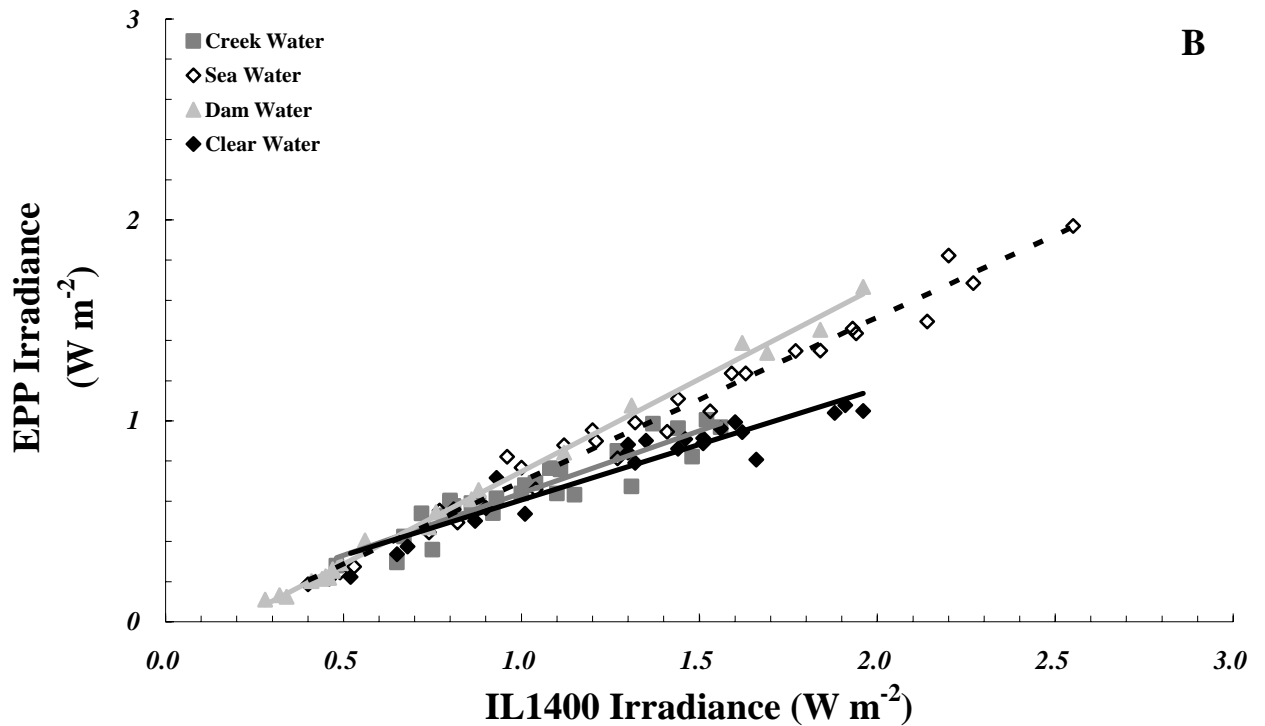


Figure 4.20: EPP2000 spectrometer to IL1400 radiometer calibration transfer data for low SZA conditions (A) and high SZA conditions (B).

4.5 Chapter Discussion

In this chapter the calibrations in air and underwater and the calculations of the immersion factors for the IL1400 radiometer, the mobile scanning spectroradiometer, the EPP2000 spectrometer, the Bentham spectroradiometer and the Solar Light UV broadband meter have been described. This will allow for the development and application of the PPO dosimeter in the following chapter.

Chapter 5

Development of the PPO Dosimeter

5.1 Introduction

As documented in Chapter 3, solar UV is known to have a highly significant impact upon the marine ecosystem. This has been documented by many previous studies using a variety of measurement methods in aquatic environments such as oceans, streams and lakes. Evidence gathered from these investigations has shown that exposure to UVB can be detrimental to numerous aquatic life forms, while UVA radiation can cause both damage and possibly even repair certain types of UVB damage to underwater animals. Polysulphone, along with other select chemical dosimeters have been tested to record underwater UV exposures, and from this quantify the relationship between water column depth and DOC levels to the distribution and penetration of biologically damaging UV underwater. However, these early studies were only able to measure UV exposures over short intervals of time. This chapter reports on the evaluation and testing of the PPO film UV dosimeter for long term usage in underwater conditions. Tests performed in this chapter include the dose response, cosine response, exposure additivity and watermarking effect relating to the PPO dosimeter as measured in a controlled underwater environment (an indoors water tank) and will also detail the overnight dark reaction and UVA and visible radiation response of the PPO dosimeter which can be used for post – exposure error correction to enhance the overall accuracy of the UV exposures measured by the PPO dosimeters in the field. The results show that the PPO dosimeter has the potential for long – term underwater UV exposure measurements.

5.2 The PPO Dosimeter

5.2.1 Fabrication and Physical Properties

PPO film has been identified from previous studies performed by Davis *et al* (1976), Lala (1984), Lester *et al* (2003) and Berre and Lala (1989) and consequently selected in this research for testing as a long – term underwater solar UV dosimeter, where long term is defined as the exposure received at a subtropical site over the time span of approximately seven days. The PPO dosimeter is fabricated by mixing PPO in powder form (General Electric Plastics, United States) together with chloroform (which acts as a solvent) at the specific ratio of 6 grams PPO powder to 50 ml chloroform. This ratio has been identified as the ideal in previous studies in order to produce high quality reproducible sheets (Lester *et al*, 2003). After being left to mix overnight, the solution is cast as a thin film at a thickness of approximately 40 microns on an automated casting table housed in a fume cupboard. Forty microns is generally the standard thickness used in the majority of all dosimetric applications with polysulphone, and it is also used for PPO as it has been shown that it is the thickness at which the PPO film reaches an optimal level of tensile durability (Lester *et al*, 2003). The casting process is very difficult to master and requires a substantial amount of effort and care in order to produce good quality sheets of reproducible thickness and composition. After being left to dry for 2 hours, the PPO film is cut into squares using a blade and is fixed to a PVC holder with an area of 3 cm x 3 cm and an opening slot of 1.2 cm x 1.6 cm. The film is stuck to the holder with electrical tape. Figure 5.1 displays a typical PPO dosimeter.

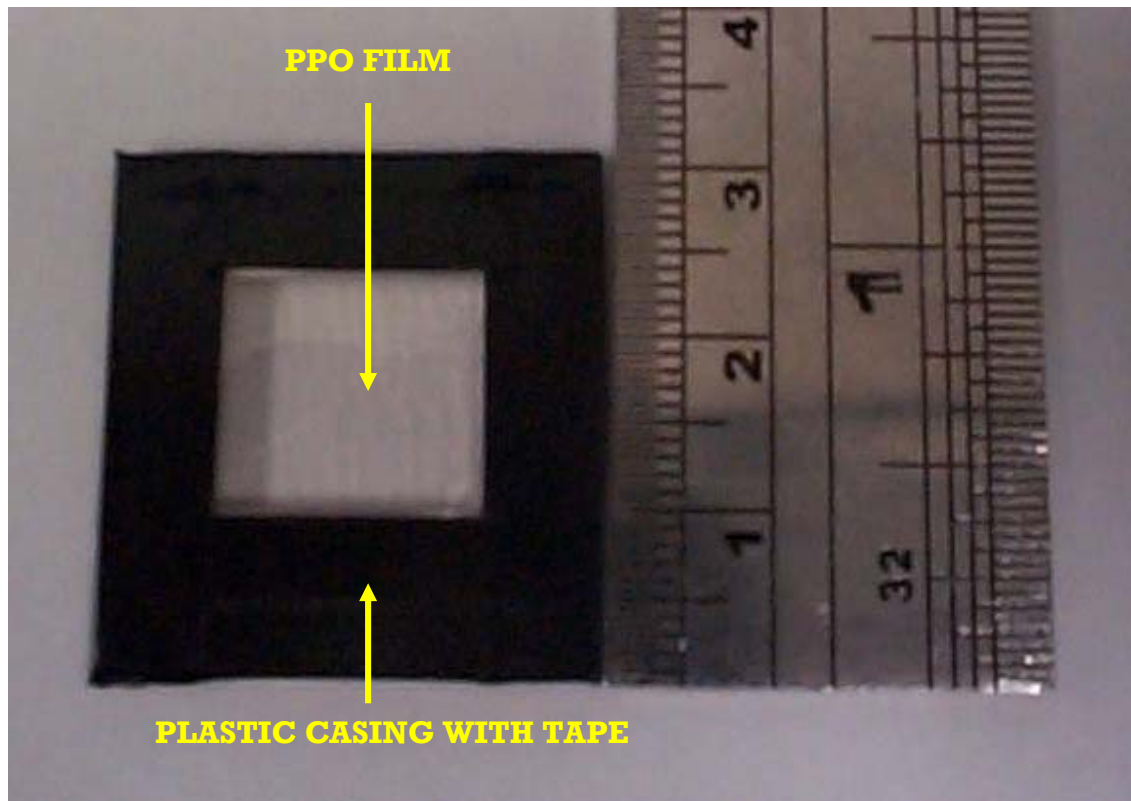


Figure 5.1: A typical PPO dosimeter.

5.2.2 PPO Dosimeter Optical Measurement

The change in optical absorbance caused by UV exposure upon the PPO film is measured in a spectrophotometer (model 1601, Shimadzu Co., Kyoto, Japan) at 320 nm, which is a wavelength where a measurably significant change in optical absorbance is known to occur (Schouten *et al*, 2007). Figure 5.2 displays a pre and post exposure optical absorption distribution for the PPO film across the UV and visible wavebands after an 18.4 kJ m^{-2} UVB exposure. The error threshold for optical absorbance measurements in the spectrophotometer has been quoted as ± 0.002 by the manufacturer. Figure 5.3 displays a picture of the spectrophotometer setup in combination with the data acquisition computer. After each UV exposure, the change in optical absorbance at 320 nm (ΔA_{320}) for each PPO dosimeter used in a

measurement campaign is measured to provide a data point, where ΔA_{320} is calculated with the following equation:

$$\Delta A_{320} = A_{320}^{FINAL} - A_{320}^{INITIAL}$$

where A_{320}^{FINAL} is the final optical absorbance measurement after exposure taken at 320 nm and $A_{320}^{INITIAL}$ is the initial absorbance measurement before exposure taken at 320 nm. Both A_{320}^{FINAL} and $A_{320}^{INITIAL}$ are measured by the spectrophotometer with the following logarithmic functions:

$$A_{320}^{FINAL} = -\log_{10} \left(\frac{I_{320}^{FINAL}}{I_{320}^{REF}} \right)$$

$$A_{320}^{INITIAL} = -\log_{10} \left(\frac{I_{320}^{INITIAL}}{I_{320}^{REF}} \right)$$

where I_{320}^{FINAL} and $I_{320}^{INITIAL}$ are measurements of the transmitted UV radiation intensity at 320 nm passing through either a used or unused PPO dosimeter film and I_{320}^{REF} is the intensity of a reference beam that has not passed through the PPO film.

To better improve the accuracy of the measurements, the ΔA_{320} value was measured over four positions across the film surface with the mean of these values used to calculate the UV exposure by means of a dose – response calibration. A specialised dosimeter holder apparatus was fabricated for this purpose. It is displayed in Figure 5.4.

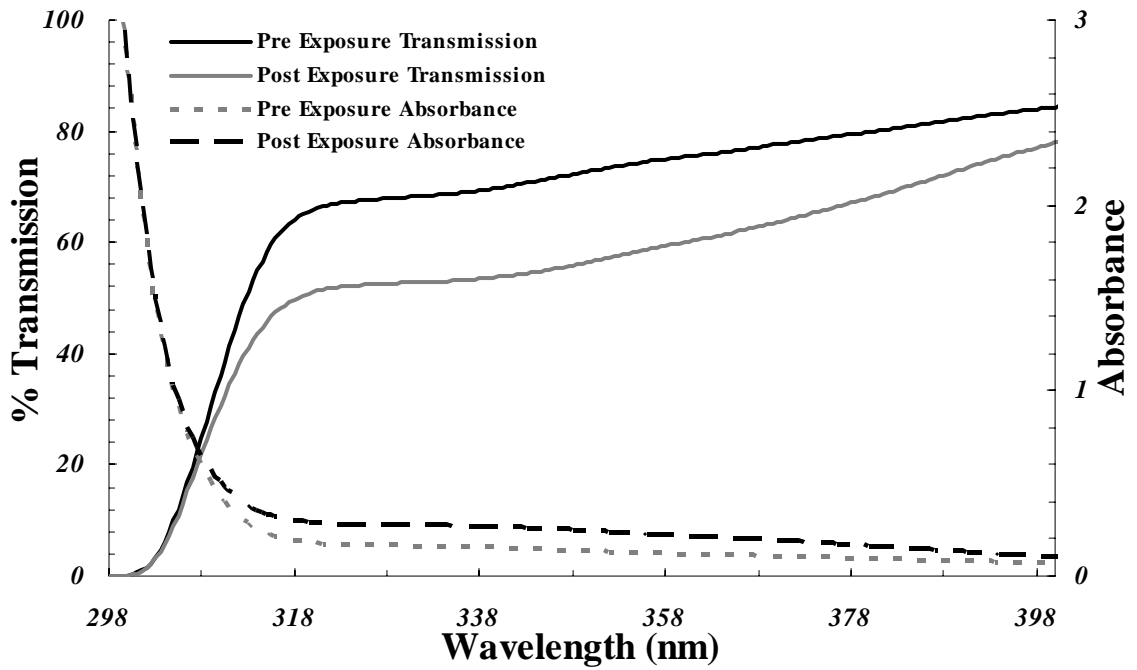


Figure 5.2: Change in optical transmission and absorbance across the entire terrestrial UV waveband for PPO film after an underwater UVB exposure of 18.4 kJ m^{-2} .



Figure 5.3: Spectrophotometer unit connected to the data acquisition computer.



Figure 5.4: Dosimeter holder apparatus employed for the measurement of each PPO dosimeter.

5.3 Optical Properties of the PPO Dosimeter in Air

5.3.1 Applications as an Erythemal and UVA Dosimeter

Recent investigations have shown that PPO can be used successfully in – air as both an erythemal and UVA dosimeter. Lester *et al* (2003) subjected the PPO dosimeter to a number of different tests in – air within a controlled laboratory environment. These tests included analysis of dose – response calibrations for different film thicknesses, effect of ambient temperature on optical absorbency, dark response, spectral response and dosimeter error estimation. The spectral response measured in the study appeared to closely resemble the action spectrum attributed to the erythemal response, which is an excellent characteristic for a dosimeter to have if it is to be employed for measurements related to human activity in the solar UV environment. In addition, a calibration curve was produced linking the gradual changes in the optical absorbency of the PPO dosimeter to the erythemal exposure measured by a scanning

spectroradiometer. A similar calibration is presented in Figure 5.5 where a progressive increase in solar erythemal exposure is calibrated against changing optical absorbance for a series of PPO dosimeters. The following chapter (Chapter 6) extends the original work of Lester *et al* (2003) and calibrates the PPO dosimeter for each season to the erythemal response.

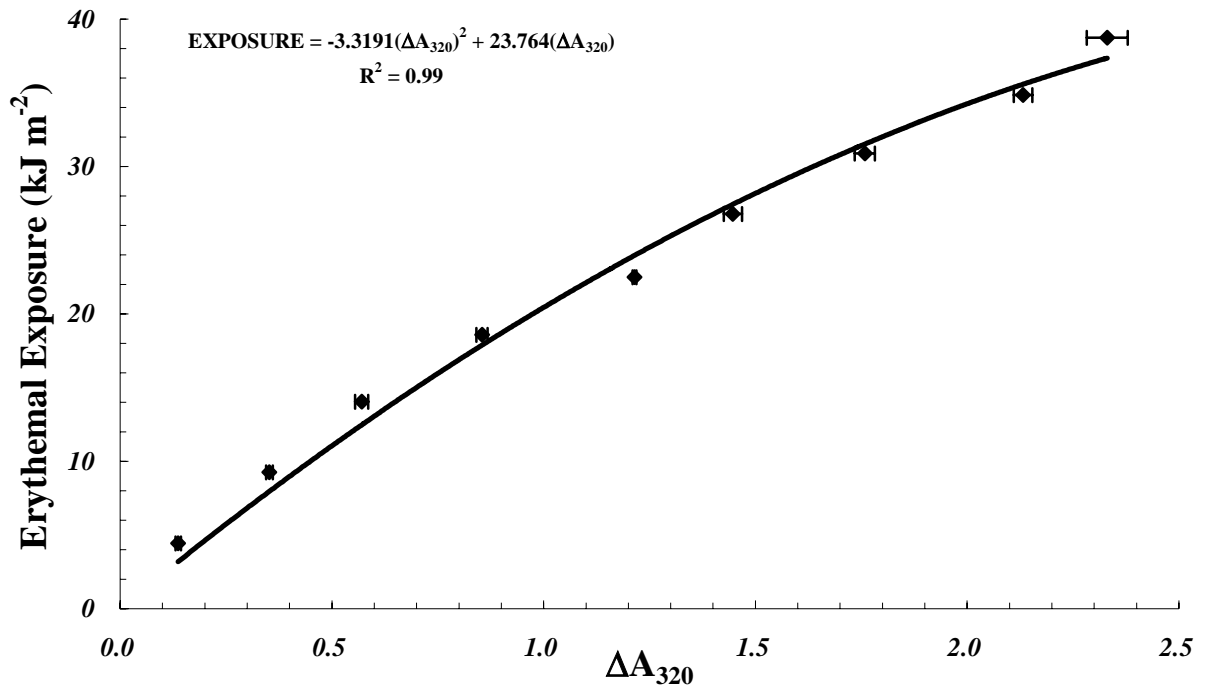


Figure 5.5: An example horizontal plane PPO film dose – response calibration made in autumn to the erythemally active wavelengths.

Turnbull & Schouten (2008) have presented data showing that PPO can also be employed to take accurate measurements of solar UVA exposures. In this research the PPO dosimeter was coupled with a simple mylar filter which blocked any UVB energy from reaching the film surface during exposure time. From this a calibration linking changing optical absorbance brought on by incident UVA wavelengths and UVA exposure measured by a scanning spectroradiometer was compiled during the months of autumn. This calibration is presented in Figure 5.6. It was found that the

PPO film in combination with the mylar filter was capable of measuring UVA exposures of potentially greater than 20 MJ m⁻² at a level of uncertainty no greater than ± 5%.

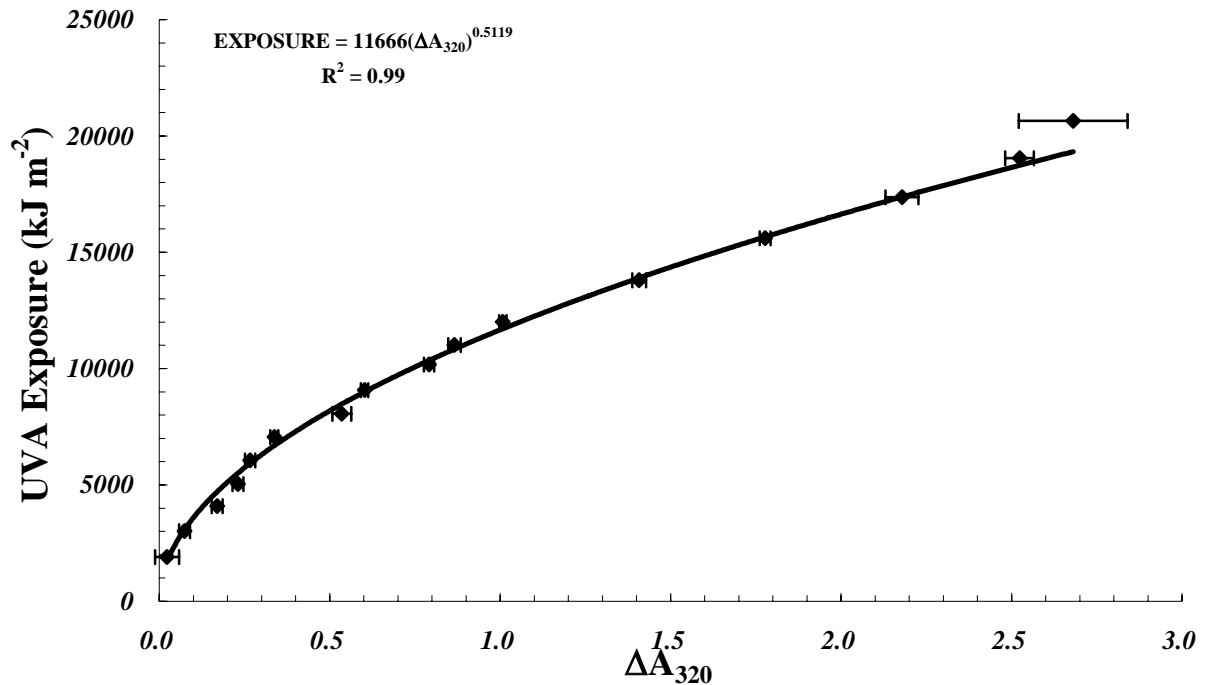


Figure 5.6: The horizontal plane PPO film dose – response calibration made in autumn to the UVA.

5.4 Analysis of the PPO Dosimeter in a Controlled Clear Water Environment

5.4.1 Water Tank, Irradiation Source Description and Water Analysis

The water tank used in the testing of the dosimeter had a length of 51 cm, a width of 37 cm and a depth of 30 cm. The water tank was painted matt black and was covered over by black felt in order to stop any outside stray light from penetrating the water. The UVB source employed was a fluorescent UV lamp (model FS40/12, Philips, Lawrence & Hanson, Toowoomba, Australia) covered by a long strip of cellulose acetate. This material was used to block out the UVC wavelengths emitted by the

lamp. The lamp was suspended in place over the top of the tank at a distance of 18 cm from the water surface. All subsequent tests on the PPO dosimeter, apart from the watermark effect test and the reaction to UVA and visible exposure test were conducted in this tank with this particular configuration.

The water used was clear tap water, kept free of any floating particulates. For all of the experiments in the controlled environment, UVB was defined as the waveband running from 298 to 320 nm. As mentioned in Section 4.4, the 320 nm cut – off has sometimes been employed by photobiologists and was deemed to be more applicable to the spectral response of the PPO film. The water remained completely stable, with no mixing or any kind of surface disturbance occurring during the duration of each experiment. The water temperatures measured in the tank during each of the experiments ranged from 12 °C to 23 °C as the tests were carried out throughout the autumn and winter months.

5.4.1.1 Dose – Response

The PPO dosimeter was calibrated for unweighted UVB exposure from 298 nm to 320 nm at two different depths in conjunction with the immersion effect corrected IL1400. The depths were 1 cm below the surface (Z_{1CM}) and 16 cm below the surface (Z_{16CM}). The PPO dosimeter was also calibrated just above the water surface in conjunction with the IL1400 calibrated for in – air conditions. In order to derive each calibration curve, batches of PPO dosimeters were exposed to the UVB source on a horizontally aligned surface for a total time of 35 hours. The exposure (measured in kJ m^{-2}) was measured at specific intervals with the IL1400. After each interval, the change in optical absorbance at 320 nm (ΔA_{320}) for each PPO dosimeter was

measured in the spectrophotometer to provide a data point. After their absorbencies were measured, the dosimeters were placed back into the water for further exposure. It is important to note that the response spectra of the IL1400 and the PPO film are different. The calibrations against each other and the spectroradiometer will only be applicable for the source spectrum employed in the calibration. The $\pm 5\%$ uncertainty of the spectroradiometer together with an estimated IL1400 transfer calibration error of $\pm 3\%$, an immersion factor uncertainty of $\pm 3\%$ and a $\pm 3\%$ final transfer uncertainty to the PPO dosimeter combine to give a total $\pm 14\%$ uncertainty in the PPO film calibration routine. This total uncertainty measurement should only be regarded as a simple approximation as the procedure of adding different error components together to produce an overall error value can sometimes lead to a sizeable overestimate of the actual mean error if the individual sources of error are not linked in any way. Therefore, in future studies using the PPO dosimeter a more accurate total uncertainty estimate should be made by finding the root mean square of all the separate errors.

By analysing the dose – response calibrations made at the two depths, it can be determined if the UVB calibration of the PPO dosimeter is reasonably the same in shallow water and if these shallow water dose – response calibrations differed at all from the surface calibration. The dose – response calibrations for PPO film on a horizontal plane at the water surface and at depths of 1 cm and 16 cm are presented in Figure 5.7. A calibration equation in polynomial form has been fitted to the calibration data at the surface and at each depth. For the surface calibration, the equation is

$$UVB_{SURFACE} = 199.24(\Delta A_{320})^2 + 174.76(\Delta A_{320})$$

with an R^2 value of 0.99 and where $UVB_{SURFACE}$ is the UVB exposure received at the water surface in units of kJ m^{-2} . For the calibration made at $Z = 1 \text{ cm}$ the equation is

$$UVB_{Z1cm} = 164.17(\Delta A_{320})^2 + 142.49(\Delta A_{320})$$

with an R^2 value of 0.99 and where $UVB_{Z1 \text{ cm}}$ is the UVB exposure received at a depth of 1 cm in units of kJ m^{-2} . For the calibration made at $Z = 16 \text{ cm}$ the equation is

$$UVB_{Z16cm} = 146.02(\Delta A_{320})^2 + 149.76(\Delta A_{320})$$

with an R^2 value of 0.99 and where UVB_{Z16cm} is the UVB exposure received at a depth of 16 cm in units of kJ m^{-2} .

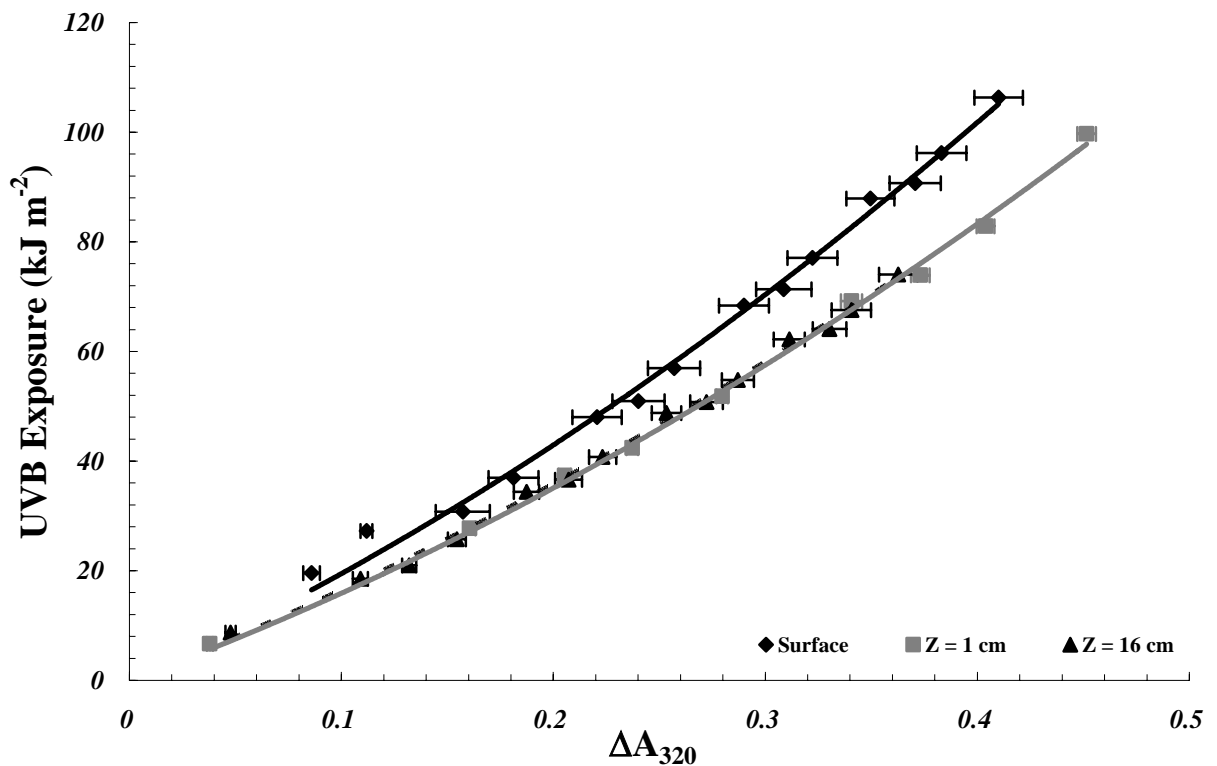


Figure 5.7: Horizontal plane PPO film calibrations of the dose – response at the water surface and at $Z_{1\text{CM}}$ and $Z_{16\text{CM}}$. The error bars represent 1δ for each of the calibrations.

The dose – response calibrations performed with the UVB source in the ideal clear water environment at the shallow depths of Z_{1CM} and at Z_{16CM} are almost completely interchangeable. However, these two dose – response calibrations do differ significantly from the dose – response calibration made at the water surface, and this difference becomes magnified with increasing levels of exposure. For instance, a discrepancy as large as 19 kJ m^{-2} exists between the dose – response calibrations at the water surface and at Z_{1CM} after a recorded ΔA_{320} of 0.4. This suggests that an in – air calibration could not be applied to calculate exposures recorded by PPO film in underwater environments without considerable errors coming into play. So it is advised that before any measurement campaign is performed in an underwater environment in the field, that at least one dose – response calibration is performed in combination with an immersion effect corrected radiometer in a tank at an arbitrary depth in a sample of water taken from the actual site. Additionally, the calibrations performed between the radiometer and the PPO film should only be used to measure exposures from the spectrum that they have been calibrated to in order to minimize errors. It should also be noted that the three calibration regimes seen in Figure 5.7 tend to curve upward with increasing exposure to a final ΔA_{320} value of about 0.5 coinciding with a UVB exposure of approximately 100 kJ m^{-2} . However, the long – term calibration regimes displayed in Figure 5.5, Figure 5.6 and in Chapters 6, 7 and 8 for both the in – air and underwater environments distinctly show that PPO film calibrations have a natural tendency to saturate with increasing exposure, gradually becoming more pronounced after reaching an approximate ΔA_{320} value of 1. Therefore, it is expected that if the PPO dosimeters used in calibrations shown in Figure 5.7 were to be further irradiated by the artificial UV source the calibrations would also eventually begin to saturate.

5.4.1.2 Cosine Response

As is the case in air, the solar UV in water arrives at a receiving plane in two components, namely the direct and the diffuse components. The direct component propagates in a direct path from the sun, while the diffuse component is scattered in a multitude of different directions by various waterborne constituents. Therefore, the response of the PPO dosimeter to UV wavelengths incident at different inclinations in water must be detailed. PPO dosimeters were aligned to a series of angles running in 10° increments from 0° through to 80° with each of their centre points in alignment to a horizontal axis. The error for each of these angular alignments was estimated to be within $\pm 2^\circ$. The dosimeters were then exposed to 35 hours of cumulative UVB exposure at a depth just below the water surface. Following this, the ΔA_{320} for each dosimeter was normalised using a previously calculated dose – response calibration and compared directly to the cosine function. The absolute error (AE) for the cosine response was calculated at each angle as the magnitude of the difference between the cosine function and the angular ΔA_{320} response normalised to a horizontally aligned ΔA_{320} response using the expression:

$$AE(\theta) = \left| \cos(\theta) - \frac{A[(\Delta A_{320})_z^\theta]^2 + B[(\Delta A_{320})_z^\theta] + C}{A[(\Delta A_{320})_z^{HORIZONTAL}]^2 + B[(\Delta A_{320})_z^{HORIZONTAL}] + C} \right|$$

where θ is the angle at which the dosimeter was positioned relative to the horizontal plane during exposure, A , B and C are calibration coefficients, z is the depth at which the dosimeter was exposed and *HORIZONTAL* represents the horizontal plane (where $\theta = 0^\circ$). The normalised underwater cosine response for the PPO dosimeter is shown in Figure 5.8. The cosine error varied from 4% to 22% for angles smaller than 80° .

Before usage in an underwater environment, it may be necessary to perform a cosine response test in a controlled environment on the particular batch of PPO film to be used. This data could then be used to calculate appropriate cosine correction factors that when applied, would minimize measurement errors arising from inherent errors in the angular response of the PPO film. Before the calculation of the cosine correction factors, the angular distribution of the incoming radiation in the respective underwater environment must be known. A general estimate of the correction required can be made by assuming that the distribution of radiation in the particular underwater environment is isotropic. The cosine response means that errors can occur not only in the exposures measured by tilted dosimeters, but also in exposures measured by dosimeters aligned to the horizontal plane within an environment where diffuse UV is present.

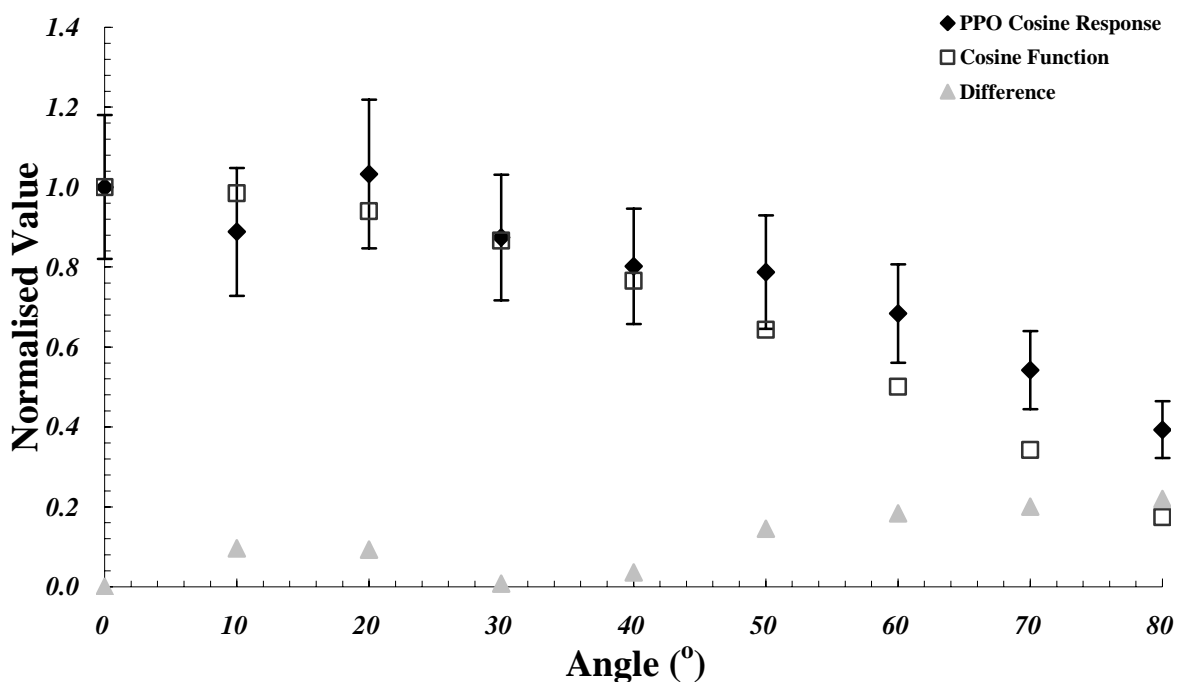


Figure 5.8: PPO dosimeter cosine response underwater at an arbitrary depth. The y – error bars represent the cumulative $\pm 9\%$ in – water interdosimeter variation following normalisation.

5.4.1.3 Independence of Dose Rate

If dose rate independence exists for the PPO dosimeter underwater, a high UVB irradiance accumulated over a short time period will deliver the same ΔA_{320} value as would be measured for a low UVB irradiance accumulated over a long period of time. To verify underwater dose rate independence, a short period high irradiance (D_1) was delivered to a batch of 15 dosimeters at Z_{1CM} over a time span of 14 hours. After this, a long period low irradiance (D_2) was delivered to another batch of 15 dosimeters at Z_{1CM} , this time having the UVB source elevated to approximately twice the height above the tank. This trial was carried out over the period of time necessary so that both exposures were equal. The respective ΔA_{320} values from each batch were then measured and compared.

The in – water interdosimeter variation for the PPO dosimeter was calculated using the same batches of dosimeters as used for the dose rate independence test. The mean and standard deviation of the ΔA_{320} for each dosimeter across four positions of the film surface was calculated and then used to find the coefficient of variation (CV) for the entire sample. This CV was then converted to a percentage value called the in – water interdosimeter variation error. Lester *et al* (2003) calculated an in – air interdosimeter variation error of approximately 6%. It was anticipated that this error will be higher for underwater measurements due to the influence of watermarking on the PPO film surface.

After a total exposure of 76 kJ m^{-2} received during the initial 14 hour time period and the consequent 23 hour time period for the high and low irradiances respectively, the ΔA_{320} values measured across the two batches of PPO dosimeters, were found to vary

by approximately 16% after averaging. Using this data, the in – water interdosimeter variation for the PPO dosimeter was calculated to be approximately 9%, which is 3% higher than the value previously calculated for measurements in – air (Lester *et. al.*, 2003). However, it is expected that this variation estimate would increase if the PPO dosimeter were to be employed in an underwater environment of high turbidity, as strong watermarking effects and film damage would possibly occur.

As mentioned in the paragraph above, the dose rate independence data showed that a statistical variance in the order of $\pm 16\%$ for measured ΔA_{320} values over different batches of PPO dosimeters may occur for similar underwater exposures after varying periods of time. This is a reasonable level of dose rate independence. To keep these uncertainties to a minimum, the calibration dosimeters should be exposed to the source spectrum over a number of days, so that a wide variety of high and low dose rates will be employed in the calibration and accounted for.

5.4.1.4 Dark Reaction

The optical density of chemical film dosimeters is known to continue to change during storage after an exposure to solar radiation (Davis *et al*, 1976). The inherent dark reaction for PPO film was quantified by measuring the overnight change in optical density each day for a series of underwater exposures each with varying dosages taken over a time period of five days.

The overnight dark reaction data (Figure 5.9) shows that the percentage ratio between the dark reaction ΔA_{320} value (measured in the morning of each day before exposure) and the cumulative ΔA_{320} value (measured as the accumulation of the increase in

optical absorbency within the PPO film from day to day) decreases as the cumulative UVB exposure increases. This means that the effect that the inherent dark reaction has upon the PPO film is gradually reduced over time assuming that there is increasing incident dosage. This overnight dark reaction trend has been fitted with a linear fit of the following form

$$\% \Delta A_{320} = -0.0705(UVB) + 12.348$$

with an R^2 value 0.7 and where UVB is the UVB exposure received at the particular depth in units of kJ m^{-2} .

The dark reaction will influence measurements recorded by a PPO dosimeter for exposures lasting longer than one day, with the effect of the dark reaction gradually decreasing over time with increasing exposure. The effect of dark reaction on the PPO dosimeter can be nullified if a dose – response calibration is carried out continuously over several days time as necessary before measurements are made in an underwater field environment so that naturally occurring random cloud variations and patterns are taken into account by the resulting calibration data. As the dose dependent dark reaction can not be measured each day at a field location, this calibration should be carried out in the season in which the dosimeters will be used. The calibration for each season will minimise the change in dark reaction caused by the variation in dose rates from day to day. This way, any over – estimations of the total exposure caused by the overnight dark reaction are taken into account within the dose – response calibration.

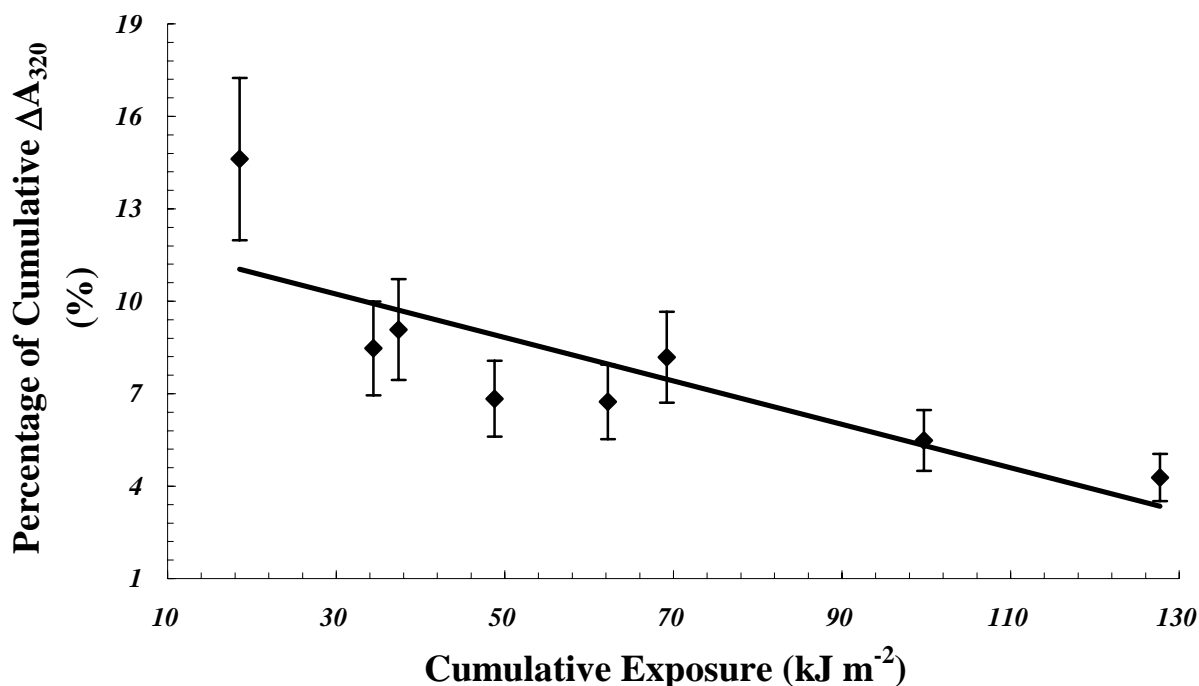


Figure 5.9: Overnight dark reaction data shown as a percentage of the cumulative ΔA_{320} value measured as the accumulation of the increase in optical absorbency within the PPO film after each daily exposure. The y – error bars represent the cumulative $\pm 9\%$ for the in – water interdosimeter variation.

5.4.1.5 Reaction to UVA and Visible Wavelengths

The PPO dosimeter's responsivity to both the visible (400 to 700 nm) and UVA (320 to 400 nm) waveband was quantified by employing both a visible and UVA waveband transmitting filter (mylar film, Cadillac Plastics, Australia) and a visible waveband transmitting filter (ST70A Sheeting, Bekeart Plastics, Australia). The mylar filter has been successfully used in previous research on top of phenothiazine dosimeters to block out UVB wavelengths (Parisi *et al*, 2005). As mentioned in Section 5.3.1, it has also been employed by Turnbull & Schouten (2008) for use with the PPO dosimeter. Two sets of PPO dosimeters, each covered by one type of filter were exposed to full sunlight over the space of five days in conjunction with an

unfiltered PPO dosimeter. At the conclusion of this time period any ΔA_{320} response caused by either UVA or visible wavelengths were detected and averaged and then compared to the unfiltered ΔA_{320} response. Ratios between the filtered and unfiltered responses were calculated to estimate the percentage effect that the respective visible and UVA wavelengths have upon the PPO dosimeter. Also, in these experiments an interdosimeter variation of 7% was estimated to occur amongst the PPO dosimeters for in – air measurements, roughly 1% higher than the in – air interdosimeter variation calculated by Lester *et al* (2003). This 7% in – air interdosimeter variation estimate will be used as the uncertainty margin for all consequent in – air measurements made with the PPO dosimeter in this dissertation.

From Figure 5.10 it can be seen that over the five day exposure period, the PPO film did not respond at all to visible wavelengths. However, a progressively increasing response to UVA wavelengths over time does occur. After 60 hours cumulative exposure time to full sunlight, the ΔA_{320} of the PPO film to UVA reaches a significant 19% of the total ΔA_{320} as measured from the unfiltered PPO film. The percentage ratio between the PPO unfiltered response and UVA response has been modelled as the following polynomial expression

$$\% \left(\frac{UVA_{RESPONSE}}{TOTAL_{RESPONSE}} \right) = -0.0009t^2 + 0.3927t$$

having an R^2 value of 0.93 and where $TOTAL_{RESPONSE}$ is the unfiltered ΔA_{320} value, $UVA_{RESPONSE}$ is the ΔA_{320} value measured after solar radiation exposure under the mylar film filter and t is the cumulative solar radiation exposure time given in hours. The results show that the PPO film could be used as a shortwave UVA (320 to 340 nm) dosimeter with the use of an appropriate UVB filter material. Previous research

by Lester *et al.* 2003 has shown that the normalized spectral response of PPO film to UVA decreases to less than 0.001 at 340 nm. So it is assumed that the induced change in optical absorbance caused by wavelengths higher than 340 nm can be regarded as negligible effectively making the UVB filtered PPO film a viable shortwave UVA dosimeter for both in – air and underwater applications. Although there is a small response to the shortwave UVA, the majority of the spectral response is in the UVB. Consequently, the PPO film can be used as a UVB dosimeter provided it is calibrated appropriately.

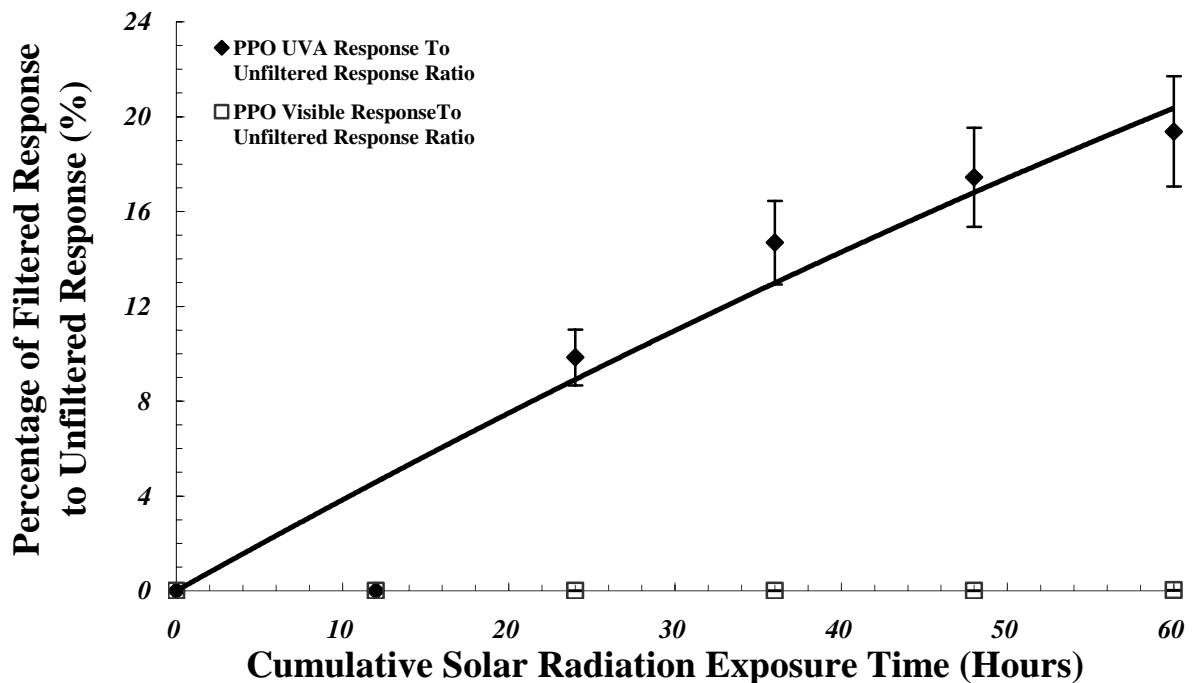


Figure 5.10: PPO film reaction to UVA and visible wavelengths on a horizontal plane after 60 hours total exposure to sunlight given as a percentage ratio. The y – error bars represent the predicted cumulative $\pm 7\%$ in – air interdosimeter variation.

5.4.1.6 Watermarking Effects

Using a temperature controlled water vessel (Grant Instruments, Cambridge), several sets of PPO dosimeters were submerged in clear stable water at a depth of 1 cm for three different temperatures without being exposed to any UV radiation. These

temperatures ranged in 20 °C increments from 0 °C up to 40 °C, which are assumed to be the minimum and maximum temperatures that would be measured throughout the year in various marine environments such as lakes and creeks found within subtropical locations. The dosimeters were submerged in the water vessel for a total of five days (120 hours in total). The ΔA_{320} value measured for each dosimeter at the end of each day was compared to an average daily ΔA_{320} value of 0.12 taken from the data set measured for the UVB dose – response calibration at Z_{1CM} . From this data any measurement errors caused by minor watermarking on the PPO film surface could be detected and quantified.

Figure 5.11 shows the percentage ratio of the daily watermark effect measurement to the average daily ΔA_{320} value over a time period of 120 hours. It appears that an increase in submersion temperature results in a measurable increase in the watermark induced ΔA_{320} value. For example, after 120 hours immersion time in 40 °C water, the accumulated watermarking on the PPO film would account for approximately 9% of the average daily ΔA_{320} value as measured in the tank.

The watermark effect results do indicate that special cleaning procedures may be necessary after the usage of PPO film underwater in order to reduce errors in the recorded ΔA_{320} value. One suggested method could be to not dry the PPO dosimeters using any kind of cloth or towel, as this could smear out watermarks and increase their effective area on the film surface, but to clean them with a blast of distilled water and leaving them to dry in a dark room, being careful not to crack or dent the film in any way. Before measurement in a spectrophotometer, each particular film should be visually inspected and checked for any remaining watermarks. If there is still some

watermarking remaining on a film's surface, the cleaning process should be repeated again.

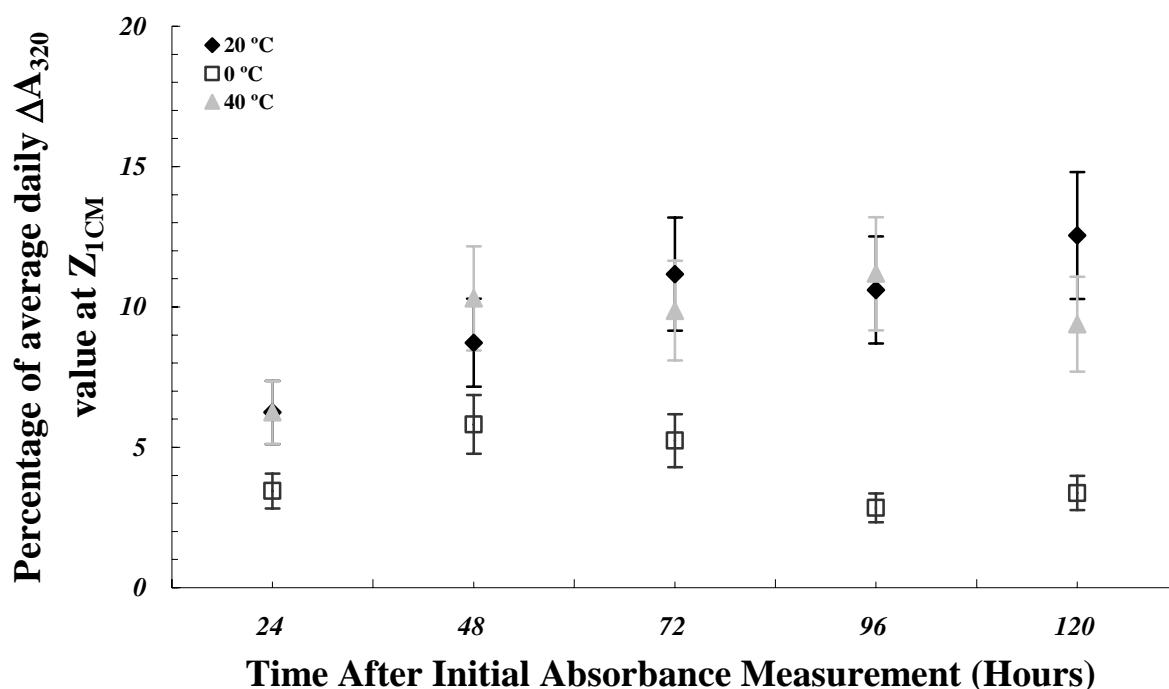


Figure 5.11: Percentage ratio of the daily watermark effect measurement to the average daily ΔA_{320} value. The y – error bars represent the cumulative $\pm 9\%$ for the in – water interdosimeter variation.

5.4.1.7 Additivity of Exposures

For the PPO dosimeter it was unclear whether multiple absorbance measurements made over a particular exposure interval have an effect on final ΔA_{320} values in comparison to a single absorbance measurement made after the same exposure interval. In order to test this, a batch of PPO dosimeters were exposed underwater to the fluorescent UV lamp at Z_{1CM} over a time span of 35 hours. Half the batch (batch A) was measured three times a day in the spectrophotometer, while the other half (batch B) were left untouched until they were measured upon the completion of the

test. An average ΔA_{320} value was then calculated individually for batch A and batch B. Following this, these two average ΔA_{320} values were compared against each other. A percentage difference of approximately 8% was calculated to exist between the average ΔA_{320} values as measured for batch A and batch B after a total UV dosage of 309 kJ m^{-2} accumulated during the 35 hour long exposure. This percentage difference falls within the 9% interdosimeter variation limit. So it appears that multiple measures of absorbance do not have any considerable influence upon final ΔA_{320} values.

5.5 Chapter Discussion

The results from this chapter confirm that PPO film can be employed as a high exposure solar UV dosimeter in underwater applications. If calibrated correctly using the proper techniques, the uncertainty in the usage of the PPO film for underwater applications is estimated to range from $\pm 15\%$ to an upper limit of $\pm 20\%$ taking into account all errors involved with transfer calibrations and the variation of the optical properties of the PPO film itself. The next stage of development described in the following three chapters will be to calibrate PPO dosimeters against the solar UV using a neutral density filter in order to extend its operational lifetime and to also calibrate and deploy the PPO dosimeter for use in three different marine environments, each having their own characteristic turbidity and DOC concentration. From this, underwater exposures recorded using the PPO dosimeters will then be compared to solar UV measurements made in the same conditions with a spectrometer at comparable solar zenith angles throughout different seasons of the year to verify the suitability of the PPO dosimeters for measurement of high UV exposures underwater.

Chapter 6

Testing of a Neutral Density Filter and Seasonal Calibrations with the PPO Dosimeter

6.1 Introduction

As Chapter 5 has shown, the PPO dosimeter is capable of measuring long – term cumulative amounts of UV exposure. However the exposure lifetime of the PPO dosimeter can be extended drastically by the use of a neutral density filter (NDF). An NDF is simply a piece of material that is attached to the top side of a dosimeter that is only partially transparent to UV wavelengths. Parisi & Kimlin (2004) have used a NDF based on developed black and white photographic film to extend the dynamic range of the polysulphone dosimeter by as much as six times beyond its usual limit. The first section of this chapter continues this research and describes how a polyethylene NDF can be calibrated and used successfully with the PPO dosimeter in order to continuously measure in – air solar sun burning (erythemal) exposures over the space of a month in low SZA conditions without the need for replacement.

Several studies such as Bodhaine *et al* (1998) have comprehensively detailed how fluctuations in atmospheric parameters and seasonal changes in SZA can have a detrimental impact upon the accuracy of radiometric instrumentation. However, there has been very few studies carried out in the past that have extensively investigated the influence of changing SZA along with variable atmospheric constituents such as column ozone upon dosimetric calibration regimes. A study was performed by Krins *et al* (2001) where polysulphone was calibrated to solar exposures over the space of two years in Munich, Germany. From this work it was discovered that by factoring seasonal stratospheric ozone patterns along with local SZA variation into the calibration data, total exposure measurement errors could be reduced by as much as 23%. Kollias *et al* (2003) has employed the polysulphone dosimeter to measure solar UVB variations over the time frame of several years in the northern hemisphere. The

researchers found that there was a seasonal shift between the UVB data measured with the polysulphone dosimeter and synthetic UVB data derived from a model produced originally by Kollias, Baqer & Sadiq (1988). Fluctuations in total atmospheric column ozone thickness occurring during the measurement campaign were believed to have been one of the main contributing factors behind this seasonal shift along with the eccentricity of the Earth's orbit and the tilt of the Earth's axis to the orbital plane. Following up on the initial work detailed by Krins *et al* (2001) and Kollias *et al* (2003), Casale *et al* (2006) extensively calibrated the polysulphone dosimeter over each season at three different field locations throughout Italy. The results from this campaign showed that a strong correlation was present between variations in the calibration profiles and variations in total column ozone levels along with SZA. At this point in time no study has analysed the effect of SZA and atmospheric column ozone upon the response of the PPO dosimeter. Prior to testing the dosimeter underwater in the subsequent chapters, the second half of this chapter will directly address this issue and will show that in – air calibrations of the PPO dosimeter to solar exposures are susceptible to atmospheric and SZA variability and change in a similar way compared to the polysulphone dosimeter.

6.2 Neutral Density Filter Testing with the PPO Dosimeter

6.2.1 Neutral Density Filter Properties

After an initial analysis, it was decided that polyethylene sourced from common waste bags would be used as the NDF material. Three possible candidates for the polyethylene based NDF material were chosen primarily due to their availability in local supermarkets and also because of their ability to withstand the elements of

nature such as wind and rain without succumbing to critical amounts of damage. These candidates were the Multix, Coles Reliance and Savings waste bags. The transmission and absorption spectra as measured for each of these waste bags is depicted in Figure 6.1 using the same spectrophotometer and equations as described in Section 5.2.2. In Figure 6.1 it can be seen that the Coles Reliance waste bag offered the lowest amount of UV transmission with a reading of 2.38% at 315 nm in comparison to 2.98% at 315 nm for the Multix waste bag and 5.29% for the Savings waste bag. The Coles Reliance waste bag also had the highest amount of UV absorption with a measurement of 1.6 at 315 nm followed by the Multix waste bag with the next highest level of 1.53 at 315 nm with the Savings waste bag having the lowest UV absorption measurement of 1.28 at 315 nm. From this data the Savings waste bag material was selected as the NDF source that was to be used in the trials. The reasoning behind this was that even though the Savings waste bag had higher UV transmission and lower UV absorption properties in comparison to the other two waste bags, hence making it more transparent to UV wavelengths, it did have near linear characteristic transmission and absorption spectra across the UV waveband for which the PPO dosimeter is most responsive (approximately 300 nm to 340 nm) which the other two waste bags did not have. This attribute of the Savings bag was desirable as it allowed for equal amounts of solar energy to be filtered through to the PPO dosimeter at each wavelength, leading to the reduction of measurement uncertainty that could be brought on by changes in the incident solar UV spectra.

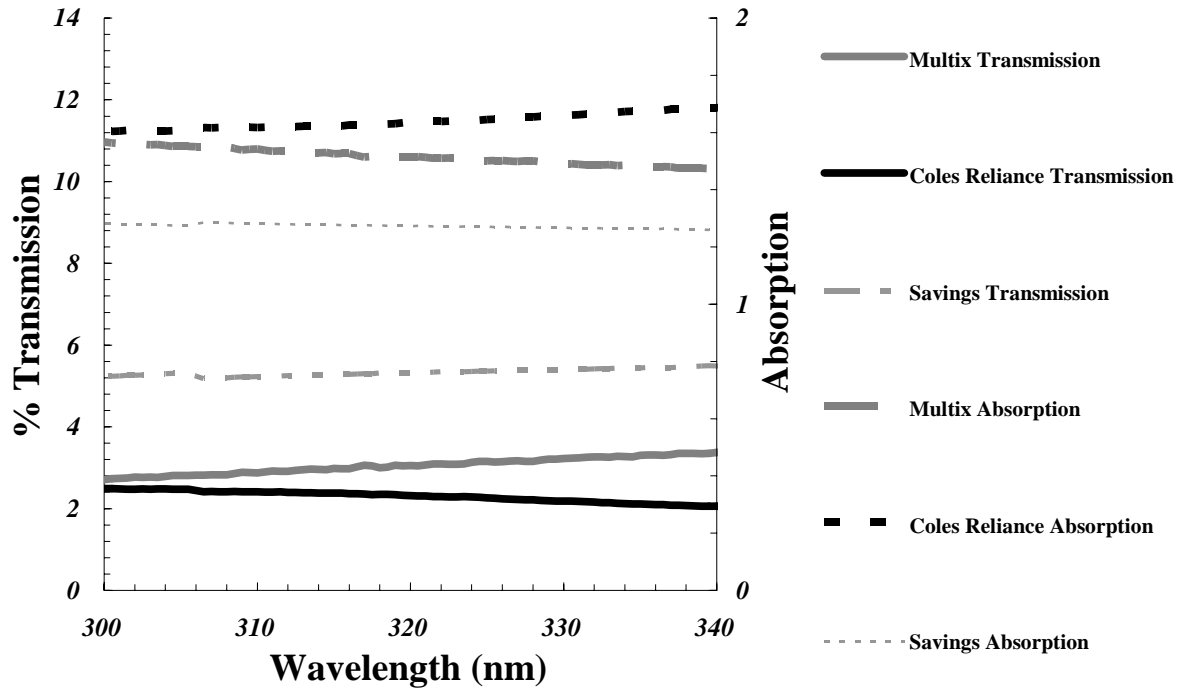


Figure 6.1: Transmission and absorption spectra across the waveband running from 300 nm to 340 nm for the Multix, Coles Reliance and Savings waste bags.

Figure 6.2 details the spectral transmission and absorption of the Savings waste bag after an equivalent solar erythemal dosage of 45 kJ m^{-2} , which equates to approximately 30 days solar exposure in mid autumn at the measurement location. From Figure 6.2 it is clear that the optical properties of the Savings waste bag do change slightly after exposure to a substantial amount of solar energy. For example, at 315 nm a difference of 3.5% is present between the pre and post exposure transmission spectra. Also at the 315 nm point, a difference of 0.08 between the pre and post exposure absorption spectra was measured to occur. These changes are taken into account in the calibrations.

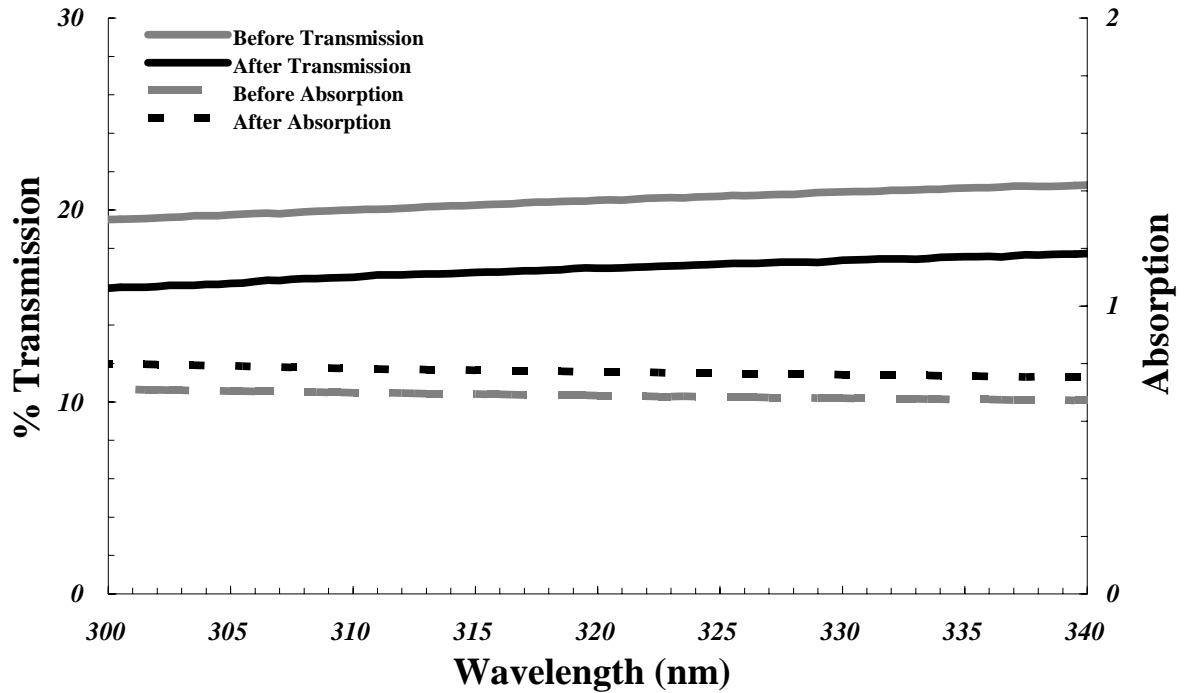


Figure 6.2: Transmission and absorption spectra across the waveband running from 300 nm to 340 nm for the Savings waste bag after a solar erythemal exposure of 45 kJ m^{-2} .

6.2.2 PPO Dosimeter and Neutral Density Filter Calibrations

The NDF and PPO dosimeter system was produced by cutting out a 1.3 cm x 1.7 cm piece of Savings waste bag material and attaching it to a PPO dosimeter by using standard electrical tape. The calibrations were performed on site at the University of Southern Queensland campus in Toowoomba, Australia (27.5° S, 151.9 ° E, 693 m altitude) using integrated measurements obtained every five minutes using the Solar Light UV broadband meter calibrated to the Bentham Spectroradiometer as described in Section 4.3.4. The first NDF and PPO dosimeter calibration series (Calibration A) ran from 5 March 2008 until 28 April 2008, while the second series (Calibration B) ran from 29 April 2008 to 27 May 2008. The dosimeters were left out for approximately seven hours each day. The response of the dosimeters in these series

was calibrated to the erythral action spectrum with respect to the horizontal plane. The erythral action spectrum is discussed in further detail in Section 6.3. A single filtered dosimeter (with an attached NDF) was removed from solar exposure every second day and a single unfiltered (without an attached NDF) dosimeter were removed from solar exposure each day during the measurement campaign. For Calibration A, the last remaining filtered and unfiltered dosimeters were left out until they were dark orange in colour, which for PPO film is a visual indication that complete optical saturation is about to take place. For Calibration B, the final filtered and unfiltered dosimeters were removed before the beginning of winter. The same numbers of filtered and unfiltered dosimeters were used in both Calibration A and Calibration B. The variation of the daily total erythral UV exposures received by the NDF and PPO dosimeters over the autumn months as measured by the Solar Light UV broadband meter calibrated to the Bentham spectroradiometer is provided in Figure 6.3. Figure 6.4 details the ozone levels detected by the OMI satellite above Toowoomba during the NDF trial period from March to May 2008. Across both of the calibration trials, local cloud coverage ranged from 0 to 8 okta.

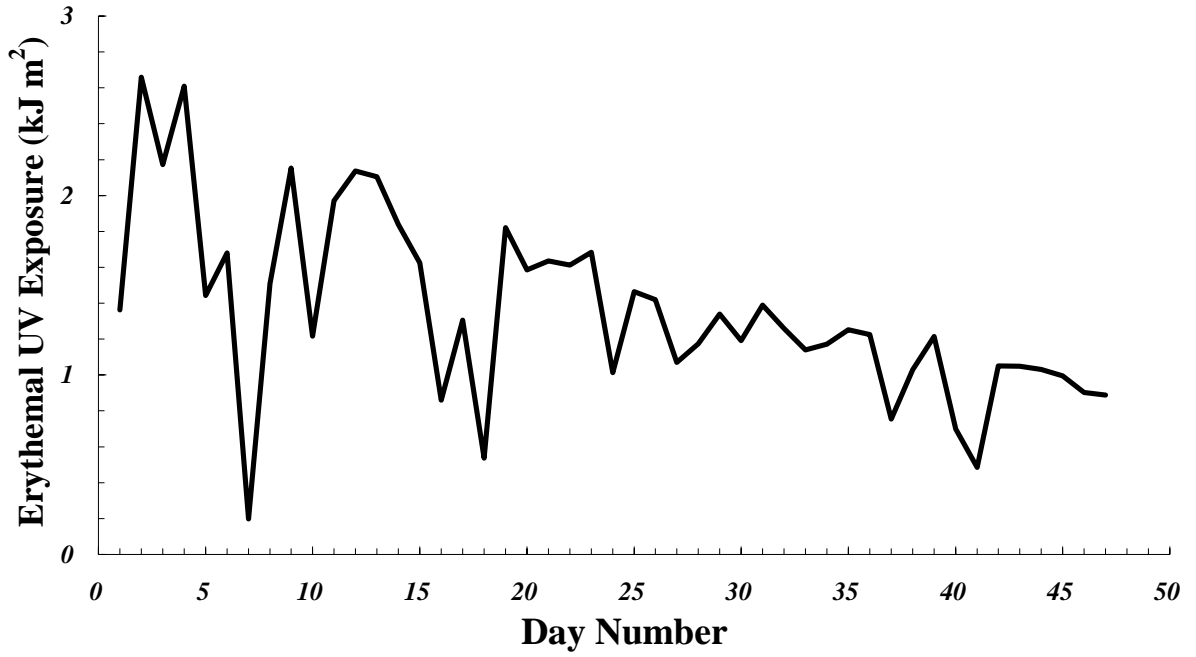


Figure 6.3: The variation of the erythemal UV exposures received by the NDF and PPO dosimeters during autumn.

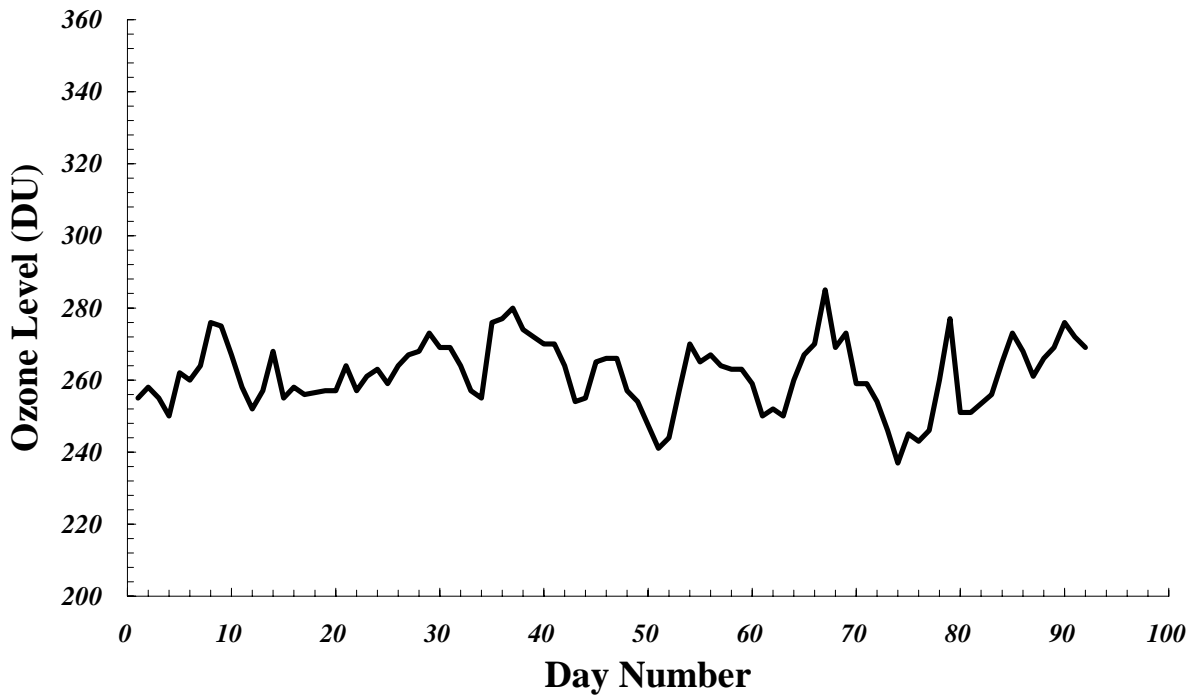


Figure 6.4: Ozone levels detected by the OMI satellite above Toowoomba during the NDF trial period (March to May 2008).

The data sets obtained for each of the filtered and unfiltered trial calibrations were fitted with second – order polynomial equations passing through the origin. The equation obtained for the Calibration A unfiltered series was:

$$UV_{ERY} = 2.85(\Delta A_{320})^2 + 14.10(\Delta A_{320})$$

with an R^2 value of 0.96 and with UV_{ERY} measured in kJ m^{-2} . For the Calibration A filtered series the calibration equation was:

$$UV_{ERY} = -1.57(\Delta A_{320})^2 + 21.58(\Delta A_{320})$$

having an R^2 value of 0.93 and UV_{ERY} given in kJ m^{-2} . The calibration equation for the Calibration B unfiltered series was given as:

$$UV_{ERY} = 8.5(\Delta A_{320})^2 - 5.86(\Delta A_{320})$$

with an R^2 value of 0.84 and UV_{ERY} once again measured in units of kJ m^{-2} . The final equation produced was for the Calibration B filtered series and it was as follows:

$$UV_{ERY} = 15.11(\Delta A_{320})^2 - 9.99(\Delta A_{320})$$

where the R^2 for this fit was 0.93 and with UV_{ERY} provided again in units of kJ m^{-2} .

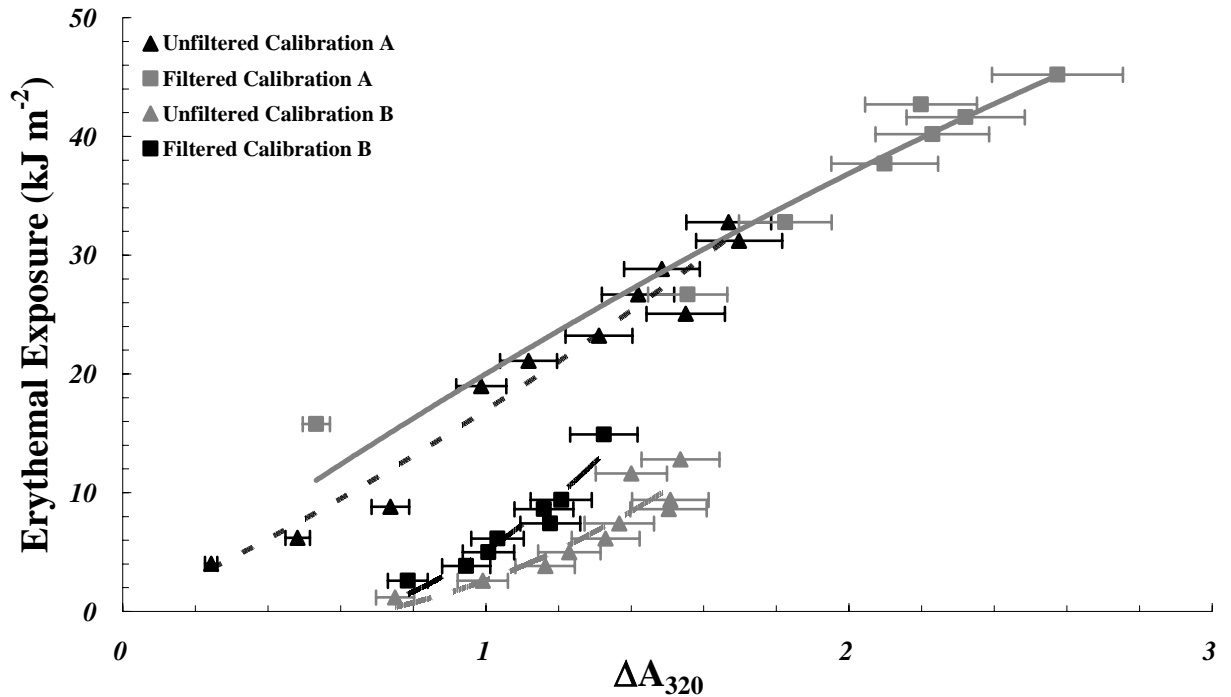


Figure 6.5: Erythemal calibrations for the filtered and unfiltered PPO dosimeters over the months of autumn.

6.3 Seasonal In – Air Erythemal Calibrations of the PPO Dosimeter

The calibrations for this investigation were again made at the University of Southern Queensland campus in Toowoomba, Australia over 12 months from March 2007 through to February 2008 inclusive. The SZA range for the autumn calibrations was 20° to 70° . The SZA range for the winter calibrations was 35° to 65° . The SZA range for the spring calibrations was 8.4° to 53° . The SZA range for the summer calibrations was 5.5° to 44° . Each calibration series ran for seven days in total. The dosimeters were exposed to the sun for approximately seven hours per day. Cloud coverage varied from 0 to 8 okta over the year – long trial period. As explained in the introduction, the calibrations were made for the PPO dosimeter over all four seasons so that the effect of different atmospheric column ozone levels and changing SZA on the response of the PPO dosimeter could be fully quantified. Four separate calibration

campaigns were carried out in each season in order to produce a substantial amount of data from which seasonal complete calibration data sets could be formulated. These complete calibrations are discussed in further detail in Section 6.3.1. A time series of the erythemal UV exposures measured every day over the in – air erythemal PPO dosimeter calibration measurement campaign is presented in Figure 6.6, with day 1 being the 12th of march 2007 and day 105 being the 20th of February 2008.

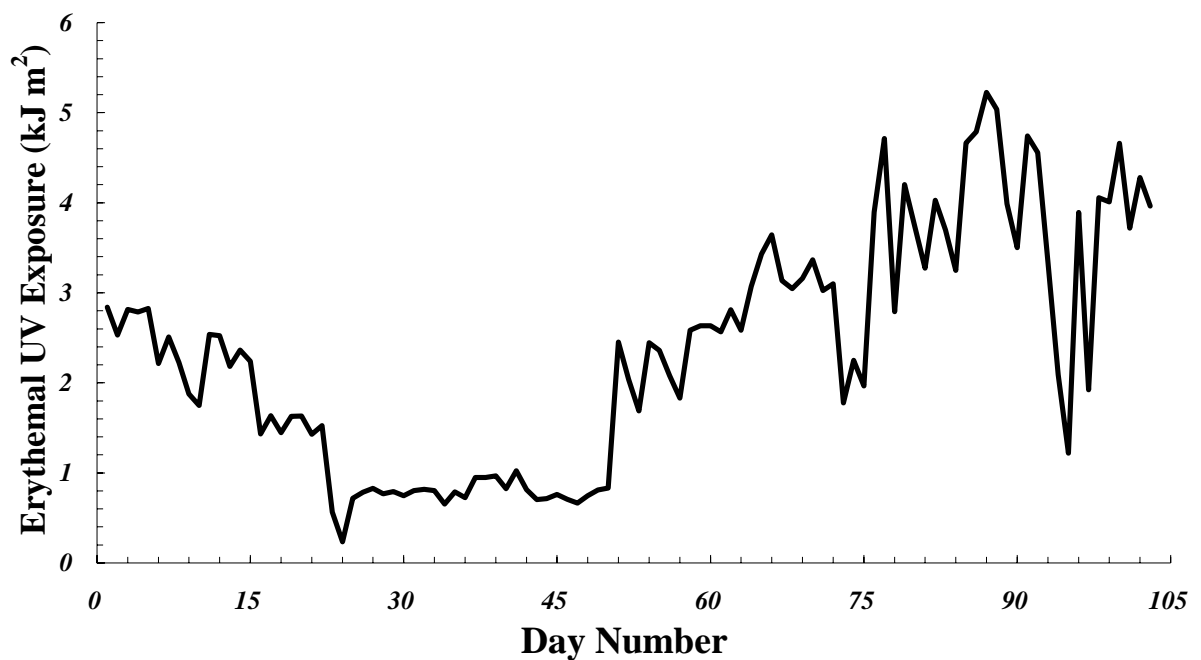


Figure 6.6: A time series of the in – air erythemal UV exposures measured over each day during the PPO dosimeter calibration measurement campaign.

As was done for the NDF and PPO dosimeter calibrations detailed in Section 6.2.2, the change in optical absorbance for each of the dosimeters in the seasonal calibrations was calibrated to the erythemally weighted UV (CIE, 1987) with respect to the horizontal plane. The erythemal action spectrum was chosen for this research as it is by far the most commonly used measure of the effect of damaging UV radiation upon the human population. The CIE (1987) produced the action spectrum quantifying the erythemal effect of solar UV radiation on human skin after collecting

and condensing results gathered from approximately sixty years of research carried out by various scientists. The three functions defining the complete shape of the erythemal action spectrum across the UV waveband are detailed below (CIE, 1987):

$$A(\lambda) = 1.0 \quad (250 \text{ nm} \leq \lambda \leq 298 \text{ nm})$$

$$A(\lambda) = 10^{0.094(298-\lambda)} \quad (298 \text{ nm} \leq \lambda \leq 328 \text{ nm})$$

$$A(\lambda) = 10^{0.015(139-\lambda)} \quad (298 \text{ nm} \leq \lambda \leq 400 \text{ nm})$$

where λ is the wavelength in nanometres.

This erythemal action spectrum as presented in Figure 6.7 shows that the high energy wavelengths below 298 nm are the most efficient at delivering the erythemal response to human skin. From 298 to 328 nm this effectiveness decreases by up to three orders of magnitude. From there, the wavelengths running from 328 nm and greater display a gradual reduction in overall erythemal effectiveness until reaching 400 nm where the erythemal response is rendered as being almost negligible.

The biologically effective UV irradiance (UV_{BE}) for a specific biological process, such as the erythemal response (UV_{ERY}) in this study, was calculated by applying this following summation over the required UV wavelength range represented by the limits of X and Y :

$$UV_{BE} = \sum_X^Y S(\lambda)A(\lambda)\Delta\lambda$$

where $S(\lambda)$ is spectral irradiance in units of $\text{W m}^{-2} \text{ nm}^{-1}$ and $A(\lambda)$ is the action spectrum (Parisi & Kimlin, 1999; WHO, 1994).

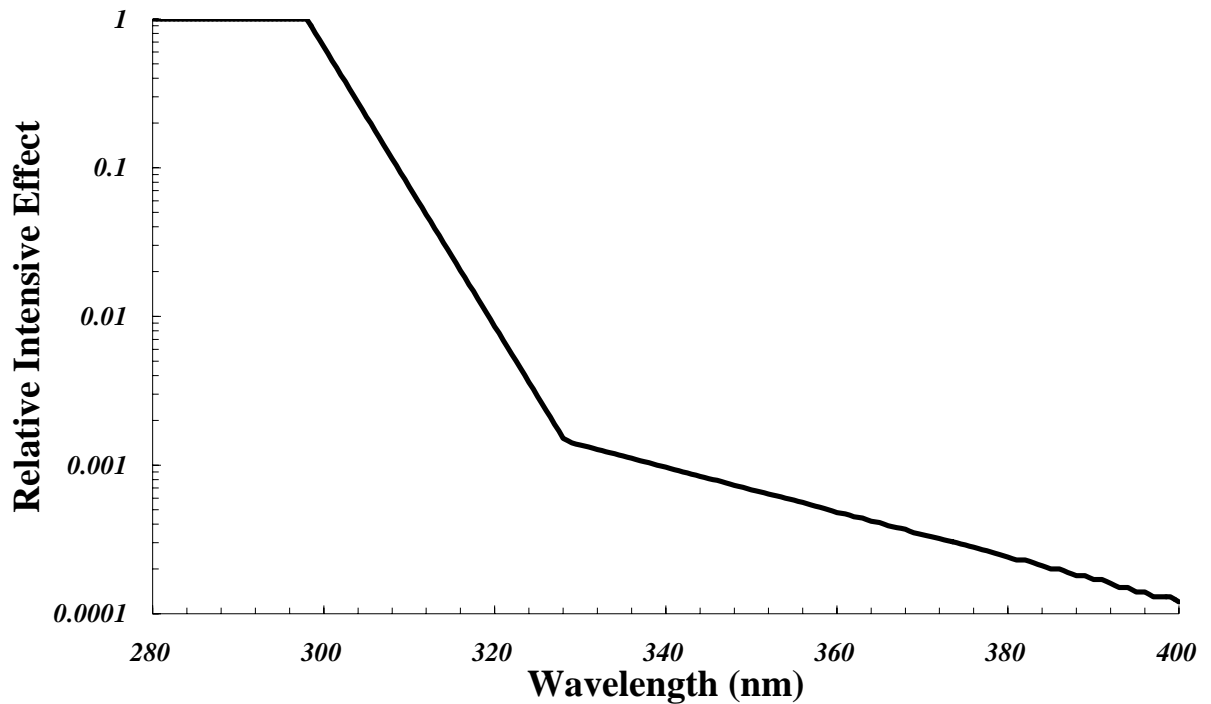


Figure 6.7: The erythemal action spectrum in the waveband running from 280 nm to 400 nm.

Over the duration of the year – long measurement campaign, column ozone levels above Toowoomba were monitored by accessing OMI satellite information (http://jwocky.gsfc.nasa.gov/ozone/ozone_v8.html) each day over the duration of the calibration campaign. This data was used in order to deduce if ozone variations had any influence upon the calibration data from season to season. Figure 6.8 shows a time series of the ozone levels measured by the OMI satellite from March 2007 to February 2008 above Toowoomba. On the graph Autumn 2007 started on day 1, winter 2007 started on day 93, spring 2007 started on day 185 and summer 2007/2008 started on day 276. Aerosol levels were not analysed as Toowoomba is a high – altitude location with an atmosphere that is relatively low in aerosol concentrations due to minimal levels of anthropogenic emission output in the region.

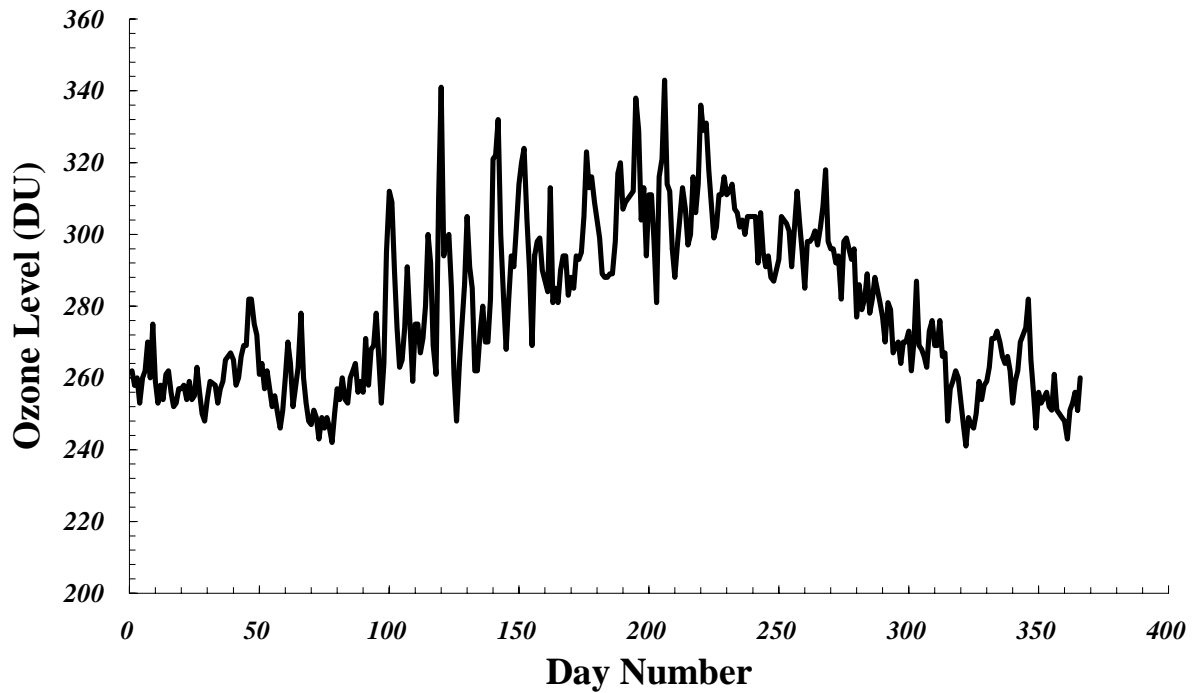


Figure 6.8: Ozone over the Toowoomba region from March 2007 to February 2008.

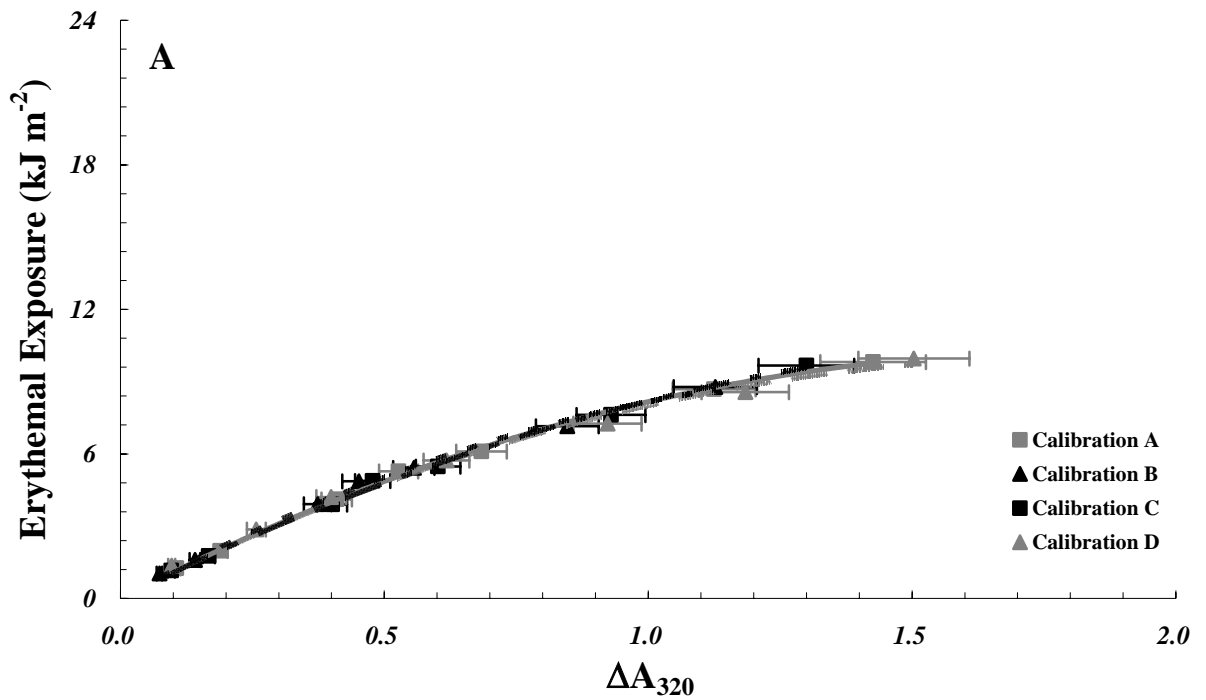
Figure 6.9 (A), (B), (C) and (D) present the in – air PPO dosimeter erythematil calibrations obtained with respect to the horizontal plane for the autumn, winter, spring and summer seasons respectively with the cumulative erythematil exposures measured by the Solar Light UV broadband meter calibrated to the Bentham spectroradiometer, with the x – axis error bars showing the $\pm 7\%$ error margin for each data point.. A second – order polynomial equation that went through the origin was used to describe the trend of each erythematil calibration data set:

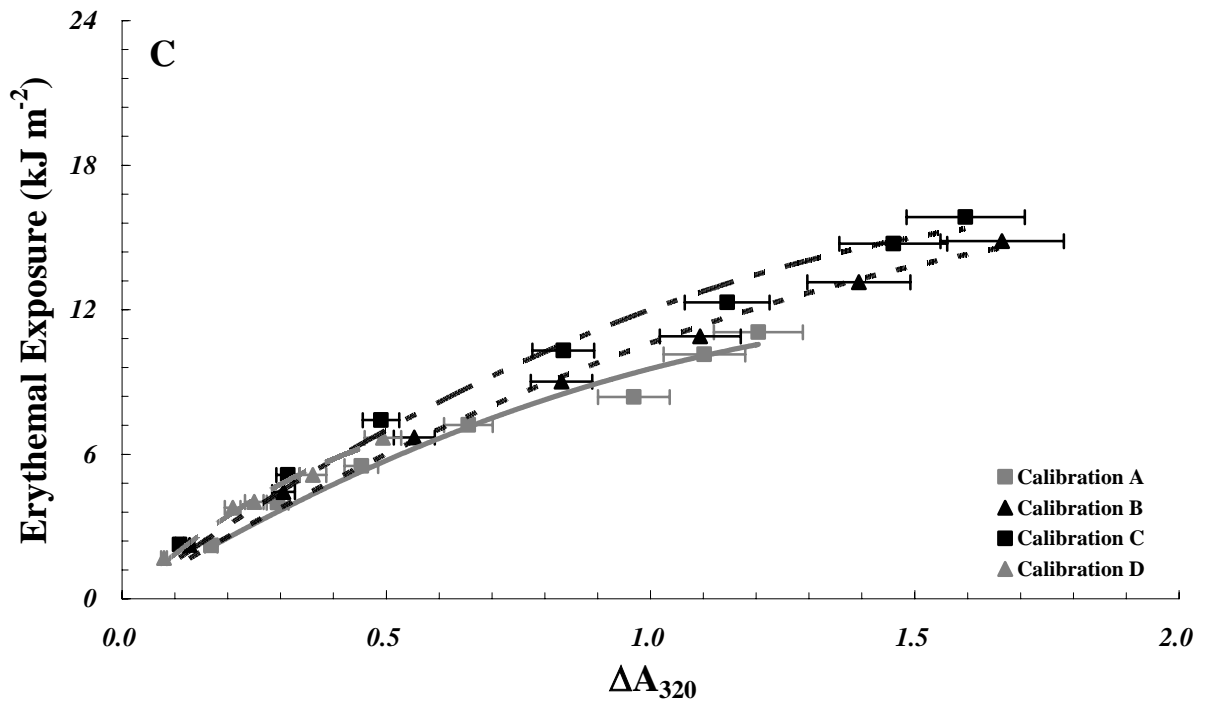
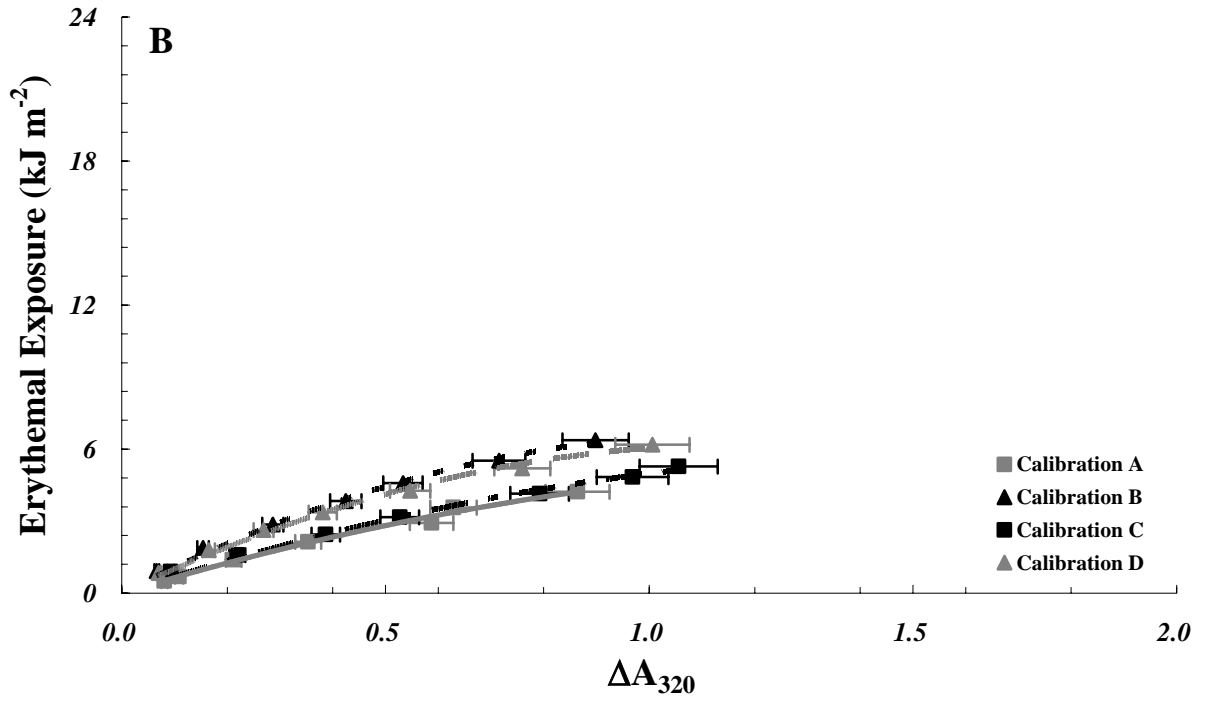
$$UV_{ERY} = -\nu(\Delta A_{320})^2 + \kappa(\Delta A_{320})$$

where UV_{ERY} is the erythematil exposure measured in units of kJ m^{-2} . Table 6.1 displays the various ν , κ and R^2 values calculated for every calibration produced throughout for each season.

Table 6.1: ν , κ and R^2 values obtained for all calibrations produced over autumn, winter, spring and summer.

CALIBRATION TYPE	ν	κ	R^2
Calibration A Autumn	3.09	11.25	0.99
Calibration B Autumn	3.78	11.95	0.99
Calibration C Autumn	2.73	10.92	0.99
Calibration D Autumn	3.05	11.05	0.99
Calibration A Winter	2.08	6.68	0.99
Calibration B Winter	4.77	11.27	0.99
Calibration C Winter	2.19	7.18	0.99
Calibration D Winter	4.39	10.44	0.99
Calibration A Spring	3.86	13.41	0.98
Calibration B Spring	2.79	13.4	0.99
Calibration C Spring	3.99	15.99	0.99
Calibration D Spring	13.19	19.79	0.99
Calibration A Summer	5.65	21.11	0.99
Calibration B Summer	2.91	17.95	0.99
Calibration C Summer	4.66	18.67	0.99
Calibration D Summer	0.84	13.09	0.99





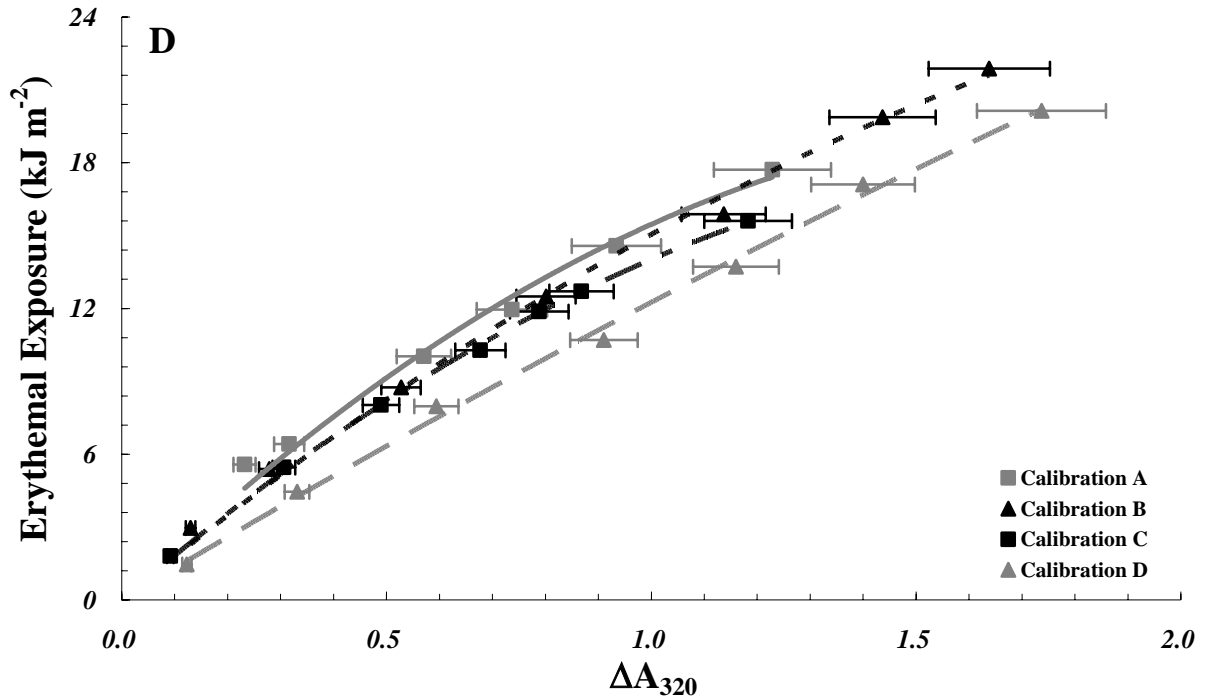


Figure 6.9: Solar erythemal exposure calibration regimes measured for the PPO dosimeter over the months of (A) autumn, (B) winter, (C) spring and (D) summer.

6.3.1 Comparison of Complete Calibration Equations

The complete calibration series developed from the weekly calibration data sets measured in each season from March 2007 to February 2008 are provided in Figure 6.10. To produce these complete calibrations, the calibration data measured for each of the four weeks per season was combined to generate four separate expanded data sets which were then directly compared against each other in order to find out if the calibrations were dependent on changing SZA or atmospheric column ozone levels. The x – axis error bars again represent the uncertainty of $\pm 7\%$ calculated for each data point. A second order polynomial equation through zero was used to model the complete calibration data.

In autumn this equation was:

$$UV_{ERY} = -3.16(\Delta A_{320})^2 + 11.3(\Delta A_{320})$$

with an R^2 value of 0.99 where UV_{ERY} is the erythemal dosage expressed as kJ m^{-2} .

For winter the equation was:

$$UV_{ERY} = -3.71(\Delta A_{320})^2 + 9.14(\Delta A_{320})$$

with an R^2 value of 0.88 where again UV_{ERY} is the erythemal exposure in units of kJ m^{-2} . The equation for spring was:

$$UV_{ERY} = -2.94(\Delta A_{320})^2 + 13.76(\Delta A_{320})$$

with an R^2 value of 0.96 where UV_{ERY} is also measured in units of kJ m^{-2} . In summer the equation was:

$$UV_{ERY} = -3.17(\Delta A_{320})^2 + 17.51(\Delta A_{320})$$

with an R^2 value of 0.96 with the UV_{ERY} exposure is given once more in kJ m^{-2} .

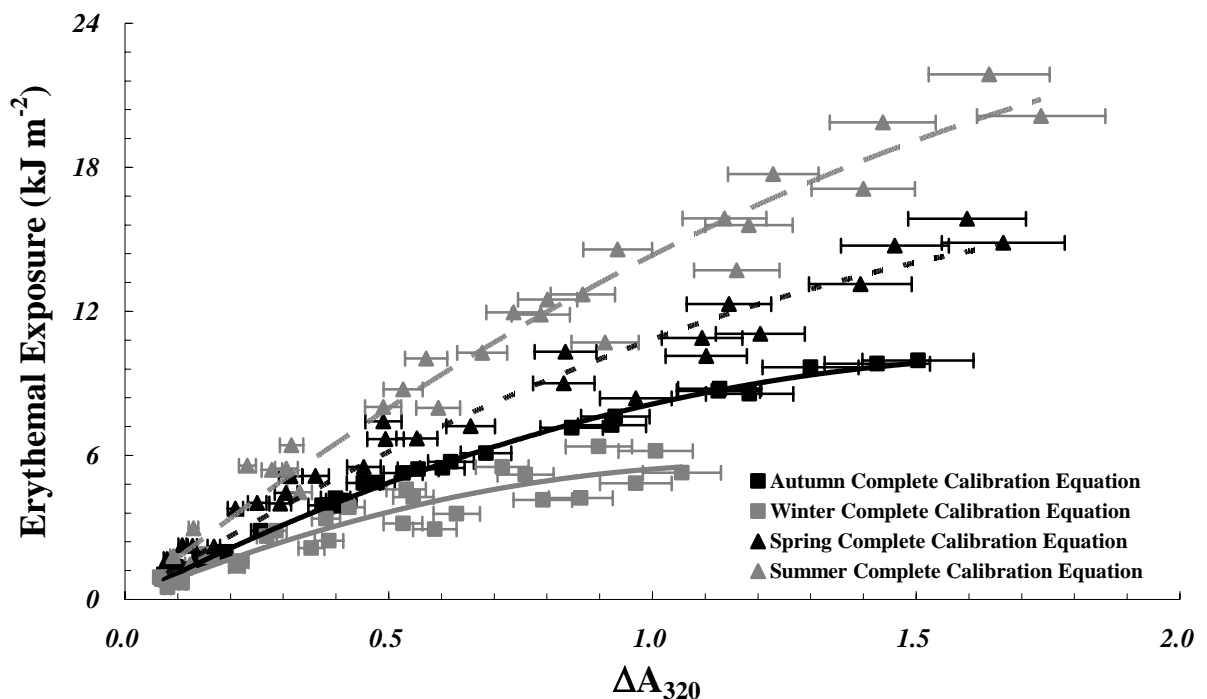


Figure 6.10: Complete solar erythemal exposure calibration equations for the PPO dosimeter for autumn, winter, spring and summer.

6.4 Chapter Discussion

From Figure 6.5 it is clearly seen that from the calibration data sets that the filtered dosimeters were capable of measuring far greater amounts of solar erythemal exposure in comparison to the unfiltered dosimeters, thus extending the effective life time of the PPO dosimeter. In Calibration A the filtered dosimeters measured an extra 14 kJ m^{-2} in comparison to the unfiltered dosimeters before the earliest beginnings of optical saturation. This equated to an extra five days of exposure time. In Calibration B the difference was not as sizeable, with the filtered dosimeters measuring 2 kJ m^{-2} more erythemal exposure than the unfiltered dosimeters, which was an extra two days worth of solar exposure for late autumn. The changes occurring in the optical properties of the Savings waste bag NDF after solar exposure as displayed in Figure 6.2 suggests that it may have to be replaced after extended periods in the field. From this, it is recommended that the Savings waste bag NDF is substituted once a month in order to limit the effect that these inherent and unavoidable optical property changes have upon the responsivity of the PPO dosimeter.

Again, from Figure 6.2 it can be seen that the spectrophotometer measured a 20% transmittance on average across the 300 nm to 340 nm waveband for the Savings waste bag. This suggests that the NDF and PPO dosimeter system could theoretically be used to measure up to five times more solar exposure at any given time in comparison to an unfiltered PPO dosimeter. However, as described in the previous paragraph, the actual observed increase in the measured exposures was much less. One possible explanation for this is that a substantial amount of the apparent absorbance and hence transmittance measured by the spectrophotometer was actually scattering, which will greatly attenuate light in the direct beam but in the context of a

sheet laying adjacent to the PPO surface most scattered light will still be intercepted by the dosimeter itself.

In addition to the measured calibrations obtained between both the filtered and unfiltered PPO dosimeters in the Calibration A and Calibration B campaigns having dissimilar magnitudes of total exposure, Figure 6.5 shows that they also have slightly different characteristic regimes. This was to be expected, as with the use of any UV NDF the incoming UV wavelengths are attenuated which alters their spectral energy distribution that in turn influences the response of the dosimeter underneath. So the PPO dosimeter must be calibrated for extended field use with an NDF attached to it. The use of an unfiltered calibration regime to calibrate extended PPO and NDF dosimeter based exposures will most certainly lead to substantial errors and hence will not suffice.

A substantial difference is also seen between the Calibration A filtered and unfiltered data sets and the Calibration B filtered and unfiltered data sets. The Calibration A measurement campaign ran at an earlier time in autumn compared to Calibration B, which meant that the Calibration A dosimeters received on average a daily erythemal exposure of 1.6 kJ m^{-2} in contrast to the Calibration B dosimeters that were exposed to a sizeably lower average daily erythemal exposure of 1.03 kJ m^{-2} . This difference in average erythemal exposures caused by the gradual increase in peak SZA over autumn, means that the average solar erythemal spectra intercepted daily by the Calibration A dosimeters would have had different characteristics such as energy distribution and cut – off wavelength when compared to the average erythemal spectra intercepted daily by the Calibration B dosimeters, leading to the significant

dissimilarities seen between the Calibration A and Calibration B data sets. Interestingly, ozone levels varied only slightly between the two calibration campaigns with an average column ozone level of 262 DU measured during Calibration A and 261 DU measured during Calibration B. So column ozone was not believed to have played any part in influencing the deviations seen between the data sets gathered for the two calibration series.

Figure 6.10 shows that there were discrepancies between the complete erythemal calibrations for the PPO dosimeter derived from the data sets measured over autumn, winter, spring and summer. The most substantial difference between all of the calibration regimes was measured to occur between the summer and winter calibrations. For example, in winter a total solar erythemal exposure of 5.5 kJ m^{-2} resulted in a change of optical absorbency of approximately 1.05 in the PPO dosimeter. In comparison, the same amount of exposure received in summer resulted in a change in optical absorbency of close to 0.3. This equated to a substantial overall difference in optical absorbency of 0.75.

The characteristic parameters calculated in the calibration trend equations derived for each season provide a picture of what is potentially causing the variability between the seasonal erythemal calibration regimes. The ν parameters given for each of the complete equations show only low differences with changes in season, with the combined average value measured for the autumn, winter, spring and summer data sets being 3.25 kJ m^{-2} with a standard deviation of $\pm 0.3 \text{ kJ m}^{-2}$, resulting in a level of variation equal to approximately 10%. Conversely, the κ parameter appears to be the main factor behind the extensive variability between the seasonal complete calibration

regimes. A combined average value for the κ parameter for the autumn, winter, spring and summer data sets was calculated as 12.75 kJ m^{-2} with a standard deviation of $\pm 3.59 \text{ kJ m}^{-2}$ which equated to a 28% level of variation, over twice as large as the level of variation estimated for the ν parameter data.

Alongside the dissimilarity existing between the response spectra for the PPO dosimeter and the erythemal effect, inconsistent levels of atmospheric column ozone may have also modulated the seasonal calibration regimes. The column ozone trend over the year – long calibration campaign given in Figure 6.8 shows that ozone levels were at their lowest during the months of autumn and summer and at their highest during the months of winter and spring. As ozone is only capable of absorbing energy from the solar wavebands with wavelengths shorter than those in the UVA, erythemal UVB wavelengths incident upon the PPO dosimeters during autumn and summer would have been attenuated to a lesser extent in comparison to the erythemal UVB wavelengths incident in winter and spring leading to changes in the features of the solar erythemal spectra from season to season. To eliminate the introduction of any major errors in field exposure measurements made in – air brought on by seasonal changes in SZA coupled with varying column ozone trends, calibrations are required to be made with respect to the source spectrum that they will be measuring. For example, if field measurements are to be made in early winter, it is highly recommended that a calibration be performed simultaneously in the same location in order to factor in current trends in the atmospheric and geometric parameters directly affecting the response of the PPO dosimeter.

This chapter has shown that the PPO dosimeter can be successfully used for the specific measurement of long – term solar erythemal UV at a substantial level of reliability as long as calibration campaigns are carried out under the necessary conditions. Additionally the employment of a polyethylene NDF has been detailed and proven to be a useful tool for application in extended measurements of the solar erythemal UV with the PPO dosimeter. The succeeding chapter will follow up on the work presented in Chapter 5 and this chapter by calibrating the PPO dosimeter for long – term underwater solar UVB exposures for four different water types over the time of an entire year.

Chapter 7

Calibration of the PPO Dosimeter in an Underwater Semi – Controlled Environment

7.1 Introduction

The information presented in Chapter 5 and 6 has shown that PPO film has excellent potential for use as a long – term underwater solar UV dosimeter. The PPO dosimeter has been calibrated to and tested in – air in the solar UV environment before by Davis *et al* (1976), Lester *et al* (2003) and also in Chapter 6 of this dissertation. However there is no documented methodology on how to properly calibrate the PPO dosimeter for water – based measurements and it has yet to be trialled in an outdoors marine environment, either real or simulated. This chapter shows that calibrations obtained in open air can not be transferred to calibrations underwater, calibrations made in one type of water can be employed for another type of water, but only within a certain range of spectral transmission and calibrations made at different depths in the same water type are interchangeable. This chapter also shows how changing SZA and the amount of local atmospheric ozone can have an effect upon underwater PPO dosimeter calibration data, just as it was shown for the in – air erythemal calibrations analysed in Chapter 6.

7.2 PPO Dosimeter Solar Calibration Campaign

The PPO dosimeter was calibrated on the horizontal plane to solar UV over the time period of approximately 25 hours total sunlight spanning 5 to 7 days outdoors to solar UV for the UVB waveband running from 298 nm to 320 nm in four different distinguishable water types which were clear drinking water drawn from the main council supply, creek water sourced from a local public Japanese Garden just outside the University of Southern Queensland Toowoomba campus, sea water obtained from a coastal location near the city of Brisbane, Australia (27° 28' 04" S, 153° 01' 40" E, 0 m elevation) and dam water sourced from an unused Agricultural engineering

research dam on site at the University of Southern Queensland Toowoomba Campus. The water types were chosen as they represent a good cross section of the different water types located around the South – East Queensland region and for their own distinct level of turbidity, DOM level and salinity. As was discussed in Chapter 5, the 320 nm UVB cut – off wavelength was chosen as it has been used occasionally in previous photobiological investigations and was more applicable to this research. The calibrations took place again in Toowoomba, Australia (27.5° S, 151.9 ° E, 693 m altitude) over a near 12 month time period between March 2007 and February 2008 inclusive. The SZA range over the autumn calibration period was 20° to 70°. The SZA range over the winter calibration period was 35° to 65°. The SZA range over the spring calibration period was 8.4° to 53°. The SZA range over the summer calibration period was 5.5° to 44°. The measurement campaign ran over all four seasons in order to investigate the effect of changing SZA and atmospheric column ozone on the underwater calibrations. Section 7.2.2 details the respective optical properties of each particular water type involved in the measurement campaign. According to the work of Lester *et al.* (2003), the response of the PPO dosimeter is not influenced in any way by fluctuations in local temperature. Therefore, changes in water temperature over the different calibration sessions would not have had any effect upon the measured ΔA_{320} data.

For each water type, one batch of dosimeters was calibrated just above the water surface (which acted as the control calibration), while another batch was placed below the water surface at a depth of about 1 cm (Z_{1CM}). UVB exposures during these calibrations were measured using the IL1400 radiometer working at the factory quoted ½ second refresh rate fitted with the underwater detector with the UVB filter.

As was the case in the initial testing of the PPO dosimeter in the controlled water tank, the IL1400 radiometer was chosen as the primary measurement instrument due to the fact that it is capable of recording the integrated UVB exposure.

Another batch of dosimeters were placed at a depth of 20 cm below the water surface ($Z_{20\text{CM}}$) in order to test for differences in calibration trends at varying depth. As a second IL1400 unit was not available for use, the exposure received at $Z_{20\text{CM}}$ in each water type had to be calculated from that measured at $Z_{1\text{CM}}$. A basic methodology using current underwater light attenuation theory was utilised in order to achieve this.

As discussed in Chapter 3, the attenuation of any form of light (including UV) into a water column is dependent upon both absorption and scattering, which are specific optical characteristics of the water type (Tedetti & Sempere, 2006). Absorption removes the incoming light completely, while scattering changes the direction in which the light moves. The characterization of the water column relies upon the derivation of the K_d as specified in Section 3.2.2, which is calculated by the following expression detailing the exponential decrease with depth of the underwater downwelling irradiance (E_d) composed of photons propagating in the downwards direction (Mishra *et al*, 2005; Mobley, 1994):

$$K_d(z, \lambda) = -\frac{1}{E_d(z, \lambda)} \frac{dE_d(z, \lambda)}{dz}$$

where $K_d(z, \lambda)$ is the attenuation coefficient given in m^{-1} or cm^{-1} , $E_d(z, \lambda)$ is the underwater downwelling irradiance in units of W m^{-2} and z is the depth of the water column in m or cm. $K_d(z, \lambda)$ is dependent on the constituent content of the water column and in turn, the distribution of the underwater light field. Dissolved and

particulate matter in the water column, especially DOM is known to greatly affect the propagation of solar UV in any water column and hence change the value of $K_d(z, \lambda)$ (Morris *et al*, 1995; Bracchini *et al*, 2004).

The equation detailed above to calculate $K_d(z, \lambda)$ can be reformatted into the Beer – Lambert – Bouguer Law, which can then be used as a model to describe the exponential decay of the underwater light field with the increase of depth, as long as a $K_d(z, \lambda)$ estimate has been calculated previously (Kinkade *et al*, 2001):

$$E_d(z, \lambda) = E(0, \lambda)e^{-K_d(z, \lambda)z}$$

where $E(0, \lambda)$ is the downwelling irradiance at an arbitrary depth just below the water surface. It is known that the spectral $K_d(z, \lambda)$ parameter should not be affected by any changes in the surface incident light field such as those caused by a change in the sun's elevation angle (Kirk, 1994). Two broadband K_d values for each particular water type were calculated and used for exposure modelling purposes throughout the entirety of the measurement campaign for both high and low SZA conditions and to factor in changes in atmospheric parameters and slight changes in the constituent composition of each particular type of water that could have occurred over time. The measurement and calculation of the K_d value for each water type is described further in Section 7.2.2.3.

7.2.1 Water Tank Description

The water tank used during the calibration campaign had a length of 66 cm, a width of 46 cm and a depth of 35 cm. The tank was made out of tinted plastic. This plastic was opaque to the UV waveband, so any UV wavelengths incident upon the sides of the tank during the calibrations would not have had any effect upon the submerged

dosimeters. Any pieces of debris that landed in the tank were removed each day in order to keep the water as close to its natural state as possible. Additionally, water levels were topped up each morning before the deployment of the dosimeters to ensure water depths remained constant. Also, at the end of each daily session, the tanks were sealed off using a lid in order to reduce evaporation and to ensure no debris fragments would fall into the water overnight.

7.2.2 Optical Properties of Each Water Type

7.2.2.1 UV Transmission and Absorption Distributions

Figure 7.1 presents the transmission and absorption spectra over the 300 to 320 nm waveband for the four water types analysed in this research. The UV transmission and absorption distributions were measured using the same spectrophotometer and equations as employed in Section 5.2.2. It can be seen that the clear, creek and sea water all share similar transmission and absorption spectra, within approximately $\pm 5\%$ of each other in transmission and within ± 0.03 of each other in absorption. However, the dam water displayed transmission and absorption spectra different to the other three water types.

Using the arbitrary comparison wavelength of 315 nm, these differences in spectral composition can be more clearly quantified. Figure 7.2 (A) and Figure 7.2 (B) presents the transmission and absorption at the arbitrarily selected wavelength of 315 nm for the four water types. The transmission spectrum for the dam water recorded a relatively low transmission value of 62% at 315 nm in comparison to 75% at 315 nm for creek water, 77% at 315 nm for sea water and 79% for the clear water. In addition,

the absorption spectrum for the dam water recorded a high level of approximately 0.21 at 315 nm. This is compared to the much lower values of 0.12 at 315 nm for the creek water, 0.11 at 315 nm for the sea water and 0.1 for the clear water.

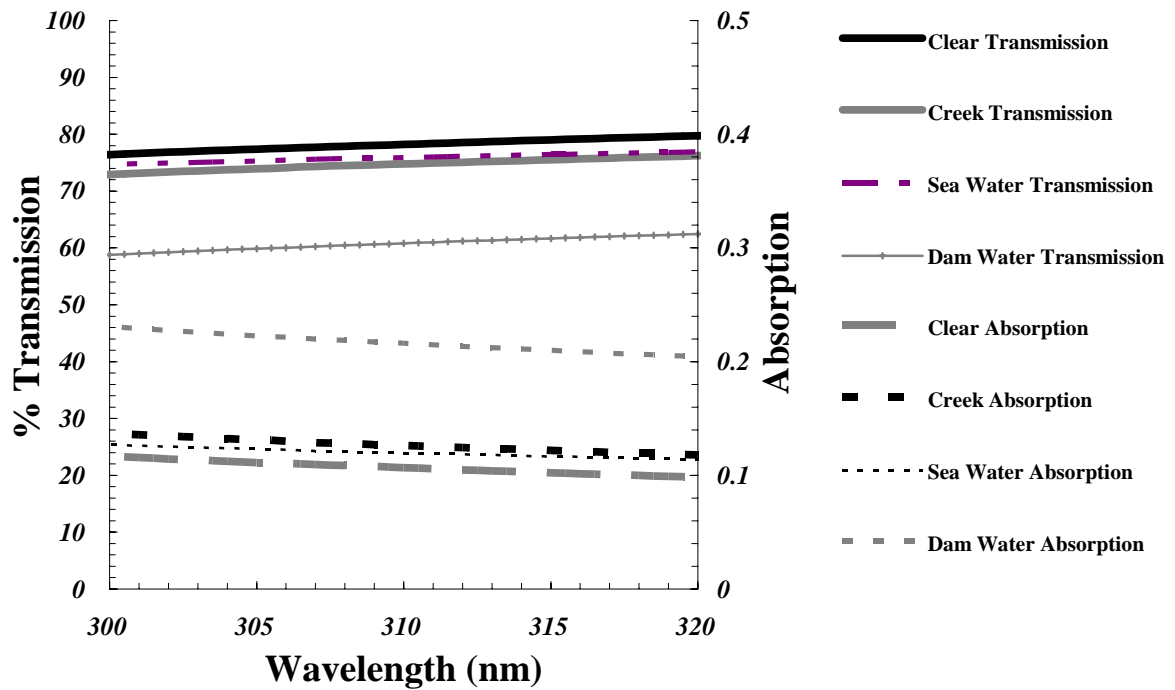


Figure 7.1: Transmission and absorption distributions for clear water, creek water, sea water and dam water.

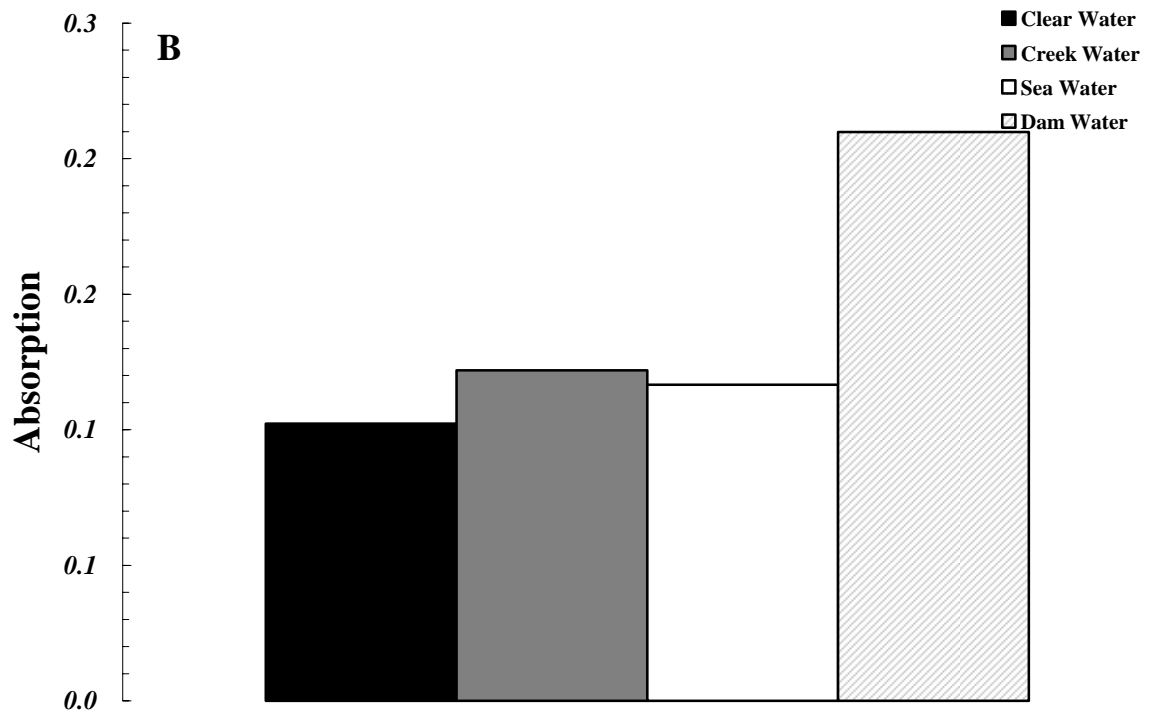
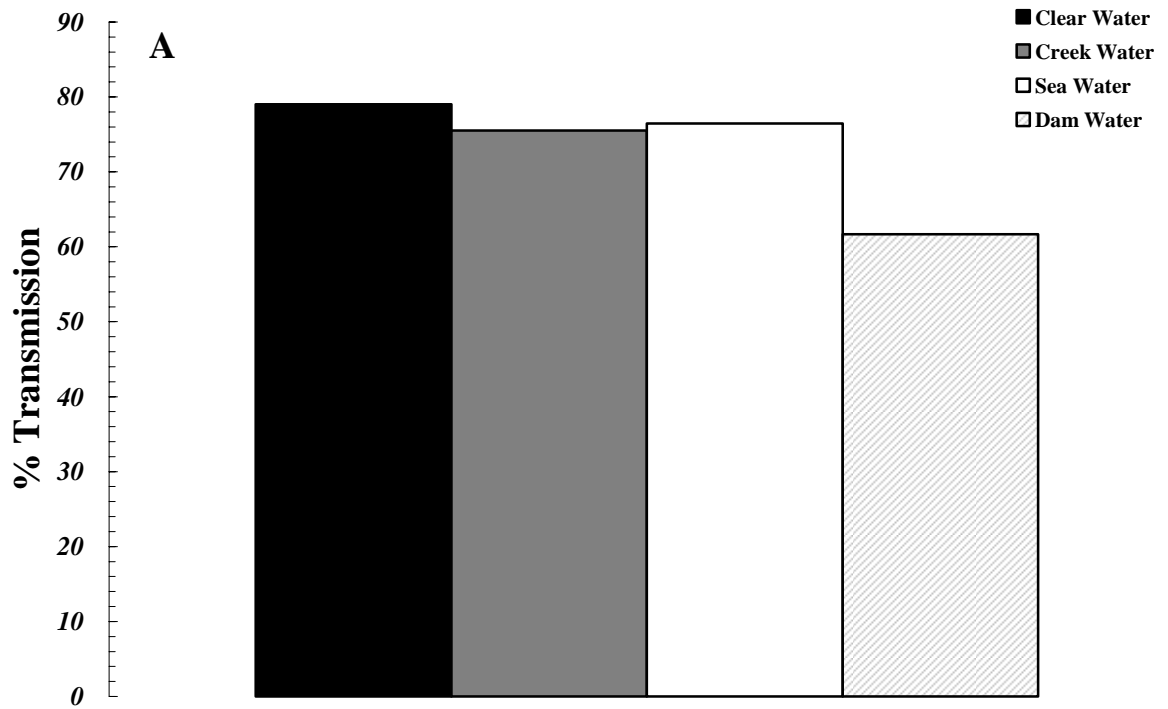


Figure 7.2: Transmission (A) and absorption (B) spectrophotometry data at 315 nm for the clear, creek, dam and sea water.

7.2.2.2 Attenuation Coefficients

The respective K_d values for each water type had to be calculated in order to properly model the solar UV exposure received at a depth of 20 cm using the Beer – Lambert – Bouguer relation. In this research, the K_d value for each water type over the 298 to 320 nm waveband was calculated using the spectral data measured using the EPP2000 spectrometer over the six month campaign running from March 2007 through to August 2007 as discussed in Section 4.4.2. Irradiance data were obtained using the spectrometer at the three different depths (Z_{1CM} , Z_{10CM} , Z_{20CM}) in each water type to create a depth profile. Linear regression techniques were applied to these profiles respectively in order to determine approximate K_d values. Direct linear comparisons between the irradiances measured by the spectrometer and the IL1400 radiometer in all four particular water types all displayed satisfactory R^2 values of between 0.87 and 0.98.

Figure 7.3 (A) and Figure 7.3 (B) display the K_d values that were calculated using the EPP2000 spectrometer in the clear, creek, sea and dam water over the measurement campaign in both low SZA (angles ranging from 20° to 61°) and high SZA (angles ranging from 39° to 75°) conditions respectively. The y – axis error bars are representative of the calculated standard error found for each K_d estimate. As was expected due to its much higher levels of turbidity and DOM content the dam water was calculated to have the highest K_d value out of all of the four water types, which was approximately 0.12 cm^{-1} for low SZA and 0.085 cm^{-1} for high SZA. In comparison to this the clear, creek and sea water types had K_d values falling near each other at 0.03 cm^{-1} , 0.036 cm^{-1} and 0.028 cm^{-1} respectively for low SZA and 0.025 cm^{-1} , 0.025 cm^{-1} and 0.036 cm^{-1} respectively for high SZA.

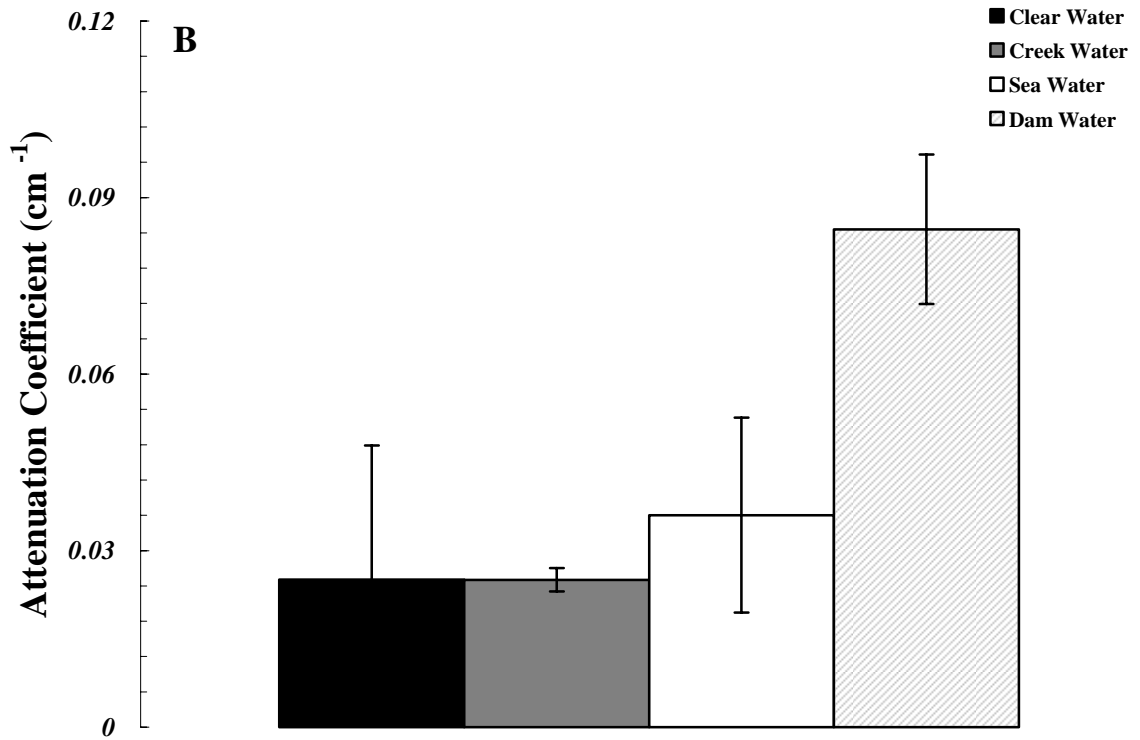
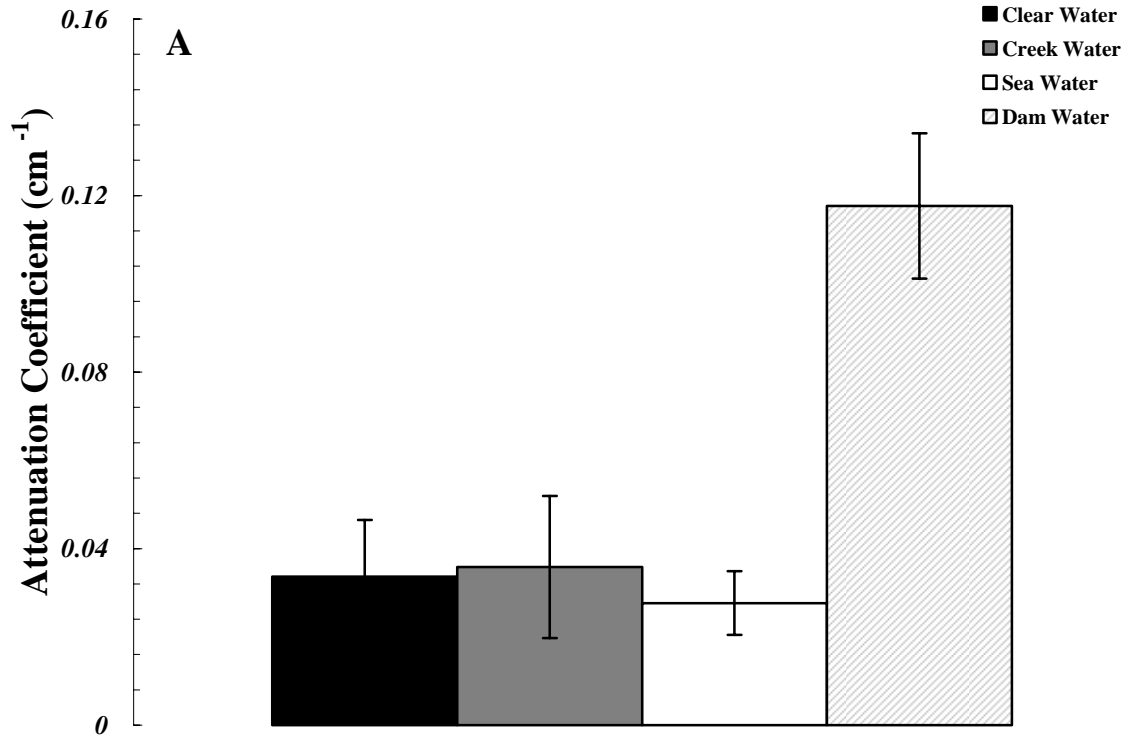


Figure 7.3: The K_d values calculated using the EPP2000 spectrometer in the clear, creek, sea and dam water for high SZA conditions (A) and the K_d values calculated

using the EPP2000 spectrometer in the clear, creek, sea and dam water for low SZA conditions (B).

7.2.3 PPO Dosimeter Solar Calibration Campaign Results

Figures 7.4 (A), 7.5 (A), 7.6 (A) and 7.7 (A) display the in – air and underwater PPO dosimeter calibrations for each water type as measured at Z_{1CM} in each particular season respectively with the cumulative UVB exposures as measured by the calibrated IL1400 broadband meter. Figures 7.4 (B), 7.5 (B), 7.6 (B) and 7.7 (B) show the underwater PPO dosimeter calibrations for each water type as measured at Z_{20CM} in all of the seasons respectively with the cumulative UVB exposure derived from the exposure at Z_{1CM} and the Beer – Lambert – Bouguer relation. A second – order polynomial equation through zero (as no change in optical absorbance represents no exposure time) was employed to model each particular calibration data set in the following form:

$$UVB_Z = -\alpha(\Delta A_{320})^2 + \beta(\Delta A_{320})$$

where UVB_Z is the UVB exposure received at the depth z in units of kJ m^{-2} . Table 7.1 displays the different α , β and R^2 values obtained for each particular calibration derived throughout the year – long measurement series.

Table 7.1: α , β and R^2 values obtained for each particular calibration over autumn, winter, spring and summer.

CALIBRATION TYPE	α	β	R^2
Control (In – Air)	86.78	322.39	0.99
Clear Water Autumn Z_{1CM}	63.77	249.68	0.99
Creek Water Autumn Z_{1CM}	68.6	248.9	0.99
Sea Water Autumn Z_{1CM}	52.48	236.93	0.99
Dam Water Autumn Z_{1CM}	99.21	296.12	0.99
Clear Water Autumn Z_{20CM}	73.37	235.11	0.99
Creek Water Autumn Z_{20CM}	15.28	171.35	0.99
Sea Water Autumn Z_{20CM}	37.56	190.74	0.98
Dam Water Autumn Z_{20CM}	2.64	29.93	0.99
Clear Water Winter Z_{1CM}	254.96	595.5	0.96
Creek Water Winter Z_{1CM}	188.96	542.93	0.99
Sea Water Winter Z_{1CM}	182.76	530.56	0.99
Dam Water Winter Z_{1CM}	299.31	643.08	0.98
Clear Water Winter Z_{20CM}	223.53	498.58	0.99
Creek Water Winter Z_{20CM}	379.98	666.83	0.99
Sea Water Winter Z_{20CM}	269.89	527.54	0.99
Dam Water Winter Z_{20CM}	251.78	357.77	0.99
Clear Water Spring Z_{1CM}	222.35	596.7	0.99
Creek Water Spring Z_{1CM}	243.7	607.01	0.99
Sea Water Spring Z_{1CM}	524.82	601.8	0.96
Dam Water Spring Z_{1CM}	115	59.26	0.88
Clear Water Spring Z_{20CM}	19.1	242.68	0.98
Creek Water Spring Z_{20CM}	58.9	357.72	0.99
Sea Water Spring Z_{20CM}	151.78	413.64	0.98
Dam Water Spring Z_{20CM}	192.03	294.74	0.98
Clear Water Summer Z_{1CM}	93.6	306.51	0.98
Creek Water Summer Z_{1CM}	50.28	246.58	0.99
Sea Water Summer Z_{1CM}	45.38	226.75	0.99
Dam Water Summer Z_{1CM}	56.9	234.03	0.99
Clear Water Summer Z_{20CM}	108.87	269.64	0.99
Creek Water Summer Z_{20CM}	403.19	519.95	0.97
Sea Water Summer Z_{20CM}	99.749	214.87	0.98
Dam Water Summer Z_{20CM}	0.85	30.21	0.97

In all of the figures, the x – axis error bars for each data point in the underwater calibrations represent an uncertainty margin of $\pm 9\%$, which was the calculated in – water dosimeter variation for PPO as found in Section 5.4.1.4 of Chapter 5. The x – axis error bars on the data points for the in – air calibration series represent a calculated error margin of approximately $\pm 7\%$, which was the estimated average

interdosimeter variation found to exist across the batch of dosimeters used for the in – air calibration as originally estimated in Chapter 5.

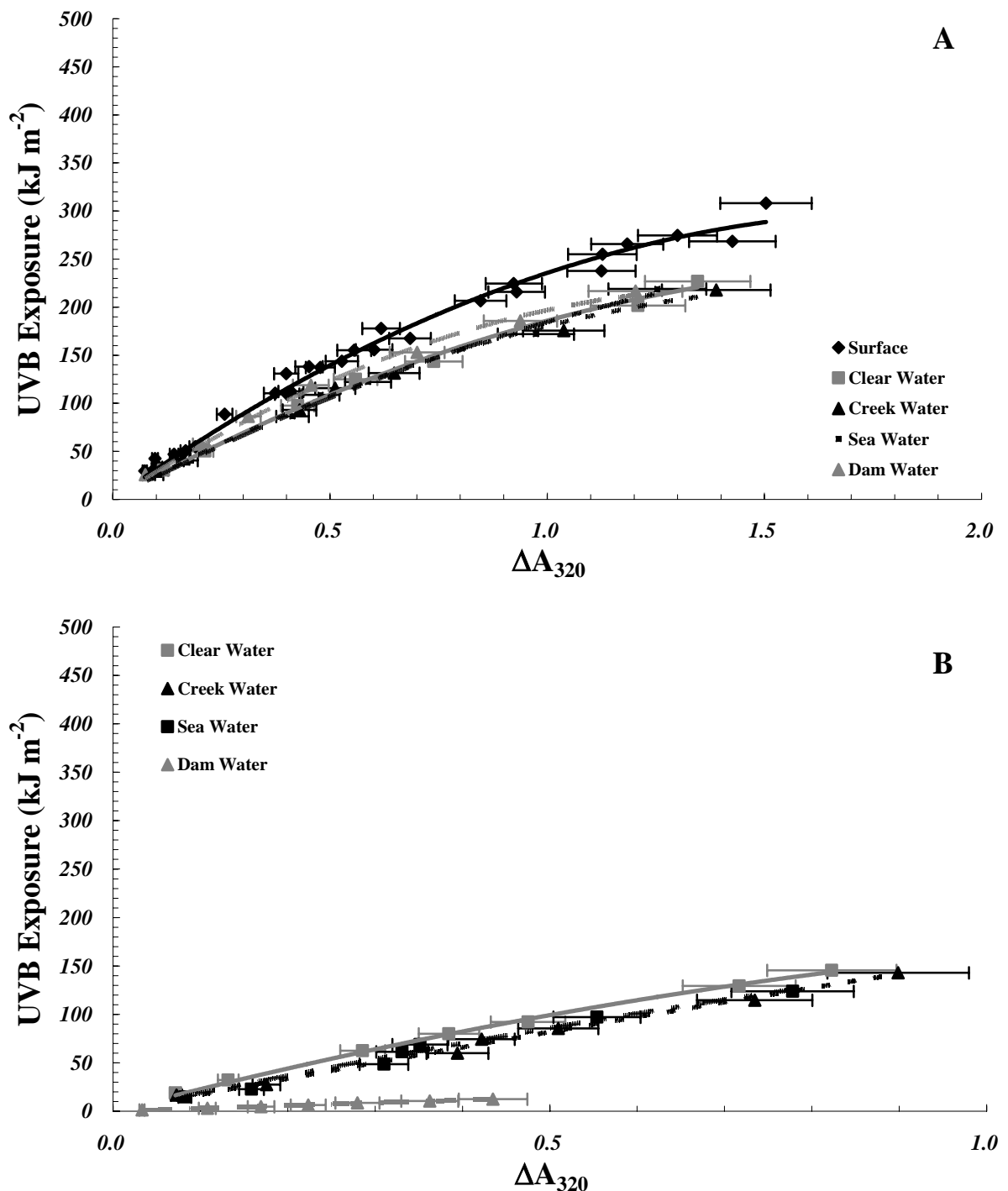


Figure 7.4: (A) Calibration curves against the solar UVB exposures over autumn for tap water, creek water, sea water and dam water at Z_{1CM} . The surface (in – air) calibration curve acts as the control. (B) Calibration curves against the solar UVB exposures over autumn for tap water, creek water, sea water and dam water at Z_{20CM} .

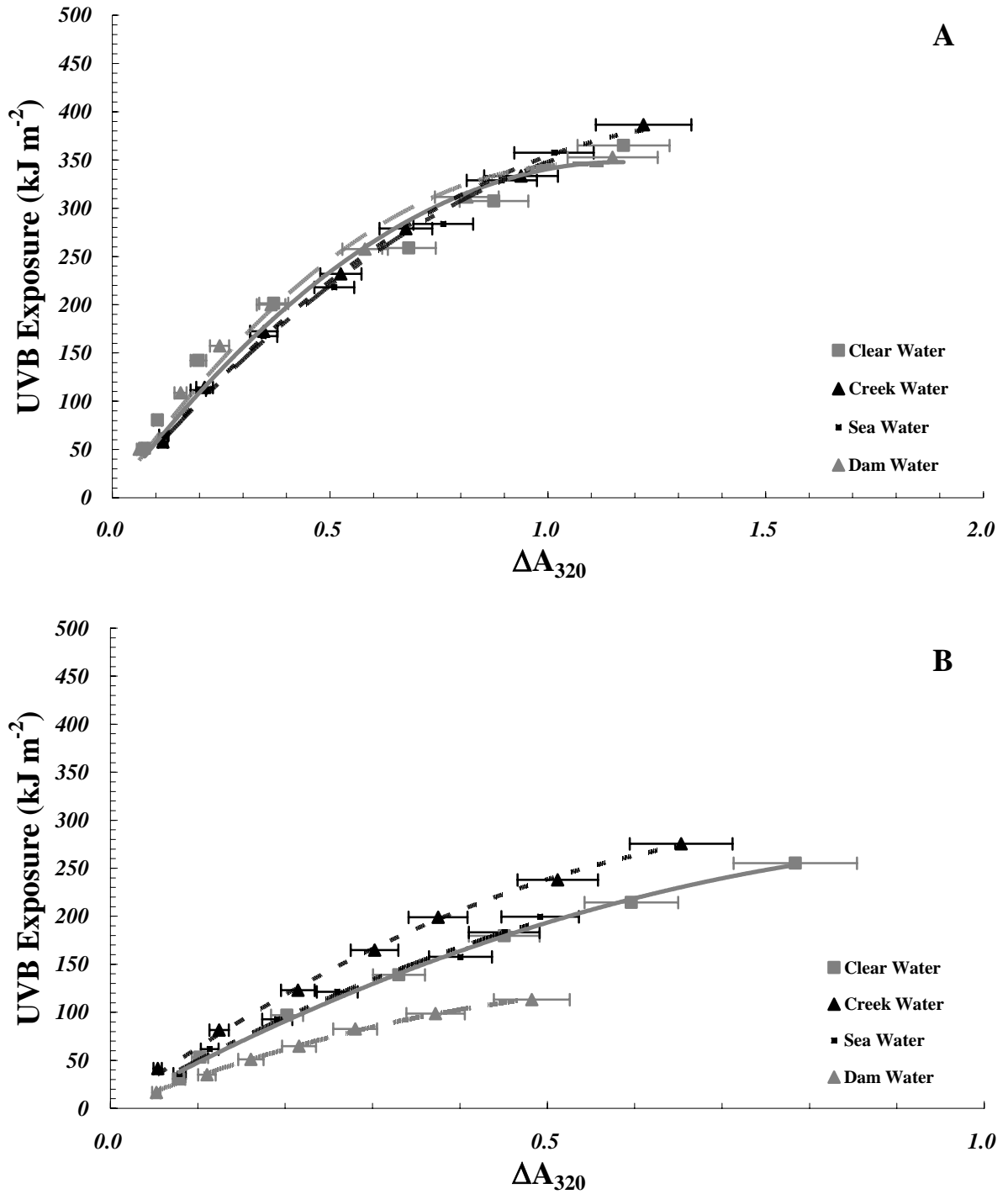


Figure 7.5: (A) Calibration curves against the solar UVB exposures over winter for tap water, creek water, sea water and dam water at Z_{1CM} . (B) Calibration curves against the solar UVB exposures over winter for tap water, creek water, sea water and dam water at Z_{20CM} .

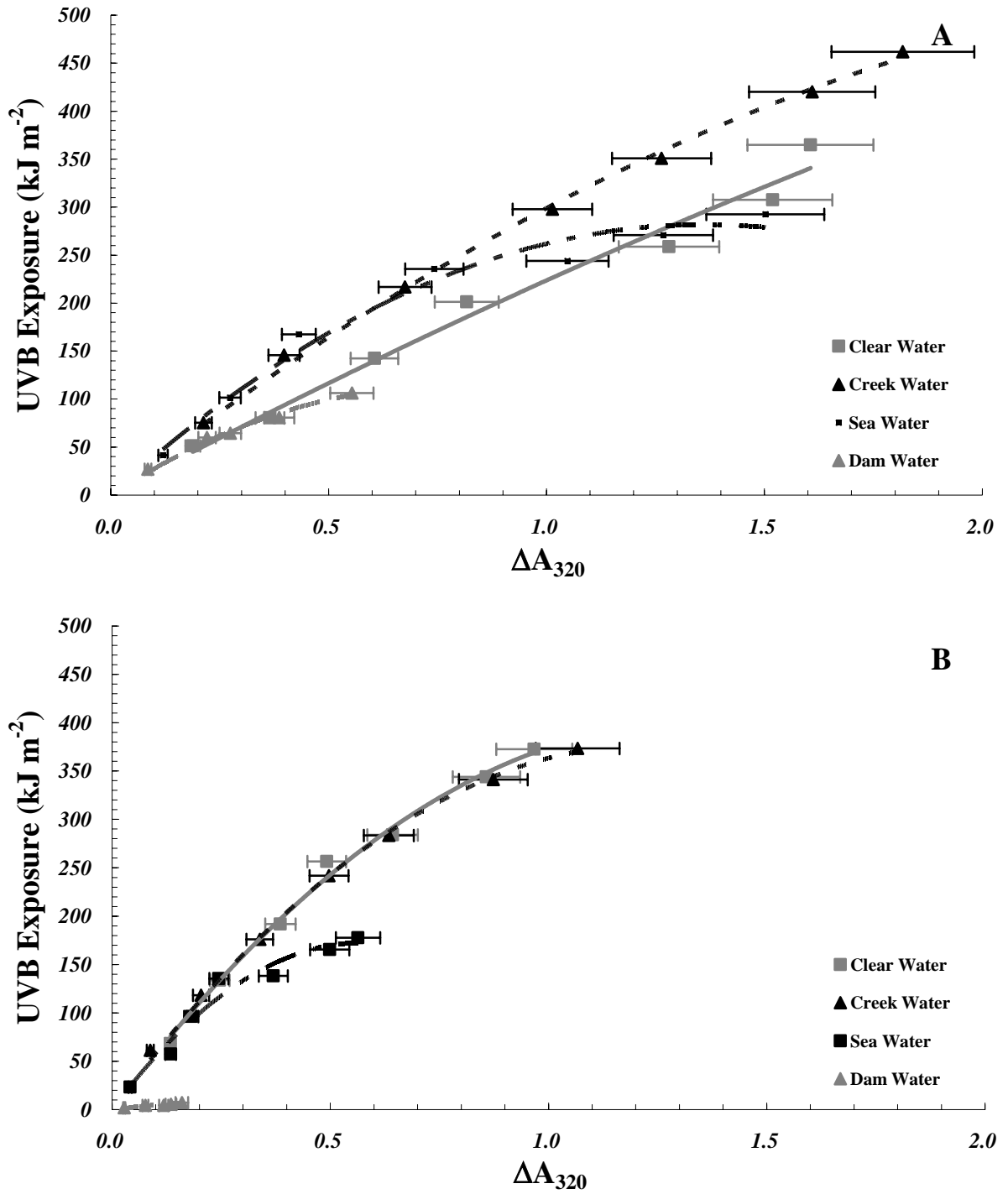


Figure 7.6: (A) Calibration curves against the solar UVB exposures over spring for tap water, creek water, sea water and dam water at Z_{1CM} . (B) Calibration curves against the solar UVB exposures over spring for tap water, creek water, sea water and dam water at Z_{20CM} .

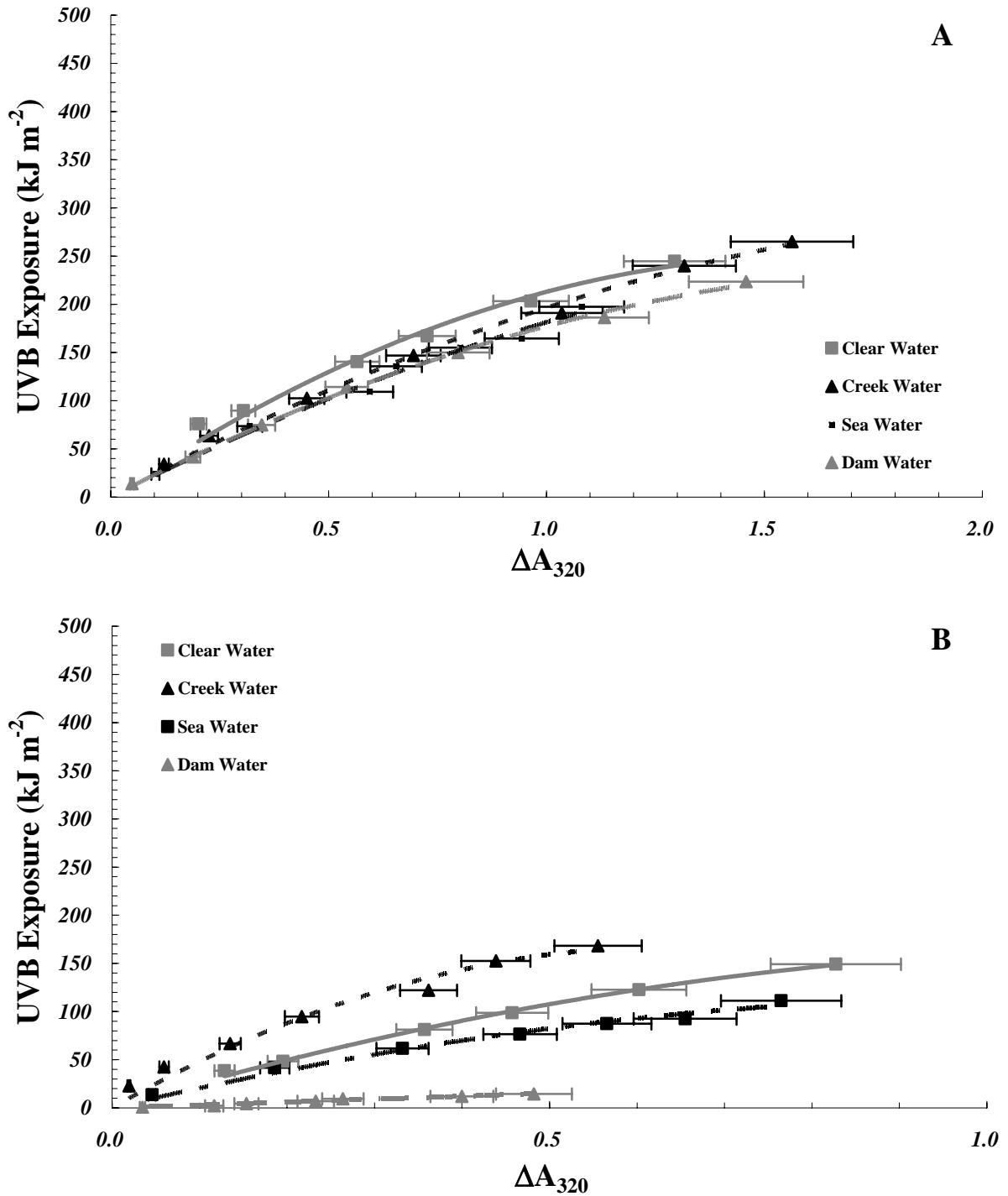


Figure 7.7: (A) Calibration curves against the solar UVB exposures over summer for tap water, creek water, sea water and dam water at Z_{1CM} . (B) Calibration curves against the solar UVB exposures over summer for tap water, creek water, sea water and dam water at Z_{20CM} .

7.2.3.1 Comparison of Complete Calibration Equations

Figure 7.8 displays the complete calibration equations derived from the data measured over the autumn, winter, spring and summer months from March 2007 to February 2008. The underwater calibration data at each depth for each particular water type was merged together for each season and compared in order to see if changing SZA or atmospheric column ozone had any influence over calibration trends. The complete calibration equations featured for all the water types do not include the calibration data obtained for the dam water at Z_{20CM}. It can be seen that three data points had noticeably lower values in comparison to the rest of the complete calibration data measured for spring after a ΔA_{320} of 1 was reached. This could have been due to deposits of dirt and organic matter settling on these dosimeters during deployment underwater. As in Figures 7.4, 7.5, 7.6 and 7.7 the x – axis error bars for each data point in the underwater calibrations again show an error of $\pm 9\%$, which was the calculated in – water dosimeter variation for PPO as determined in Section 5.4.1.4. A polynomial trend equation was applied to all of the complete calibration data sets with the UVB exposure of kJ m^{-2} over the 298 nm to 320 nm waveband. For autumn the equation took on the following form:

$$UVB = -43.422(\Delta A_{320})^2 + 221.8(\Delta A_{320})$$

with an R^2 value of 0.96. For winter the following equation emerged:

$$UVB = -203.09(\Delta A_{320})^2 + 544.51(\Delta A_{320})$$

with an R^2 value of 0.97. In spring the complete calibration equation was found to be:

$$UVB = -119.42(\Delta A_{320})^2 + 437.99(\Delta A_{320})$$

with an R^2 value of 0.87. In summer the equation was:

$$UVB = -58.611(\Delta A_{320})^2 + 248.67(\Delta A_{320})$$

with an R^2 value of 0.89.

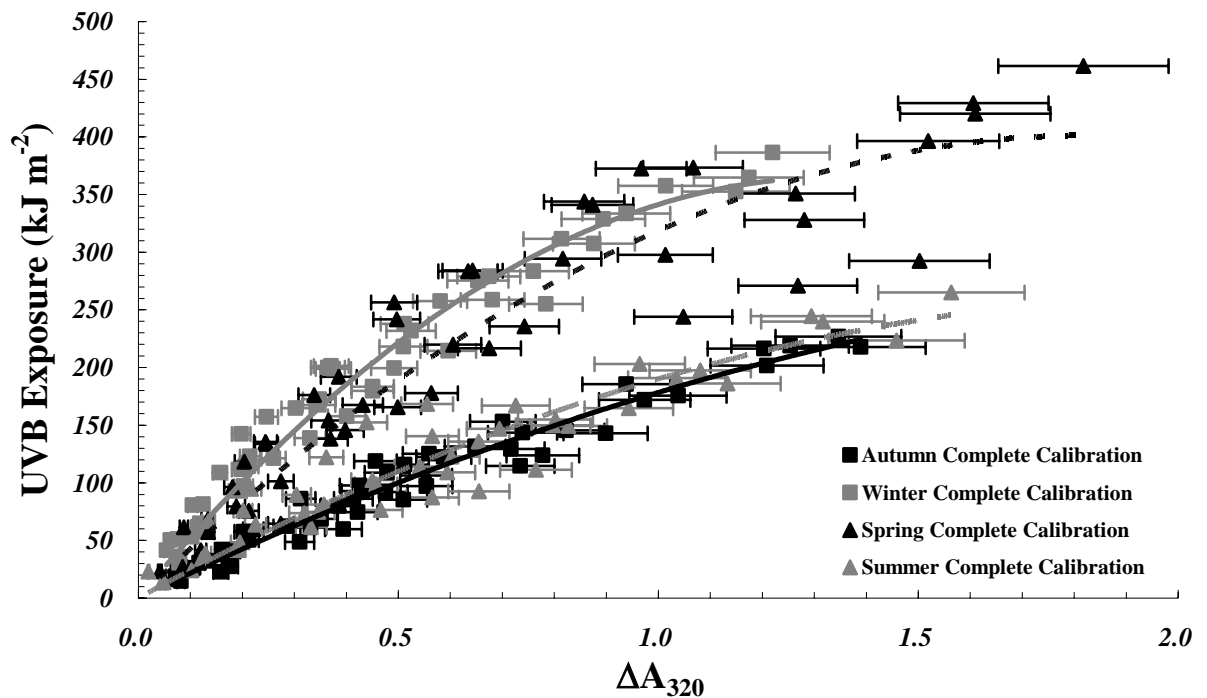


Figure 7.8: Comparison between underwater complete calibrations obtained over the months of autumn, winter, spring and summer.

7.3 Chapter Discussion

For each season, as seen in Section 7.2.3, the calibrations obtained at a depth of approximately 1 cm in each water type were all measured to be in close proximity to each other, mostly within the 9% error estimated to exist for the dosimeters. Based on this result, it can be assumed that a single shallow calibration in clear water should be transferable to measurements made in different water types that have a percentage transmission in the range of 40% to 80% as encountered in the water types employed in this research. However, these calibrations do differ to the calibration made in air with the difference becoming more pronounced with increasing cumulative exposure, reaching a discrepancy of as much as approximately 50 kJ at a ΔA_{320} value of 1.2 as seen in Figure 7.4 (A). So it is not appropriate to apply an air based calibration

equation to dosimetric measurements made underwater, without incurring substantial errors in the measured exposures.

Over autumn, winter, spring and summer the calibrations measured at $Z_{20\text{CM}}$ in each water type were also all found to be in close proximity to each other, apart from the dam water calibrations, which presented regimes completely different to the three other water types. Also, the summer calibrations obtained for all water types at the $Z_{20\text{CM}}$ depth were spread out over a greater range in comparison to the calibrations developed at $Z_{20\text{CM}}$ in the other three seasons. This could have been caused by multiple interruptions in the calibration process due to local storms and rain coupled with extremely high levels of cloud present in the atmosphere during exposure time. This high level of cloud coverage would have led to the $Z_{20\text{CM}}$ dosimeters receiving a distribution of anisotropic radiation at the bottom of the tank dissimilar to that received by the dosimeters in the previous calibrations carried out in the months of autumn, winter and spring.

From the spectrophotometry data in Figure 7.1 and Figure 7.2 it is clear to see that the dam water has the lowest level of UV transmission and in turn the highest amount of UV absorption across the 300 to 320 nm waveband when compared to the other three water types due to having a high concentration of DOM constituents. So it appears that calibrations made at deeper depths (lower than $Z_{1\text{CM}}$) are transferable from one water type to another, but only within a certain spectral transmission (or absorption) range. In this research it appears that this range is approximately $\pm 5\%$ UV transmission difference (or ± 0.03 UV absorption difference) between each water type for calibrations to be completely transferable with minimal error. Researchers would

have to keep this in mind when calibrating dosimeters to measure exposures deeper than just below the water surface.

Similar to the results seen in the solar erythemat PPO dosimeter calibration in Chapter 6, the direct comparison between the complete calibration equations for the PPO dosimeter underwater show that there is a definite difference between the calibration regimes obtained over the months of winter and spring when compared to those obtained in summer and autumn. This discrepancy between the calibration sets could be attributed not only to the change in the sun's position between these different seasons, but also to a progressive increase in column ozone levels over the measurement site as was also believed to be the case in Chapter 6.

Both the α and β calibration parameters displayed high levels of instability from season to season reflecting their possible dependence upon SZA and column ozone levels. The α parameters estimated for the underwater complete calibration equations displayed an overall average value of 106.1 kJ m^{-2} with a standard deviation of 72.5 kJ m^{-2} resulting in a sizeable variance level of 68%. The β parameters that were calculated over each season showed marginally lower levels of volatility having a percentage variation of 43% from an average value of 363.2 kJ m^{-2} together with a standard deviation of 154.5 kJ m^{-2} . This was different to what was seen with the in – air erythemat calibrations described in Chapter 6, as only the second calibration parameter (κ) was seen to be influenced by changes in atmospheric and geometric factors.

Figure 6.8 in Section 6.2.2 displays a significant increase in column ozone levels above Toowoomba that began in very late autumn (May) and continued towards the end of spring (November). Autumn and summer column ozone levels were on average 258 DU and 265 DU respectively. In comparison, winter and spring column ozone levels were much higher on average at 289 DU and 305 DU respectively. It is well known that the shorter UV wavelengths, especially those in the UVB are blocked by a much greater amount when there are increased levels of ozone present in the atmosphere. This coupled with the change in SZA would have a direct effect on the UV spectrum that is received here on the Earth. The UVB spectra received by the dosimeters during the winter and spring calibration campaigns would have had a different cut – off point, and in turn, have had a different composition in comparison to the spectra received by the dosimeters during the autumn and summer calibration campaigns. Consequently, when calibrating the PPO film for underwater usage, researchers should obtain calibration data for the season in which they will be recording measurements. Similar results to this have been discovered by other researchers investigating the effect of fluctuations in column ozone upon the response of broadband UV meters. As an example, Bodhaine *et al* (1998) has found that if the influence of ozone is ignored during calibration, UV measurements made with broadband meters can produce errors of 10% or greater.

From this analysis it appears that ozone has a more pronounced effect on the solar spectrum than SZA. This could be a possibility at a subtropical location such as Toowoomba, even though the ozone fluctuations are relatively small when compared to those that occur at higher latitudes. If this was not the case, the spring and autumn calibration regimes would have been seen to be closer together. The summer and

winter calibration regimes should have also appeared on the opposite sides of the spring and autumn calibration regimes.

In all the water types, the total UVB energy received after the 25 hour exposure period at Z_{ICM} was measured to be within approximately $300 \pm 100 \text{ kJ m}^{-2}$ for each water type. This is significantly greater than the 40 kJ m^{-2} maximum reached by Dunne (1999) when using polysulphone as an underwater dosimeter. Additionally, at the final measurement point, the PPO film dosimeters had yet to fully degrade and would have definitely been able to measure another substantial UVB dosage. This additional dosage is estimated to approximately another 200 kJ m^{-2} to 300 kJ m^{-2} before complete optical saturation is achieved, which could then be even further extended with the application of a polyethylene NDF as detailed in Chapter 6.

These results expand upon the initial data provided in Chapter 5 and Chapter 6 and show that the PPO dosimeter can be calibrated and employed to measure UVB exposures in aquatic environments under a variety of atmospheric conditions in a number of distinct water types. Chapter 8 will now use the underwater calibrations acquired throughout the research developed in this chapter and will apply them to field trials made in two real – world and one field simulated aquatic environment in order to define and test the operational limitations and overall accuracy of the PPO dosimeter.

Chapter 8

Deployment of the PPO Dosimeter in Real – World Aquatic Environments

8.1 Introduction

In the previous three chapters, the PPO dosimeter has proven to be capable of receiving both in – air and underwater exposures that are significantly greater than those of the more commonly used polysulphone dosimeter, within a range of accuracy close to what would be expected of dosimetric measurements made in air provided that the necessary calibrations are completed correctly by factoring in different column ozone levels, SZA ranges, varying water turbidity and DOM. This chapter details a final measurement campaign carried out in two real world aquatic environments and a simulated sea water environment using a batch of PPO dosimeters set at different depths and aligned to a range of different angles and geographical directions by means of attachment to a custom built dosimeter submersible float (DSF) unit over the space of a year at a sub – tropical location. Results obtained from this measurement campaign were used to compute a K_d value for the sea water in each particular season. These K_d values were found to be in close agreement to standalone K_d values derived from results taken using the EPP2000 spectrometer in the same sea water.

8.2 Dosimeter Submersible Float Specifications

The DSF employed for the field measurement campaign was fabricated by combining an aluminium frame and a PVC ballast cylinder with a total height of 64 cm, a width of 26 cm and a cross – sectional length of 67 cm. The PVC ballast cylinder had a volume of approximately 13 litres. This cylinder was filled with either small stones or gravel in order to ensure that the float would remain in its required upright stationary position throughout the duration of given series of measurements. Four steel hook

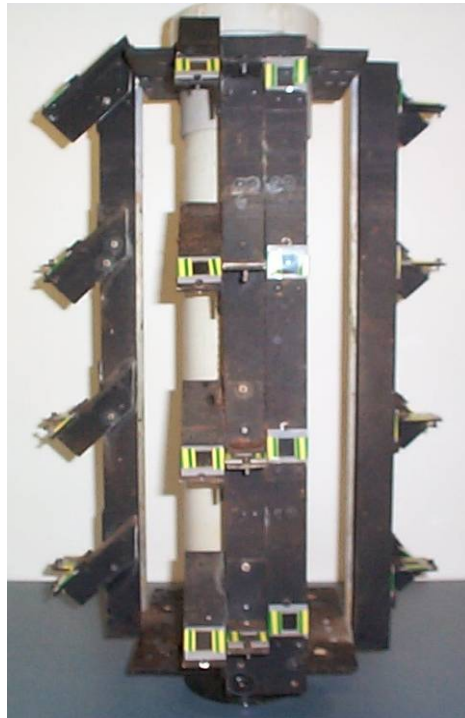
anchors were also inserted through holes in the floor of the DSF and straight into the ground in order to increase its stability in the water during windy conditions.

The DSF had a column of four dosimeter attachment sites resting on each of its four sides. Each side of the DSF was positioned around the PVC ballast cylinder in 90° increments so that measurements for each geographical direction (north, south, east and west) could be made. In each of the four sides each attachment site was separated by a distance of 15 cm. The top attachment site was designed to remain above the water level at all times throughout each measurement series, while the three lower attachment sites were to receive UVB exposures underwater. These three underwater attachment sites received UVB exposures at depths of 5 cm ($Z_{5\text{CM}}$), 20 cm ($Z_{20\text{CM}}$) and 35 cm ($Z_{35\text{CM}}$) respectively.

All the attachment sites were able to hold up to three dosimeters at a time without obstruction, with each dosimeter set to different angular inclinations which were 0° to the horizontal (horizontally aligned), 45° to the horizontal (diagonally aligned) and 90° to the horizontal (vertically aligned). In all of the different water types, each of the dosimeters were checked regularly for any mud, moss or organic matter residue build up on their surfaces. Figure 8.1 (A) displays the north side of the DSF with a full payload of PPO dosimeters ready for deployment. Figure 8.1 (B) shows the top – down view of the DSF. Due to the geometry of the DSF, some minor shading of the $Z_{20\text{CM}}$ and the $Z_{35\text{CM}}$ dosimeters was found to occur during the measurements carried out in each underwater environment, influencing the amount of diffuse irradiance scattered upon the dosimeters. This shading took place most generally during high SZA conditions, such as in the early morning and in the late afternoon, where solar

UV was incident predominantly on the sides of the DSF in comparison to low SZA conditions in which solar UV was incident towards the top of the DSF. Also, the horizontal and 45° dosimeters at each level and direction on the DSF were subjected to relatively slight amounts of shade each day due to their close proximity to each other.

A



B

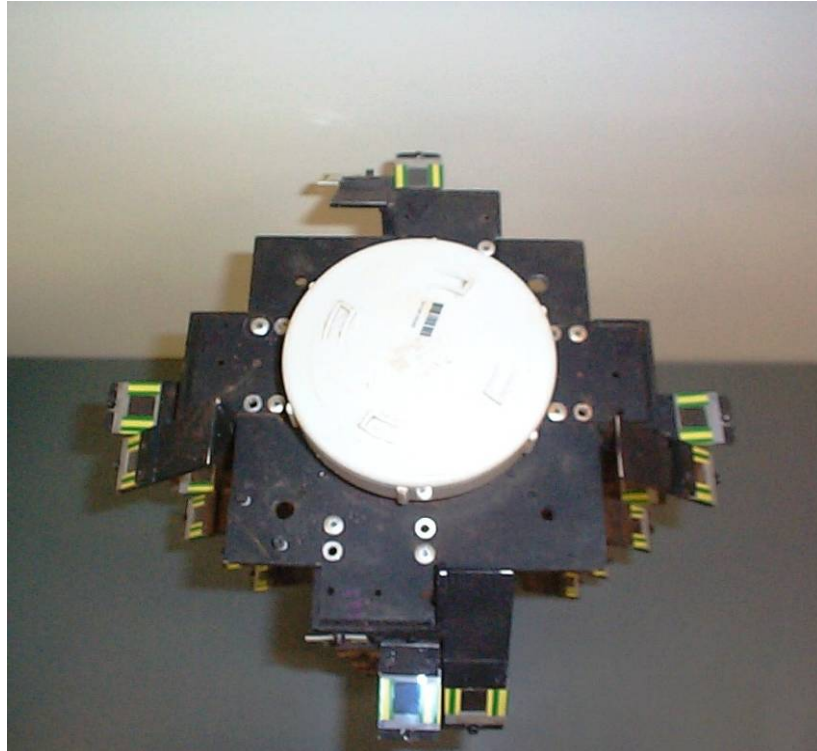


Figure 8.1: (A) North side view of the DSF and (B) the top – down view of the DSF.

8.3 Underwater UV Exposures at Different Aquatic Locales

8.3.1 Japanese Gardens Creek

A creek situated in a Japanese Garden located on the boundary of the University of Southern Queensland Toowoomba campus was used as the first field site in which to test the PPO dosimeter with the DSF. Figure 8.2 shows a panorama of the creek in the Japanese Gardens locale. The optical properties of the water found in this creek were detailed in Section 7.2.2 of Chapter 7. The creek had a measured length of 95 metres, width of 65 metres and an approximated depth of 4 metres. Measurements were carried out using the DSF in the creek in each season from early July 2007 to early April 2008. The number of days that the DSF was deployed in the environment was determined by the visible deterioration state of the dosimeters located at the top attachment site. If it could be seen that these dosimeters were becoming optically

saturated (distinguished by a change in appearance of the film from clear to orange) the measurement series was brought to an end. This protocol was employed not only for the creek water measurements, but also for the agricultural dam water measurements and the sea water measurements. The length of time it took for the top attachment site dosimeters to degrade changed slightly for each particular season across the year – long measurement series. Winter measurements ran over the space of 12 days inclusive from 16 July to 27 July 2007. Spring measurements ran over the space of 9 days inclusive from 1 October to 9 October 2007. Summer measurements ran over the space of 10 days inclusive from 18 February to 28 February 2008. Autumn measurements ran over the space of 10 days inclusive from 31 March to 9 April 2008. During the deployments, the DSF was placed in a position located far enough away from the shoreline of the creek so that shading from nearby plants and trees was minimal. The positioning of the DSF in the creek is depicted in Figure 8.3.



Figure 8.2: The Japanese Gardens Lake located on the University of Southern Queensland campus grounds.



Figure 8.3: Positioning of the DSF in the Japanese Gardens Lake.

8.3.2 University of Southern Queensland Research Dam

The second site selected for the PPO dosimeter field trials was an abandoned agricultural engineering research dam again located on site at the University of Southern Queensland, Toowoomba campus. A picture of the agricultural dam is provided in Figure 8.4. Figure 8.5 shows the position of the DSF in the agricultural dam as it was for each of the four seasonal trials. The optical properties of the water within the agricultural dam have been presented in Section 7.2.2 of Chapter 7. The agricultural dam had a measured length of 21 metres, width of 19 metres and an estimated depth of 3 metres. UVB exposure measurements were carried out using the DSF in the agricultural dam in four seasons from July 2007 to December 2008. Winter measurements ran over the space of 12 days inclusive from 2 July to 13 July 2007. Spring measurements ran over the space of 9 days inclusive from 15 October to 23 October 2007. Autumn measurements ran over the space of 8 days from 16 April to 23 April 2008. The autumn measurement series was initially planned to run for 10 days in total but flooding of the dam after overnight torrential rain brought the trial to a halt. Summer measurements in the agricultural dam could not be made in late 2007 or in early 2008 due to inclement weather conditions. However, supplementary measurements were performed over the following summer for 6 days inclusive from 1 December 2008 to 6 December 2008. Due to heavy evening rainfall and considerable winds over the campaign, three surface level dosimeters (east horizontal, south horizontal and west diagonal) were destroyed in this trial.



Figure 8.4: The agricultural dam located on the University of Southern Queensland campus grounds.

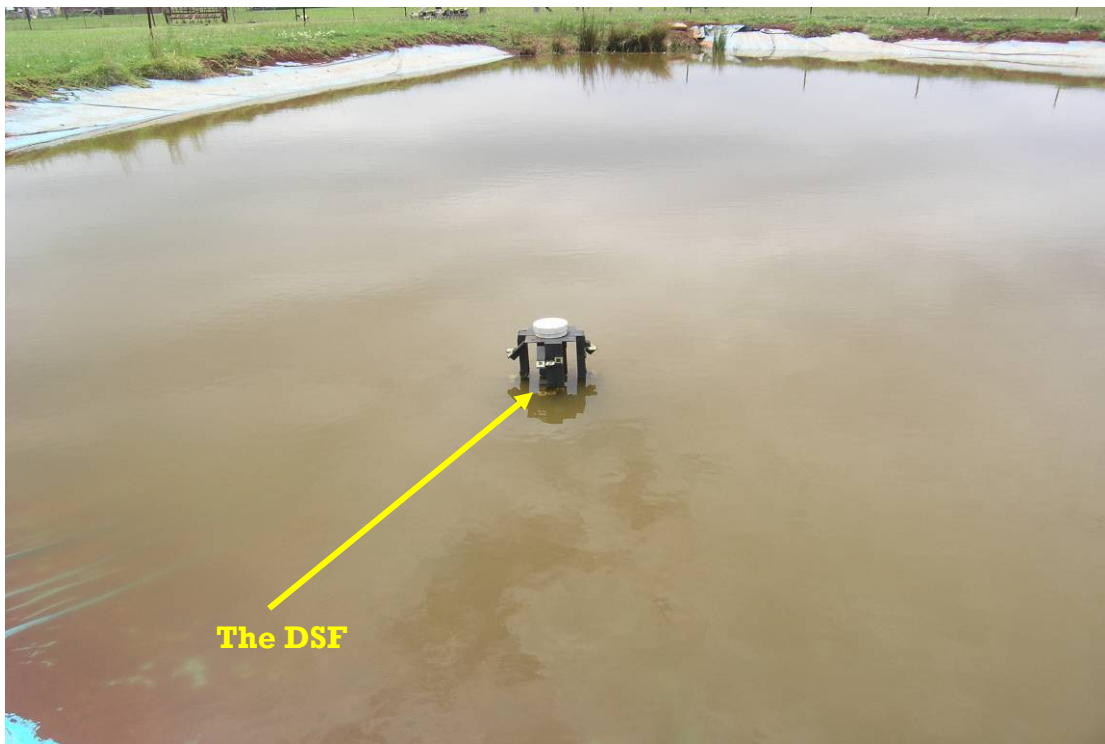


Figure 8.5: Positioning of the DSF in the agricultural dam.

8.3.3 Simulated Sea Water Environment

As the nearest coastline to Toowoomba is over 120 km away, it was decided that the final site for the PPO dosimeter field trials would be carried out in a large field simulated sea water environment instead of in the ocean itself. This negated the complexities that come into play during oceanic measurement campaigns such as high winds, turbulence, tidal changes and possible vandalism. The simulated sea water environment, as shown in Figure 8.6, consisted of a circular steel water tank which had a circumference of 10 metres and a depth of 1 ¼ metres. The sea water used in the tank was sourced from a coastal location near the city of Brisbane, Australia (27° 28' 04" S, 153° 01' 40" E, 0 m elevation) as was the case with the sea water used in the semi – controlled calibration campaigns detailed in Chapter 7. The optical properties characteristic to the sea water were previously given in Section 7.2.2 of Chapter 7. Figure 8.7 depicts how the DSF was positioned exactly in the centre of the tank so that it would receive only a minimal amount of shading during the early morning and the late afternoon. In order to eliminate any leakage from the tank and the seepage of rust into the sea water, the tank was covered with three layers of extra strength pond liner. Measurements were carried out using the DSF in the sea water tank in each season from June 2007 to July 2008. Spring measurements ran over the space of 9 days inclusive from 14 November to 22 November 2007. Autumn measurements ran over the space of 10 days inclusive from 31 March to 9 April 2008. Winter measurements ran over the space of 12 days inclusive from 30 June to 11 July 2008.

Very few useable results were obtained in an initial summer measurement series carried out in late February 2008 due to heavy amounts of rain and substantial cloud cover present in the Toowoomba area at the time. To remedy this, a second trial was

performed in early summer 2008/2009 over a period of 6 days inclusive running from 1 December to 6 December. A greater number of sunlight hours were available during this second trial in comparison to the first trial. However, more torrential rain and storms did occur late each afternoon, again reducing the total amount of solar exposure incident upon the dosimeters.



Figure 8.6: The simulated sea water environment located on the University of Southern Queensland campus grounds.

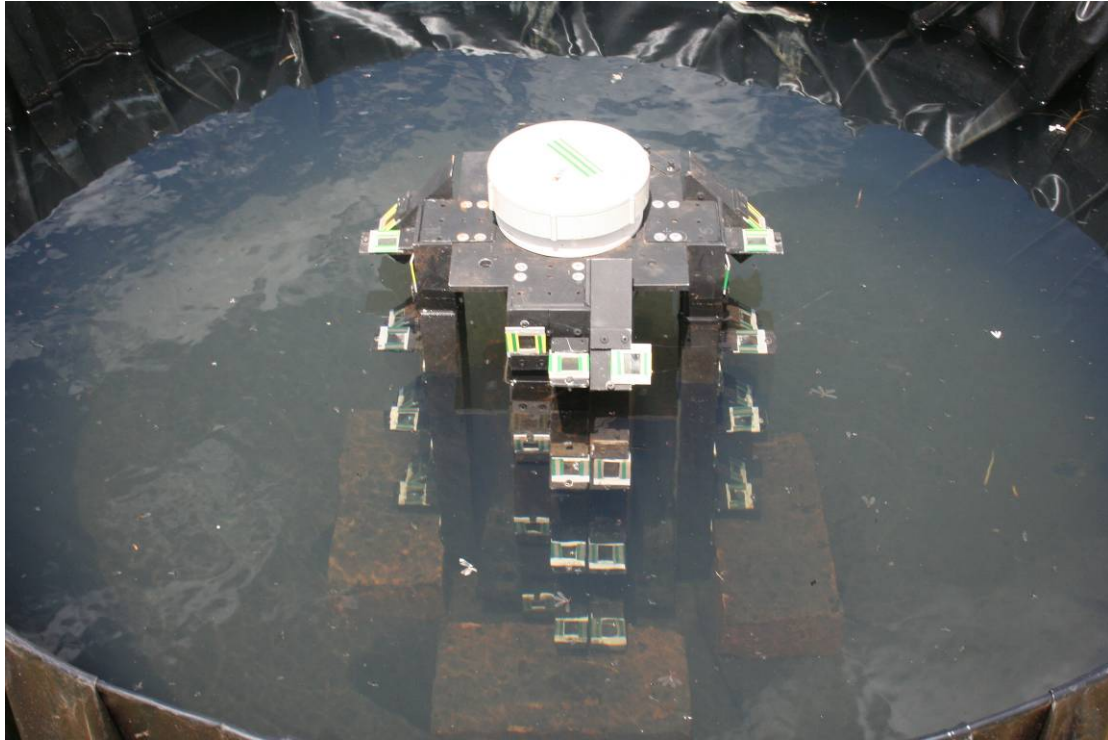


Figure 8.7: Positioning of the DSF in the simulated sea water environment.

8.3.4 PPO Dosimeter Calibrations for Each Location

From the analysis performed in Chapter 7 it was decided that in order to maintain adequate levels of accuracy, separate seasonal calibrations for the particular water types in each of the field locations would be used to calculate the UVB exposures recorded by the PPO dosimeters during the field measurement campaign. These calibrations were derived from the data detailed in Section 7.2.3 of Chapter 7. The Z_{1CM} and Z_{20CM} calibration data sets measured in each season for the creek water and sea water were merged together to create larger and more definitive data sets from which field – based UVB exposures could be measured. For the dam water the Z_{20CM} data was not used as it did not improve upon the accuracy of the existing Z_{1CM} data. The calibration data sets used for the creek, simulated sea water environment and dam are shown in Figure 8.8 (A), (B) and (C) respectively. The x – axis error bars

correspond to the usual $\pm 9\%$ underwater measurement uncertainty with the PPO dosimeter.

For the in – air measurements made with the PPO dosimeters at the top of the DSF, solar UVB calibrations measured for each season were used. These calibrations were carried out over the same time period as the year – long underwater calibration campaign and had been developed by employing integrated spectral UVB data obtained by the Bentham spectroradiometer. Figure 8.9 displays these in – air UVB calibrations as measured for autumn, winter, spring and summer seasons. The $\pm 7\%$ error inherent for all in – air PPO dosimeter measurements is represented by the x – axis error bars.

As was the case with the PPO dosimeter UVB calibrations measured in Chapter 8 a second – order polynomial equation of the following form was used to describe the characteristic trend for each of the underwater UVB calibration data sets:

$$UVB_{EXPOSURE} = -\alpha(\Delta A_{320})^2 + \beta(\Delta A_{320})$$

where $UVB_{EXPOSURE}$ is the UVB exposure intercepted by a PPO dosimeter at a given depth in units of kJ m^{-2} . Table 8.1 shows the α , β and R^2 values calculated for the modified underwater UVB calibrations for each season.

Due to the higher UVB exposure levels experienced by the PPO dosimeters on the water surface during the field measurements, a second order polynomial equation was found to not provide enough predictive accuracy when used with the seasonal in – air UVB calibration data. So a power law was used to model the overall trend of each of the in – air data sets instead:

$$UVB_{EXPOSURE} = \alpha(\Delta A_{320})^\beta$$

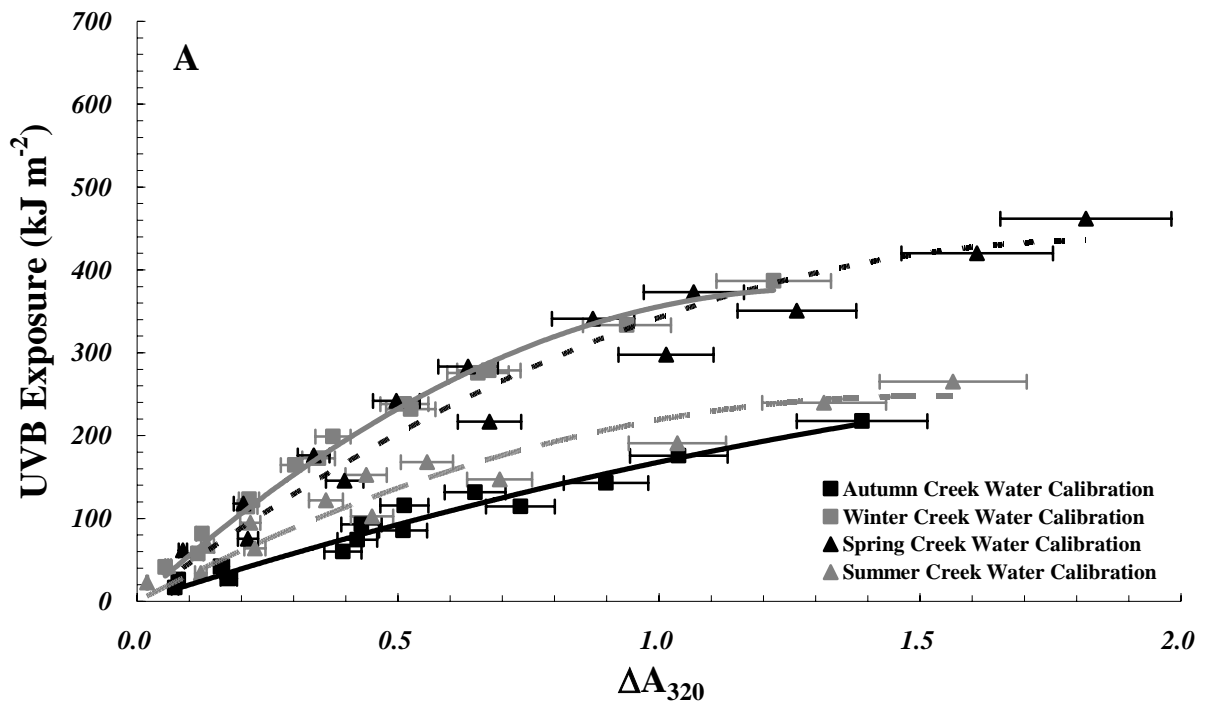
where $UVB_{EXPOSURE}$ is the UVB exposure measured by a PPO dosimeter at the water surface in kJ m^{-2} . Table 8.1 includes the α , β and R^2 values calculated for the in – air seasonal calibration equations.

Table 8.1: α , β and R^2 values obtained for the combined creek water, sea water, dam water UVB underwater calibrations measured over autumn, winter, spring and summer.

CALIBRATION TYPE	α	β	R^2
Creek Water Autumn	34.94	202.96	0.96
Sea Water Autumn	24.01	201.51	0.97
Dam Water Autumn	99.21	296.12	0.99
Creek Water Winter	218.3	574.05	0.99
Sea Water Winter	143.62	493.16	0.99
Dam Water Winter	299.31	643.08	0.98
Creek Water Spring	125.59	468.02	0.94
Sea Water Spring	165.47	431.08	0.96
Dam Water Spring	192.03	294.74	0.98
Creek Water Summer	108.1	327.29	0.91
Sea Water Summer	0.17	176.29	0.94
Dam Water Summer	56.9	234.03	0.99

Table 8.2: α , β and R^2 values obtained for the in – air UVB calibrations measured over autumn, winter, spring and summer.

CALIBRATION TYPE	α	β	R^2
UVB Autumn	232.78	0.8	0.99
UVB Winter	232.25	0.8	0.97
UVB Spring	317.95	0.78	0.9
UVB Summer	367.12	0.83	0.96



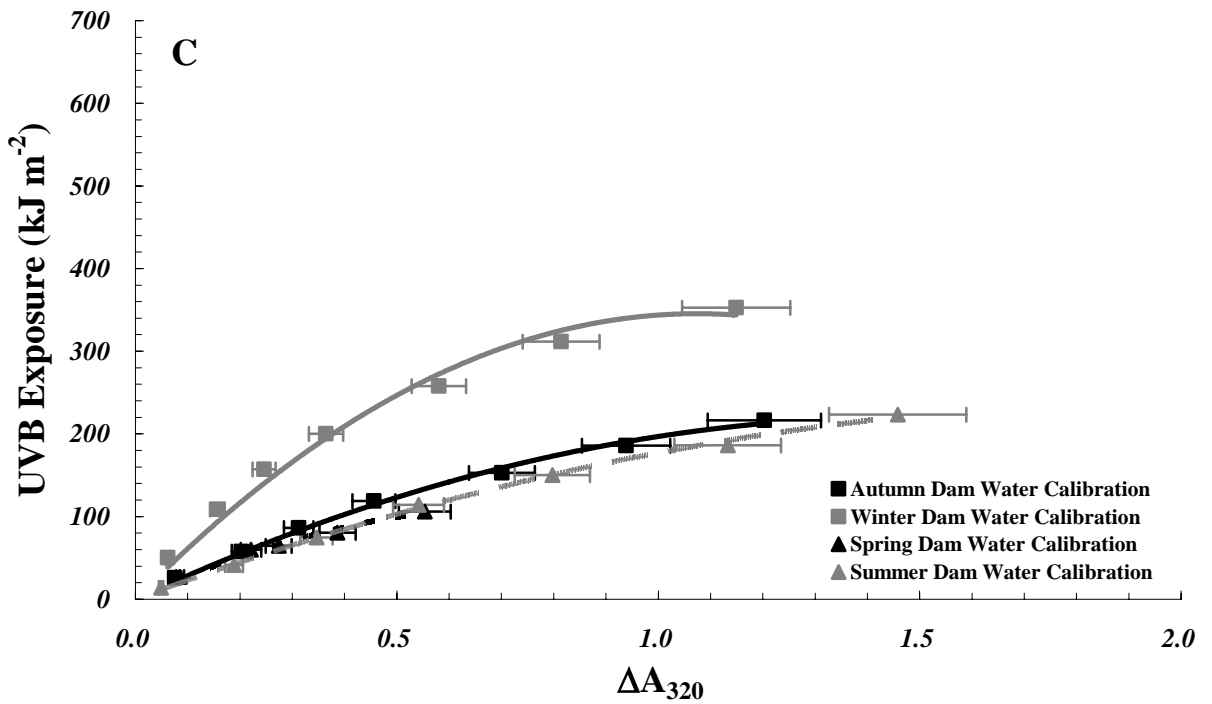
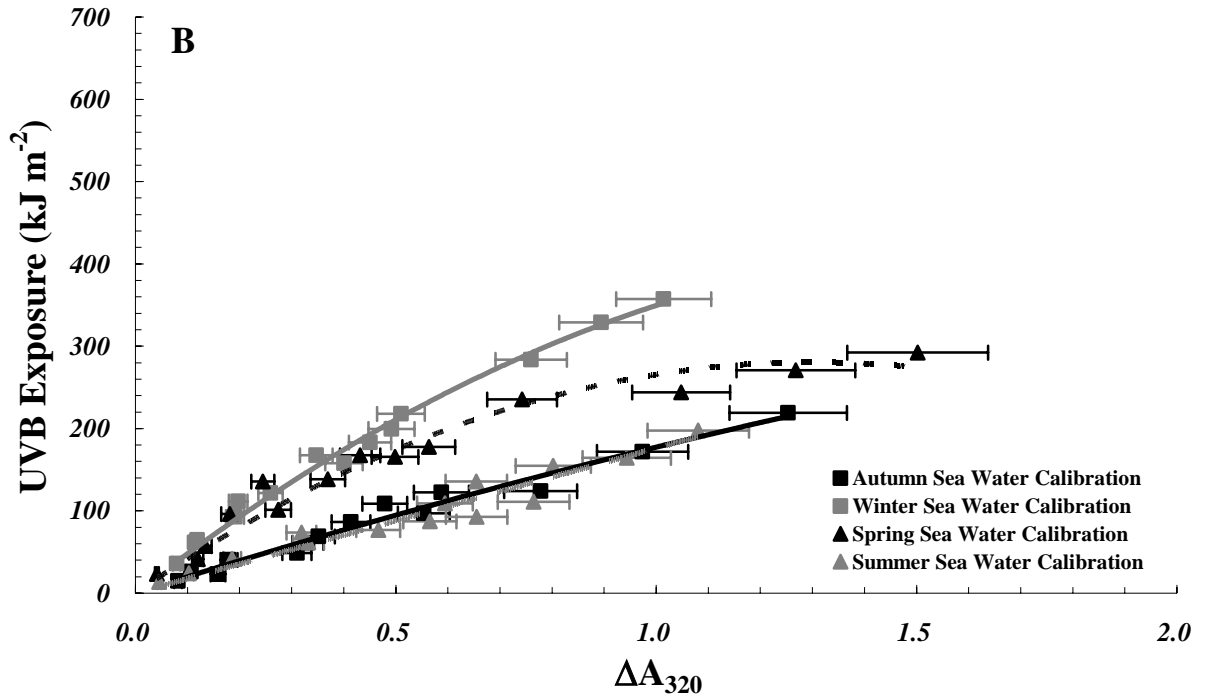


Figure 8.8: Creek (A), sea (B) and dam (C) underwater calibrations used to obtain field UVB exposures for each season.

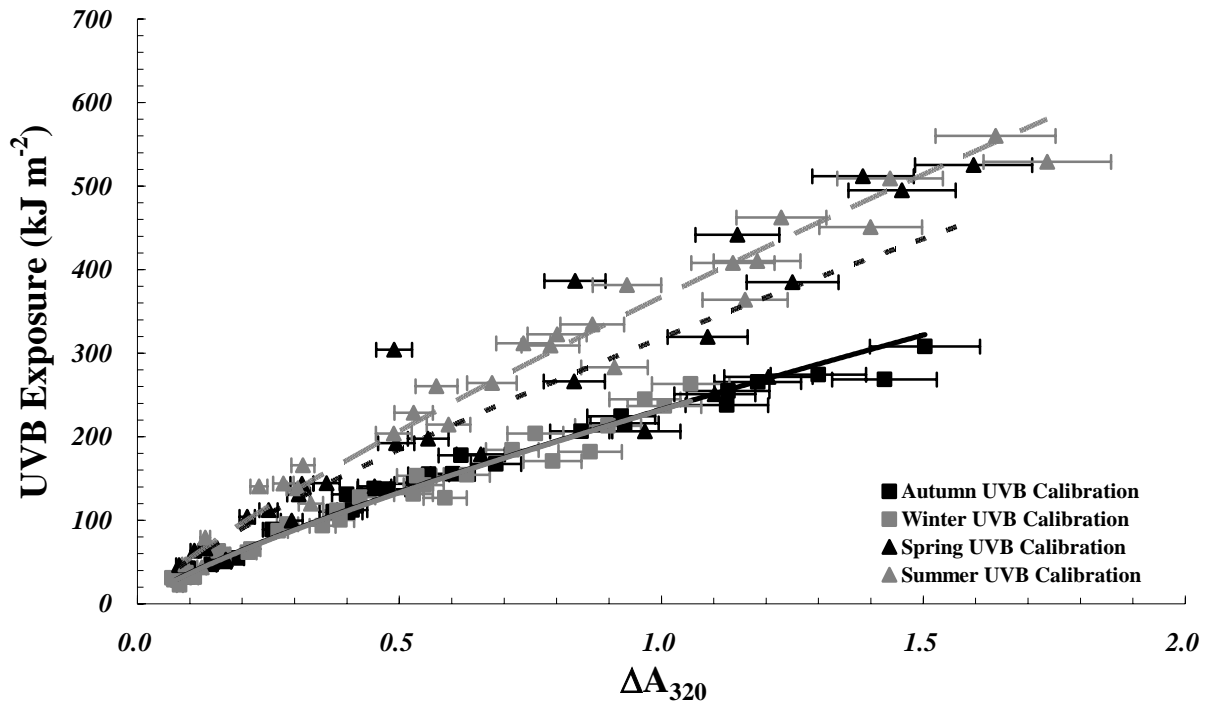


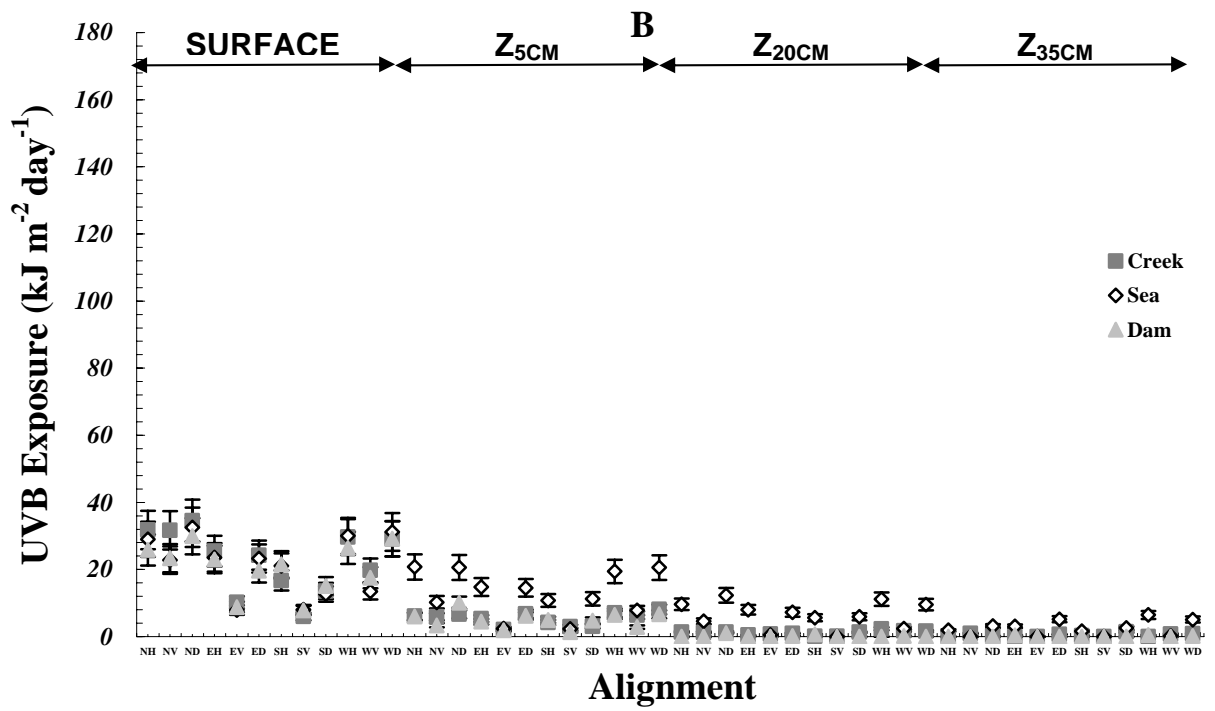
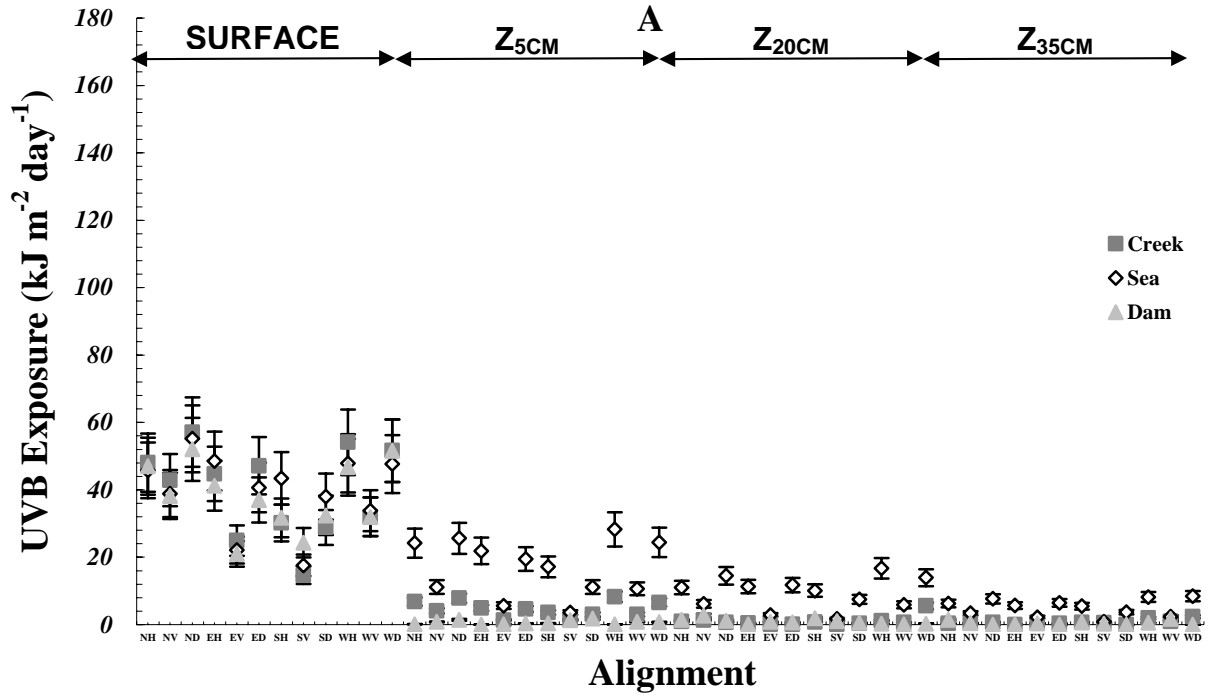
Figure 8.9: In – air UVB calibrations employed for the water surface field measurements made in each season.

8.4 Measurement Campaign Results

8.4.1 Creek Water

Measurement data collected with the DSF in the creek in autumn, winter, spring and summer can be seen in Figure 8.10 (A), (B), (C) and (D) respectively. The first 12 data blocks on the x – axis represent the daily averaged UVB exposures measured at the water surface running in order from the north, east, south and west cycling over the 0° , 90° , 45° orientations for each particular direction. This order continues for each following set of 12 data blocks along the x – axis for all the depths from 5 cm to 20 cm to 35 cm. The UVB exposure error was approximated as an accumulative $\pm 18\%$ uncertainty that results from errors generated during measurement and analysis procedures. This $\pm 18\%$ error threshold and the data presentation scheme remained

the same for both the dam water and sea water measurements. At the water surface for each season it can be clearly seen from the figures that relatively high levels of UVB exposure were received by the dosimeters, which was to be expected as they were not submerged. Throughout each season at the water surface the largest exposures were generally recorded at either the north or west alignments usually at an inclination of 45°. The horizontally aligned dosimeters commonly intercepted UVB dosages comparable if not slightly less than those received at the 45° inclination, with the vertically aligned dosimeters measuring the lowest amounts of solar UVB.



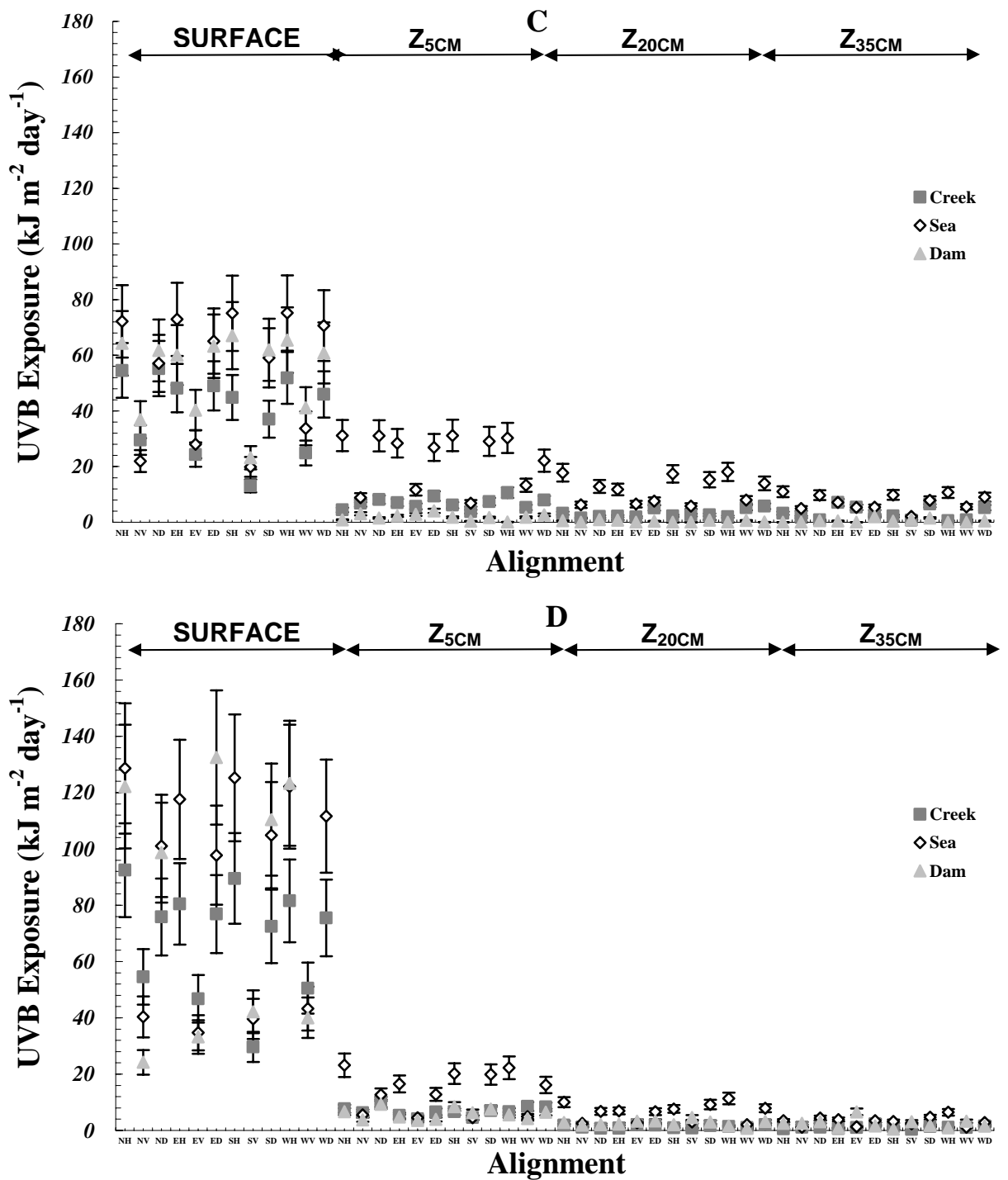


Figure 8.10: UVB exposure distributions in the creek, sea and dam water in autumn
 (A), winter (B), spring (C) and summer (D).

In the creek, measurements were able to be obtained at a depth of 5 cm across each particular measurement position. The general distribution of the exposures at this depth was extremely similar to what was seen with the exposures measured at the surface of the water. The highest exposures were again usually seen at either the north or west alignments at the 45° inclination, except for the data collected in spring where the dosimeter aligned to the horizontal directed to the west received the most UVB. However, in each season the magnitude of the UVB exposures at the 5 cm depth was considerably reduced in comparison to the measurements made at the surface across every single position. For example, in autumn the maximum daily averaged exposure received at the surface was $57 \text{ kJ m}^{-2} \text{ day}^{-1}$ recorded at the north 45° position. In comparison, at the same position 5 cm underwater the measurement recorded was $7.8 \text{ kJ m}^{-2} \text{ day}^{-1}$, a sizeable 86% reduction with respect to the surface UVB exposure. Again, in spring the maximum exposure was received at the north 45° position with a value of $55 \text{ kJ m}^{-2} \text{ day}^{-1}$. The measurement made at the same position 5 cm underwater was far less at $8 \text{ kJ m}^{-2} \text{ day}^{-1}$, which represented another reduction in UVB exposure of approximately 86%. This was surprising as the spectrophotometry results showed that the creek water had a reasonably high UVB transmission level. As the DSF was anchored at a location in the creek so that it was not influenced by any shade produced by shoreline plants and trees, the most plausible explanation for the drastic reduction in UVB exposure would be due to the large clusters of organic matter produced by local wildlife such as ducks and birds and decaying plant matter that was observed to be floating through the water at regular intervals. This organic matter could have blocked the incoming UVB effectively shading the dosimeters positioned underwater.

Throughout the measurement campaign very few reliable UVB exposures were measured during any season at the 20 cm and the 35 cm depths in the creek. Even in summer where solar output is at its highest levels, it appears that the UVB wavelengths failed to penetrate the creek water any further than 5 cm. This result meant that no depth profiles could be obtained for the creek water.

8.4.2 Sea Water

UVB exposure data measured using the DSF in the simulated sea water environment averaged over each day in autumn, winter, spring and summer can be seen in Figure 8.10 (A), (B), (C) and (D) respectively. As was shown in the creek water, it is seen from the figures that across every position UVB exposures received by the dosimeters at the water surface were far greater than those intercepted underwater. Over the seasons the highest exposures on the surface of the sea water were generally measured at either the west or north directions at the 45° or horizontal alignments. Again, due to the fact they were not exposed to the same amount of sky view as the 45° or horizontal dosimeters, the vertically aligned dosimeters measured UVB levels usually no more than half that measured by their 45° and horizontal counterparts oriented towards the same direction. As an example, in the spring measurement campaign, along the eastern orientation at the surface, the vertically aligned dosimeter measured an average daily UVB exposure of 28 kJ m⁻² day⁻¹, while comparatively the dosimeter at the horizontal alignment measured 73 kJ m⁻² day⁻¹ and the dosimeter at the 45° alignment measured 65 kJ m⁻² day⁻¹.

Unlike the underwater measurements made in both the creek and the agricultural dam, significant UVB measurements were able to be made at each depth from 5 cm down

to 35 cm across the entirety of the measurement campaign. As was seen in the creek series of measurements, data obtained at the first depth underwater was significantly less in magnitude in comparison to measurements made at the water surface. For instance, in winter the value for UVB exposure obtained along the east direction at the horizontal inclination was measured to be $24 \text{ kJ m}^{-2} \text{ day}^{-1}$ in comparison to $15 \text{ kJ m}^{-2} \text{ day}^{-1}$ which was measured at the same position 5 cm underwater. This represented a decrease of roughly 38% in total UVB exposure.

From 5 cm deep to 20 cm deep and then again from 20 cm deep to 35 cm deep further considerable attenuation of the incoming UVB exposure was found to occur for every measurement series in the sea water. A good example of this can be seen in the spring measurement set, from the 5 cm depth to the 20 cm depth where a drop in UVB exposure of approximately 46% occurs at the horizontally aligned position facing south. Once more, at this same position, from the 20 cm depth to the 35 cm depth, a reduction of around 41% in the UVB exposure was measured to exist between the two. Another example of high UVB attenuation is seen at the 45° alignment along the east direction in the autumn data set, where a reduction in UVB exposure of 37% was recorded between the 5 cm and 20 cm depths with a further 50% reduction in UVB exposure occurring between the 20 cm and 35 cm depths.

Unlike the creek water and the agricultural dam, it was found that the decrease in UVB exposure with increasing depth could be modelled with a good level of accuracy by using power law functions fitted to all of the exposure depth profiles for the sea water at each azimuth in every season. These functions each have the form:

$$UVB_{EXPOSURE} = \psi z^{-\omega}$$

where $UVB_{EXPOSURE}$ is the UVB dosage measured by the dosimeter during the exposure time in units of kJ m^{-2} and z is the depth in units of cm. Averaged UVB exposure depth profiles at 5 cm, 20 cm and 35 cm produced from the horizontally aligned sea water exposure distribution data can be viewed in Figure 8.11 for each season. The y – axis errors bars represent a calculated $\pm 18\%$ range of uncertainty inherent within each data point. The ψ , ω and R^2 data for each specific depth profile are provided in Table 8.3. From Figure 8.11 it can be seen that the UVB data obtained in the sea water in summer are smaller overall in magnitude in comparison to the measurements made in autumn and spring and only slightly greater than the UVB measurements made in winter. This was due to a substantial amount of cloud coverage and rain being prevalent for roughly three days out of the six day summer measurement campaign greatly reducing incident amounts of solar UVB.

Table 8.3: ψ , ω and R^2 values calculated for the sea water UVB depth distributions for autumn, winter, spring and summer.

SEASON	ψ	ω	R^2
Autumn	64.75	0.61	0.93
Winter	61.53	0.76	0.88
Spring	77.36	0.56	0.96
Summer	74.69	0.77	0.96

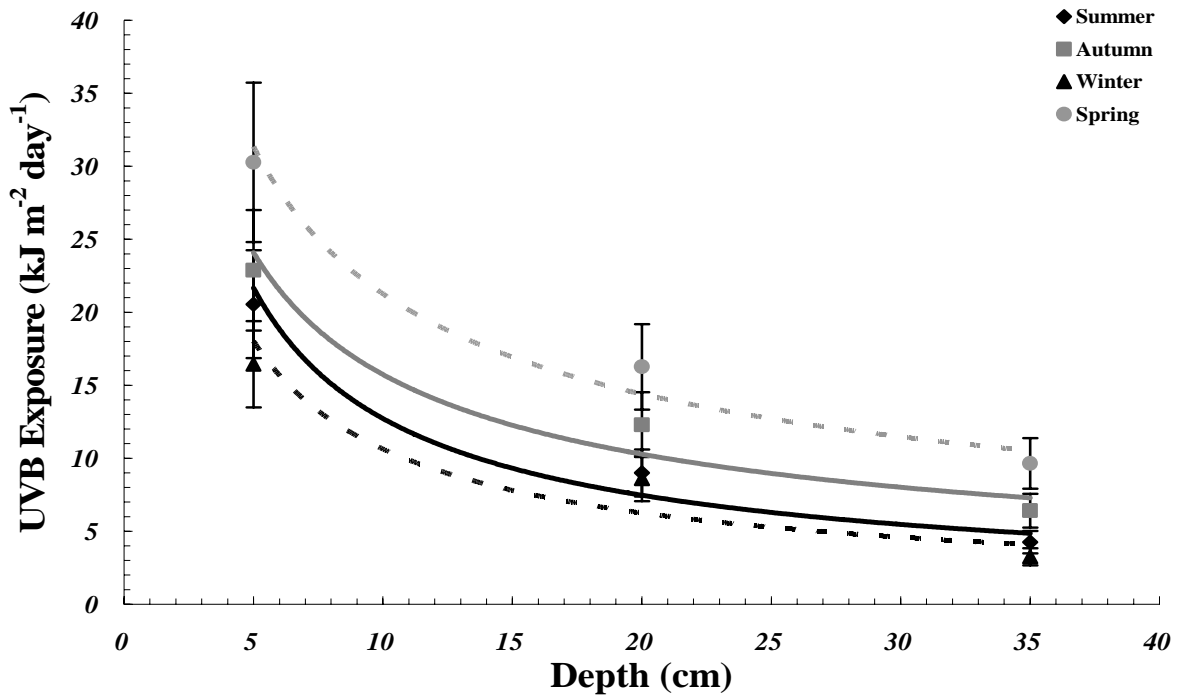


Figure 8.11: Averaged UVB exposure depth regimes as extracted from horizontally aligned sea water exposure distribution data for each season of the year.

8.4.3 Agricultural dam

Daily averaged UVB exposure measurement data recorded with the DSF in the agricultural dam in autumn, winter, spring and summer can be seen in Figure 8.10 (A), (B), (C) and (D) respectively. As was the case with the creek water and the sea water, the levels of UVB exposure recorded just above the water surface were the highest. Due to the very high level of UVB absorption present in the agricultural dam, no reliable data could be measured by the dosimeters underwater, except for some relatively small values found in each campaign. However, it is unclear if these measurements are reliable, as there were high amounts of soil discharge in the water that mildly stained the PPO dosimeter film. It is possible that this staining could have led to incorrect absorption values being measured by the spectrophotometer.

Therefore, similarly to the creek water, no depth profiles could be provided for the agricultural dam water.

8.4.4 Attenuation Coefficient Calculation for the PPO Dosimeters

To calculate K_d values with the PPO dosimeters only calibrated UVB exposure data measured at the 0° angular inclination were used. The calibrated UVB exposure data gathered at each of the three depths were used in conjunction with the modified Beer – Lambert – Bouguer Law. Linear regression analysis was performed with the modified Beer Lambert Bouguer Law in order to extract the value for K_d . A final K_d estimate was determined by averaging together the particular K_d values calculated for each geographical direction.

8.4.5 Attenuation Coefficient Calculation for the Calibrated EPP2000 Spectrometer

Evaluation of K_d values for each of the three different water types were made using the same underwater UVB spectral irradiance data collected with the EPP2000 spectrometer during the measurement campaign over two cloud free days in early autumn and two additional cloud free days in mid winter for the calibration between the IL1400 broadband meter and the EPP2000 spectrometer. Over the range of SZA encountered throughout the measurements made each day, for each water type at each depth, a UVB irradiance value was calculated by integrating the spectral UVB irradiance across the UVB waveband. This integrated UVB value was then included in a series of depth profiles. The modified Beer – Lambert – Bouguer Law was again used together with the depth profiles to find the necessary K_d values in a similar way to how it was used with the dosimetric measurements, except irradiance data was used in the linear regression process instead of exposure data.

8.4.6 Comparison of the Attenuation Coefficients Calculated in the Sea Water with the EPP2000 Spectrometer and the Dosimeters

Figure 8.12 compares the K_d values calculated from the sea water UVB exposure depth regimes compared to the averaged sea water K_d value calculated using the EPP2000 spectrometer. The percentage variation calculated directly as $\frac{\sigma}{\mu} \cdot 100\%$ for each K_d estimation applicable to both the dosimeters and the EPP2000 spectrometer is represented in the figure by the y – axis error bars. σ is defined as the standard deviation across all of the K_d estimates obtained for each separate season and μ is defined as the mean across all of the K_d estimates obtained for each separate season. Using the dosimeters, the K_d value in the sea water was estimated to be 0.045 cm^{-1} in summer, 0.073 cm^{-1} in winter, 0.043 cm^{-1} in autumn and 0.039 cm^{-1} in spring. The average value of these four measurements was found to be 0.049 with a standard deviation of ± 0.017 . The averaged K_d values determined with the EPP2000 spectrometer from the solar spectral UVB data sets obtained in early autumn and mid winter were found to be 0.028 cm^{-1} with a standard deviation of ± 0.025 and 0.036 with a standard deviation of ± 0.014 respectively.

Almost all of the K_d values were found to be in relatively close agreement with each other in accordance to the estimated error margins. However, the winter K_d estimation calculated with the dosimeters was found to be substantially greater in value in comparison with all the other K_d approximations. This could have occurred due to the shading of the lower sections of the DSF in the sea water tank during high SZA conditions that are prevalent during winter especially in the early to mid morning and early to late afternoon, as discussed in Section 8.2. The dosimeters positioned primarily at the depths of 20 cm and 35 cm in the tank would have received a lower

amount of UVB exposure during these intervals each day in comparison to their counterparts in the autumn, spring and summer measurement campaigns. By inspection of the modified Beer – Lambert – Law used to calculate the K_d values for the dosimeters, it can be clearly seen that any reduction in measured UVB leads to an inevitable increase in the K_d estimate.

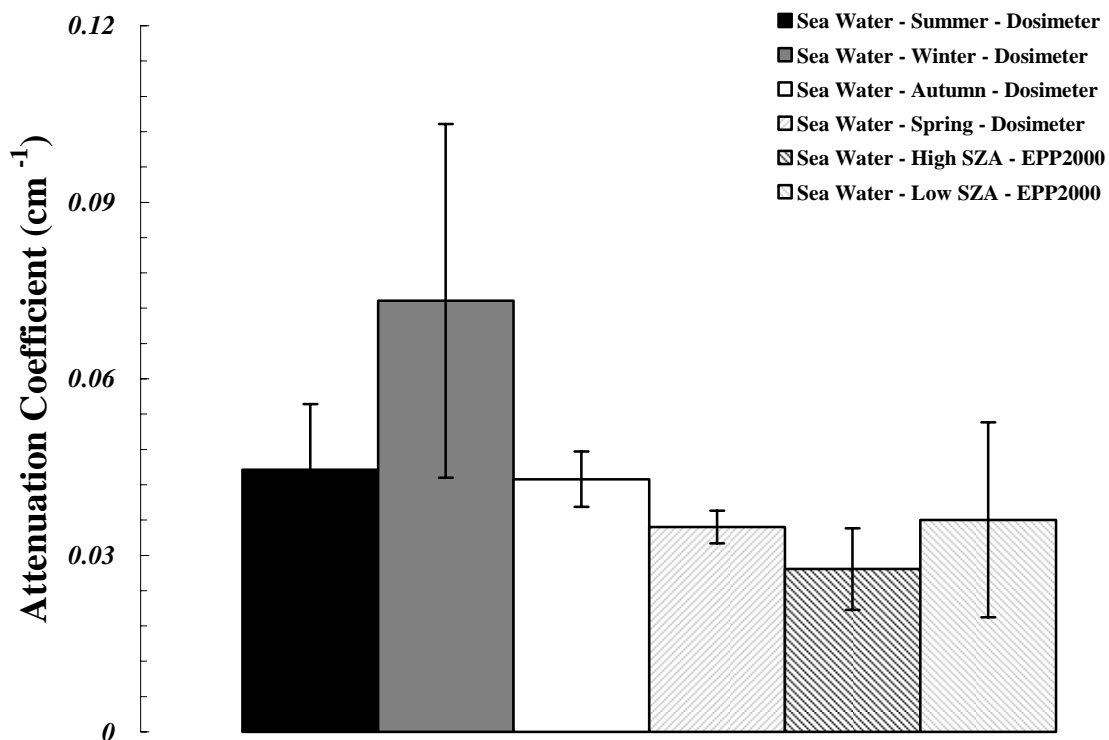


Figure 8.12: K_d values calculated from the sea water UVB exposure depth regimes compared to the K_d value calculated using the EPP2000 spectrometer for sea water.

8.5 Chapter Discussion

The results produced in this research show that the PPO dosimeter provides comparable UVB exposure data compared to the spectrometric alternative within a good level of accuracy in types of water with little amounts of DOM and particulate matter, such as the sea water. The PPO dosimeter is useful in water with increased turbidity and DOM content for depths up to approximately 5 cm. However, the

usefulness of the PPO dosimeter at any depths greater than approximately 5 cm may be reduced in water with increased levels of water turbidity and DOM content, which both in turn reduce the overall UVB transmission and enhance the UVB absorption capabilities of the water leading to a reduction in the penetrative ability of the UVB. This was the case with the creek water and the agricultural dam water. In addition, in order to achieve accurate results with the PPO dosimeter, a rigid calibration regime such as the one carried out for this research must be applied in order to allow for variations in the solar UVB spectrum brought on by changes in the sun's position from season to season and to take into account any influence of column ozone fluctuations which may occur throughout the year.

It was seen from the measurements made with dosimeters in the creek water and in the agricultural engineering dam water that only small amounts of UVB exposure could be reliably recorded at the shallow depth of 5 cm in close to ideal conditions, with no UV recorded beneath that depth, even in high solar UVB conditions through summer, early autumn and late spring. This suggests that there is a characteristic limit to the depth at which the PPO dosimeter can be used underwater in water types with relatively high amounts of turbidity DOM content. In this research it appears that this limit is reached just below the 5 cm depth in water types having less than or equal to 75% UV transmission at a wavelength of 315 nm, which was the value obtained for the creek water. However it can be used up to at least 35 cm in sea water.

As mentioned in Section 6.4 as being the cause of discrepancies in NDF measurements, one possible reason for the differences between the usable depth ranges for the creek and sea water types, despite having similar optical characteristics,

could be due to the fact that a substantial amount of the absorbance and hence transmittance measured by the spectrophotometer was actually scattering, which will greatly attenuate light in the direct beam but for a PPO dosimeter employed underwater a substantial amount of direct beam and scattered light will still be intercepted. Therefore, as recommended in Section 6.4, any measurement of the transmittance of water should be evaluated using a scattered transmission accessory, such as an integrating sphere.

Not only do these water types like that found in the creek and the agricultural dam inhibit and attenuate the penetration of the solar UVB, but these water types are more likely to have free floating particulates and suspended masses of organic matter that could possibly condense on the dosimeter film and block out the UVB which would lead to distorted outcomes. Also, in creek, dam and estuary water type environments there is the possibility of the dosimeters being shaded by falling branches, leaves and other types of assorted plant matter which would further add to measurement uncertainty. One way to overcome these types of issues that occur at natural water locales such as dams, creeks and estuaries would be to check on and clean the dosimeters at regular intervals. However, this would be time consuming for the researcher and defeats the main purpose of the dosimeter, which is being able to leave it unattended underwater for extensive periods.

At this point in time it is recommended that this dosimeter only be used in 'cleaner' underwater locations distanced from influencing natural environmental factors like wildlife, shoreline trees and plants that have the potential to deposit various types of organic matter into the water. One such example of a 'cleaner' water locale would be

in the ocean itself, preferably near or on a reef where frequent subsurface mixing takes place which would keep the water fresh and clear of any major contaminants. Fjords, such as those found in the Arctic regions and similar water bodies in Antarctica may also be an ideal location for PPO dosimeter measurements as the water found in them is sourced from glaciers or ice bergs, which is generally clear with an extremely high UV transmission capability. The PPO dosimeter could also be deployed in free flowing creeks, as the water in these locations is kept relatively clean due to its constant movement.

On the other hand, if the total incident UV exposure incident on various living organisms needs to be completely quantified, the attachments of organic matter to the surface of the PPO film during deployment is not a problem because organic matter naturally becomes attached to life forms over time in real underwater environments. This build up of organic matter most commonly occurs on sedentary organisms such as corals, seaweeds and seagrasses. Therefore, the PPO dosimeter would provide a useful measure of the total protection provided by organic matter to these particular types of aquatic life.

Chapter 9

Conclusions

9.1 Conclusions

Solar UV has a far reaching influence upon the underwater ecosystem, directly affecting the sensitive balance between aquatic animal and plant species across all regions of the food chain. In order to simplify the process involved in gathering underwater UV exposure data made difficult and complicated by the use of electronic optical measurement instrumentation such as spectroradiometers, radiometers and spectrometers, this dissertation has developed, tested and evaluated the novel use of the PPO dosimeter in underwater environments.

The first research objective as specified in Section 1.2 was met with the analysis of the optical and physical properties of the PPO dosimeter in clean impurity free water within a controlled laboratory environment using a solar UV fluorescent tube source. From this it was found that the PPO dosimeter could be successfully calibrated and prepared for underwater use. However, in – air to underwater calibration transfers were deemed to be unworkable without introducing substantial errors. Underwater cosine response was measured to be sufficient up to an incident angle of 80° . In addition, dosimetric measurement repeatability and measurement error in ideal underwater conditions was found to be only 2% to 3% greater than that of in – air measurements. Also, watermarking effects were discovered to affect measurements by up to 13% after 120 hours worth of submersion time. This problem was easily alleviated by spraying the dosimeters with a blast of distilled water after extraction from the water (Schouten *et al*, 2007).

The goals set out in the second research objective detailed in Section 1.2 were completed after an extensive year long calibration campaign with the PPO dosimeter

calibrated against both the solar erythemal action spectrum in – air and to the solar UVB spectrum underwater at different depths in a semi – controlled tank environment during the months of autumn, winter, spring and summer in the clear, creek, sea and dam water types. In these in – air and underwater calibration series it was discovered that the PPO dosimeter had the ability to receive exposures over a longer time span, in the order of roughly seven times as much, in comparison to the polysulphone dosimeter that has been the chemical dosimeter of choice for researchers for over twenty years. Testing of a polyethylene based NDF showed that the response of the PPO dosimeter could be even further extended before reaching optical saturation. It was also found that in both in – air and underwater conditions, the PPO film response varied with modulations of the incident solar spectrum composition resulting naturally from changing SZA and atmospheric column ozone. Based on this it was recommended that the PPO dosimeter only be calibrated specifically in the season in which it is to be used, preferably at the same time as measurements were being made in the field. Moreover, PPO dosimeter response underwater was found to be dependent upon water type, but only when the characteristic transmission spectra between two water types was different on average by more than 5% over the UVB waveband (Schouten *et al*, 2008).

Research objective three as provided in Section 1.2 was successfully completed following the deployment of the PPO dosimeter with the novel DSF unit over an entire year to measure the angular distribution of the solar UVB in a creek, a stagnant dam and in a simulated field sea water environment each having a characteristic water type with its own turbidity and DOM level. UVB exposures were measured down to a depth of 5 cm in the creek water and the dam water and down to a depth of 35 cm in

the sea water. It is assumed that the PPO dosimeter would be capable of measuring exposures even deeper than 35 cm in the sea water. After completion of the field measurement campaign, PPO dosimeter measurements taken from the sea water measurements were used to calculate a series of K_d values specific for each season. These K_d values showed good levels of agreement when compared to attenuation coefficient calculations made using the calibrated EPP200 spectrometer in the same sea water. Quantitatively, the K_d value estimates when averaged across all the seasons were found to be 0.05 cm^{-1} as measured by the PPO dosimeters compared to 0.032 cm^{-1} as measured by the EPP2000 spectrometer. With shading effects factored out for the PPO dosimeter measurements, the K_d value calculated using the PPO dosimeters got even closer to the EPP2000 spectrometer's estimate, reducing to 0.042 cm^{-1} (Schouten *et al*, 2009).

From these outcomes, it is believed that the PPO dosimeter will prove to be an easily deployable, inexpensive and ultimately invaluable tool for marine scientists, particularly marine biologists interested in the effects of long – term solar UV radiation exposure upon aquatic life forms and environments such as coral reefs and solar UV physicists who aim to better quantify the distribution of the solar UV radiation field in underwater environments without having to use cumbersome optical meters. Health professionals may also find the PPO dosimeter useful for estimating UV dosages on humans engaged in a wide variety of aquatic activities such as swimming in pools, creeks, dams and at the beach and also during snorkelling and diving activities.

9.2 Future Work

Several follow up investigations, such as the examples detailed below, could be conducted to further enhance the understanding of the physical and optical characteristics and also the working limitations of the PPO dosimeter, ultimately assisting and increasing the usability and applicability of the PPO dosimeter for both in – air and marine UV measurement campaigns:

- Deploy the PPO dosimeter in a wider range of water types different to the ones analysed in this dissertation ranging from the most extremely turbid water such as that found in stagnant mangroves to the most clean and pure water such as glacial stream water in order to completely determine the absolute spectral transmission range within which the PPO dosimeter can be used most effectively with minimal error;
- Further detailed analysis could be performed with the PPO dosimeter by obtaining more UV depth profiles and normalising them to water surface exposures over a wider range of atmospheric conditions and seasonal changes in SZA. From this information it could be definitively deduced if underwater UV exposures do vary from season to season;
- Take measurements with the PPO dosimeter together with a submersible radiometer across a progressively increasing depth range at an aquatic location in water with relatively few impurities to estimate the exact sensitivity at which PPO film no longer produces a response in close to ideal conditions, and in doing so find the minimum operational sensitivity of the PPO dosimeter;

- Quantify the dose – response of the PPO dosimeter over a range of different angles to determine if varying badge orientation and inclination has any influence over calibrations of the PPO film to the solar UV;
- Use the PPO dosimeter to measure long – term UV exposure over coral reefs by attaching the PPO film badge to hard corals with waterproof glue. The data gathered by the PPO dosimeters could then be used to model zooxanthellae mortality rates and in turn coral bleaching and coral mortality rates against UV exposure, and hence determine if UV really has any influence upon coral health;
- Follow up on the initial in – air research conducted by Turnbull and Schouten (2008) and calibrate the PPO dosimeter with the mylar filter to the shortwave UVA waveband underwater. In this work basic optical and physical properties of the dosimeter system would have to be detailed such as cosine response, spectral response, temperature effect, dose – rate independence, interdosimeter variation and exposure additivity. Calibrations to the solar UV would also have to be performed in each season in multiple water types;
- Extend the preliminary in – air research carried out in Section 6.2 and calibrate the PPO dosimeter with the NDF to the UVB waveband underwater. Again, as with the PPO film and mylar filter system the optical and physical properties of the PPO film and NDF dosimeter system would have to be quantified, and calibrations would have to be made in each season to the solar UV in a variety of different water types. These calibrations may be stretched over the space of several years due to the increased exposure capability of the NDF dosimeter that would become even more pronounced in water types with restricted levels of UV transmission;

- Measure UV exposures with the PPO dosimeter continuously over several years time both in – air and underwater to encompass as many changing atmospheric conditions as possible including column ozone, aerosols and SZA. From this vast amount of information, it would be possible to create correction factor data sets for different column ozone levels, aerosol concentrations and SZA to further improve the accuracy of the PPO dosimeter;
- Placement of the PPO film on human subjects to determine solar UV exposure levels encountered during aquatic leisure activities such as swimming, snorkelling and diving, for which there has been very little information published. In these activities humans generally go in and out of water in cycles. Due to this, a special hybrid PPO film calibration to the solar UV combining both in – air and underwater calibration regimes may need to be formulated for this research.

References

- Bais, A.F., Zerefos, C.S., Meleti, C., Ziomas, I.C. & Tourpali, K. 1993, 'Spectral measurements of solar UVB radiation and its relations to total ozone, SO₂ and clouds,' *Journal of Geophysical Research*, Vol. 98(D3), pp. 5199-5204.
- Bais, A.F., Kazantzidis, A., Kazadzis, S., Balis, D., Zerefos, C.S. & Meleti, C. 2002, 'Effects of aerosol optical depth and single scattering albedo on surface UV irradiance,' in Proceedings of SPIE Vol. 4482 *Ultraviolet Ground- and Space-based Measurements, Models and Effects*, edited by James R. Slusser, Jay R. Herman, Wei Gao (SPIE, Bellingham, WA, 2002) 15-22.
- Baker, K. S. & Smith R. C. 1982, 'Bio-optical classification and model of natural waters,' *Limnology and Oceanography*, Vol. 27, pp. 500-509.
- Banaszak A.T. & Neale P.J. 2001, 'Ultraviolet radiation sensitivity of photosynthesis in phytoplankton from an estuarine environment,' *Limnology and Oceanography*, Vol. 46, pp. 592-603
- Barbieri, E.S., Villafane, V.E. & Helbling, E.W. 2002, 'Experimental assessment of UV effects upon temperate marine phytoplankton when exposed to variable radiation regimes' *Limnology and Oceanography*, Vol. 47, pp. 1648-1655.
- Barton, I.J. & Paltridge, G.W. 1979, 'The Australian climatology of biologically effective ultraviolet radiation,' *Australian Journal of Dermatology*, Vol. 20, pp. 68-74.
- Basher, R.E. 1996, 'Perspectives on monitoring ozone and solar ultraviolet radiation,' *Transactions of the Menzies Foundation*, Vol. 15, pp. 81-88.
- Bates, D.R. 1984, 'Rayleigh scattering by air,' *Planetary and Space Science*, Vol. 32, pp. 785-790.
- Belmont, P., Hargreaves, B.R., Morris, D.P. & Williamson, C.E. 2007, 'Estimation attenuation of ultraviolet radiation in streams: Field and laboratory methods,' *Photochemistry and Photobiology*, Vol. 83, pp. 1339-1347.
- Bell, G.M. & Hoar, W.S. 1950, 'Some effects of ultraviolet radiation on sockeye salmon eggs and alevins,' *Canadian Journal of Research*, Vol. 28, pp. 35-43.
- Bernhard, G., Booth, C.R. & McPeters, R.D. 2003, 'Calculation of total column ozone from global UV spectra at high latitudes,' *Journal of Geophysical Research*, Vol. 108(D17), 4532, doi:10.1029/2003JD003450
- Berhnard, G., Booth, C.R., & Ehramjian, J.C. 2004, 'Version 2 data of the National Science Foundation's ultraviolet radiation monitoring network: South Pole,' *Journal of Geophysical Research*, Vol. 109, D21207, doi:1029/2004JD004937

- Berhnaard, G., Booth, C.R., Ehramjian, J.C. & Nichol, S.E. 2006, 'UV climatology at McMurdo station, Antarctica, based on Version 2 data of the National Science Foundation's ultraviolet monitoring network,' *Journal of Geophysical Research*, Vol. 111, D11201, doi: 10.1029/2005JD005857
- Berre, B. & Lala, D. 1989, 'Investigation on photochemical dosimeters for ultraviolet radiation,' *Solar Energy*, Vol. 42(5), pp. 405-416.
- Bigelow, D.S., Slusser, J.R., Beaubien, A.F. & Gibson, J.H., 1998 'The USDA ultraviolet radiation monitoring program,' *Bulletin of the American Meteorological Society*, Vol. 79(4), pp. 601-615.
- Birkeland, C. 1997, *Life and Death of Coral Reefs*, Springer Publishing, United States.
- Bissett, W.P., Schofield, O., Glenn, S, Cullen, J.J., Miller, W.L., Plueddemann, A.J. & Mobley, C.D. 2001, 'Resolving the impacts and feedback of ocean optics on upper ocean ecology,' *Oceanography*, Vol. 14, pp. 30-53.
- Blaustein, A.R. & Kiesecker, J.M. 1997, 'The effects of ultraviolet – B radiation on amphibians in natural ecosystems,' in D.P. Hader (ed.) *The Effects of Ozone Depletion of Aquatic Ecosystems*, R.G. Landes Company, United States.
- Blumthaler, M. & Ambach, W. 1988, 'Solar UVB albedo of various surfaces,' *Photochemistry and Photobiology*, Vol. 48, pp. 85-88.
- Blumthaler, M. 1993, 'Solar UV measurements,' in M. Tevini (ed.), *UV-B Radiation and Ozone Depletion*, Lewis, Boca Raton.
- Blumthaler, M., Ambach, W. & Salzberger, M. 1994, 'Effects of cloudiness on global and diffuse UV irradiance in a high – mountain area,' *Theoretical and Applied Climatology*, Vol. 50, pp. 23-30.
- Blumthaler, M., Ambach, W. & Ellinger, R. 1997, 'Increase in solar UV radiation with altitude,' *Journal of Photochemistry and Photobiology B: Biology*, Vol. 39, pp. 130-134.
- Bodhaine, B. A., Dutton, E. G., McKenzie, R. L. & Johnston, P. V. 1998, 'Calibrating broadband UV instruments: ozone and solar zenith angle dependence,' *Journal of Atmospheric and Oceanic Technology*, Vol 15, pp. 916-926.
- Bodhaine, B.A., Wood, N.B., Dutton, E.G. & Slusser, J.R. 1999, 'On Rayleigh Optical Depth Calculations,' *Journal of Atmospheric and Oceanic Technology*, Vol. 16, pp. 1854-1861.
- Boeing, W.J., Leech, D.M., Williamson, C.E., Cooke, S. & Torres, L. 2004, 'Damaging UV radiation and invertebrate predation: conflicting selective pressures for zooplankton vertical distribution in the water column of low DOC lakes,' *Oecologia*, Vol. 138, pp. 603-612.

- Boelen, P., Obernosterer, I., Vink, A.A. & Buma, A.G.J. 1999, 'Attenuation of biologically effective UV radiation in tropical Atlantic waters measured with a biochemical DNA dosimeter,' *Photochemistry and Photobiology*, Vol. 69(1), pp. 34-40.
- Bojkov, R.D., Fioletov, V.E. & Diaz, S.B. 1995, 'The relationship between solar UV irradiance and total ozone from observations over southern Argentina,' *Geophysical Research Letters*, Vol. 22(10), pp. 1249-1252.
- Bracchini, L., Loisselle, S., Dattilo, A.M., Mazzuoli, S., Cozar, A. & Rossi, C. 2004, 'The spatial distribution of optical properties in the ultraviolet and visible in an aquatic ecosystem,' *Photochemistry and Photobiology*, Vol. 80, pp. 139-149.
- Brooks, P.D., O'Reilly, C.M., Diamond, S.A., Campbell, D.H., Knapp, R., Bradford, D., Corn, P.S., Hossack, B. & Tonnessen, K. 2005, 'Spatial and temporal variability in the amount and source of dissolved organic carbon: Implications for UV exposure in amphibian habitats,' *Ecosystems*, Vol. 8(5), pp. 478-487.
- Brown B.E., Dunn R.P., Goodson M.S. & Douglas A.E. 2000, 'Bleaching patterns in reef corals,' *Nature*, Vol. 404 (6774), pp. 142-143.
- Buchheim, J. 1998, *Coral Reef Bleaching*, Odyssey Expeditions-Marine Biology Learning Center Publications, viewed 1 December 2006, <<http://www.marinebiology.org/coralbleaching.htm>>
- Bukata, R.P., Jerome, J.H., Kondratyev, K.Y. & Pozdnyakov, D.V. 1995, *Optical properties and remote sensing of inland and coastal waters*, CRC Press, United States.
- Calbo, J., Pages, D. & Gonzalez, J. 2005, 'Empirical studies of cloud effects on UV radiation: A review,' *Reviews of Geophysics*, Vol. 43, RG2002, doi: 10.1029/2004rg000155
- Caldwell, M.M. 1981, 'Plant response to solar ultraviolet radiation,' in O.L. Lange, P.S. Nobel, C.B. Osmond & H. Ziegler (eds.), *Encyclopaedia Plant Physiology*, Springer, New York.
- Casale, G.R., Borra, M., Colosimo, A., Colucci, M., Mititello, A., Siani, A.M. & Sisto, R. 2006, 'Variability among polysulphone calibration curves,' *Physics in Medicine and Biology*, Vol. 51, pp. 4413-4427.
- Cede, A., Blumthaler, M., Luccini, E., Piacentini, R.D. & Nunez, L. 2002, 'Effects of clouds on erythemal and total irradiance as derived from data of the Argentine network,' *Geophysical Research Letters*, Vol. 29(24), 2223, doi:10.1029/2002GL015708.
- Chaplin, M., 2009, *Water absorption spectrum*, viewed 18 June 2009, <<http://www.lsbu.ac.uk/water/vibrat.html>>

Chowdahry, J., Cairns, B., Mishchenko, M.I., Hobbs, P.V., Cota, G.F., Redemann, J., Rutledge, K., Holben, B.N. & Russell, E. 2005, 'Retrieval of aerosol scattering and absorption properties from photopolarimetric observations over the ocean during the CLAMS experiment,' *Journal of the Atmospheric Sciences*, Vol 62, pp. 1093-1117.

CIE (International Commission on Illumination) 1987, 'A reference action spectrum for ultraviolet induced erythema in human skin,' *CIE-Journal*, Vol. 5(1), pp. 17-22.

CIE (International Commission on Illumination) 1992, 'Personal Dosimetry of UV radiation,' Publication No. CIE 98.

Cole, G.A. 1975, *Textbook of Limnology*, The C.V. Mosby Company, United States.

Conde, D., Aubriot, L. & Sommaruga, R. 2000, 'Changes in UV penetration associated with marine intrusions and freshwater discharge in a shallow coastal lagoon of the Southern Atlantic Ocean,' *Marine Ecology Progress Series*, Vol. 207, pp. 19-31.

Conde, D., Aubriot, L., Bonilla, S. & Sommaruga, R. 2002, 'Marine intrusion in a coastal lagoon enhance the negative effect of solar UV radiation on phytoplankton photosynthetic rates,' *Marine Ecology Progress Series*, Vol. 240, pp. 57-70.

Coombes, C.A. & Harrison, A.W. 1988, 'Angular distribution of overcast sky short wavelength radiance,' *Solar Energy*, Vol. 40(2), pp. 161-166.

Crawford, J., Shetter, R.E., Lefer, B., Cantrell, C., Junkermann, S., Madronich, S. & Calvert, J. 2003, 'Cloud impacts on UV spectral actinic flux observed during the international photolysis frequency measurement and model intercomparison (IPMMI),' *Journal of Geophysical Research*, Vol. 108(D16), 8545, doi:10.1029/2002JD002731

CSIRO (Commonwealth Scientific and Industrial Research Organisation) 1997, *National Measurement Laboratory Measurement Report On One Tungsten Halogen Lamp No. M28623*, CSIRO, Lindfield.

Crump, D., Lean, D., Berrill, M., Coulson, D. & Toy, L. 1999, 'Spectral irradiance in pond water: Influence of water chemistry,' *Photochemistry and Photobiology*, Vol. 70(6), pp. 893-901.

Davis, A., Deane, G.W.H., Gordon, D., Howell, G.V. & Ledbury, K.J. 1976, 'A world-wide program for the continuous monitoring of solar UV radiation using poly (phenylene oxide) film, and consideration of the results,' *Journal of Applied Polymer Science*, Vol. 20, pp. 1165-1174.

Davies – Colley, R.J. & Smith, D.G. 1995, 'Optically pure waters in Waikoropupu ('Pupu') Springs, Nelson, New Zealand,' *New Zealand Journal of Marine and Freshwater Research*, Vol. 29, pp. 251-256.

- D'Croz, L., Mate, J.L. & Oke J.E. 2001, 'Responses to elevated sea water temperature and UV radiation in the coral *porites lobata* from upwelling and non – upwelling environments on the pacific coast of Panama,' *Bulletin of Marine Science*, Vol. 69(1), pp. 203-214.
- Deckert, R & Michael, K.J. 2006, 'Lensing effect on underwater levels of UV radiation,' *Journal of Geophysical Research*, Vol. 111, C05014, doi:10.1029/2005JC003332.
- Den Outer, P.N., Slaper, H., Tax, R.B. 2005, 'UV radiation in the Netherlands: Assessing long – term variability and trends in relation to ozone and clouds,' *Journal of Geophysical Research*, Vol. 110, D02203, doi:10.1029/2004JD004824.
- Diffey, B. L. 1991, 'Solar ultraviolet radiation effects on biological systems,' *Physics in Medicine and Biology*, Vol. 36 (3), pp. 299-328.
- di Sarra, A., Cacciani, M., Chamard, P., Cornwall, C., DeLuisi, J.J., Di Iorio, T., Disterhoft, P., Fiocco, G., Fua, D. & Monteleone, F. 2002, 'Effects of dust and ozone on the ultraviolet irradiance at the Mediterranean island of Lampedusa during PAUR II,' *Journal of Geophysical Research*, Vol. 107(D18), 8135, doi:10.11029/2000JD000139
- Dring, M.J., Wagner, A., Franklin, L.A., Kuhlenkamp, R. & Luning, K. 2001, 'Seasonal and diurnal variations in ultraviolet-B and ultraviolet-A irradiances at and below the sea surface at Helgoland (North Sea) over a 6-year period,' *Helgoland Marine Research*, Vol. 55, pp. 3-11.
- Ducklow, H.W., Carlson, C.A., Bates, N.R., Knap, A.H. & Michaels, A.F. 1995, 'Dissolved organic carbon as a component of the biological pump in the North Atlantic Ocean,' *Philosophical Transactions of the Royal Society of London Series B: Biological Sciences*, Vol. 348, pp. 161-167.
- Dunne, R.P. & Brown, B.E. 1996, 'Penetration of solar UVB radiation in shallow tropical waters and its potential biological effects on coral reefs; results from the central Indian Ocean and Andaman Sea,' *Marine Ecology Progress Series*, Vol. 144, pp. 109-118.
- Dunne, R.P. 1999, 'Polysulphone film as an underwater dosimeter for solar ultraviolet-B radiation in tropical latitudes,' *Marine Ecology Progress Series*, Vol. 189, pp. 53-63.
- Feister, U., Grasnack, K.H. & Grewe, R. 1992, 'Instruments for broadband UV radiation measurements,' *Solar Energy*, Vol. 49(6), pp. 535-540.
- Feister, U. & Grewe, R. 1995, 'Spectral albedo measurements in the UV and visible region over different types of surfaces,' *Photochemistry and Photobiology*, Vol. 62(4), pp. 736-744.
- Fenchel, T., King G.M. & Blackburn, T.H. 1998, *Bacterial Biogeochemistry: The Ecophysiology of Mineral Cycling*, Academic Press, San Diego.

- Fioletov, V.E., Kerr, J.B. & Wardle, D.I. 1997, 'The relationship between total ozone and spectral UV irradiance from Brewer observations and its use for derivation of total ozone from UV measurements,' *Geophysical Research Letters*, Vol. 24(23), pp. 2997-3000.
- Flannery, T. 2005, *The weather makers: the history and future impact of climate change*, The Text Publishing Company, Australia.
- Fleischmann, E.M. 1989, 'The measurement and penetration of ultraviolet radiation into tropical marine water,' *Limnology and Oceanography*, Vol. 34(8), pp. 1623-1629.
- Frazer, P. 1996, 'Chemistry of Stratospheric Ozone and Ozone Depletion,' *Cancer Forum*, Vol. 20(3), pp. 162-168.
- Frederick, J.E. 1993, 'Yearly review. Ultraviolet sunlight reaching the earth's surface: a review of recent research,' *Photochemistry and Photobiology*, Vol. 57, pp. 175-178.
- Freedman, R.A. & Kaufmann, W. J. 2002, *Universe*, W.H. Freeman, United States.
- Frenette, J., Arts, M.T. & Morin, J. 2003, 'Spectral gradients of downwelling light in a fluvial lake (Lake Saint-Pierre, St-Lawrence River),' *Aquatic Ecology*, Vol. 37, pp. 77-85.
- Frost, P.C., Larson, J.H., Kinsman, L.E., Lamberti, G.A. & Bridgham, S.D. 2005, 'Attenuation of ultraviolet radiation in streams of northern Michigan,' *Journal of the North American Benthological Society*, Vol. 24(2), pp. 246-255.
- Frost, P.C., Mack, A., Larson, J.H., Bridgham, S.D. & Lamberti, G.A. 2006, 'Environmental controls of UVB radiation in forested streams of northern Michigan,' *Photochemistry and Photobiology*, Vol. 82(3), pp. 781-786.
- Garcia – Pichel, F. 1994, 'A model for the internal self – shading in planktonic organisms and its implications for the usefulness of ultraviolet sunscreens,' *Limnology and Oceanography*, Vol. 39, pp. 1704-1717.
- Gianelli, S.M., Carlson, B.E. & Lacis, A.A. 2005, 'Aerosol retrievals using rotating shadowband spectroradiometer data,' *Journal of Geophysical Research*, Vol. 110, D05203, doi:10.1029/2004JD005329.
- Gibson, J.A.E., Vincent, W.F., Nieke, B. & Pienitz, R. 2000, 'Control of biological exposure to UV radiation in the Arctic Ocean: Comparison of the roles of ozone and riverine dissolved organic matter,' *Arctic*, Vol. 53(4), pp. 372-282).
- Gleason, D. F. & Wellington, G. M. 1993, 'Ultraviolet radiation and coral bleaching,' *Nature*, Vol. 365, pp. 836-838.
- Goyot, G. 1998, *Physics of the Environment and Climate*, Praxis Publishing, West Sussex.

- Grant, R.H., Heisler, G.M. & Gao, W. 1997a, 'Clear sky radiance distributions in ultraviolet wavelength bands,' *Theoretical and Applied Climatology*, Vol. 56, pp. 123-135.
- Grant, R.H., Heisler, G.M. & Gao, W. 1997b, 'Ultraviolet sky radiance distributions of translucent overcast skies,' *Theoretical and Applied Climatology*, Vol. 58, pp. 129-139.
- Grant, R.H. & Heisler, G.M. 1997, 'Obscured overcast sky radiance distributions for ultraviolet and photosynthetically active radiation,' *Journal of Applied Meteorology*, Vol. 36, pp. 1336-1345.
- Grant, R.H. & Gao, W. 2003, 'Diffuse fraction of UV radiation under partly cloudy skies as defined by the automated surface observation system (ASOS),' *Journal of Geophysical Research*, Vol. 108(D2), 4046, doi:10.1029/2002JD002201
- Hader, D.P. & Worrest, R.C. 1997, 'Consequences of the effects of increased solar ultraviolet radiation on aquatic ecosystems,' in D.P. Hader (ed.) *The Effects of Ozone Depletion of Aquatic Ecosystems*, R.G. Landes Company, United States.
- Hader, D.P., Kumar, H.D., Smith, R.C. & Worrest, R.C. 1998, 'Effects on aquatic ecosystems,' *Journal of Photochemistry and Photobiology B: Biology*, Vol. 46, pp. 53-68.
- Hader, D.P., Kumar, H.D., Smith, R.C. & Worrest, R.C. 2003, 'Aquatic ecosystems: effects of solar ultraviolet radiation and interactions with other climatic change factors,' *Photochemical and Photobiological Sciences*, Vol. 2, pp. 39-50.
- Hanelt, D., Tug, H., Bischof, K., Gross, C., Lippert, H., Sawall, T. & Wiencke, C. 2001, 'Light regime in an Arctic fjord: a study related to stratospheric ozone depletion as a basis for determination of UV effects on algal growth,' *Marine Biology*, Vol. 138, pp. 649-658.
- Hargreaves, B.R. 2003, 'Water column optics and penetration of UVR,' in E.W. Helbling and H. Zagarese (eds.), *UV effects in aquatic organisms and ecosystems*, The Royal Society of Chemistry, Cambridge.
- Harriott, V.J. 1985, 'Mortality rates of scleractinian corals before and during a mass bleaching event,' *Marine Ecology Progress Series*, Vol. 21, pp. 81-88.
- Helbling, E.W., Gao, K., Goncalves, R.J., Wu, H. & Villafane, V.E. 2003, 'Utilization of solar UV radiation by coastal phytoplankton assemblages off SE China when exposed to fast mixing,' *Marine Ecology Progress Series*, Vol. 259, pp. 59-66.
- Helbling, E.W., Villafane, V.E. & Holm-Hansen, O. 1994 'Effects of ultraviolet radiation on Antarctic marine phytoplankton photosynthesis with particular attention to the influence of mixing,' in C.S. Weiler & P.A. Penhale (eds.) *Ultraviolet radiation in Antarctica: measurements and biological effects*, American Geophysical Union, United States.

Herndl, G.J. 1997, 'Role of ultraviolet radiation on bacterioplankton activity,' in D.P. Hader (ed.) *The Effects of Ozone Depletion of Aquatic Ecosystems*, R.G. Landes Company, United States.

Hoegh – Guldberg, O. 1999, 'Climate change, coral bleaching and the future of the world's coral reefs,' *Marine and Freshwater Research*, Vol. 50, pp. 839-866.

Hooker, S.B. & Zibordi, G. 2005, 'Advanced methods for characterising the immersion factor of irradiance sensors,' *Journal of Atmospheric and Oceanic Technology*, Vol. 22, pp. 757-770.

Hojerslev, N.K. 1974, 'Daylight measurement for photosynthetic studies in the western Mediterranean,' University of Copenhagen Institute of Physical Oceanography Technical Report.

Horneck, G. 1997, 'Biological UV Dosimetry,' in D.P. Hader (ed.) *The Effects of Ozone Depletion of Aquatic Ecosystems*, R.G. Landes Company, United States.

Houghton, J.T. 2002, *The Physics of Atmospheres*, Cambridge University Press, United Kingdom.

Huber, M., Blumthaler, M., Ambach, W. & Staehelin, J. 1995, 'Total atmospheric ozone determined from spectral measurements of direct solar UV irradiance,' *Geophysical Research Letters*, Vol. 22(1), pp. 53-56.

Hunter, J.R., Taylor, J.H. & Moser, H.G. 1979, 'Effect of ultraviolet irradiation on eggs and larvae of the northern anchovy, *Engraulis mordax*, and the pacific mackerel, *Scomber japonicus*, during the embryonic stage,' *Photochemistry and Photobiology*, Vol. 29, pp. 325-338.

Ignatov, A., Minnis, P., Loeb, N., Wielicki, B., Miller, W., Sun – Mack, S., Tanre, D., Remer, L., Laszlo, I. & Geier, E. 2005, 'Two MODIS products over ocean on the terra and aqua CERES SSF datasets,' *Journal of the Atmospheric Sciences*, Vol. 62, pp. 1008-1031.

Ingle, J. D. & Crouch, S.R. 1988, *Spectrochemical Analysis*. Prentice – Hall, United States.

International Association for the Properties of Water and Steam (IAPWS) 1997, 'Release on the refractive index of ordinary water substance as a function of wavelength, temperature and pressure,' Technical Report.

International Light Inc. 1998, 'Instruction Manual: IL1400A Radiometer/Photometer,' Technical Report.

International Light 2009, *SED(SEL) 240 – International Light Technologies Inc.*, viewed 24 June 2009,
< <http://www.intl-lighttech.com/products/detectors/detectordata/se240>>

Iribarne, J.V. & Cho, H.-R. 1980, *Atmospheric Physics*, D. Riedel Publishing Company, Netherlands.

Jacovides, C.P., Karalis, J.D. & Steven, M.D. 1993, 'Spectral distribution of solar radiation in Athens,' *Theoretical and Applied Climatology*, Vol. 47, pp. 321-239.

Jankowski, J.J., Kieber, D.J., Mopper, K. & Neale, P.J. 2000, 'Development and intercalibration of ultraviolet solar actinometers,' *Photochemistry and Photobiology*, Vol. 71, pp. 431-440.

Jeffrey, W. H., Aas, P., Lyons, M. M., Coffin, R. B., Pledger R. J & Mitchell, D. L. 1996, 'Ambient solar radiation-induced photodamage in marine bacterioplankton,' *Photochemistry and Photobiology*, Vol. 64, pp. 419-427.

Johnsen, S. & Sosik, H. 2004, 'Shedding light on light in the ocean,' *Oceanus Magazine*, Vol. 43(2), pp. 1-5.

Johnsen, S. & Widder, E.A. 2001, 'Ultraviolet absorption in transparent zooplankton and its implications for depth distribution and visual predation,' *Marine Biology*, Vol. 138, pp. 717-730.

Jokela, K., Leszczynski, K., Visuri, R. & Ylianttila, L. 1995, 'Increase in UV exposure in Finland in 1993,' *Photochemistry and Photobiology*, Vol. 62(1), pp. 101-107.

Jokiel, P.L. 1980, 'Solar ultraviolet radiation and coral reef epifauna,' *Science*, Vol. 297, pp. 1069-1071.

Kahn, R., Wen – Hao, L., Martonchik, J.V., Bruegge, C.J., Diner, D.J., Gaitley, B.J., Abdou, W., Dubovik, O., Holben, B., Smirnov, A., Jin, Z. & Clark, D. 2005, 'MISR calibration and implications for low – light – level aerosol retrieval over dark water,' *Journal of the Atmospheric Sciences*, Vol. 62, pp. 1032-1052.

Karentz, D., Bothwell, M.L., Coffin, R.B., Hanson, A., Herndl, G.J., Kilham, S.S., Lesser, M.P., Lindell, M., Moeller, R.E., Morris, D.P., Neale, P.J., Sanders, R.W., Weiler, C.S. & Wetzel, R.G. 1994, 'Impact of UV-B radiation on pelagic freshwater ecosystems: Report of working group on bacteria and phytoplankton,' *Archiv Fur Hydrobiologie*, Vol. 43, pp. 31-69.

Karl, D., Letelier, R., Tupas, L., Dore, J., Christian, J. & D.Hebel 1997, 'The role of nitrogen fixation in the biogeochemical cycling in the Subtropical North Pacific Ocean,' *Nature*, Vol. 388, pp. 533-538.

Karoly, D.J. 1997, 'Physics of stratospheric ozone and UV – B radiation,' *Australian Meteorological Magazine*, Vol. 46, pp. 179-184.

Kasten, F. & Young A. T. 1989, 'Revised optical air mass tables and approximation formula', *Applied Optics*, Vol. 28, pp. 4735 - 4738.

Kerr, J.B. 2003, 'Understanding the factors that affect surface UV radiation,' in Proceedings of SPIE Vol. 5156 *Ultraviolet Ground- and Space-based Measurements, Models and Effects III*, edited by James R. Slusser, Jay R. Herman, Wei Gao (SPIE, Bellingham, WA, 2003) 1-14.

KNMI (Koninklijk Nederlands Meteorologisch Instituut) 2008, *OMI Instrument*, viewed 18 December 2008,
< <http://www.knmi.nl/omi/research/instrument/index.php> >

Kim, Y.J., Kim, J.E., Ryu, S.Y. & Ogunjobi, K.O. 2003a, 'UV irradiance monitoring and effects of aerosol optical depth on the ground-based measurement of ultraviolet irradiance at Kwangju, Korea,' in Proceedings of SPIE Vol. 4896 *Ultraviolet Ground- and Space-based Measurements, Models and Effects II*, edited by Wei Gao, Jay R. Herman, Guanyu Shi, Kazuo Shibasaki, James R. Slusser, (SPIE, Bellingham, WA, 2003a) 173-180.

Kimlin, M.G., Parisi, A.V. & Mainstone, J.S. 2000, 'Effect of short term ozone variations on human ultraviolet radiation exposure,' *Radiation Protection in Australasia*, Vol. 17(2), pp. 51-59.

Kinkade, C.S., Marra, J., Dickey, T.D. & Weller, R. 2001, 'An annual cycle of phytoplankton biomass in the Arabian Sea, 1994-1995, as determined by moored sensors,' *Deep-Sea Research II*, Vol. 48, pp. 1285-1301.

Kirk, J.T.O. 1994, *Light and photosynthesis in aquatic ecosystems*. Cambridge University Press, Cambridge.

Kollias, N., Baqer, A.H. & Sadiq, I. 1988, 'Measurements of solar middle ultraviolet radiation in a desert environment,' *Photochemistry and Photobiology*, Vol. 47, pp. 565-569.

Kollias, N., Baqer, A., Sadiq, I., Gillies, R. & Ou – Yang, H. 2003, 'Measurement of solar UVB variations by polysulphone film,' *Photochemistry and Photobiology*, Vol. 78(3), pp. 220-224.

Komhyr, W.D., Grass, R.D., Evans, R.D., Leonard, R.K., Quincy, D.M., Hofmann, D.J. & Koenig, G.L. 1994, 'Unprecedented 1993 ozone decrease over the United States from Dobson spectrophotometer observations,' *Geophysical Research Letters*, Vol. 21(3), pp. 201-204.

Koussoulaki, A., Danielidis, D.B., Häder, D.P. & R. Santas, 1998, 'Assessment of *Euglena gracilis* as a biological dosimeter for solar UV-A and UV-B radiation under field conditions,' *Internet Journal of Science, Biological Chemistry*, viewed 1 December 2006, <http://www.photobiology.com/v1/santas3/euglen.htm>

Kouwenberg, J. H. M., Browman, H. I., Cullen, J. J., Davis R. F., St-Pierre J.-F. & Runge J. A. 1999a, 'Biological weighting of ultraviolet (280-400 nm) induced mortality in marine zooplankton and fish. I. Atlantic cod (*Gadus morhua*) eggs,' *Marine Biology*, Vol. 134, pp. 269-284.

- Kouwenberg, J. H. M., Browman, H. I., Cullen, J. J., Davis R. F., St-Pierre J.-F. & Runge J. A. 1999b, 'Biological weighting of ultraviolet (280-400 nm) induced mortality in marine zooplankton and fish. II. *Calanus finmarchicus* (Copepoda) eggs,' *Marine Biology*, Vol. 134, pp. 285-293.
- Krins, A., Dorschel, B., Knuschke, P., Seidlitz, H.K. & Thiel, S. 2001, 'Determination of the calibration factor of polysulphone film UV dosimeters for terrestrial solar radiation,' *Radiation Protection Dosimetry*, Vol. 95, pp. 345-352.
- Kuchinke, C., Fienberg, K. & Nunez, M. 2004, 'The angular distribution of UV-B sky radiance under cloudy conditions: A comparison of measurements and radiative transfer calculations using a fractal cloud model,' *Journal of Applied Meteorology*, Vol. 43(5), pp. 751-761.
- Kuwahara, V.S., Toda, T., Hamasaki, K., Kikuchi, T. & Taguchi, S. 2000, 'Variability in the relative penetration of ultraviolet radiation to photosynthetically available radiation in temperate coastal waters, Japan,' *Journal of Oceanography*, Vol. 56, pp. 399-408.
- Kylling, A., Webb, A.R., Kift, R., Gobbi, G. P., Ammannato, L., Barnaba, F., Bais, A., Kazadzis, S., Wendisch, M., Jakel, E., Schmidt, S., Kniffka, A., Thiel, S., Junkermann, W., Blumthaler, M., Silbernagl, R., Schallhart, B., Schmitt, R., Kjeldstad, B., Thorseth, T. M., Scheirer, R. & Mayer, B. 2005, 'Spectral actinic flux in the lower troposphere: measurement and 1 – D simulations for cloudless, broken cloud and overcast situations,' *Atmospheric Chemistry and Physics*, Vol. 5, pp. 1975-1997.
- Lala, D. 1984, 'Photochemical measurement of ultraviolet solar radiation,' *Symposium Proceedings: Recent Advances in Pyranometry*, IEA Solar R&D SMHI, Norrkoping, Sweden, pp. 269-283.
- Laurion, I., Vincent, W.F. & Lean, D.R.S. 1997, 'Underwater ultraviolet radiation: development of spectral models of northern latitude high lakes,' *Photochemistry and Photobiology*, Vol. 65, pp. 107-114.
- Leech, D.M., Williamson, C.E., Moeller, R.E. & Hargreaves, B.R. 2005, 'Effects of ultraviolet radiation on the seasonal vertical distribution of zooplankton: a database analysis,' *Archiv fur Hydrobiologie*, Vol. 162, pp. 445-464.
- Lenoble, J. 1993, *Atmospheric Radiative Transfer*. Deepak Publishing, United States.
- Lesser, M. P., Stochaj, W. R., Tapley, D. W., & Shick, J. M. 1990, 'Bleaching in coral reef anthozoans: effects of irradiance, ultraviolet radiation, and temperature on the activities of protective enzymes against active oxygen,' *Coral Reefs*, Vol. 8, pp. 225-232.
- Lesser, M.P. 1996, 'Elevated temperatures and ultraviolet radiation cause oxidative stress and inhibit photosynthesis on symbiotic dinoflagellates,' *Limnology and Oceanography*, Vol. 41(2), pp. 271-283.

- Lesser, M.P., Lamare, M.D. & Barker, M.F. 2004, 'Transmission of ultraviolet radiation through the Antarctic annual sea ice and its biological effects on sea urchin embryos,' *Limnology and Oceanography*, Vol. 49(6), pp. 1957-1963.
- Lester, R.A., Parisi, A.V., Kimlin, M.G. & Sabburg, J. 2003, 'Optical properties of poly(2,6-dimethyl-1,4-phenylene oxide) film and its potential for a long term solar ultraviolet dosimeter,' *Physics in Medicine and Biology*, Vol. 48, pp. 3685-3698.
- Levy, R.C., Remer, L.A., Martins, J.V., Kaufman, Y.J., Plana – Fattori, A., Redemann, J. & Wenny, B. 2005, 'Evaluation of the MODIS aerosol retrievals over ocean and land during CLAMS,' *Journal of the Atmospheric Sciences*, Vol. 62, pp. 974-992.
- Li, S., Paulsson, M. & Bjorn, L.O. 2002, 'Temperature-dependent formation and photorepair of DNA damage and induced by UV-B radiation in suspension-cultured tobacco cells,' *Journal of Photochemistry and Photobiology B: Biology*, Vol. 66, pp. 67-72.
- Lindell, M.J., Graneli, W. & Tranvik, L.J., 'Enhanced bacterial growth in response to photochemical transformation of dissolved organic matter,' *Limnology and Oceanography*, Vol. 40(1), pp. 195-199.
- Madronich, S. 1993, 'The atmosphere and UV-B radiation,' in A.R. Young, L.O. Bjorn, J. Moan & W. Nultch (eds.), *Environmental UV Photobiology*, Plenum Press, New York.
- Madronich, S., McKenzie, R.L., Bjorn, L.O. & Caldwell, M.M. 1998, 'Changes in biologically active ultraviolet radiation reaching the Earth's surface,' *Journal of Photochemistry and Photobiology B: Biology*, Vol. 46, pp. 5-19.
- Mason, N.J. & Pathak, S.K. 1997, 'Spectroscopic studies of ozone – the Earth's UV filter,' *Contemporary Physics*, Vol. 38(4), pp. 289-299.
- McKenzie, R.L., 1991, 'Application of a simple model to calculate latitudinal and hemispheric differences in ultraviolet radiation,' *Weather and Climate*, Vol. 11, pp. 3-14.
- McKenzie, R.L. & Bodeker, G. 1996, 'UV and ozone: An update,' *Water & Atmosphere*, Vol. 4(1), pp. 7-12.
- McKenzie, R.L., Kotcamp, M. & Ireland, W. 1996, 'Upwelling UV spectral irradiances and surface albedo measurements at Lauder, New Zealand,' *Geophysical Research Letters*, Vol. 23(14), pp. 1757-1760.
- McKenzie, R.L., Bodeker, G. & Connor, B. 1999, 'Increased UV radiation in New Zealand: A cautionary tale,' *Water & Atmosphere*, Vol. 7(4), pp. 7-8.
- McKenzie, R.L., Connor, B. & Bodeker, G. 1999, 'Increased summertime UV radiation in response to ozone loss,' *Science*, Vol. 285, pp. 1709-1711.

- McPeters, R.D. & Labow, G.J. 1996, 'An assessment of the accuracy of 14.5 years of Nimbus 7 TOMS version 7 ozone data by comparison with the Dobson network,' *Geophysical Research Letters*, Vol. 23(25), pp. 3695-3698.
- McPeters, R.D., Hollandsworth, S.M., Flynn, L.E., Herman, J.R. & Seftor, C.J. 1996, 'Long – term ozone trends derived from the 16 – year combined Nimbus 7/Meteor 3 TOMS version 7 record,' *Geophysical Research Letters*, Vol. 23(25), pp. 3699-3702.
- Meleti, C. & Cappellani, F. 2000, 'Measurements of aerosol optical depth at Ispra: Analysis of the correlation with UV-B, UV-A, and total solar irradiance,' *Journal of Geophysical Research*, Vol. 105(D4), pp. 4971-4978.
- Meloni, D., Casale, G.R., Siani, A.M., Palmieri, S. & Cappellani, F. 2000, 'Solar UV dose patterns in Italy,' *Photochemistry and Photobiology*, Vol. 71(6), pp. 681-690.
- Mishra, D.R., Narumalani, S., Rundquist, D. & Lawson, M. 2005, 'Characterising the vertical diffuse attenuation coefficient for downwelling irradiance in coastal waters: Implications for water penetration by high resolution satellite data,' *Photogrammetry and Remote Sensing*, Vol. 60, pp. 48-64.
- Mobley, C.D. 1994, *Light and water: Radiative transfer in natural waters*, Academic Press, San Diego.
- Moeller, R. E., Gilroy, S., Williamson, C. E., Grad, G. & Sommaruga, R. 2005, 'Dietary acquisition of photoprotective compounds (mycosporine-like amino acids, carotenoids) and acclimation to ultraviolet radiation in a freshwater copepod,' *Limnology and Oceanography*, Vol. 50, pp. 427-439.
- Moore, P. 1995, *The Guinness Book of Astronomy*, Guinness, United Kingdom.
- Morris, D.P. & Hargreaves, B.R. 1997, 'The Role of Photochemical Degradation of Dissolved Organic Carbon in Regulating the UV Transparency of Three Lakes on the Pocono Plateau,' *Limnology and Oceanography*, Vol. 42(2), pp. 239-249.
- Morris, D.P., Zagarese, H., Williamson, C.E., Balseiro, E.G., Hargreaves, B.R., Modenutti, B., Moller, R. & Quimalinos, C. 1995, 'The attenuation of solar UV in lakes and the role of dissolved organic carbon,' *Limnology and Oceanography*, Vol. 40(8), pp. 1381-1391.
- Morrow, J.H. & Booth, C.R. 1997, 'Instrumentation and methodology for ultraviolet radiation measurements in aquatic environments,' in D.P. Hader (ed.) *The Effects of Ozone Depletion of Aquatic Ecosystems*, R.G. Landes Company, United States.
- NASA (National Aeronautics and Space Administration) 2008, *Earth Observing System (EOS) Aura*, viewed 18 December 2008,
< <http://aura.gsfc.nasa.gov/instruments/omi/index.html> >
- Neale, P.J., Davis, R.F., Cullen, J.J. 1998, 'Interactive effects of ozone depletion and vertical mixing on photosynthesis of Antarctic phytoplankton,' *Nature* Vol. 392, pp. 585–589

- Neale, P.J., Helbling, E.W. & Zagarese, H.E. 2003, 'Modulation of UVR exposure and effects by vertical mixing and advection,' in E.W. Helbling and H Zagarese (eds.), *UV effects in aquatic organisms and ecosystems*, The Royal Society of Chemistry, Cambridge.
- Neale, P.J., Bossard, P., Huot, Y. & Sommaruga, R. 2001, 'Incident and *in situ* irradiance in Lakes Cadagno and Lucerne: A comparison of methods and models,' *Aquatic Sciences*, Vol. 63, pp. 250-264.
- Newton, J.W., Tyler, D.D. & Slodki, M.E. 1979, 'Effect of ultraviolet – B (280 – 320) radiation on blue – green algae (cyanobacteria), possible biological indicators of stratospheric ozone depletion,' *Applied and Environmental Microbiology*, Vol. 37, pp. 1137-1141.
- Nichol, S.E., Pfister, G., Bodeker, G.E., McKenzie, R.L., Wood, S.W. & Bernhard, G. 2003, 'Moderation of cloud reduction of UV in the Antarctic due to high surface albedo,' *Journal of Applied Meteorology*, Vol. 42(8), pp. 1174-1183.
- Nunez, N., Forgan, B. & Roy, C. 1994, 'Estimating ultraviolet radiation at the Earth's surface,' *International Journal of Biometeorology*, Vol. 38, pp. 5-17.
- Ohde, T. & Siegel, H. 2003, 'Derivation of immersion factors for the hyperspectral TriOS radiance sensor,' *Journal of Optics A: Pure and Applied Optics*, Vol. 5(3), pp. L12-L14.
- O'Toole, A. 1994, 'The Canadian ozone watch and UV index,' in R.H. Briggs & M.E.B. Joyner (eds.), *NATO ASI Series Stratospheric Ozone Depletion/UV – B Radiation in the Biosphere*, Springer – Verlag, Berlin.
- Pan, B., Ghosh, S., Xing, B. 2008, 'Dissolved Organic Matter Conformation and Its Interaction with Pyrene As Affected by Water Chemistry and Concentration,' *Environmental Science and Technology*, Vol. 42, pp. 1594-1599.
- Parsons, P., Neale, R., Wolski, P. & Green, A. 1998, 'The shady side of solar protection,' *Medical Journal of Australia*, Vol. 168, pp. 327-330.
- Parisi, A.V. & Kimlin M. 1997a, 'Ozone and ultraviolet radiation,' *Australasian Science*, Vol. 18(1), pp. 44-46.
- Parisi, A.V. & Kimlin M. 1997b, 'Why do UV levels vary?,' *Australasian Science*, Vol. 18(2), pp. 39-41.
- Parisi, A.V. & Kimlin, M.G. 1999, 'Horizontal and sun-normal biologically effective ultraviolet irradiances,' *Photochemistry and Photobiology*, Vol. 53(1-3), pp. 70-74.
- Parisi, A.V., Sabburg, J. & Kimlin, M.G. 2004, *Scattered And Filtered Solar UV Measurements*, Kluwer Academic Publishers, Netherlands.

- Parisi A.V. & Kimlin, M.G. 2004, 'Personal solar UV exposure measurements employing modified polysulphone with an extended dynamic range,' *Photochemistry and Photobiology*, Vol. 79(5), pp. 411-415.
- Parisi, A.V. & Downs, N. 2004, 'Variation of the enhanced biologically damaging solar UV due to clouds,' *Photochemical and Photobiological Sciences*, Vol. 3., pp. 643-647.
- Parisi, A.V. 2005, 'Physics concepts of solar ultraviolet radiation by distance education,' *European Journal of Physics*, Vol. 26, pp. 313-320.
- Parisi, A.V., Kimlin, M.G., Turnbull, D.J. & Macaranas, J. 2005, 'Potential of phenothiazine as a thin film dosimeter for UVA exposures,' *Photochemical and Photobiological Sciences*, Vol. 4, pp. 907-910.
- Parisi, A.V. & Turner, J. 2006, 'Variations in the short wavelength cut – off of the solar UV spectra,' *Photochemical and Photobiological Sciences*, Vol. 5, pp. 331-335.
- Pfister, G., McKenzie, R.L., Liley, J.B., Thomas, A., Forgan, B.W. & Long, C.N. 2003, 'Cloud coverage based on all-sky imaging and its impact on surface solar irradiance,' *Journal of Applied Meteorology*, Vol. 42, pp. 1421-1434.
- Piacentini, R.D., Cede, A. & Barcena, H. 2003, 'Extreme solar total and UV irradiances due to cloud effect measured near the summer solstice at the high – altitude desertic plateau Puna of Atacama (Argentina),' *Journal of Atmospheric and Solar Terrestrial Physics*, Vol. 65(6), pp. 727-731.
- Piazena, H. 1996, 'The effect of altitude upon the solar UV-B and UV-A irradiance in the tropical Chilean Andes,' *Solar Energy*, Vol. 57(2), pp. 133-140.
- Pickett, J.E. 1994, 'Effect of stratospheric ozone depletion on terrestrial ultraviolet radiation: a review and analysis in relation to polymer degradation,' *Polymer Degradation and Stability*, Vol. 43, pp. 353-362.
- Plumb, R.A. 1989, 'Atmospheric ozone – Physics and Chemistry,' *Transactions of the Menzies Foundation*, Vol. 15, pp. 3 – 13.
- Pounds, A.J. 2001, 'Climate and amphibian declines,' *Nature*, Vol. 410, pp. 639-640.
- Rae, R., Howard-Williams, C., Hawes, I., Schwarz, A-M. & Vincent, W.F. 2001, 'Penetration of solar ultraviolet radiation into New Zealand lakes: influence of dissolved organic carbon and catchment vegetation,' *Limnology*, Vol. 2, pp. 79-89.
- Rae, R., Hawes, I., Hanelt, D. & Howard-Williams, C. 2001, *Ultraviolet light: Is it harming New Zealand lakes*, National Institute of Water and Atmospheric Research, viewed 14 November 2006, <http://www.niwascience.co.nz/pubs/wa/09-1/uv.htm>.
- Rautio, M. & Korhola, A. 2002, 'Effects of ultraviolet radiation and dissolved organic carbon on the survival of subarctic zooplankton,' *Polar Biology*, Vol. 25, pp. 460-468.

- Redemann, J., Schmid, B., Eilers, J.A., Kahn, R., Levy, R.C., Russell, P.B., Livingston, J.M., Hobbs, P.V., Smith Jr., W.L. & Holben, B.N. 2005, 'Suborbital measurements of spectral aerosol optical depth and its variability at subsatellite grid scales in support of CLAMS 2001,' *Journal of the Atmospheric Sciences*, Vol. 62, pp. 993-1007.
- Regan, J.D., Carrier, W.L., Gucinski, H., Olla, B.L., Yoshida, H., Fujimura, R.K. & Wicklund, R.I. 1992, 'DNA as a solar dosimeter in the ocean,' *Photochemistry and Photobiology*, Vol. 56, pp. 35-42.
- Reinart, A., Arst, H. & Pierson D.C. 2005, 'Optical properties and light climate in Lake Verevi,' *Hydrobiologia*, Vol. 547, pp. 41-49.
- Reitner, B., Herndl, G.J. & Herzig, A. 1997, 'Role of ultraviolet-B radiation on photochemical and microbial oxygen consumption in a humic rich shallow lake,' *Limnology and Oceanography*, Vol. 42, pp. 950-960.
- Remer, L.A., Kaufman, Y.J., Tanre, D., Mattoo, S., Chu, D.A., Martins, J.V., Li, R.-R., Ichoku, C., Levy, R.C., Kleidman, R.G., Eck, T.F., Vermote, E. & Holben, B.N. 2005, 'The MODIS aerosol algorithm, products and validation,' *Journal of the Atmospheric Sciences*, Vol. 62, pp. 947-973.
- Rikus, L. 1996, 'Prediction of UV-B dosage at the surface,' *Cancer Forum*, Vol. 20(3), pp. 179-187.
- Roleda, M.Y., Wiencke, C., Hanelt, D. & Bischof, K 2007, 'Sensitivity of the early life stages of macroalgae from the northern hemisphere to ultraviolet radiation,' *Photochemistry and Photobiology*, Vol. 83(4), pp. 851-862.
- Roos, J.C. & Vincent, W.F. 1998, 'Temperature dependence of UV radiation effects on Antarctic cyanobacteria,' *Journal of Phycology*, Vol. 34, pp. 118-125.
- Rosales, A., Pedroni, J.V. & Tocho, J.O. 2006, 'Global spectral UV-radiometer with automatic shadowband,' *Photochemistry and Photobiology*, Vol. 82, pp. 844-849.
- Rousseaux, M.C., Ballare, C.L., Giordano, C.V., Scopel, A.L., Zima, A.M., Szwarcberg – Bracchitta, M., Searles, P.S., Caldwell, M.M. & Díaz, S.B. 1999, 'Ozone depletion and UVB radiation: Impact on plant DNA damage in southern South America,' *Proceedings of the National Academy of Science*, Vol. 96(26), pp. 15310-15315.
- Roy, C.R., Gies, H.P. & Elliot, G. 1990, 'Ozone depletion,' *Nature*, Vol. 347, pp. 235-235.
- Sabburg, J. & Wong, J. 2000, 'The effect of clouds on enhancing UVB irradiance at the Earth's surface: A one year study,' *Geophysical Research Letters*, Vol. 27(20), pp. 3337-3340.
- Sabburg, J., Parisi, A.V. & Wong, J. 2001, 'Effect of cloud on UVA and exposure to humans,' *Photochemistry and Photobiology*, Vol. 74(3), pp. 412-416.

- Sabburg, J.M., Parisi, A.V. & Kimlin, M.G. 2003, 'Enhanced spectral UV irradiance: A 1 year preliminary study,' *Atmospheric Research*, Vol. 66, pp. 261-272.
- Sabburg, J. & Parisi, A. 2006, 'Spectral dependency of cloud enhanced UV irradiance,' *Atmospheric Research*, Vol. 81(3). pp. 206-214.
- Schick, J.M., Lesser, M.P. & Jokiel, P.L. 1996, 'Effects of ultraviolet radiation on corals and other coral reef organisms,' *Global Change Biology*, Vol. 2(6), pp. 527-545.
- Schouten, P.W., Parisi, A.V. & Turnbull, D.J. 2007, 'Evaluation of a high exposure solar UV dosimeter for underwater use,' *Photochemistry and Photobiology*, Vol. 83, pp. 931-937.
- Schouten, P.W., Parisi, A.V. & Turnbull, D.J. 2008, 'Field calibrations of a long – term UV dosimeter for aquatic UVB exposures,' *Journal of Photochemistry and Photobiology B: Biology*, Vol. 91 (2-3). pp. 108-116.
- Schouten, P.W., Parisi, A.V. & Turnbull, D.J. 2009, 'Applicability of the Polyphenylene Oxide Film Dosimeter to High UV Exposures in Aquatic Environments,' Accepted for publication in *Journal of Photochemistry and Photobiology B: Biology*.
- Schmucki, D.A. & Philipona, R. 2002, 'UV radiation in the Alps: The altitude effect,' in Proceedings of SPIE Vol. 4482 *Ultraviolet Ground- and Space-based Measurements, Models and Effects*, edited by James R. Slusser, Jay R. Herman, Wei Gao (SPIE, Bellingham, WA, 2002) 234-239.
- Schubert, H., Sagert, S. & Forster, R.M. 2001, 'Evaluation of the different levels of variability in the underwater light field of a shallow estuary,' *Helgoland Marine Research*, Vol. 55, pp. 12-22.
- Serway, R.A., Moses, C.J. & Moyer, C.A. 2005, *Modern Physics*, Brooks/Cole – Thompson Learning, Belmont.
- Shick J.M. & Dunlap W.C. 2002, 'Mycosporine – like amino acids and related gadusols: biosynthesis, accumulation, and UV – protective functions in aquatic organisms,' *Annual Review of Physiology*, Vol. 64, pp. 223-262.
- Setlow, R.B. 1974, 'The wavelengths in sunlight effective in producing skin cancer: a theoretical analysis,' *Proceedings of the National Academy of Sciences USA*, Vol. 71, pp. 3363–3366.
- Siebeck, O. 1988, 'Experimental investigation of UV tolerance in hermatypic corals (Scleractinia),' *Marine Ecology Progress Series*, Vol. 43, pp. 95-103.
- Siegel, D.A. & Michaels, A.F. 1996, 'Quantification of non – algal light attenuation in the Sargasso Sea: implications for biogeochemistry and remote sensing', *Deep Sea Research II*, Vol. 43, pp. 321-346.

- Simon, P.C. 1997, 'Extraterrestrial solar irradiances in the near and medium UV ranges,' in C.S. Zerefos and A.F. Bais (eds.) *Solar Ultraviolet Modelling, Measurement and Effects*, Springer, Berlin.
- Sinha, R.P., Lebert, M., Kumar, A. & Hader, D.P. 1995, 'Disintegration of phycobilisomes in rice field cyanobacterium *Nostoc* sp. Following UV irradiation,' *Biochemistry and Molecular Biology International*, Vol. 37, pp. 697-706.
- Sinha, R.P., Singh, N., Kumar, A., Kumar, H.D. & Hader, D.P. 1996, 'Effects of UV irradiation on certain physiological and biochemical processes in cyanobacteria,' *Journal of Photochemistry and Photobiology B: Biology*, Vol. 32, pp. 107-114.
- Sinha, R.P., Singh, N., Kumar, A., Kumar, H.D. & Hader, D.P. 1997, Impacts of ultraviolet – B irradiation on nitrogen – fixing cyanobacteria of rice paddy fields,' *Journal of Plant Physiology*, Vol. 150, pp. 188-193.
- Sinha, R.P. & Hader, D.P. 1997, 'Impacts of UV – B irradiation on rice – field cyanobacteria,' in D.P. Hader (ed.) *The Effects of Ozone Depletion of Aquatic Ecosystems*, R.G. Landes Company, United States.
- Sinha, R.P., Sinha, J.P., Groniger, A. & Hader, D.P. 2002, 'Polychromatic action spectrum for the induction of a mycosporine-like amino acid in a rice-field cyanobacterium, *Anabaena* sp.,' *Journal of Photochemistry and Photobiology B: Biology*, Vol 66, pp. 47-53.
- Slusser, J., Gibson, J., Bigelow, D., Kolinski, D., Mou, W., Koenig, G., & Beaubien, A. 1999, 'Comparison of column ozone retrievals by use of an UV multifilter rotating shadow – band radiometer with those from Brewer and Dobson spectrophotometers,' *Applied Optics*, Vol. 38(9), pp. 1543-1551.
- Smith, R. C. & Baker, K. S. 1981, 'Optical properties of the clearest natural waters (200 – 800 nm),' *Applied Optics*, Vol. 20, pp. 177-184.
- Smith, R.C., Tyler, J.E. & Goldman C.R. 1973, 'Optical properties and color of Lake Tahoe and Crater Lake,' *Limnology and Oceanography*, Vol. 18(2), pp. 189-199.
- Smith Sr., W.L., Zhou, D.K., Larar, A.M., Mango, S.A., Howell, H.B., Knuteson, R.O., Revercomb, H.E. & Smith Jr. W.L. 2005, 'The NPOESS airborne sounding testbed interferometer – remotely sensed surface and atmospheric conditions during CLAMS,' *Journal of the Atmospheric Sciences*, Vol. 62, pp. 1118-1134.
- Solar Light Co. 2009, *501 UV – Biometer*, viewed 14 January 2009, < <http://www.solar.com/501.htm>>
- Sommaruga, R. & Psenner, R. 1997, 'Ultraviolet radiation in a high mountain lake of the Austrian Alps: Air and underwater measurements,' *Photochemistry and Photobiology*, Vol. 65(6), pp. 957-963.

- Stamnes, K., Slusser, J. & Bowen, M. 1991, 'Derivation of total ozone abundance and cloud effects from spectral irradiance measurements,' *Applied Optics*, Vol. 30(30), pp. 4418-4426.
- Stamnes, K. 2002a, 'Ultraviolet and visible radiation in the atmosphere – ocean system: a tutorial review of modelling capabilities,' *Optical Engineering*, Vol. 41, pp. 3008-3018.
- Stamnes, K. 2002b, 'Modelling and measurements of UV radiation in the atmosphere-ocean system: A review,' in Proceedings of SPIE Vol. 4482 *Ultraviolet Ground- and Space-based Measurements, Models and Effects*, edited by James R. Slusser, Jay R. Herman, Wei Gao (SPIE, Bellingham, WA, 2002) 1-14.
- Sturman, A.P. & Tapper, N.J. 1997, *The Weather and Climate of Australia and New Zealand*, Oxford University Press, Melbourne.
- Tedetti, M. & Sempéré, R. 2005, 'Penetration of ultraviolet radiation in the marine environment. A review,' *Photochemistry and Photobiology*, Vol. 82(2), pp. 389-397.
- Tett, P. 2005, *The environment – light*, viewed 14 November 2008, < <http://www.lifesciences.napier.ac.uk/teaching/Env/En9light.html>>
- Thomas, D.N. & Lara, R.J. 1995, 'Photodegradation of algal derived dissolved organic carbon,' *Marine Ecology Progress Series*, Vol. 116, pp. 309-310.
- Tranvik, L. & Kokalj, S. 1998, 'Decreased biodegradability of algal DOC due to interactive effects of UV radiation and humic matter,' *Aquatic Microbial Ecology*, Vol. 14, pp. 301-307.
- Turnbull, D. J. & Parisi, A. 2005, 'Measuring the diffuse component of solar UV beneath shade structures: a practical activity for an Australian summer,' *Teaching Science*, Vol. 51(1), pp. 22-24.
- Turnbull, D.J. & Schouten, P. 2008, 'Utilising polyphenylene oxide for high exposure solar UVA dosimetry,' *Atmospheric Chemistry and Physics*, Vol. 8, pp. 2759-2762.
- Turner, J. Parisi, A.P. & Turnbull, D.J. 2008, 'Reflected solar radiation from horizontal, vertical and inclined surfaces: Ultraviolet and visible spectral and broadband behaviour due to solar zenith angle, orientation and surface type,' *Journal of Photochemistry and Photobiology B: Biology*, Vol. 92(1), pp. 29-37.
- Tyagi R., Kumar H. D., Vyas D. & Kumar A. 1991, 'Effects of ultraviolet – Bradiation on growth, pigmentation, $\text{NaH}^{14}\text{CO}_3$ uptake and nitrogen metabolism in *Nosoc muscorum*,' in ' in Y.P. Abrol, P.N. Wattal, A. Gnanam, Govindjee, D.R. Ort, A.H. Teramura (eds.), *Impact of Global Climatic Changes on Photosynthesis and Plant Productivity*, Oxford and IBH Publishing, New Delhi.
- Tzortziou, M., Osburn, C.L. & Neale P.J. 2007, 'Photobleaching of dissolved organic material from a tidal marsh-estuarine system of the Chesapeake Bay,' *Photochemistry and Photobiology*, Vol. 83, pp. 782-792.

United Nations Environment Programme (UNEP), *Aquatic Ecosystems*, viewed 18 June 2009, <<http://www.gcric.org/UNEP1998/UNEP98p49.html>>

Urbach, F. 1997, 'Ultraviolet radiation and skin cancer of humans,' *Journal of Photochemistry and Photobiology B: Biology*, Vol. 40, pp.3-7.

Vaishampayan, A., Sinha, R.P., Hader, D.P., Dey, T., Gupta, A.K., Bhan, U. & Rao, A.L. 2002, 'Cyanobacterial fertilisers in rice agriculture,' *Botanical Review*, Vol. 67, pp. 453-516.

Vasilkov, A.P., Herman, J.R., Ahmad, Z., Kahru, M. & Mitchell, B.G. 2005, 'Assessment of the ultraviolet radiation field in ocean waters from space based measurements and full radiative transfer equations,' *Applied Optics*, Vol. 44, pp. 2863-2869.

Vincent, W.F. & Roy, S. 1993, 'Solar ultraviolet radiation and aquatic primary production: Damage, protection and recovery,' *Environmental Reviews*, Vol. 1, pp.1-12.

Vincent, W.F., Rae, R., Laurion, I., Howard-Williams, C. & Priscu, J.C. 1998, 'Transparency of Antarctic ice-covered lakes to solar UV radiation,' *Limnology and Oceanography*, Vol. 43(4), pp. 618-624.

Vincent, W.F., Laurion, I. & Pienitz, R. 1998, 'Arctic and Antarctic lakes as optical indicators of global change,' *Annals of Glaciology*, Vol. 27, pp. 691-696.

Vinebrooke, R.D. & Leavitt, P.R. 1999, 'Differential responses of littoral communities to ultraviolet radiation in an alpine lake,' *Ecology*, Vol. 80, pp. 223-237.

Voss, K.J., Welton, E.J., Quinn, P.K., Frouin, R., Miller, R. and Reynolds, R.M. 2001, 'Aerosol optical depth measurements during the Aerosols99 experiment,' *Journal of Geophysical Research*, Vol. 106(D18), pp. 20811-20819.

Warner, M.E., Fitt, W.K. and Schmidt, G.W. 1996, 'The effects of elevated temperature on the photosynthetic efficiency of zooxanthellae in hospite from four different species of reef coral: a novel approach,' *Plant, Cell and Environment*, Vol. 19, pp. 291-299.

Webb, A.R. 1998, *UVB Instrumentation and Applications*, Gordon and Breach, Amsterdam.

Weihs, P., Webb, A.R., Hutchinson, S. & Middleton, G.W. 2000, 'Measurements of the diffuse UV sky radiance during broken cloud conditions,' *Journal of Geophysical Research*, Vol. 105(D4), pp. 4937-4944.

Wenny, B.N., Saxena, V.K. & Frederick, J.E. 2001, 'Aerosol optical depth measurements and their impact on surface levels of ultraviolet-B radiation,' *Journal of Geophysical Research*, Vol. 106(D15), pp.17311-17319.

- Wetzel, R.G. 2001, *Limnology: Lake and river ecosystems*, Academic Press, United States.
- WHO (World Health Organisation) 1994, 'Environmental health criteria 160: Ultraviolet radiation,' Geneva.
- WMO (World Meteorological Organisation) 2007, 'Scientific Assessment of Ozone Depletion: 2006,' Geneva.
- Wilhelm, S.W., Jeffrey, W.H., Suttle, C.A. & Mitchell, D.L. 2002, 'Estimation of biologically damaging UV levels in marine surface waters with DNA and viral dosimeters,' *Photochemistry and Photobiology*, Vol. 76(3), pp. 268-273.
- Williamson, C.E. 1996, *Effects of UV Radiation on Freshwater Ecosystems*, viewed 1 December 2008, <<http://www.gbhap.com/fulltext/130/T960006F130.htm>>
- Williamson C. E., Stemberger, R. S., Morris, D. P., Frost, T. M., Paulsen, S. G. 1996, 'Ultraviolet radiation in North American lakes: Attenuation estimates from DOC measurements and implications for plankton communities,' *Limnology and oceanography*, Vol. 41(5), pp. 1024-1034.
- Williamson, C. 2005, *The ecology of UV – An introduction*, viewed 1 December 2008, <<http://www.orgs.muohio.edu/uvlakes/UVecology/Intro/intro.html#uvatten>>
- Winiacki, S. & Frederick, J.E. 2005, 'Ultraviolet radiation and clouds: Couplings to tropospheric air quality,' *Journal of Geophysical Research*, Vol. 110, D22202, doi: 10.1029/2005JD006199
- Wong, C.F., Toomey, S., Fleming R.A. & Thomas B.W. 1995, 'UV-B radiometry and dosimetry for solar measurements,' *Health Physics*, Vol. 68, pp. 175-184.
- Wong, C.F. & Parisi, A.V. 1999, 'Assessment of ultraviolet radiation exposures in photobiological experiments,' *Protection Against the Hazards of UVR, Internet Conference*, 18 Jan – 5 Feb 1999.
- Xenopoulos, M.A., Prairie Y.T. & Bird D.F. 2000, 'The influence of UVB, stratospheric ozone variability and thermal stratification on the phytoplankton biomass dynamics in a mesohumic lake,' *Canadian Journal of Fisheries and Aquatic Science*, Vol. 57, pp. 600-609.
- Huot, Y., Jeffrey, W.H., Davis, R.F. & Cullen J.J. 2000, 'Damage to DNA in Bacterioplankton: A Model of Damage by Ultraviolet Radiation and its Repair as Influenced by Vertical Mixing,' *Photochemistry and Photobiology*, Vol. 72(1), pp. 62-74.
- Zagarese, H.E. & Williamson, C.E. 2001, 'The implications of solar UV radiation exposure for fish and fisheries,' *Fish and Fisheries*, Vol. 2, pp. 250-260.

Zibordi, G. 2005, 'Immersion factor of in – water radiance sensors: Assessment for a class of radiometers,' *Journal of Atmospheric and Oceanic Technology*, Vol. 23, pp. 302-313.

Zibordi G., Hooker, S.B., Mueller, J. & Lazin, G. 2004, 'Characterisation of the immersion factor for a series of in-water optical radiometers,' *Journal of Atmospheric and Oceanic Technology*, Vol. 21, pp. 501-514.

APPENDICES

Conference Presentations and Publications from this Research

Better Characterisation of the Underwater Solar UV Environment Using a High Exposure Dosimeter

Peter Schouten, University of Southern Queensland, Australia.

Dr Alfio Parisi, University of Southern Queensland, Australia.

Abstract:

The effect of solar UV radiation (UV) upon the marine ecosystem has been well documented by many previous studies using a wide range of measurement and modeling techniques adapted to an extensive variety of underwater environments such as oceans, lakes, streams and creek beds. From these investigations it has been discovered that UVB radiation (wavelengths running from 280 to 320 nm) has a broad range of negative effects on aquatic biota, while the less energetic UVA radiation (wavelengths running from 320 to 400 nm) has the capability to both repair and damage various types of underwater life. Solar UV radiation also has the potential to cause damage to unprotected humans involved in various aquatic activities such as swimming, snorkeling and diving.

The penetration and distribution of the UV field in an underwater environment is primarily dependent upon the water column depth and dissolved organic carbon (DOC) level of the water, and therefore the capability of the UV to cause biological damage is also dependent upon these factors. Various chemical dosimeters have been fabricated and tested to measure the UV underwater, and in turn quantify the relationship between water column depth and DOC levels to the UV field distribution, but have only been able to record UV exposures over short time increments thus limiting the extent of the data.

It has now become necessary to build upon this initial research and develop a chemical dosimeter that is capable of measuring long-term SUV exposure in any type of underwater environment. Poly (2,6-dimethyl-1, 4-phenylene oxide) (PPO) has been identified and chosen as a candidate for this objective. This presentation will deliver several preliminary results relating to the development of the PPO dosimeter for use underwater and will discuss the future directions that this research will take.

Live Presentation made at the Showcasing Toowoomba Area Health Research Conference, Toowoomba, Australia, 25 August 2006.

Development of a High Exposure Underwater Solar UV Dosimeter

Peter Schouten, University of Southern Queensland, Australia.

Dr Alfio Parisi, University of Southern Queensland, Australia.

Dr David Turnbull, University of Southern Queensland, Australia.

Abstract:

The penetration and distribution of the Solar Ultraviolet Radiation (UV) field in any natural underwater environment depends on the column depth and dissolved organic carbon (DOC) level of the water, and therefore the capability of the UV to cause biological damage to the aquatic biota is also dependent upon these parameters. Several solid-state chemical dosimeters have been fabricated and tested to measure the underwater UV, and in turn quantify the relationship between water column depth and DOC levels to the underwater UV field distribution. However, these dosimeters have only had the ability to measure UV exposures over short temporal increments, thus limiting the scope of the data.

It has now become necessary to build upon this initial research and develop a chemical dosimeter that is capable of measuring long-term UV exposure in any type of underwater environment. Poly (2,6-dimethyl-1, 4-phenylene oxide) (PPO) has been identified and selected as a prime candidate for this objective. The optical properties of PPO have already been tested in air. However, before being deployed for trials in actual marine environments, the immersed optical properties of the PPO dosimeter have to be tested in a controlled laboratory environment using solar simulation techniques in order to confirm the suitability of PPO for this purpose. The optical properties that have been investigated to date include the dose response, spectral response, angular variation, dark reaction and exposure repeatability.

This presentation will deliver these results and will also discuss the future directions that this research will take.

Poster Presentation made at the Australian Institute of Physics 2006 Conference, Brisbane, Australia, 7 December 2006.

Utilising Polyphenylene Oxide for Long Term Solar UVA Dosimetry

Dr David Turnbull, University of Southern Queensland, Australia.

Peter Schouten, University of Southern Queensland, Australia.

Abstract:

Exposure to UV radiation is known to be a causative factor in the induction of skin cancers and other sun-related disorders. Most acute responses of humans to UV exposure occur as a result of UVB (280 to 315 nm) exposures, as these wavelengths are highly sensitive in creating a human biological response. However, this does not mean that UVA radiation has no impact on human UV exposures and health. UVA can cause erythema in human skin, yet, the exposures required to create such a response is much larger than UVB radiation. UVA radiation penetrates much deeper into human skin tissue than UVB, resulting in impacts that are not as acute, taking many years to manifest. Past research has shown that UVA (315 to 400 nm) plays a significant role in human skin carcinogenesis. Studies have also shown that UVA plays an important role in skin damage, immune suppression, DNA damage, photoageing and wrinkling. Researchers at the University of Southern Queensland have developed a personal UV dosimeter that can quantitatively assess long term solar UVA exposures. The chemical polyphenylene oxide, cast in thin film form and which is responsive to both the UVA and UVB part of the spectrum was used and filtered with mylar. This combined system responded to the UVA wavelengths only and underwent a change in optical absorbance as a result of UVA exposure. Preliminary results indicate that this UVA dosimeter saturates reasonably slowly when exposed to sunlight and can measure exposures of more than 20 MJm^{-2} of solar UVA radiation with an uncertainty level of no more than $\pm 5\%$.

Poster presentation made at the 12th Congress of the European Society for Photobiology, Bath, England, 1 – 6 September 2007.

Application of Poly (2,6-dimethyl-1, 4-phenylene oxide) Film for the Long – Term Measurement of Underwater Solar UVB

Peter Schouten, University of Southern Queensland, Australia.

Dr Alfio Parisi, University of Southern Queensland, Australia.

Dr David Turnbull, University of Southern Queensland, Australia.

Abstract:

For underwater ultraviolet radiation (UV) measurements, the usage of chemical dosimeters has been relatively low in comparison to measurements made with optical meters. However, dosimeters such as the Poly (2,6-dimethyl-1, 4-phenylene oxide) film (PPO) offer an inexpensive, easy to deploy and accurate alternative to the optical meters, and could prove to be an invaluable tool for researchers investigating the underwater effects of solar UV. To date, no literature has been produced detailing how to adequately calibrate and deploy chemical dosimeters for long-term underwater usage. The following paper details a basic methodology on how to calibrate the PPO dosimeter for underwater use and also demonstrates how in-air and in-water dosimetric calibrations cannot be transferred while shallow calibrations for different water types can be with only a small reduction in accuracy.

Live Presentation made at the Celebration of 100 Years of UV Radiation Research Conference, Davos, Switzerland, 18 September 2007.

Development of a Long Term Solar UVA Dosimeter

Dr David Turnbull, University of Southern Queensland, Australia.
Peter Schouten, University of Southern Queensland, Australia.

Abstract:

Exposure to UV radiation is known to be a causative factor in the induction of skin cancers and other sun-related disorders. Most acute responses of humans to UV exposure occur as a result of UVB (280 to 315 nm) exposures, as these wavelengths are highly sensitive in creating a human biological response. However, this does not mean that UVA radiation has no impact on human UV exposures and health. UVA can cause erythema in human skin, yet, the exposures required to create such a response is much larger than UVB radiation. UVA radiation penetrates much deeper into human skin tissue than UVB, resulting in impacts that are not as acute, taking many years to manifest. Past research has shown that UVA (315 to 400 nm) plays a significant role in human skin carcinogenesis. Studies have also shown that UVA plays an important role in skin damage, immune suppression, DNA damage, photoageing and wrinkling. Researchers at the University of Southern Queensland have developed a personal UV dosimeter that can quantitatively assess long term solar UVA exposures. The chemical polyphenylene oxide, cast in thin film form and which is responsive to both the UVA and UVB part of the spectrum was used and filtered with mylar. This combined system responded to the UVA wavelengths only and underwent a change in optical absorbance as a result of UVA exposure. Preliminary results indicate that this UVA dosimeter saturates reasonably slowly when exposed to sunlight and can measure exposures of more than 20 MJm^{-2} of solar UVA radiation with an uncertainty level of no more than $\pm 5\%$.

Poster Presentation made at the Celebration of 100 Years of UV Radiation Research Conference, Davos, Switzerland, 18 – 20 September 2007.

Calibration of Poly (2,6-dimethyl-1, 4-phenylene oxide) film for Long – Term Underwater Solar UV Exposures

Peter Schouten, University of Southern Queensland, Australia.

Dr Alfio Parisi, University of Southern Queensland, Australia.

Abstract:

The sizeable reduction in the protective ozone layer over recent decades has coincided with an increase in the amount of biologically damaging solar ultraviolet radiation (UV_{BE}) reaching the Earth's surface. Not only does this intensification of the UV_{BE} affect terrestrial life forms, but it also has a negative influence upon numerous organisms inhabiting marine environments such as rivers and dams. Coupled with the enhanced evaporative effect of global warming, these organisms living underwater have even less protection against the UV_{BE} than was once present.

Various methodologies using a wide range of measurement systems have been employed previously in order to determine the amount of UV_{BE} incident upon various aquatic organisms in a number of different water bodies. Broadband meters and spectroradiometers have been employed to take underwater measurements. However, these measurement campaigns are limited by the fact that radiometric equipment requires a human controller, constant power supply and regular calibrations in order to function properly. Dosimetric measurements have also been made underwater using two distinct types of dosimeter. The first type based on a synthetic chemical, like polysulphone, and the second type based on a biological matter, such as a DNA sample. The studies made using biological dosimeters have displayed very good results, however the time and skill necessary to make these types dosimeters can outweigh their usefulness. The chemical dosimeters are easier to make and have also provided useable data, but only for short periods of exposure, usually no more than a day.

Previous research has shown that Poly (2,6-dimethyl-1, 4-phenylene oxide) film (PPO) has the potential for use as a long – term underwater solar UV dosimeter. However, there is no documented methodology on how to properly calibrate the PPO dosimeter for marine – based measurements and it has yet to be trialled in a real marine environment. This presentation will detail the calibration methodology required for accurate measurements in a wide variety of different water types found around the South – East Queensland region.

Live Presentation made at the Australian Institute of Physics Postgraduates Meeting, Brisbane, Australia, 9 November 2007.

Measurement of Solar UVB Exposures in Sea Water with a High – Exposure Dosimeter

Peter Schouten, University of Southern Queensland, Australia.

Dr Alfio Parisi, University of Southern Queensland, Australia.

Dr David Turnbull, University of Southern Queensland, Australia.

Abstract:

For several decades, marine scientists have investigated the underwater ultraviolet light environment using a wide variety of spectroradiometric and radiometric equipment. These types of instruments are extremely useful for taking underwater measurements of the solar UV within a short window of time, for example recording fluctuations in UV levels caused by rapidly changing environmental parameters, like cloud cover or water turbidity. However, over long phases these spectroradiometers and radiometers become increasingly problematic to use, with high amounts of maintenance time necessary involving routine calibrations and corrections for the immersion effect.

However, to supplement the short – term underwater measurements using spectroradiometers and radiometers, a new long – term dosimetric system employing Poly (2,6-dimethyl-1, 4-phenylene oxide) (PPO) film has been developed. The PPO film dosimeter has proven to be capable of measuring underwater UV dosages of at least five times that of the more commonly used polysulphone dosimeter, at a level of accuracy close to what would be expected of dosimetric measurements made in air provided that the necessary calibrations are completed correctly.

This presentation details a measurement campaign made in a simulated sea water environment using a batch of PPO dosimeters set at different depths and aligned to a range of different inclinations and azimuths by means of attachment to a custom built dosimeter submersible float (DSF) unit. The results obtained from this measurement campaign were used to compute a diffuse attenuation coefficient (K_d) for the sea water. This K_d value was compared to a K_d value derived from results taken using a radiometer in the same water.

Live Presentation made at the American Society of Photobiology 2008 Conference, Burlingame, California, United States, 24 June 2008.

For this presentation the lead author was awarded with a Frederick Urbach Memorial Travel Award valued at US \$400.

Usage of the Polyphenylene Oxide Dosimeter to Measure Solar UVB and Erythemal UV Exposures over Extended Intervals

Peter Schouten, University of Southern Queensland, Australia.

Dr Alfio Parisi, University of Southern Queensland, Australia.

Dr David Turnbull, University of Southern Queensland, Australia.

Abstract:

For over thirty years scientists have been using chemical film dosimeters to measure levels of solar ultraviolet radiation (UV) exposure on human subjects in a multitude of different environments, for example on the sporting field or under shade structures. Over this time the most commonly used dosimeter has been the polysulphone dosimeter. The polysulphone dosimeter has proven to be very useful for short term exposure measurements, such as typically over the duration of a single day in subtropical regions. However, the inherently small optical saturation limit of polysulphone does not allow it to be used for long periods of time. Another chemical film dosimeter, the poly 2,6-dimethyl-1,4-phenylene oxide (PPO) film dosimeter has been extensively tested and characterised by researchers at the University of Southern Queensland in order to overcome the limitation of the relatively short dynamic range of polysulphone. Over the period of a year, numerous batches of PPO dosimeters have been calibrated to the solar ultraviolet – B (UVB) (280 to 320 nm) and the erythemal (sun burning) UV in air by employing a scanning spectroradiometer (Bentham Instruments, Reading UK) over the space of a week for each particular batch. Calibrations were obtained in each season in order to ascertain the influence of different solar zenith angle ranges and fluctuations in atmospheric conditions on the PPO film. This presentation will highlight data from this research as well as detail possible applications for the PPO dosimeter for use in health related research.

Poster Presentation made at the Australian Health and Medical Research Conference, Brisbane, Australia, 20 November 2008.

Using the Polyphenylene Oxide Dosimeter for Extended Underwater UV Measurements

Peter Schouten, University of Southern Queensland, Australia.
Dr Alfio Parisi, University of Southern Queensland, Australia.
Dr David Turnbull, University of Southern Queensland, Australia.
Nathan Downs, University of Southern Queensland, Australia.

Abstract:

The current global warming situation together with recent fluctuating trends in atmospheric ozone levels have resulted in changes occurring to the penetrative ability and distribution of the solar ultraviolet (UV) light field as measured in underwater locales such as in lakes and the ocean. The UV, in particular the UVB, has been shown by numerous studies in the past to have a detrimental effect on many forms of underwater life, ranging from the big to the small, each having their own special niche within the delicate marine ecosystem, which has direct consequences to our own life on the land. So it is extremely important that we measure and document the attributes of the UV underwater so we can enhance our understanding of its widespread effect upon the aquatic world.

The underwater UV light environment has been measured in the past using a multitude of spectroradiometric and radiometric equipment. These instruments have been highly useful for taking underwater measurements of the UV sporadically over a short time frame. However, over long periods of time these spectroradiometers and radiometers become harder to employ, with sizeable amounts of time needed to accurately calibrate and correct them.

This presentation provides measurements extracted from a year long measurement campaign conducted in a simulated sea water environment using a series of Polyphenylene Oxide (PPO) dosimeters immersed at varying depths and aligned to three different inclinations and four azimuths by using a custom built dosimeter submersible float (DSF). The results taken from this campaign were used to calculate an average diffuse attenuation coefficient (K_d) for the sea water in the UVB waveband. This K_d value was compared to another K_d value estimated using data taken using a spectrometer in the same water. Results taken from a long – term calibration completed using a prototype PPO dosimeter in conjunction with a neutral density filter (NDF) will also be presented.

Poster Presentation made at the Australian Institute of Physics 2008 Conference, Adelaide, Australia, 1 December 2008.

Paper 1: Schouten, P.W., Parisi, A.V. & Turnbull, D.J. 2007, 'Evaluation of a high exposure solar UV dosimeter for underwater use,' *Photochemistry and Photobiology*, Vol. 83, pp. 931-937. (Authors preprint copy shown here).

Photochemistry and Photobiology, 2007, 83: 1-7

Evaluation of a High Exposure Solar UV Dosimeter for Underwater Use

Peter W. Schouten^{*1}, Alfio V. Parisi^{1,2} and David J. Turnbull^{1,2}

¹Department of Biological and Physical Sciences, Faculty of Sciences, University of Southern Queensland, Toowoomba, Australia

²Centre for Rural and Remote Area Health, Faculty of Sciences, University of Southern Queensland, Toowoomba, Australia

Received 26 October 2006; accepted 1 February 2007; DOI: 10.1111/j.1751-1097.2007.00085.x

ABSTRACT

Solar ultraviolet radiation (UV) is known to have a significant effect upon the marine ecosystem. This has been documented by many previous studies using a variety of measurement methods in aquatic environments such as oceans, streams and lakes. Evidence gathered from these investigations has shown that UVB radiation (280–320 nm) can negatively affect numerous aquatic life forms, while UVA radiation (320–400 nm) can both damage and possibly even repair certain types of underwater life. Chemical dosimeters such as polysulphone have been tested to record underwater UV exposures and in turn quantify the relationship between water column depth and dissolved organic carbon levels to the distribution of biologically damaging UV underwater. However, these studies have only been able to intercept UV exposures over relatively short time intervals. This paper reports on the evaluation of a high exposure UV dosimeter for underwater use. The UV dosimeter was fabricated from poly 2,6-dimethyl-1,4-phenylene oxide (PPO) film. This paper presents the dose response, cosine response, exposure additivity and watermarking effect relating to the PPO dosimeter as measured in a controlled underwater environment and will also detail the overnight dark reaction and UVA and visible radiation response of the PPO dosimeter, which can be used for error correction to improve the reliability of the UV data measured by the PPO dosimeters. These results show that this dosimeter has the potential for long-term underwater UV exposure measurements.

INTRODUCTION

The measurement of solar ultraviolet radiation (UV) within the marine environment has been a subject of major interest for scientists for many decades. For example, previous investigations (1–5) have mainly investigated how the UV along with other wavebands in the electromagnetic spectrum (most commonly the visible waveband) penetrate and interact with the organic constituents and physical properties of various water bodies such as oceans and lakes by using various types of optical instrumentation such as spectrometers and broadband meters. An extensive review of this particular field has been provided by Tedetti and Sempéré (6).

In underwater conditions, the usage of broadband meters and spectrometers becomes complex where more routine

maintenance is required in comparison with when they operate on land and also additional calibrations are required to correct for the immersion effect (7). UV chemical dosimeters such as the tried and tested polysulphone (8,9) provide an easily deployable and inexpensive method for measuring UV exposure in comparison with the more expensive and problematical spectrometer and broadband meter alternatives.

Several UV chemical dosimeters such as o-nitrobenzaldehyde (10) and polysulphone (11,12) have been used previously in marine environments. However, these dosimeters only have the capability to record a cumulative exposure over small temporal increments, usually no greater than a 2 day period. This small dynamic range greatly reduces the amount of time over which a UV exposure can be measured in the field. Polysulphone dosimeters could be removed and replaced over regular periods of time in order to increase the amount of cumulative exposure measured. However, this would require a researcher to be on site nearly every day or every other day. So there is a need for a chemical dosimeter that can be employed for underwater use that is capable of measuring large amounts of UV radiation over a long time period. Poly 2,6-dimethyl-1,4-phenylene oxide (PPO) would be ideal for this purpose as it would allow for unattended measurements to be made at marine locales over extensive amounts of time.

Initial research conducted by Davis *et al.* (13) showed that PPO film could be successfully employed to measure high amounts of UV exposure over significant periods of time. Lester *et al.* (14) followed up on this work and presented data detailing the cosine response, temperature effects, spectral response and reproducibility for in-air PPO film usage. In this investigation, Lester *et al.* (14) found that PPO film has a dynamic range extending to 2 MJ m^{-2} of UVB before complete saturation, equivalent to 4 days exposure to solar UV in summer at subtropical regions. This represents a four-fold increase in dynamic range in comparison with polysulphone. In addition to this, in-air studies performed by Berre and Lala (15) have shown that PPO film dosimeters have an error equal to or better than 20% when compared with UV data collected by a radiometer.

It is a natural extension from these studies to further test the optical properties and operational limitations of the PPO film in underwater environments in order to develop a dosimeter capable of measuring long-term UV exposures with good accuracy. This, in turn, will greatly increase the extent of data available to the researcher and most importantly, will help to better quantify underwater solar UV exposure. However,

*Corresponding author email: schouten@usq.edu.au (Peter W. Schouten)
© 2007 American Society for Photobiology 0031-8655/07

before being deployed in actual marine environments, the optical and physical properties of the PPO dosimeter for use underwater have to be quantified in a controlled underwater environment. This paper reports on the properties of dose-response calibrations at different depths, cosine response, dose rate independence, interdosimeter variation, watermark effect, dark reaction, additivity of exposures and in-air response to visible and UVA wavelengths. The results are presented in order to verify the suitability of PPO film for underwater usage.

MATERIALS AND METHODS

Dosimeter preparation and analysis. A UV responsive dosimeter capable of receiving long-term exposures was developed specifically for underwater usage. In this paper, a long-term exposure is defined as that received at a subtropical site over a period of approximately a week. The chemical PPO film was selected for this objective. This dosimeter consists of the chemical PPO cast in thin film form at a thickness of approximately 0.04 mm. The PPO film is placed into a polyvinyl chloride (PVC) holder with an area of 3 × 3 cm and an opening slot of 1.2 × 1.6 cm. The film is held in place on the holder with standard electrical tape. The change in optical absorbance caused by UV exposure upon the PPO film was measured by a spectrophotometer (model 1601; Shimadzu Co., Kyoto, Japan) at 320 nm, which is a wavelength where a measurably significant change in optical absorbance occurs. The error threshold for optical absorbance measurements in the spectrophotometer has been quoted as ±0.002 by the manufacturer. This error was found to have an influence of between ±0.04% and ±4.7%, respectively, when compared with the highest and lowest optical absorbencies measured during testing. However, as the dosimeters will predominantly be used when the changes in optical absorbencies are high, the error will normally be at the low end of the range at ±0.04%. Figure 1 displays a typical optical absorption and transmission distribution for PPO film across the UV waveband. After each underwater exposure and before measurement in the spectrophotometer, the PPO film was cleaned with a burst of distilled water and left to dry in a darkened space.

Water tank, irradiation source description and water type analysis. The water tank used in the testing of the dosimeter had a length of 51 cm, a width of 37 cm and a depth of 30 cm. The water tank was painted matt black and was covered over by black felt in order to stop any outside stray light from penetrating the water. The UVB source employed was a fluorescent UV lamp (model FS40/12; Philips, Lawrence & Hanson, Toowoomba, Australia) covered by a long strip of cellulose acetate. This material was used to block out the UVC wavelengths emitted by the lamp. The lamp was suspended in place over the top of the tank at a distance of 18 cm from the water surface. All subsequent tests on the PPO dosimeter, apart from the watermark effect test and the reaction to UVA and visible exposure test were conducted in this tank with this particular configuration.

The water used was clear tap water, kept free of any floating particulates. For all of the experiments, UVB was defined as the waveband running from 280 to 320 nm. The 320 nm cut-off has sometimes been employed by photobiologists and was more applicable to our investigation. Figure 2 displays the transmission and absorption spectra measured using the spectrophotometer from 298 to 320 nm for a sample of this water at a typical temperature of 15°C. The water remained completely stable, with no mixing or surface disturbance occurring during the duration of each experiment. The water temperatures measured in the tank during each of the experiments ranged from 12°C to 23°C.

Immersion effect and radiometer calibration. The measurement of any type of electromagnetic radiation underwater by radiometric equipment is not a straightforward process. A wavelength-dependent property known as the immersion effect comes into play whenever an optical collector is submerged underwater. This is caused by a greater amount of light being backscattered out of the collector during a water-based measurement in comparison with a similar air-based measurement. This results from the difference between the refractive indices for air and water at the collector interface (16). In order to

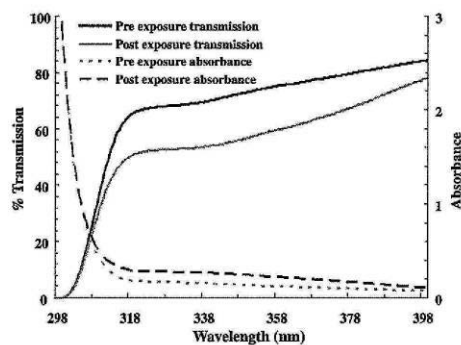


Figure 1. Change in optical transmission and absorbance in the UV waveband for PPO film after an underwater UVB exposure of 18.4 kJ m⁻².

correct for this, an IL1400 radiometer (International Light, Newburyport, MA) using a UVB filter (UVB-1; International Light) was calibrated for underwater use against a scanning spectroradiometer using a similar methodology as specified by Zibordi (17), Hooker & Zibordi (18) and Zibordi *et al.* (19). It was estimated that a variation of less than 1% would exist between the immersion factors calculated over the range of temperatures recorded during each experiment. Hence, only one set of immersion factor values, calculated at 23°C was used in the calibrations. The IL1400 was used as the primary measurement instrument instead of the spectroradiometer as it has the capability to integrate UV exposures over time. The underwater calibration of the IL1400 against the spectroradiometer took into account the different immersion effect and cosine response of the IL1400 in comparison with the spectroradiometer.

The spectroradiometer unit consisted of a diffuser input optic (type D6; Bentham Instruments, Reading, UK) capable of collecting spectral data ranging from 280 to 400 nm with wavelength dispersal performed by a double holographic grating monochromator (model DH10; Jobin Yvon, France) with 1200 lines mm⁻¹ gratings. The variations in the spectral irradiance measured by this particular spectroradiometer have been reported to be within approximately ±5% (20). Before each scanning session, the spectroradiometer was wavelength calibrated against a mercury UV spectral output and absolute irradiance was calibrated against a secondary standard quartz tungsten halogen lamp (250 W) powered by a stabilized current of 9.500 ± 0.005 A (model

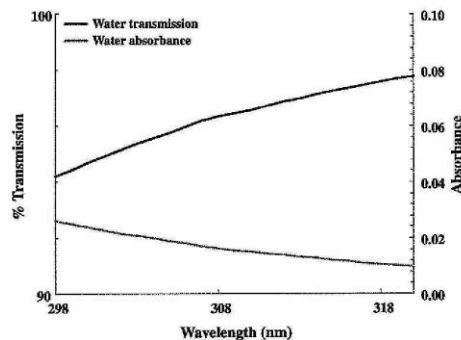


Figure 2. Transmission and absorption spectra of a sample of the clear tap water from 298 nm through to 320 nm at 15°C.

PD36 20AD; Kenwood, Hazlet, NJ). The absolute irradiance calibration standard originates from the National Standards Laboratory at the CSIRO, Lindfield, Australia.

Underwater dosimeter deployment and calibration. The PPO dosimeter was calibrated for unweighted UVB exposure from 280 to 320 nm at two different depths in conjunction with the immersion effect corrected IL1400. The depths were 1 cm below the surface ($Z_{1\text{cm}}$) and 16 cm below the surface ($Z_{16\text{cm}}$). The PPO dosimeter was also calibrated just above the water surface in conjunction with the IL1400 calibrated for in-air conditions. In order to derive each calibration curve, batches of PPO dosimeters were exposed to the UVB source on a horizontally aligned surface for a total time of 35 h. The exposure (J m^{-2}) was measured at specific intervals with the IL1400. After each interval, the change in optical absorbance at 320 nm (ΔA_{320}) for each PPO dosimeter was measured by the spectrophotometer to provide a data point, where ΔA_{320} was calculated by the following:

$$\Delta A_{320} = A_{320}^{\text{FINAL}} - A_{320}^{\text{INITIAL}}$$

where A_{320}^{FINAL} is the final optical absorbance measurement after exposure taken at 320 nm and A_{320}^{INITIAL} is the initial absorbance measurement before exposure taken at 320 nm. To increase the accuracy of the calibrations, the ΔA_{320} value was calculated over four positions across the film surface with the mean of these values used to calculate the UVB exposure. After their absorbencies were measured, the dosimeters were placed back into the water for further exposure. It is important to note that the response spectra of the IL1400 and the PPO film are different. The calibrations against each other and the spectroradiometer will only be applicable for the source spectrum employed in the calibration. The $\pm 5\%$ uncertainty of the spectroradiometer together with an estimated IL1400 transfer calibration error of $\pm 3\%$, an immersion factor uncertainty of $\pm 3\%$ and a $\pm 3\%$ final transfer uncertainty to the PPO dosimeter combine to give a total $\pm 14\%$ uncertainty in the PPO film calibration routine.

Dose rate independence and interdosimeter variation. If dose rate independence exists for the PPO dosimeter underwater, a high UVB irradiance accumulated over a short time period will deliver the same ΔA_{320} value as would be measured for a low UVB irradiance accumulated over a long period of time. To verify dose rate independence, a short period high irradiance (D_1) was delivered to a batch of 15 dosimeters at $Z_{1\text{cm}}$ over a time span of 14 h. After this, a long period low irradiance (D_2) was delivered to another batch of 15 dosimeters at $Z_{1\text{cm}}$, this time having the UVB source elevated to approximately twice the height above the tank. This trial was carried out over the period of time necessary so that both exposures were equal. The respective ΔA_{320} values from each batch were then measured and compared.

The in-water interdosimeter variation for the PPO dosimeter was calculated using the same batches of dosimeters as used for the dose rate independence test. The mean and standard deviation of the ΔA_{320} for each dosimeter across four positions of the film surface was calculated and then used to find the coefficient of variation (CV) for the entire sample. This CV was then converted to a percentage value called the in-water interdosimeter variation error. Lester *et al.* (14) calculated an in-air interdosimeter variation error of approximately 6%. It is anticipated that this error will be higher for underwater measurements due to the influence of watermarking on the PPO film surface.

Watermark effect. Using a temperature-controlled water vessel (Grant Instruments, Cambridge, UK), several sets of PPO dosimeters were submerged in clear stable water at a depth of 1 cm for three different temperatures without being exposed to any form of radiation. These temperatures ranged in 20°C increments from 0°C up to 40°C , which are assumed to be the minimum and maximum temperatures that would be measured throughout the year in various marine environments such as lakes and creeks found within subtropical locales. The dosimeters were submerged in the water vessel for a total of 5 days (120 h in total). The ΔA_{320} value measured for each dosimeter at the end of each day was compared with an average daily ΔA_{320} value of 0.12 taken from the data set measured for the UVB dose-response calibration at $Z_{1\text{cm}}$. From this data any measurement errors caused by minor watermarking on the PPO film surface could be detected and quantified.

Underwater cosine response of dosimeter. As is the case in air, the solar UV in water arrives at a receiving plane in two components, namely the direct and the diffuse components. The direct component propagates in a direct path from the sun, while the diffuse component is scattered in a multitude of different directions by various waterborne constituents. Therefore, the response of the PPO dosimeter to UV wavelengths incident at different inclinations in water must be detailed. PPO dosimeters were aligned to a series of angles running in 10° increments from 0° through to 80° with each of their center points in alignment to a horizontal axis. The error for each of these angular alignments was estimated to be within $\pm 2^\circ$. The dosimeters were then exposed to 35 h of cumulative UVB exposure at a depth just below the water surface. Following this, the ΔA_{320} for each dosimeter was normalized using a previously calculated dose-response calibration and compared directly to the cosine function. The absolute error (AE) for the cosine response was calculated at each angle as the magnitude of the difference between the cosine function and the angular ΔA_{320} response normalized to a horizontally aligned ΔA_{320} response using the expression:

$$AE(\theta) = \left| \cos(\theta) - \frac{A[(\Delta A_{320})_Z^\theta]^2 + B[(\Delta A_{320})_Z^\theta] + C}{A[(\Delta A_{320})_Z^{\text{HORIZONTAL}}]^2 + B[(\Delta A_{320})_Z^{\text{HORIZONTAL}}] + C} \right|$$

where θ is the angle at which the dosimeter was positioned relative to the horizontal plane during exposure, A , B and C are calibration coefficients, Z is the depth at which the dosimeter was exposed and HORIZONTAL represents the horizontal plane (where $\theta = 0^\circ$).

Overnight dark reaction. The optical density of chemical film dosimeters is known to continue to change during storage after an exposure to solar radiation (21). The inherent dark reaction for PPO film was quantified by measuring the overnight change in optical density each day for a series of underwater exposures each with varying dosages taken over a time period of 5 days.

Reaction to UVA and visible exposure. The PPO dosimeter's responsivity to both the visible (400–700 nm) and UVA (320–400 nm) waveband was quantified by employing both a visible and UVA waveband transmitting filter (mylar film; Cadillac Plastics, Australia) and a visible waveband transmitting filter (S770A Sheet-ing; Bekeart Plastics, Australia). The mylar filter has been successfully used in previous research on top of phenothiazine dosimeters to block out UVB wavelengths (22). Two sets of PPO dosimeters, each covered by one type of filter were exposed to full sunlight over the space of 5 days in conjunction with an unfiltered PPO dosimeter. At the conclusion of this time period any ΔA_{320} response caused by either UVA or visible wavelengths was detected and averaged and then compared with the unfiltered ΔA_{320} response. Ratios between the filtered and unfiltered responses were calculated to estimate the percentage effect that the respective visible and UVA wavelengths have upon the PPO dosimeter.

Additivity of exposures. For the PPO dosimeter, it was unclear whether multiple absorbance measurements made over a particular exposure interval have an effect on final ΔA_{320} values in comparison with a single absorbance measurement made after precisely the same exposure interval. In order to test this, a batch of PPO dosimeters was exposed underwater to the fluorescent UV lamp at $Z_{1\text{cm}}$ over a time span of 35 h. Half the batch (batch A) was measured three times a day in the spectrophotometer, while the other half (batch B) were left untouched until they were measured upon the completion of the test. An average ΔA_{320} value was then calculated individually for batch A and batch B. Following this, these two average ΔA_{320} values were compared against each other.

RESULTS

Immersion effect and radiometer calibration

The immersion effect factors in the UVB waveband for the scanning spectroradiometer are presented in Fig. 3. It can be seen that the immersion factors fluctuate across the UVB waveband, tending to decrease in magnitude slightly with increasing wavelength. The immersion effect corrected spectral

irradiances in the UVB waveband are depicted in Fig. 4 at just above the water surface, at a depth of 1 cm and at a depth of 16 cm. For each scan a peak can be seen at 313 nm, which is due to the spectral emission from mercury constituents in the UV source lamp. For the scan taken at $Z_{16\text{cm}}$, the two irregular troughs at 300 nm and at 317 nm can be attributed to photon noise, due to the spectroradiometer reaching the limit of its performance range at this depth.

Dosimeter calibration variation underwater

By analyzing the dose-response calibrations made at the two depths, it could be seen if the UVB calibration of the PPO dosimeter was interchangeable in shallow water and if these shallow water dose-response calibrations differed at all from the surface calibration. The dose-response calibrations for PPO film on a horizontal plane at the water surface and at depths of 1 and 16 cm are displayed in Fig. 5. A calibration

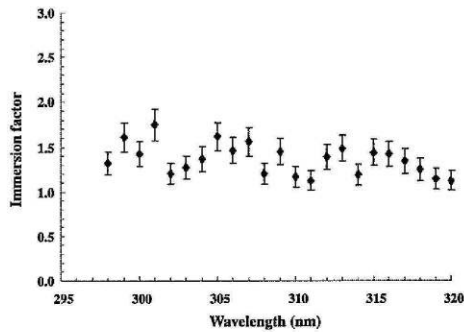


Figure 3. Immersion effect factors from 298 nm through to 320 nm as calculated for the spectroradiometer. The y-error bars represent the cumulative $\pm 5\%$ variation estimated to exist within each scan.

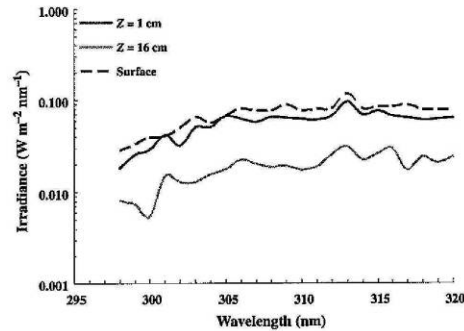


Figure 4. Profile of immersion effect corrected spectral irradiances from 298 nm through to 320 nm in the water tank at the water surface, at $Z_{1\text{cm}}$ and $Z_{16\text{cm}}$.

equation in polynomial form has been fitted to the calibration data at the surface and at each depth. For the surface calibration, the equation is:

$$\Delta A_{320} = -1 \times 10^{-5}(\text{UVB}_{\text{SURFACE}})^2 + 0.0052(\text{UVB}_{\text{SURFACE}})$$

with an R^2 value of 0.99 and where $\text{UVB}_{\text{SURFACE}}$ is the UVB exposure received at the water surface in units of kJ m^{-2} .

For the calibration made at $Z = 1$ cm the equation is

$$\Delta A_{320} = -2 \times 10^{-5}(\text{UVB}_{Z_{1\text{cm}}})^2 + 0.0062(\text{UVB}_{Z_{1\text{cm}}})$$

with an R^2 value of 0.99 and where $\text{UVB}_{Z_{1\text{cm}}}$ is the UVB exposure received at a depth of 1 cm in units of kJ m^{-2} .

For the calibration made at $Z = 16$ cm the equation is

$$\Delta A_{320} = -2 \times 10^{-5}(\text{UVB}_{Z_{16\text{cm}}})^2 + 0.0063(\text{UVB}_{Z_{16\text{cm}}})$$

with an R^2 value of 0.99 and where $\text{UVB}_{Z_{16\text{cm}}}$ is the UVB exposure received at a depth of 16 cm in units of kJ m^{-2} .

Dose rate independence and interdosimeter variation

After a total exposure of 76 kJ m^{-2} received during the initial 14 h time period and the consequent 23 h time period for the high and low irradiances, respectively, the ΔA_{320} values measured across the two batches of PPO dosimeters were found to vary by approximately 16%. Using this data, the in-water interdosimeter variation for the PPO dosimeter was calculated to be approximately 9%, which is 3% higher than the value previously calculated for measurements in-air (11).

Watermark effect

Figure 6 shows the percentage ratio of the daily watermark effect measurement to the average daily ΔA_{320} value over a time period of 120 h. It appears that an increase in submersion temperature results in a measurable increase in the watermark-induced ΔA_{320} value. For example, after 120 h immersion time in 40°C water, the accumulated watermarking on the PPO film would account for approximately 13% of the average daily ΔA_{320} value as measured in the tank.

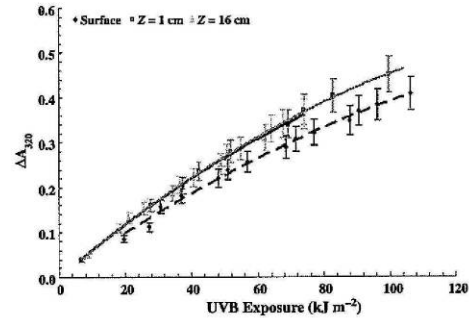


Figure 5. Horizontal plane PPO film dose-response calibrations at the water surface and at $Z_{1\text{cm}}$ and $Z_{16\text{cm}}$. The error bars represent the $\pm 9\%$ for the in-water interdosimeter variation.

Underwater cosine response of dosimeter

The normalized underwater cosine response for the PPO dosimeter is shown in Fig. 7. The cosine error varied from 4% to 22% for angles smaller than 50°.

Overnight dark reaction

The overnight dark reaction data (Fig. 8) shows that the percentage ratio between the dark reaction ΔA_{320} value (measured in the morning of each day before exposure) and the cumulative ΔA_{320} value (measured as the accumulation of the increase in optical absorbency within the PPO film from day to day) decreases as the cumulative UVB exposure increases. This means that the effect that inherent dark reaction has upon the PPO film gradually diminishes over time, assuming there is increasing incident dosage. This overnight dark reaction trend has been fitted with a power law of the following form

$$\% \Delta A_{320} = 68.583(\text{UVB})^{-0.5572}$$

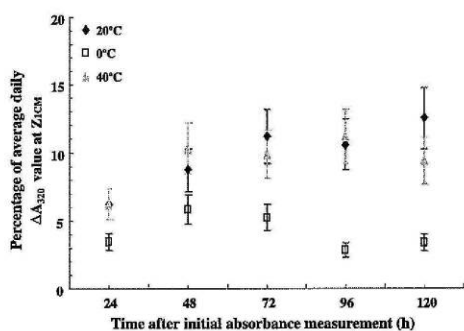


Figure 6. Percentage ratio of the daily watermark effect measurement to the average daily ΔA_{320} value. The y-error bars represent the cumulative $\pm 9\%$ for the in-water interdosimeter variation.

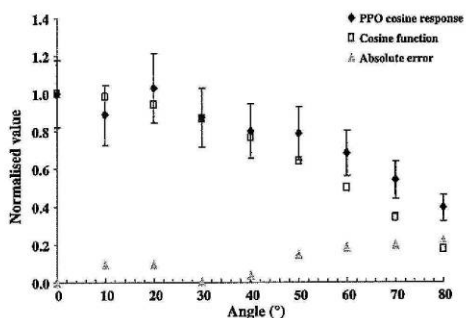


Figure 7. PPO film cosine response underwater at an arbitrary depth. The y-error bars represent the cumulative $\pm 9\%$ in-water interdosimeter variation after normalization.

with an R^2 value 0.89 and where UVB is the UVB exposure received at the particular depth in units of kJ m^{-2} .

Reaction to UVA and visible exposure

From Fig. 9, it can be seen that over the 5 day exposure period, the PPO film did not respond at all to visible wavelengths. However, a progressively increasing response to UVA wavelengths over time does occur. After 60 h cumulative exposure time to full sunlight, the ΔA_{320} of the PPO film to UVA reaches a significant 19% of the total ΔA_{320} as measured from the unfiltered PPO film. The percentage ratio between the PPO unfiltered response and UVA response has been modeled as the following polynomial expression

$$\% \left(\frac{\text{UVA}_{\text{RESPONSE}}}{\text{TOTAL}_{\text{RESPONSE}}} \right) = -0.0009(t)^2 + 0.3927(t)$$

having an R^2 value of 0.93 and where $\text{TOTAL}_{\text{RESPONSE}}$ is the unfiltered ΔA_{320} value, $\text{UVA}_{\text{RESPONSE}}$ is the ΔA_{320} value measured after solar radiation exposure under the mylar film filter and t is the cumulative solar radiation exposure time given in hours.

Additivity of exposures

A percentage difference of approximately 8% was calculated to exist between the average ΔA_{320} values as measured for batch A and batch B after a total dosage of 309 kJ m^{-2} accumulated during the 35 h long exposure. This percentage difference falls within the 9% interdosimeter variation limit. So it appears that multiple measures of absorbance do not have any considerable influence upon final ΔA_{320} values.

DISCUSSION

This paper has extended the previous research (13–15) by detailing how PPO film responds to UV in underwater conditions. The dose-response calibrations performed with

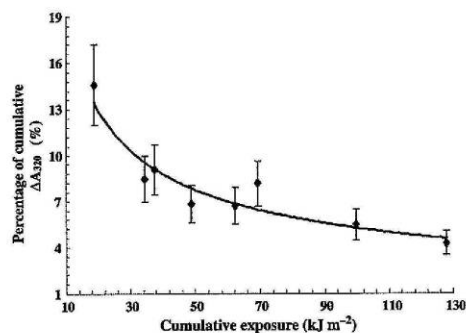


Figure 8. Overnight dark reaction data shown as a percentage of the cumulative ΔA_{320} value measured as the accumulation of the increase in optical absorbency within the PPO film after each daily exposure. The y-error bars represent the cumulative $\pm 9\%$ for the in-water interdosimeter variation.

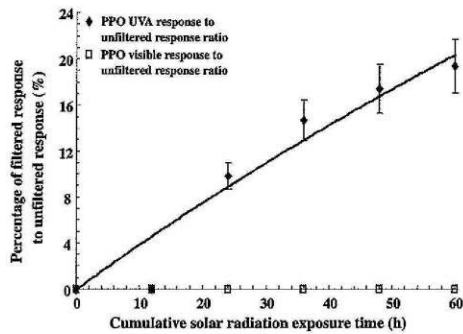


Figure 9. PPO film reaction to UVA and visible wavelengths on a horizontal plane after 60 h total exposure to sunlight given as a percentage ratio. The γ -error bars represent the cumulative $\pm 6\%$ in-air interdosimeter variation.

the UVB source in the ideal clear water environment at the shallow depths of $Z_{1\text{cm}}$ and at $Z_{16\text{cm}}$ are almost completely interchangeable. However, these two dose-response calibrations do differ significantly from the dose-response calibration made at the water surface. For instance, a discrepancy as large as 19 kJ m^{-2} exists between the dose-response calibrations at the water surface and at $Z_{1\text{cm}}$ after a recorded ΔA_{320} of 0.4. This suggests that an in-air calibration could not be applied to calculate exposures recorded by PPO film in underwater environments without considerable errors coming into play. So it is advised that before any measurement campaign is performed in an underwater environment in the field that at least one dose-response calibration is performed in a tank at an arbitrary depth in a sample of water taken from the actual site in combination with an immersion effect corrected radiometer. The calibrations performed between the radiometer and the PPO film should only be used to measure exposures from the spectrum that they have been calibrated to in order to minimize errors.

Within each batch of PPO dosimeters, underwater interdosimeter variations were found to be approximately 9%, which is only 3% more than the variation calculated in air (14). However, it is expected that this variation estimate would increase if the PPO dosimeter were to be employed in an underwater environment of high turbidity, as strong watermarking effects and film damage would almost certainly occur. The dose rate independence data shows that repeatability discrepancies in the order of $\pm 16\%$ for measured ΔA_{320} values over different batches of PPO dosimeters may occur for similar underwater exposures after varying periods of time. This does not represent a high level of dose rate independence as this result does not overlap with the calculated interdosimeter variation. To keep these uncertainties to a minimum, the calibration dosimeters should be exposed to the source spectrum over a number of days, so that a wide variety of high and low dose rates will be employed in the calibration and accounted for.

The watermark effect results indicate that special cleaning procedures may be required after the usage of PPO film underwater in order to reduce errors in the recorded ΔA_{320}

value. One suggested method could be to not dry the PPO dosimeters using a cloth or towel, as this could smear out watermarks and increase their effective area, but to clean them with distilled water and leave them to dry in a dark room. Before measurement, each particular film should be visually inspected and checked for any remaining watermarks. If there is still some watermarking remaining on a film's surface, the cleaning process should be repeated again.

Before usage in an underwater environment, it may be necessary to perform a cosine response test in a controlled environment on the particular batch of PPO film to be used. This data could then be used to calculate appropriate cosine correction factors that when applied, would minimize measurement errors arising from inherent errors in the angular response of the PPO film. Before the calculation of the cosine correction factors, the angular distribution of the incoming radiation in the respective underwater environment must be known. A general estimate of the correction required can be made by assuming that the distribution of radiation in this environment is isotropic. The imperfect cosine response means that errors can occur not only in the exposures measured by tilted dosimeters, but also in exposures measured by dosimeters aligned to the horizontal plane within a diffuse UV environment.

Dark reaction will influence measurements recorded by a PPO dosimeter for exposures lasting longer than 1 day, with the effect of the dark reaction gradually decreasing over time with increasing exposure. The effect of dark reaction can be nullified if a dose-response calibration is carried out before measurements are made in an underwater field environment. As the dose-dependent dark reaction cannot be measured each day at a field location, this calibration should be carried out in the season in which the dosimeters will be used. The calibration for each season will minimize the change in dark reaction caused by the variation in dose rates from day to day. This way, any overestimations of the total exposure caused by the overnight dark reaction are completely taken into account within the dose-response calibration.

The results show that the PPO film could be used as a shortwave UVA (320–340 nm) dosimeter with the use of an appropriate UVB filter material. However, it is not certain over what range of UVA wavelengths the PPO film is reacting to. Previous studies (14) show that the normalized spectral response of PPO film to UVA decreases to less than 0.001 at 340 nm. So it is assumed that the induced change in optical absorbance caused by wavelengths higher than 340 nm can be regarded as negligible effectively making the UVB filtered PPO film a viable shortwave UVA dosimeter for both in-air and underwater applications. Although there is a small response to the shortwave UVA, the majority of the spectral response is in the UVB. Consequently, the PPO film can be used as a UVB dosimeter provided it is calibrated appropriately.

The results show that PPO film can be employed as a high exposure solar UV dosimeter in underwater applications. If calibrated correctly, the uncertainty in the usage of the PPO film for underwater applications is estimated to range from $\pm 15\%$ to an upper limit of $\pm 20\%$ taking into account all errors involved with transfer calibrations and the variation of the optical properties of the PPO film itself. The next stage of development will be to calibrate PPO dosimeters against the solar UV in several marine environments such as streams and

dams, each having their own characteristic turbidity and dissolved organic carbon concentration. Underwater exposures recorded using the PPO dosimeters will then be compared with radiometric solar UV measurements made in the same conditions at comparable solar zenith angles throughout different seasons of the year to completely verify the accuracy of the PPO dosimeters for measurement of high UV exposures underwater.

Acknowledgements—The authors would like to thank both Graham Holmes and Oliver Kinder from the Faculty of Sciences, University of Southern Queensland for their technical assistance throughout this project.

REFERENCES

- Davies-Colley, R. J. and D. G. Smith (1995) Optically pure waters in Waikoropupu ("Pupu") Springs, Nelson, New Zealand. *New Zeal. J. Mar. Fresh.* **29**, 251–256.
- Hargreaves, B. R. (2003) Water column optics and penetration of UVR. In *UV Effects in Aquatic Organisms and Ecosystems* (Edited by E. W. Helbling and H. Zagarese), pp. 59–105. The Royal Society of Chemistry, Cambridge.
- Neale, P. J., E. W. Helbling and H. E. Zagarese (2003) Modulation of UVR exposure and effects by vertical mixing and advection. In *UV Effects in Aquatic Organisms and Ecosystems* (Edited by E. W. Helbling and H. Zagarese), pp. 107–134. The Royal Society of Chemistry, Cambridge.
- Neale, P. J., P. Bossard, Y. Huot and R. Sommaruga (2001) Incident and *in situ* irradiance in Lakes Cadagno and Lucerne: A comparison of methods and models. *Aquat. Sci.* **63**, 250–264.
- Smith, R. C., J. E. Tyler and C. R. Goldman (1973) Optical properties and color of Lake Tahoe and Crater Lake. *Limnol. Oceanogr.* **18**(2), 189–199.
- Tedetti, M. and R. Sempéré (2005) Penetration of ultraviolet radiation in the marine environment. A review. *Photochem. Photobiol.* **82**(2), 389–397.
- Austin, R. W. (1976) *Air-water radiance calibration factor*, Technical Memorandum ML-76-004, Visibility Laboratory, p. 8. Scripps Institute of Oceanography, La Jolla, CA.
- Davis, A., G. H. W. Deane and B. L. Diffey (1976a) Possible dosimeter for ultraviolet radiation. *Nature* **261**, 169–170.
- Davis, A., B. L. Diffey and B. K. Tate (1981) A personal dosimeter for biologically effective solar UV-B radiation. *Photochem. Photobiol.* **34**, 283–286.
- Fleischmann, E. M. (1989) The measurement and penetration of ultraviolet radiation into tropical marine water. *Limnol. Oceanogr.* **34**(8), 1623–1629.
- Frost, P. C., A. Mack, J. H. Larson, S. D. Bridgman and G. A. Lamberti (2006) Environmental controls of UVB radiation in forested streams of northern Michigan. *Photochem. Photobiol.* **82**, 781–786.
- Dunne, R. P. (1999) Polysulphone film as an underwater dosimeter for solar ultraviolet-B radiation in tropical latitudes. *Mar. Ecol.-Prog. Ser.* **189**, 53–63.
- Davis, A., G. W. H. Deane, D. Gordon, G. V. Howell and K. J. Ledbury (1976) A world-wide program for the continuous monitoring of solar UV radiation using poly (phenylene oxide) film, and consideration of the results. *J. Appl. Polym. Sci.* **20**, 1165–1174.
- Lester, R. A., A. V. Parisi, M. G. Kimlin and J. Sabburg (2003) Optical properties of poly(2,6-dimethyl-1,4-phenylene oxide) film and its potential for a long term solar ultraviolet dosimeter. *Phys. Med. Biol.* **48**, 3685–3698.
- Berre, B. and D. Lala (1989) Investigation on photochemical dosimeters for ultraviolet radiation. *Sol. Energy* **42**, 405–416.
- Ohde, T. and H. Siegel (2003) Derivation of immersion factors for the hyperspectral TriOS radiance sensor. *J. Opt. A-Pure Appl. Opt.* **5**, L12–L14.
- Zibordi, G. (2005) Immersion factor of in-water radiance sensors: Assessment for a class of radiometers. *J. Atmos. Ocean. Tech.* **23**, 302–313.
- Hooker, S. B. and G. Zibordi (2005) Advanced methods for characterising the immersion factor of irradiance sensors. *J. Atmos. Ocean. Tech.* **22**, 757–770.
- Zibordi, G., S. B. Hooker, J. Mueller and G. Lazin (2004) Characterisation of the immersion factor for a series of in-water optical radiometers. *J. Atmos. Ocean. Tech.* **21**, 501–514.
- Wong, C. F., S. Toomey, R. A. Fleming and B. W. Thomas (1995) UV-B radiometry and dosimetry for solar measurements. *Health Phys.* **68**, 175–184.
- Parisi, A. V., J. Sabburg and M. G. Kimlin (2004) *Scattered and Filtered Solar UV Measurements*, pp. 70–71. Kluwer Academic Publishers, The Netherlands.
- Parisi, A. V., M. G. Kimlin, D. J. Turnbull and J. Macararas (2005) Potential of phenothiazine as a thin film dosimeter for UVA exposures. *Photochem. Photobiol. Sci.* **4**, 907–910.



ELSEVIER

Available online at www.sciencedirect.com



Journal of Photochemistry and Photobiology B: Biology 91 (2008) 108–116

Journal of
Photochemistry
and
Photobiology
B: Biology

www.elsevier.com/locate/jphotobiol

Field calibrations of a long-term UV dosimeter for aquatic UVB exposures

P.W. Schouten^{a,*}, A.V. Parisi^{a,b}, D.J. Turnbull^{a,b}

^a Department of Biological and Physical Sciences, Faculty of Sciences, University of Southern Queensland, Toowoomba 4350, Australia
^b Centre for Rural and Remote Area Health, Faculty of Sciences, University of Southern Queensland, Toowoomba 4350, Australia

Received 10 December 2007; received in revised form 5 February 2008; accepted 13 February 2008
Available online 20 February 2008

Abstract

Various methodologies using a wide range of measurement systems have been employed previously in order to determine the amount of UV that could be incident upon various aquatic organisms in a number of different aquatic locales. Broadband meters and spectroradiometers have been employed extensively to take underwater measurements. However, these measurement campaigns are limited by the fact that radiometric equipment requires a human controller, constant power supply and regular calibrations and corrections in order to function properly. Dosimetric measurements have also been made underwater using two distinct types of dosimeter. The first type based on a synthetic chemical, like polysulphone, and the second type based on a biological matter, such as a DNA sample. The studies made using biological dosimeters have displayed very good results, however the time and skill necessary to make these types of dosimeters can outweigh their usefulness. The chemical dosimeters are easier to make and have also provided useable data, but only for short periods of exposure, usually no more than a day. Previous research has shown that Poly (2,6-dimethyl-1,4-phenylene oxide) (PPO) has excellent potential for use as a long-term underwater solar UVB dosimeter. However, there is no documented methodology on how to properly calibrate the PPO dosimeter for water-based measurements and it has yet to be trialled in an outdoors marine environment, either real or simulated. This manuscript shows that calibrations obtained in air can not be transferred to calibrations made in water, calibrations made in one type of water can be employed for another type of water, but only within a certain range of spectral transmission and calibrations made at different depths in the same water type are interchangeable. It was also discovered that changing solar zenith angle had an effect upon calibration data. This research addressed these issues by formulating and developing a calibration methodology required for accurate underwater long-term UVB measurements in the field using the PPO film dosimeter.
© 2008 Elsevier B.V. All rights reserved.

Keywords: Dosimeter; PPO; Underwater; Ultraviolet; Marine; Solar

1. Introduction

The sizeable reduction in the protective ozone layer over recent decades has coincided with an increase in the amount of biologically damaging solar ultraviolet radiation (UV_{BE}) reaching the Earth's surface. Not only does this intensification of the UV_{BE} affect terrestrial life forms, but it also has a negative influence upon a wide and varied number of organisms inhabiting marine environments such as rivers and dams. Coupled with the enhanced evaporative

effect of global warming, these organisms living underwater have even less protection against the UV_{BE} than was once present.

Several studies have analysed the behaviour of the solar UV underwater with varying degrees of success. One recent notable investigation was made by Frost et al. [1] where spectral data was obtained over a range of different depths in order to calculate attenuation factor values in the UV waveband for a variety of different streams each with their own particular dissolved organic matter (DOM) levels. Some other notable similar investigations detailing underwater solar UV spectral irradiance and its relationship with DOM and other marine constituents have been published

* Corresponding author.
E-mail address: schouten@usq.edu.au (P.W. Schouten).

by: Bracchini et al. [2] in shallow lake water; Conde, Aubriot and Sommaruga [3] in lagoon waters within the Southern Atlantic Ocean; Crump et al. [4] in shallow pond water; Vincent et al. [5] in Antarctic ice covered lakes; and Sommaruga and Psenner [6] in a high altitude mountain lake in Austria. Most recently, Belmont et al. [7] analysed diffuse attenuation factors for river water in both the laboratory and field environments using radiometric instrumentation set to multiple wavelength channels.

All of these measurement campaigns have been limited by the fact that the spectroradiometric equipment used required a constant power supply, a human controller and regular calibrations in order to operate correctly. Also, due to the high cost of spectroradiometric equipment, usually only one spectroradiometer can be employed during a series of measurements. This greatly reduces the amount of measurement data available for analysis and also does not allow for precise same-time comparisons to be made with the data, for example comparisons between measurements made at different angles and at different depths.

These problems can be alleviated with the use of a high exposure UV dosimeter applicable underwater, as many dosimeters can be deployed at different angles and depths at the same time at a cost far less than that of a conventional spectroradiometer. Also, no human operator is required apart from their initial calibration, setting-up and collection and they require no external power source to operate.

However, despite their usefulness, it is important to note that dosimetric measurements are not a complete replacement for spectroradiometric measurements in the underwater environment. Spectroradiometers and radiometers are still necessary to record short term changes in underwater UV irradiance levels, such as those brought on by rapidly evolving systems, such as cloud coverage.

Dosimetric measurements have been made underwater using two distinct types of dosimeter. The first type based on a synthetic chemical, such as the commonly used polysulphone, and the second type based on a biological composition, such as a particular DNA sample. One example of this DNA dosimeter technique is seen in Regan et al. [8]. Out of these two dosimetric techniques, the biological dosimeters (most often those based on DNA) have been the most commonly used in marine applications.

Boelen et al. [9] has delivered one of the most extensive underwater biological dosimeter investigations to date. Using DNA dosimeters fabricated out of calf thymus DNA, the authors developed distributions of DNA damaging UV irradiance as a function of depth with good accuracy when compared against spectroradiometric measurements. Other notable examinations have been carried out by Koussoulaki et al. [10] using *Euglena gracilis* cultures and Li et al. [11] by calibrating tobacco cells against UVB related DNA damaging effects. These studies have all shown good results, however the time and skill necessary to make biologically active dosimeters appear to outweigh their usefulness.

Only three chemical dosimeter types have been deployed in the underwater environment. The first and most commonly used is polysulphone. Dunne [12] evaluated UVB radiation with polysulphone dosimeters in a variety of different types of seawater at tropical latitudes. The author found that polysulphone had a practical depth range of between 2.2 and 7.0 m, dependent upon seawater turbidity with a 5% error margin. However, exposures of between 1.5 and 40.0 kJ m⁻² could only be measured. Polysulphone was also successfully employed by Frost et al. [13] to estimate diffuse attenuation coefficient values in shaded water bodies in the North-east region of the United States. The second type of chemical dosimeter used for underwater UV measurements has been the *o*-nitrobenzaldehyde dosimeter, which was used in one study carried out by Fleischmann [14] at Discovery Bay in Jamaica. This dosimeter only measures UV exposures over a period of the order of a day and this study measured UV exposures with the *o*-nitrobenzaldehyde dosimeter to calculate the typical depth distribution and variation of solar UV throughout a single day. The third and final dosimeter to be tested underwater was the PPO film dosimeter by Schouten et al. [15]. This investigation analysed various optical and physical properties of PPO film, such as the cosine response, reproducibility after exposure, dose rate independence, watermarking effects, dark reaction, UVA and visible wavelength response and exposure additivity.

Currently, it is not known if: calibrations measured in air can be reassigned to calibrations made in water; calibrations obtained in one water type can be used for another water type; and calibrations made at separate depths in the same water type are interchangeable. Also unknown at this stage is the effect of solar zenith angle (SZA) upon underwater calibration regimes. This manuscript will extend the previous work presented in this field by answering these important research questions and giving a detailed documentation of the methodology required to calibrate the PPO dosimeter for underwater measurements in the real marine environment.

2. Materials and methods

2.1. Dosimeter description and measurement technique

For this investigation, the UV responsive polymer film PPO dosimeter was tested and calibrated in outdoor aquatic environments long-term. In this work, a long-term exposure is defined as an exposure received in an outdoor aquatic environment at a subtropical site over a one week time interval at any time of the year. The physical dosimeter consists of the chemical PPO cast in thin film form at a thickness of approximately 40 µm. The PPO film is placed into a polyvinyl chloride (PVC) holder of size 3.3 cm and an aperture of 1.2–1.6 cm. The film is secured to the holder with standard electrical tape. The change in optical absorbance caused by UV exposure upon the PPO film is measured by a spectrophotometer (model 1601, Shimadzu

Co., Kyoto, Japan) at 320 nm, which is a wavelength where a measurably significant change in optical absorbance is known to occur [15]. The error threshold for optical absorbance measurements in the spectrophotometer has been quoted as ± 0.002 by the manufacturer. After each UV exposure, the change in optical absorbance at 320 nm (ΔA_{320}) for each PPO dosimeter used in a measurement campaign is measured to provide a data point, where ΔA_{320} is calculated with the following equation:

$$\Delta A_{320} = A_{320}^{\text{FINAL}} - A_{320}^{\text{INITIAL}}$$

where A_{320}^{FINAL} is the final optical absorbance measurement taken at the wavelength of the maximum change in optical absorbance at 320 nm as described by Schouten et al. [15] after exposure to the sun and A_{320}^{INITIAL} is the initial absorbance measurement taken at the same wavelength of 320 nm before exposure to the sun. After every underwater exposure and before measurement in the spectrophotometer, any residues or particulates remaining on the PPO film surface were removed with a distilled water jet and then left to dry in a dark box.

To better improve the accuracy of the measurements, the ΔA_{320} value is measured over four positions across the film surface with the mean of these values used to calculate the UV exposure by means of interpolation from a dose-response calibration.

2.2. Dose response calibrations

The PPO dosimeter was calibrated on the horizontal plane to solar UV over the time period of approximately 25 h sunlight spanning 5–7 days outdoors to solar UV for the UVB waveband running from 300 to 320 nm in four different water types. These were clear tap water, sea water, moderately turbid creek water and highly turbid stagnant dam water. The 320 nm cut-off has been used occasionally in photobiological investigations and was more applicable to our research. The calibrations took place in Too-

woomba, Australia (27.5° S, 151.9° E, 693 m altitude) over the six month time period between March and August inclusive, representing the autumn (low SZA) and winter (high SZA) seasons. The SZA range over the autumn calibration period was 20°–70°. The SZA range over the winter calibration period was 35°–65°. The measurement campaign ran over both autumn and winter in order to investigate the effect of changing SZA on the underwater calibrations. The water types were chosen as they represent a good cross section of the different water types and for their own distinct level of turbidity, DOM (dissolved organic matter) level and salinity. Fig. 1 shows the respective UV transmission and absorption distributions from 300 to 320 nm for each water type, measured using a spectrophotometer (model 1601, Shimadzu Co., Kyoto, Japan). According to the work of Lester et al. [16], the response of the PPO dosimeter is not influenced in any way by fluctuations in local temperature. Therefore, changes in temperature over the different calibration sessions would not have had any effect upon the measured ΔA_{320} data.

For each water type, one batch of dosimeters was calibrated just above the water surface (which acted as the control calibration), while another batch was placed below the water surface at a depth of about 1 cm ($Z_{1\text{CM}}$). UV exposures during these calibrations were measured using an IL1400 radiometer working at a 1/2 second refresh rate (International Light, Newburyport, MA) fitted with an underwater detector with a UVB filter having a response running from 265 to 332 nm (UVB-1, International Light). The IL1400 radiometer was chosen as the primary measurement instrument due to the fact that it is capable of recording the integrated UVB exposure.

Another batch of dosimeters were placed at a depth of 20 cm below the water surface ($Z_{20\text{CM}}$) in order to test for differences in calibration trends at varying depth. As a second IL1400 unit was not available for use, the exposure received at $Z_{20\text{CM}}$ in each water type had to be calculated from that at $Z_{1\text{CM}}$. A basic methodology using

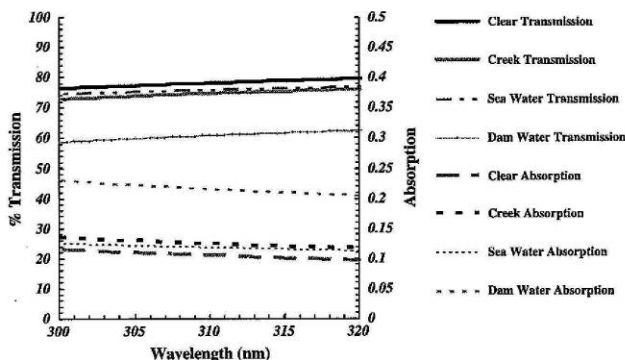


Fig. 1. Transmission and absorption distributions for tap water, creek water, sea water and water taken from a stagnant water reserve.

current underwater light attenuation theory was utilised in order to achieve this.

The attenuation of any form of light (including UV) into a water column is dependent upon both absorption and scattering, which are specific optical characteristics of the water type [17]. Absorption removes the incoming light completely, while scattering changes the direction in which the light moves. The characterization of the water column relies upon a single parameter known as the diffuse attenuation coefficient K_d . This parameter is calculated by the following expression which details the exponential decrease with depth of the underwater downwelling irradiance (E_d) which is composed of photons propagating in the downwards direction ([18,19]):

$$K_d(\lambda, z) = -\frac{1}{E_d(\lambda, z)} \frac{dE_d(\lambda, z)}{dz}$$

where $K_d(\lambda, z)$ is the diffuse attenuation coefficient given in m^{-1} , $E_d(\lambda, z)$ is the underwater downwelling irradiance in units of $W m^{-2}$ and z is the depth of the water column in m. $K_d(\lambda, z)$ is dependent on the constituent content of the water column and in turn, the distribution of the underwater light field. Dissolved and particulate matter in the water column, especially dissolved organic matter (DOM) is known to greatly affect the propagation of solar UV in any water column and hence change the value of $K_d(\lambda, z)$ ([2,20]). $K_d(\lambda, z)$ is not affected by any changes in the surface incident light field such as those caused by a change in the sun's elevation angle [21].

The equation detailed above to calculate $K_d(\lambda, z)$ can be written in another form, which can then be used as a simple model, based upon the Beer–Lambert–Bouguer relation to describe the exponential decay of the underwater light field with increasing depth, if $K_d(\lambda, z)$ has already been calculated [22]:

$$E_d(\lambda, z) = E(0, \lambda)e^{-K_d(\lambda, z)z}$$

where $E(0, \lambda)$ is the downwelling irradiance at a depth just below the water surface. In this research, the K_d value for

each water type over the 300–320 nm waveband was calculated using spectral data measured using the spectrometer mentioned in the next section over a six month campaign running from March 2007 through to August 2007. Irradiance data was obtained using the spectrometer at three different depths in each water type to create a depth profile. Linear regression techniques were applied to these profiles respectively in order to determine approximate K_d values. Direct linear comparisons between the irradiances measured by the spectrometer and the IL1400 radiometer in all four particular water types all displayed satisfactory R^2 values of between 0.87 and 0.98.

Column ozone levels above Toowoomba were monitored by accessing OMI satellite information (http://jwocky.gsfc.nasa.gov/ozone/ozone_v8.html) each day over the duration of the calibration campaign. This data was used in order to deduce if ozone variations had any influence upon the calibration data from season to season. Fig. 2 shows a time series of the ozone levels measured by the OMI satellite from March to August 2007 above Toowoomba. Aerosol levels were not analysed as Toowoomba is a high-altitude location with an atmosphere that is relatively low in aerosol concentrations.

2.3. Immersion effect

To ensure the highest levels of accuracy, the IL1400 radiometer was calibrated for underwater use against a standardised immersion effect corrected spectrometer (StellarNet EPP2000 C-UV-VIS, Tampa, Florida). The immersion effect comes into play when an optical meter is submerged underwater to take a light measurement. A larger amount of light is backscattered out of the meter during a water-based measurement in comparison to an air-based measurement. This is due to the discrepancies between the refractive indices for air and water at the collector interface. The methodology employed to calculate these immersion factors was based upon the work of Zibordi [23], Hooker and Zibordi [24] and Zibordi et al. [25].

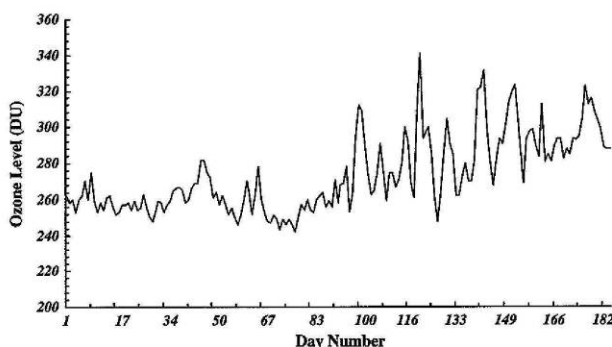


Fig. 2. Time series of OMI measured column ozone levels present over Toowoomba from March 2007 to August 2007 where day 1 is 1 March 2007.

2.4. Water tank description

The water tank used during the calibration campaign had a length of 66 cm, a width of 46 cm and a depth of 35 cm. The tank was made out of tinted plastic. This plastic is opaque to the UV waveband, so any UV wavelengths incident upon the sides of the tank during the calibrations would not have had any effect upon the submerged dosimeters. Any pieces of debris that landed in the tank were removed each day in order to keep the water as close to its natural state as possible. Also, at the end of each daily session, the tanks were sealed off using a lid in order to reduce evaporation and to ensure no debris fragments would fall into the water overnight.

3. Results

3.1. Water type spectrophotometry

Fig. 1 presents the transmission and absorption spectra over the 300–320 nm waveband for the four water types analysed in this research. It can be seen that the clear, creek and sea water all share similar transmission and absorption spectra, within approximately ±5% of each other in transmission and within ±0.03 arbitrary units of each other in absorption. However, the dam water displayed transmission and absorption spectra far different to the other three water types. The transmission spectrum for the dam water recorded a relatively low transmission value of 61% at 310 nm in comparison to 75% at 310 nm for creek water, 76% at 310 nm for sea water and 79% at 310 nm for clear water. In turn, the absorption spectrum for the dam water recorded a high level of approximately 0.22 at 310 nm. This is compared to 0.13 at 310 nm for the creek water, 0.12 at 310 nm for the sea water and 0.10 at 310 nm for the clear water.

3.2. Immersion effect

The immersion factors calculated for the spectrometer can be seen in Fig. 3. It is clear from this graph that the immersion factor remains relatively static across the 300–320 nm waveband. There is a slight fluctuation in the immersion factor value from 300 to 305 nm. This can be attributed to the lower response of the spectrometer at in this region.

3.3. Dose response calibrations

Figs. 4 and 6 display the in-air and underwater PPO dosimeter calibrations for each water type as measured at Z_{1CM} in autumn and winter respectively with the cumulative UVB exposures as measured by the IL1400 broadband meter. Figs. 5 and 7 displays the in-air and underwater PPO dosimeter calibrations for each water type as measured at Z_{20CM} in autumn and winter respectively with the cumulative UVB exposure derived from the Beer–Lambert–Bouguer relation. A second-order polynomial equation normalised to zero (as no change in optical absorbance represents no exposure time) was employed to model each particular calibration data set in the following form:

$$UVB_z = -\alpha(\Delta A_{320})^2 + \beta(\Delta A_{320})$$

where UVB_z is the UVB exposure received at the depth z in units of kJ m^{-2} . Table 1 displays the different α , β and R^2 values obtained for each particular calibration.

In Figs. 4–7, the x -axis error bars for each data point in the underwater calibrations represent an uncertainty margin of ±9%, which was the calculated in-water dosimeter variation for PPO as found by Schouten et al. [15]. The x -axis error bars on the data points for the in-air calibration series represent a calculated error margin of approximately ±7%, which was the estimated average

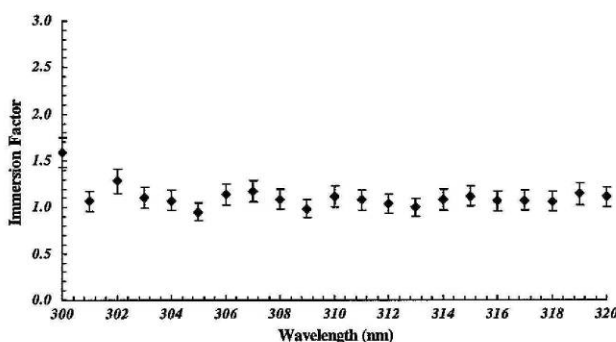


Fig. 3. Immersion effect coefficients across the modified UVB waveband as measured for the StellarNet EPP2000 spectrometer in a controlled environment.

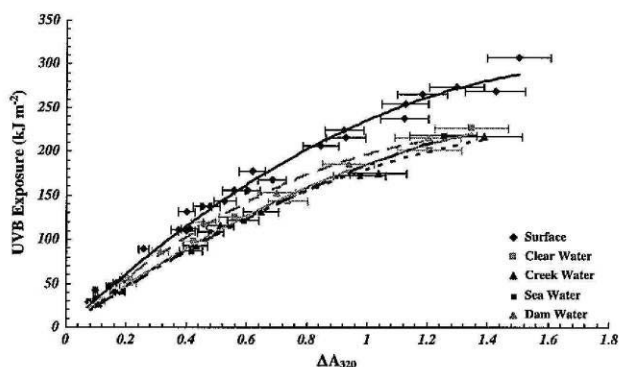


Fig. 4. Calibration curves as made against the solar UVB exposures over autumn for tap water, creek water, sea water and water taken from a stagnant water reserve at Z_{1CM} . The surface (in-air) calibration curve acts as the control.

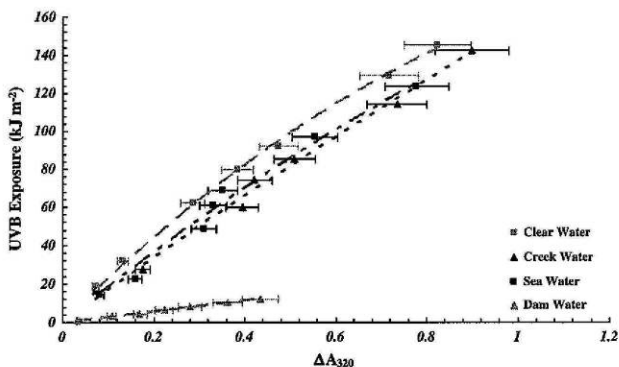


Fig. 5. Calibration curves as made against the solar UVB exposures over autumn for tap water, creek water, sea water and water taken from a stagnant water reserve at Z_{20CM} .

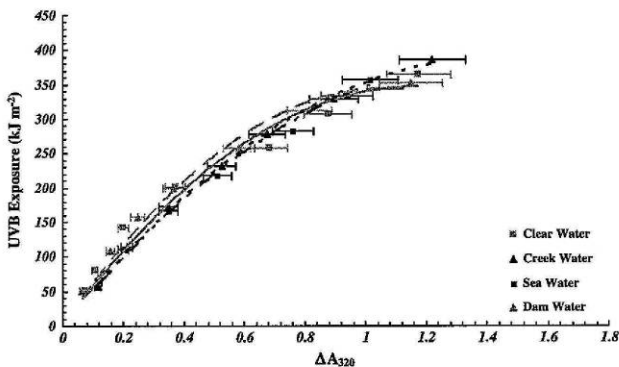


Fig. 6. Calibration curves as made against the solar UVB exposures over winter for tap water, creek water, sea water and water taken from a stagnant water reserve at Z_{1CM} .

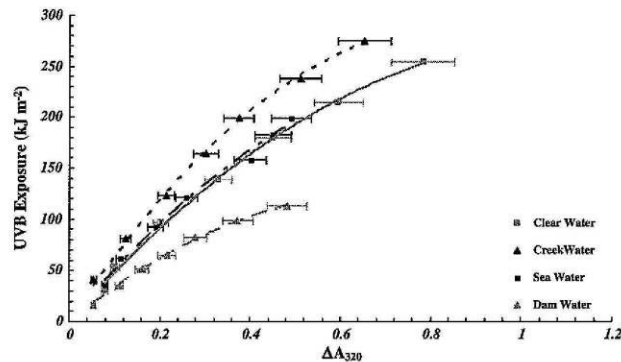


Fig. 7. Calibration curves as made against the solar UVB exposures over winter for tap water, creek water, sea water and water taken from a stagnant water reserve at Z_{20CM} .

Table 1
 α , β and R^2 values obtained for each particular calibration over autumn and winter

Calibration type	α	β	R^2
Control	86.78	322.39	0.99
Clear water autumn Z_{1CM}	63.77	249.68	0.99
Creek water autumn Z_{1CM}	68.6	248.9	0.99
Sea water autumn Z_{1CM}	52.48	236.93	0.99
Dam water autumn Z_{1CM}	99.21	296.12	0.99
Clear water autumn Z_{20CM}	73.37	235.11	0.99
Creek water autumn Z_{20CM}	15.28	171.35	0.99
Sea water autumn Z_{20CM}	37.56	190.74	0.98
Dam water autumn Z_{20CM}	2.64	29.93	0.99
Clear water winter Z_{1CM}	254.96	595.5	0.96
Creek water winter Z_{1CM}	188.96	542.93	0.99
Sea water winter Z_{1CM}	182.76	530.56	0.99
Dam water winter Z_{1CM}	299.31	643.08	0.98
Clear water winter Z_{20CM}	223.53	498.58	0.99
Creek water winter Z_{20CM}	379.98	666.83	0.99
Sea water winter Z_{20CM}	269.89	527.54	0.99
Dam water winter Z_{20CM}	251.78	357.77	0.99

interdosimeter variation found to exist across the batch of dosimeters used for the in-air calibration.

Fig. 8 displays the master calibration equations derived from the data measured over the autumn and winter months of 2007. The autumn underwater calibration data was merged together and compared to the combined winter underwater calibration data in order to see if SZA had any influence over calibration trends. The master calibration equations featured for autumn and winter do not include the calibration data obtained for the dam water at Z_{20CM} . As in Figs. 3–6, the x-axis error bars for each data point in the underwater calibrations shown an error of $\pm 9\%$, which was the calculated in-water dosimeter variation for PPO as determined by Schouten et al. [15]. A polynomial trend equation was applied to both the autumn and winter master calibration data sets. For autumn the equation took on the following form:

$$UVB = -43.422(\Delta A_{320})^2 + 221.8(\Delta A_{320})$$

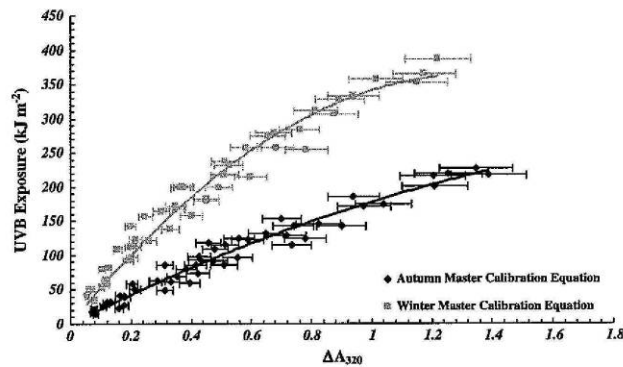


Fig. 8. Comparison between underwater master calibrations obtained over autumn and winter.

with an R^2 value of 0.96 where UVB is the UVB exposure received in units of kJ m^{-2} across the 300–320 nm waveband. For winter the following equation emerged:

$$\text{UVB} = -203.09(\Delta A_{320})^2 + 544.51(\Delta A_{320})$$

with an R^2 value of 0.97 where again UVB is the UVB exposure received in units of kJ m^{-2} across the 300–320 nm waveband.

4. Discussion

For each season, the calibrations obtained at a depth of approximately 1 cm in each water type were all measured to be in close proximity to each other, mostly within the 9% error estimated to exist for the dosimeters. Based on this result, it can be assumed that a single shallow calibration in clear water should be transferable to measurements made in different water types that have a percentage transmission in the range of 40–80% as encountered in the water types employed in this research. However these calibrations do differ to the calibration made in air with the difference becoming more pronounced with increasing cumulative exposure, reaching a discrepancy of as much as approximately 50 kJ at a ΔA_{320} value of 1.2. So it is not appropriate to apply an air based calibration equation to dosimetric measurements made underwater, without incurring substantial errors in the measured exposures.

Over autumn and winter, the calibrations measured at $Z_{20\text{CM}}$ in each water type were also all found to be in close proximity to each other, apart from the dam water calibration, which presented a regime completely different to the three other water types. From the spectrophotometry data shown in Fig. 1 it is clear to see that the dam water has the lowest level of UV transmission and in turn the highest amount of UV absorption across the 300–320 nm waveband when compared to the other three water types due to having a high concentration of DOM constituents. So it appears that calibrations made at deeper depths (lower than $Z_{1\text{CM}}$) are transferable from one water type to another, but only within a certain spectral transmission (or absorption) range. In this research it appears that this range is approximately $\pm 5\%$ UV transmission difference (or ± 0.03 UV absorption difference) between each water type for calibrations to be completely transferable with minimal error. Researchers would have to keep this in mind when calibrating dosimeters to measure exposures deeper than just below the water surface.

The direct comparison between the master calibration equations for autumn and winter show that there is a definite difference between the calibration regimes obtained over the autumn months when compared to those obtained in the winter months. This discrepancy between the calibration sets could be attributed not only to the change in the sun's position between the two seasons, but also to a progressive increase in column ozone levels over the measurement site. Fig. 8 displays this significant increase in column

ozone levels above Toowoomba that began in late autumn (May) and continued towards the end of winter (August). It is well known that the shorter UV wavelengths, especially those in the UVB are blocked by a much greater amount when there are increased levels of ozone present in the atmosphere. This has a direct effect on the UV spectrum present here on the Earth. The UVB spectra received by the dosimeters during the winter calibration campaign would have had a different cut-off point, and in turn, have had a different composition in comparison to the spectra received by the dosimeters during the autumn calibration campaign. Consequently, when calibrating the PPO film for underwater usage, researchers should obtain calibration data for the season in which they will be recording measurements. Similar results to this have been discovered by other researchers investigating the effect of fluctuations in column ozone upon the response of broadband UV meters. In particular, Bodhaine et. al. [26] found that if the influence of ozone is ignored during calibration, UV measurements made with broadband meters can produce errors of 10% or greater.

The total UVB energy received after the 25 h exposure period was measured to be approximately 200 kJ m^{-2} for each water type. This is significantly greater than the 40 kJ m^{-2} maximum reached by Dunne [12] when using polysulphone as an underwater dosimeter. Additionally, at the final measurement point, the PPO film dosimeters had yet to fully degrade and would be able to accept another substantial UVB dosage. This additional dosage is estimated to approximately another 200 kJ m^{-2} before complete optical saturation is achieved. These results show that the PPO dosimeter can be calibrated and employed to measure UVB exposures in aquatic environments under a variety of atmospheric conditions in a number of distinct water types.

Acknowledgements

The authors would like to thank both Graham Holmes and Oliver Kinder from the Faculty of Sciences, University of Southern Queensland for their technical assistance throughout this project.

References

- [1] P.C. Frost, J.H. Larson, L.E. Kinsman, G.A. Lamberti, S.D. Bridgman, *J. N. Am. Benthol. Soc.* 24 (2) (2005) 246–255.
- [2] L. Bracchini, S. Loiselte, A.M. Dattilo, S. Mazzuoli, A. Cozar, C. Rossi, *Photochem. Photobiol.* 80 (2004) 139–149.
- [3] D. Conde, L. Aubriot, R. Sommaruga, *Mar. Ecol. Prog. Ser.* 207 (2000) 19–31.
- [4] D. Crump, D. Lean, M. Berrill, D. Coulson, L. Toy, *Photochem. Photobiol.* 70 (6) (1999) 893–901.
- [5] W.F. Vincent, R. Rae, I. Laurion, C. Howard-Williams, J.C. Priscu, *Limnol. Oceanogr.* 43 (4) (1998) 618–624.
- [6] R. Sommaruga, R. Psenner, *Photochem. Photobiol.* 65 (6) (1997) 957–963.
- [7] P. Belmont, B.R. Hargreaves, D.P. Morris, C.E. Williamson, *Photochem. Photobiol.* 83 (2007) 1339–1347.

- [8] J.D. Regan, W.L. Carrier, H. Gucinski, B.L. Olla, H. Yoshida, R.K. Fujimura, R.I. Wicklund, *Photochem. Photobiol.* 56 (1992) 35–42.
- [9] P. Boelen, I. Obernosterer, A.A. Vink, A.G.J. Buma, *Photochem. Photobiol.* 69 (1) (1999) 34–40.
- [10] A. Koussoulaki, D.B. Daniefidis, D.P. Häder, R. Santas, *Internet J. Sci. Biol. Chem.* (1998). <<http://www.photobiology.com/v1/santas3/euglen.htm>>.
- [11] S. Li, M. Paulsson, L.O. Bjorn, *J. Photochem. Photobiol. B* 66 (2002) 67–72.
- [12] R.P. Dunne, *Mar. Ecol. Prog. Ser.* 189 (1999) 53–63.
- [13] P.C. Frost, A. Mack, J.H. Larson, S.D. Bridgham, G.A. Lamberti, *Photochem. Photobiol.* 82 (3) (2006) 781–786.
- [14] E.M. Fleischmann, *Limnol. Oceanogr.* 34 (8) (1989) 1623–1629.
- [15] P. Schouten, A. Parisi, D.J. Turnbull, *Photochem. Photobiol.* 83 (4) (2007) 931–937.
- [16] R.A. Lester, A.V. Parisi, M.G. Kimlin, J. Samburg, *Phys. Med. Biol.* 48 (2003) 3685–3698.
- [17] M. Tedetti, R. Sempéré, *Photochem. Photobiol.* 82 (2) (2005) 389–397.
- [18] D.R. Mishra, S. Narumalani, D. Rundquist, M. Lawson, *ISPRS J. Photogramm.* 60 (2005) 48–64.
- [19] C.D. Mobley, *Light and Water: Radiative Transfer in Natural Waters*, Academic Press, San Diego, 1994.
- [20] D.P. Morris, H. Zagarese, C.E. Williamson, E.G. Balseiro, B.R. Hargreaves, B. Modenutti, R. Moller, C. Quimalinos, *Limnol. Oceanogr.* 40 (8) (1995) 1381–1391.
- [21] J.T. O Kirk, *Light and Photosynthesis in Aquatic Ecosystems*, Cambridge University Press, Cambridge, 1994.
- [22] C.S. Kinkade, J. Marra, T.D. Dickey, R. Weller, *Deep-Sea Res. II* 48 (2001) 1285–1301.
- [23] G. Zibordi, *J. Atmos. Ocean. Technol.* 23 (2005) 302–313.
- [24] S.B. Hooker, G. Zibordi, *J. Atmos. Ocean. Technol.* 22 (2005) 757–770.
- [25] G. Zibordi, S.B. Hooker, J. Mueller, G. Lazin, *J. Atmos. Ocean. Technol.* 21 (2004) 501–514.
- [26] B.A. Bodhaine, E.G. Dutton, R.L. McKenzie, P.V. Johnston, *J. Atmos. Ocean. Technol.* 15 (1998) 916–926.

Utilising polyphenylene oxide for high exposure solar UVA dosimetry

D. J. Turnbull and P. W. Schouten

Faculty of Sciences, University of Southern Queensland, Toowoomba, 4350, Australia

Received: 26 November 2007 – Published in Atmos. Chem. Phys. Discuss.: 6 February 2008

Revised: 24 April 2008 – Accepted: 8 May 2008 – Published: 23 May 2008

Abstract. A personal UV dosimeter that can quantitatively assess high exposure solar UVA exposures has been developed. The chemical polyphenylene oxide has been previously reported on its ability to measure high UVB exposures. This current research has found that polyphenylene oxide, cast in thin film form, is responsive to both the UVA and UVB parts of the solar spectrum. Further to this, the UVB wavelengths were filtered out with the use of mylar. This combined system responded to the UVA wavelengths only and underwent a change in optical absorbance as a result of UVA exposure. Preliminary results indicate that this UVA dosimeter saturates steadily when exposed to sunlight and can measure exposures of more than 20 MJ/m² of solar UVA radiation with an uncertainty level of no more than ±5%.

1 Introduction

Exposure to UV radiation is known to be a causative factor in the induction of skin cancers and other sun-related disorders. Most acute responses of humans to UV exposure occur as a result of UVB (280 to 315 nm) exposures, as these wavelengths are highly effective in creating a human biological response. However, this does not mean that UVA radiation has no impact on human UV exposures and health. UVA can cause erythema in human skin, yet, the exposures required to create such a response is much larger than UVB radiation. UVA radiation penetrates much deeper into human skin tissue than UVB, resulting in impacts that are not as acute, taking many years to manifest. Past research has shown that UVA (315 to 400 nm) plays a significant role in human skin carcinogenesis, immune suppression, DNA damage, photoageing and wrinkling (Agar et al., 2004; Moan et

al., 1999; Garland et al., 2003). Skin cancer is considered the most common malignant neoplasm in Australia and the USA (Krieger and Armstrong, 1996; Glanz and Mayer, 2005; NCI, 2006). Over 1600 Australians die from skin cancer each year and a further 380 000 Australians are treated for skin cancer each year (NCCI, 2003; AIHW, 2004; AIHW, 2005). Skin cancer is Australia's most expensive cancer with estimated amounts of \$264 million and \$30 million spent in Australia during 2001 on NMSC and melanoma respectively (AIHW, 2005). As a result, it is essential to decrease the amount of exposure to damaging solar UV radiation that the population experiences. This requires methods to understand the solar UV radiation environment that humans live in. Spectroradiometers, broadband meters and dosimeters are often utilised for the measurement of incident solar UV radiation. Quantification of the individual level of solar UV radiation exposure requires personal dosimetry due to changes in the position of people compared to the radiation source. Dosimetry is very useful as researchers can leave the dosimeters in situ for extended periods of time to monitor long term UV trends. However, dosimeters need to be calibrated against a spectroradiometer or broadband meter. On the other hand, spectroradiometers and broadband meters are more useful for analysing the effect of changing atmospheric variables (e.g. clouds, aerosols and ozone) upon UV dosages.

Commonly used UV chemical dosimeters are polysulphone and phenothiazine. Phenothiazine has been used for measuring UVA wavelengths in various environments (Parisi et al., 2005). However, phenothiazine only has the capability to record a cumulative exposure over a small time period, usually three to four hours. This small dynamic range greatly reduces the amount of time over which a UVA exposure can be measured in the field. Therefore, a chemical dosimeter that is capable of measuring large amounts of UVA radiation over a long time period would be very useful. Research conducted by Davis et al. (1976) showed that Poly (2,6-dimethyl-1, 4-phenylene oxide) (PPO) film could



Correspondence to: D. J. Turnbull
(turnbull@usq.edu.au)

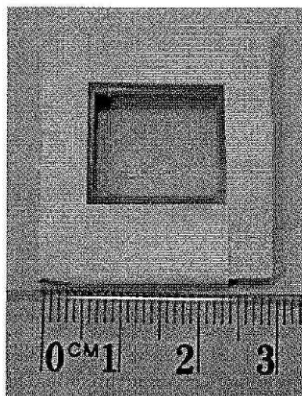


Fig. 1. A sample PPO dosimeter with the mylar film attachment.

be employed to measure high levels of UV exposure. Further research found PPO to be ideal for this purpose as it would allow for unattended UVB measurements to be made at various locations over a time period of at least one week with high levels of accuracy when compared against radiometric measurements (Davis et al., 1981; Berre and Lala, 1989; Lester et al., 2003). Schouten et al. (2007) found that PPO has a progressively increasing response to UVA wavelengths over time. PPO dosimeters have been utilised in the measurement of global UVB and erythral exposures, however, they have not been used to measure solar UVA exposures. The aim of this paper was to extend the previous research that has employed PPO dosimeters for the measurement of solar UVB and erythral exposures to investigate the suitability of PPO for the measurement of high exposure solar UVA irradiances.

2 Materials and methods

2.1 PPO

PPO film of approximately $40\ \mu\text{m}$ thickness was attached with adhesive tape to a plastic holder. The holders for the dosimeters were $3\times 3\ \text{cm}$ in area and fabricated from thin polyvinylchloride with an aperture of approximately $1.2\times 1.6\ \text{cm}$ (Fig. 1). A UV/visible spectrophotometer (model 1601, Shimadzu Co., Kyoto, Japan) was used to measure the pre and post exposure absorbance of the dosimeter. The uncertainty range for optical absorbance measurements in the spectrophotometer has been stated as ± 0.002 by the manufacturer. PPO is responsive to both the UVA and UVB part of the solar spectrum, therefore the UVB wavelengths were filtered by placing $120\ \mu\text{m}$ thick mylar film (Cadillac Plastics, Australia) on top of the PPO film. For each dosime-

ter, the change in optical absorbance (ΔA_{320}) due to UV exposure was measured at $320\ \text{nm}$ (with mylar removed) at four different sites over the dosimeter in order to minimise any errors due to any possible minor variations in the PPO film over the size of the dosimeter. The change in optical absorbance was measured at $320\ \text{nm}$ as previous studies have shown that this is the wavelength where the greatest overall UV energy induced change occurs (Lester et al., 2003; Schouten et al., 2007). The post exposure absorbance was measured at a standardized time following exposure to minimize any error associated with the post exposure "dark reaction" of the PPO (Lester et al., 2003; Schouten et al., 2007). Lester et al. (2003) has shown previously that the PPO dosimeter is not a temperature dependent system, so fluctuations in temperature over the exposure time period will not have any influence upon the subsequent measurement error.

2.2 Calibration

The dosimeters were calibrated for UVA exposures by exposing a series of dosimeters on a horizontal plane, to relatively clear sky solar UV from approximately 08:00 to 16:00 h Australian Eastern Standard Time (EST) for a total of 22 days. One dosimeter was removed from solar exposure at regular periods of time ranging from one to two days with the last dosimeter being removed after 22 days. The dosimeters were brought in at the end of each day to ensure that they did not receive any overnight damage. These calibrations ran over the months of April and May at a subtropical Southern Hemisphere site at the University of Southern Queensland, Toowoomba, Australia ($27.6^\circ\ \text{S}$, $151.9^\circ\ \text{E}$, altitude $693\ \text{m}$). The solar zenith angle (SZA) ranged from 30° to 75° . The PPO dosimeters were calibrated on a horizontal plane with a UVA meter (501 UVA Biometer, Solar Light Co., Philadelphia, USA). The UVA meter was calibrated against a scanning spectroradiometer (Bentham Instruments, Ltd, Reading, UK). The spectroradiometer is based on a double grating monochromator, a UV sensitive detector and amplifier with software variable gain provided by a programmable high voltage power supply. The container in which the spectroradiometer is housed is temperature stabilised with a Peltier system and the temperature set to 25°C . The temperature inside the container at each scan is recorded by the software. For the times that the temperature inside the container housing the spectroradiometer varied by more than 1°C from the set temperature due to hot ambient temperatures, the manufacturer supplied temperature correction factor of $-0.4\%/^\circ\text{C}$ was applied in the post processing to the spectral irradiance data collected at each $0.5\ \text{nm}$ increment. This correction was the same at all wavelengths. The wavelength shift of the instrument due to temperature as provided by the manufacturer is $0.005\ \text{nm}/^\circ\text{C}$. Consequently, any wavelength shift was minimal and no correction for wavelength shift has been applied. The input optics of the spectroradiometer are provided by a PTFE (polytetrafluoro ethylene)

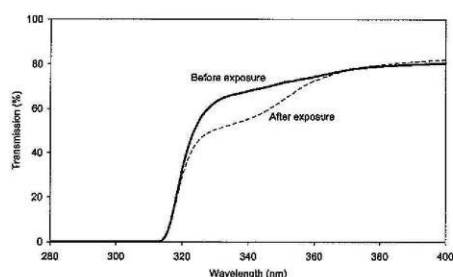


Fig. 2. The spectral transmission of mylar film before and after a total solar UVA exposure of 20 MJ/m^2 .

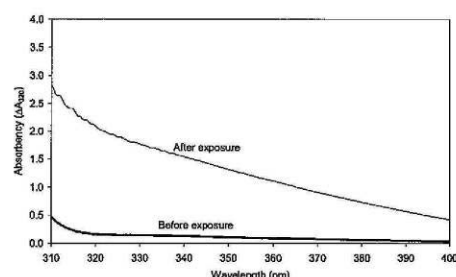


Fig. 3. The absorption spectrum of PPO before and after a total solar UVA exposure of 20 MJ/m^2 .

diffuser and connected by an optical fibre to the input slit of the monochromator. The spectroradiometer is programmed to start scanning the global UV spectrum from 280 to 400 nm in 0.5 nm increments from dawn, and thereafter every 10 min till dusk. The instrument is wavelength calibrated to the UV spectral lines of a mercury lamp and irradiance calibrated to a 150 Watt quartz tungsten halogen lamp with calibration traceable to the National Physical Laboratory, UK standard.

To produce the calibration curve, the UVA exposure (MJ/m^2) was measured over specific intervals with the UVA meter. This measurement was then calibrated to the scanning spectroradiometer by employing a transfer equation with a calculated R^2 value of no less than 0.99. After each interval, the ΔA_{320} for a single PPO dosimeter was measured by the spectrophotometer to provide a single data point, where ΔA_{320} was calculated by the following

$$\Delta A_{320} = A_{320}^{\text{FINAL}} - A_{320}^{\text{INITIAL}} \quad (1)$$

where A_{320}^{FINAL} is the final optical absorbance measurement after exposure taken at 320 nm and A_{320}^{INITIAL} is the initial absorbance measurement before exposure taken at 320 nm. After the absorbency was measured, the dosimeter was then removed from the batch.

2.3 Reproducibility

To test the reproducibility of the dosimeters for the measurement of solar UVA, ten dosimeters (with mylar filter) were exposed simultaneously to solar UV over a three hour period on a horizontal plane. These exposures were conducted on an unshaded sports oval in autumn under clear sky conditions to ensure that the dosimeters were exposed to all of the incident solar UV radiation, both direct and diffuse radiation from the sky.

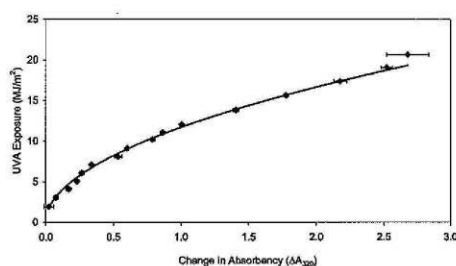


Fig. 4. Calibration curve of PPO for UVA exposures. The error bars represent the standard deviation in each series of absorbency measurements.

3 Results

3.1 Filtered exposures

The spectral transmission of the mylar film was measured pre-exposure and post-exposure to solar UV to test for any significant changes. The change in spectral transmission of the mylar film is provided in Fig. 2. The maximum change was approximately 13% from 331 to 337 nm. The change in absorbency of the PPO film pre- and post-exposure is provided in Fig. 3.

3.2 Calibration

The calibration of the PPO dosimeters for solar UVA exposure is shown in Fig. 4. The data points are the averages of the four ΔA 's measured for each dosimeter and the error bars on the x-axis values are the standard deviation of the four measurements. A power law was fitted to the calibration data with the form of:

$$\text{UVA} = 11.7(x^{0.51}) \text{ MJ/m}^2 \quad (2)$$

where x is the change in absorbency. The resulting R^2 for the calibration was greater than 0.99.

3.3 Reproducibility

For the reproducibility tests, all dosimeters received the same exposure of solar UV producing a mean ΔA_{320} of 0.598 with a standard deviation of no more than 3% and a coefficient of variation equal to approximately 5%. This variation may be due to minor variations over the surface of the sheet of PPO film, from which the dosimeters were fabricated, that are inherent in the casting process and are difficult to eliminate. Variation can also be influenced by dust particles that may have accumulated on the surface of the dosimeters during the exposure period.

4 Discussion

PPO film has never before been used to measure solar UVA exposures, however, preliminary results indicate that this UVA dosimeter saturates reasonably slowly when exposed to sunlight and can measure exposures of more than 20 MJ/m² of solar UVA radiation with an uncertainty level of no more than $\pm 5\%$. For the Toowoomba measurement site, this equates to approximately two weeks of full day UVA exposures under clear sky conditions. This exposure period will be extended for higher latitude sites and also for varying atmospheric conditions.

The size and lightweight properties of the dosimeter means that it can be attached to any anatomical site on the human body in different environments such as underneath shade or in a vehicle in order to measure the solar UVA exposures with a level of ease, simplicity and cost-effectiveness not associated with counterpart radiometric measurements. The usage of the dosimeter requires the calibration against a calibrated UVA meter. The profile of the calibration curve will vary with the season and this can be overcome by calibrating the dosimeter in the season that it will be employed to measure the solar UVA exposures. Schouten et al. (2008) found that when the PPO dosimeter is calibrated to UVB wavelengths over different seasons there was a slight but definite variation between calibration profiles. However, when PPO is calibrated to UVA wavelengths this variation will be significantly reduced due to the fact that UVA wavelengths are not affected by atmospheric parameters to the extent that UVB wavelengths are.

Acknowledgements. This research was supported by a Project Grant awarded by the Cancer Council Queensland.

Edited by: M. Blumthaler

Atmos. Chem. Phys., 8, 2759–2762, 2008

References

- Agar, N. S., Halliday, G. M., Barnetson, R. S., Ananthaswamy, H. N., Wheeler, M., and Jones, A. M.: The basal layer in human squamous tumors harbors more UVA than UVB fingerprint mutations: a role for UVA in human skin carcinogenesis, *Proc. Nat. Acad. Sci.*, 101, 4954–4959, 2004.
- AIHW (Australian Institute of Health and Welfare) & Australasian Association of Cancer Registries (AACR): Cancer in Australia 2001, Cancer Series Number 28, Canberra, AIHW, 2004.
- AIHW (Australian Institute of Health and Welfare): Health system expenditures on cancer and other neoplasms in Australia, 2000–01, Health and Welfare Expenditure Series Number 22, Canberra, AIHW, 2005.
- Berre, B. and Lala, D.: Investigation on photochemical dosimeters for ultraviolet radiation, *Sol. Ener.*, 42, 405–416, 1989.
- Davis, A., Deane, G. W. H., Gordon, D., Howell, G. V., and Ledbury, K. J.: A world-wide program for the continuous monitoring of solar UV radiation using poly (phenylene oxide) film, and consideration of the results, *J. Appl. Polym. Sci.*, 20, 1165–1174, 1976.
- Davis, A., Diffey, B. L., and Tate, B. K.: A personal dosimeter for biologically effective solar UV-B radiation, *Photochem. Photobiol.*, 34, 283–286, 1981.
- Garland, C. F., Garland, F. C., and Gorham, E. D.: Epidemiologic evidence for different roles of ultraviolet A and B radiation in melanoma mortality rates, *Ann. Epidemiol.*, 13, 395–404, 2003.
- Glanz, K. and Mayer, J. A.: Reducing ultraviolet radiation exposure to prevent skin cancer, *Am. J. Prev. Med.*, 29, 131–142, 2005.
- Krieger, A. and Armstrong, B.: International trends in skin cancer, *Can. Forum*, 20, 192–194, 1996.
- Lester, R. A., Parisi, A. V., Kimlin, M. G., and Sabburg, J.: Optical properties of poly(2,6-dimethyl-1,4-phenylene oxide) film and its potential for a long term solar ultraviolet dosimeter, *Phys. Med. Biol.*, 48, 3685–3698, 2003.
- Moan, J., Dahlback, A., and Setlow, R. B.: Epidemiological support for an hypothesis for melanoma induction indicating a role for UVA radiation, *Photochem. Photobiol.*, 70, 243–247, 1999.
- NCCI (National Cancer Control Initiative): The 2002 national non-melanoma skin cancer survey, A report by the NCCI Non-melanoma Skin Cancer Working Group, edited by: Staples, M. P., Melbourne, NCCI, 2003.
- NCI (National Cancer Institute): <http://www.cancer.gov/cancertopics/commoncancers>, accessed 15 December 2006.
- Parisi, A. V., Kimlin, M. G., Turnbull, D. J., and Macaranas, J.: Potential of phenothiazine as a thin film dosimeter for UV-A exposures, *Photochem. Photobiol. Sci.*, 4, 907–910, 2005.
- Schouten, P. W., Parisi, A. V., and Turnbull, D. J.: Evaluation of a high exposure solar UV dosimeter for underwater use, *Photochem. Photobiol.*, 83, 1–7, 2007.
- Schouten, P. W., Parisi, A. V., and Turnbull, D. J.: Field calibrations of a long term UV dosimeter for aquatic UVB exposures, *J. Photochem. Photobiol. B Biol.*, doi:10.1016/j.jphotobiol.2008.02.004, in press, 2008.

www.atmos-chem-phys.net/8/2759/2008/

Paper 4: Schouten, P.W., Parisi, A.V. & Turnbull, D.J. 2009, 'Applicability of the Polyphenylene Oxide Film Dosimeter to High UV Exposures in Aquatic Environments,' *Journal of Photochemistry and Photobiology B: Biology*, Accepted for publication.

**Applicability of the Polyphenylene Oxide Film Dosimeter to High UV
Exposures in Aquatic Environments**

P W Schouten ^{a*}, A V Parisi ^{a,b} & D J Turnbull ^{a,b}

^a Department of Biological and Physical Sciences, Faculty of Sciences, University of Southern Queensland, Toowoomba, Australia 4350.

^b Centre for Rural and Remote Area Health, Faculty of Sciences, University of Southern Queensland, Toowoomba, Australia 4350.

Keywords: Solar UV, Ultraviolet, Underwater, Aquatic, Marine, Field, Dosimeter, Badge, Film

*To whom correspondence should be addressed at: schouten@usq.edu.au

ABSTRACT

Previous research has proven that the Poly (2,6-dimethyl-1, 4-phenylene oxide) (PPO) dosimeter is capable of receiving both in-air and underwater UV exposures that are significantly greater than those of the more commonly used polysulphone dosimeter, within a range of accuracy close to what would be expected of dosimetric measurements made in-air provided that the necessary calibrations are completed correctly by factoring in different atmospheric column ozone levels, SZA ranges, varying water turbidity and DOM levels. However, there is yet to be an investigation detailing the performance of the PPO dosimeter and its ability to measure UV in an actual field environment over an extended period of time. This research aims to bridge this gap in the knowledge by presenting a measurement campaign carried out in two real world aquatic environments and a simulated sea water environment using a batch of PPO dosimeters set at different depths and aligned to a range of different angles and geographical directions by means of attachment to a custom built dosimeter submersible float (DSF) unit over the space of a year at a sub-tropical location. Results obtained from this measurement campaign were used to compute a K_d value for the sea water in each particular season. These K_d values were found to be in close agreement to standalone K_d values derived from results taken using a standard calibrated spectrometer in the same sea water.

INTRODUCTION

The current global warming trend in unison with recent fluctuations in atmospheric column ozone levels have resulted in changes occurring to the penetrative ability and distribution of the solar ultraviolet (UV) (280 to 400 nm) light field as measured in underwater locations such as in lakes, creeks, dams and the ocean. The solar UV, in particular the ultraviolet-B (UVB) (280 to 320 nm), has been shown by a vast number of studies to have a significantly detrimental effect on many different types of underwater life, ranging from the big to the small, each having their own special niche within the delicate marine ecosystem, which has direct consequences to our own life here on Earth [1, 2, 3, 4, 5]. Therefore, it is of utmost importance that the attributes of the underwater UV are measured and documented in order to enhance our understanding of its widespread influence upon the aquatic world.

The influence of solar UV radiation upon aquatic ecosystems is presently a highly investigated topic [6]. It is a well known fact that solar UV, in both its ultraviolet-A (UVA) (320 to 400 nm) and UVB components, does have a detrimental impact upon marine organisms. Following varying levels of solar UV exposure, reduced rates in reproduction, growth and development and a higher amount of mutations have been seen to occur in species such as phytoplankton, zooplankton, fish eggs and larvae, and also macroalgae [7].

Increases in the amount of incoming solar UV into a marine ecosystem, such as those caused by decreases on atmospheric ozone levels for instance, can lead to decreases in biomass productivity, which affect each level of the food chain, working all the way to the top with reduced food production available for human consumption [8]. In

addition to this, there would be a noticeable reduction in the global sink capacity for carbon dioxide alongside wide scale changes in marine species composition [8, 9].

So there is a definite need for the continual measurement and monitoring of solar UV in a wide variety of underwater environments in order to further quantify and predict the damaging influence solar UV has upon the fragile aquatic life cycle. For underwater UV measurements, UV dosimeters have often been overlooked as a measurement tool by researchers, with most investigations employing spectroradiometers, spectrometers or radiometers to do the bulk of the work. These instruments have been highly useful for taking underwater measurements of the UV sporadically over a short time frame. However, over long periods of time these spectroradiometers and radiometers become harder to employ, with sizeable amounts of time and effort needed to accurately calibrate and maintain them.

There are several recent examples of underwater UV measurement work using spectroradiometers, spectrometers or radiometers in numerous types of water bodies located across the world. Hanelt et al. [10] used a spectroradiometer system with a custom diffuser housing to measure UVB radiation distributions in an arctic fjord. Dring et al. [11] used an underwater light sensor to make daily UV measurements in the Helgoland region of the North Sea over a time period of six years. Frenette et al. [12] measured the depth profiles of both UV and photosynthetically active radiation (PAR) in Lake Saint Pierre, Quebec with a spectroradiometer. Reinhart et al. [13] also employed a spectroradiometer to measure both spectral UV and PAR at set depth increments in order to estimate various optical properties of Lake Verevi, Estonia. Also, again with the use of a spectroradiometer, Schubert et al. [14] investigated

variations in UV and PAR spectral irradiance levels in a shallow estuary on the southern coastline of the Baltic Sea. In comparison to this there have been only a few underwater investigations made with UV dosimeters.

Polysulphone has been deployed previously in underwater locales in the field in two different studies. The first was carried out by Dunne [15], where UVB radiation was measured using polysulphone dosimeters in seawater at tropical latitudes. The author discovered that the polysulphone dosimeters could obtain a UVB response within a 5% error threshold over a depth range of between 2.2 and 7.0 m, depending upon the turbidity of the seawater. Only small exposures of between 1.5 to 40.0 kJ m⁻² could be measured during deployment time. The second most recent study was completed by Frost et al. [16] who successfully used polysulphone to estimate attenuation coefficients in shaded water bodies in the North-east region of the United States.

Although these studies were successful in measuring underwater solar UVB, polysulphone is still restricted by the fact that it only has a limited dynamic range in comparison to Poly (2,6-dimethyl-1, 4-phenylene oxide) (PPO) film. This difference in dynamic range has been shown to be many times greater than polysulphone at sub-tropical latitudes [17]. This allows the PPO dosimeter to stay in use in the field for a much longer period of time when compared to polysulphone. Even though it has a much greater dynamic range, the PPO dosimeter has similar optical and physical characteristics to the polysulphone dosimeter. It has no temperature dependence, a relatively minimal dark reaction effect, a good cosine response, in-air variation of less than $\pm 10\%$ and like the polysulphone dosimeter it possesses a response spectrum that closely resembles the erythemal action spectrum [17]. Previous investigations have

shown that the PPO film dosimeter can be used to measure in-air personal UV exposures on humans over extended time intervals [18, 19, 20]. Following up on this work, PPO film dosimeters have been tested for use underwater in two recent studies carried out in controlled environments [21, 22].

Results have been presented describing general optical properties of the PPO dosimeter when submerged in clean tap water in an indoors laboratory environment [21]. The properties that were analysed in this study included UVB dose-response depth profiling, cosine response, interdosimeter variation, dose rate independence, UVA and visible wavelength responsivity, water marking effect with temperature dependence and exposure additivity. From this work it was found that PPO could be used as a viable underwater dosimeter as long as strict calibration and error correction procedures were implemented.

Following this, the calibration methodology necessary to produce accurate UVB measurements with the PPO dosimeter outdoors in the field was investigated in four different varieties of water each having their own characteristic spectral transmission and absorption characteristics [22]. This research discovered that calibrations for the PPO dosimeter can be transferred from one water type to another at any depth, as long as the water types under analysis had similar overall spectral transmission and absorption properties. It was also found that calibrations measured for the PPO dosimeter in air could not be employed for use in the underwater environment. In addition, it was shown that the PPO film could be exposed to seven to eight times as much solar UV in comparison to polysulphone before the beginning of optical saturation when underwater. This investigation along with the outcomes provided by

Casale et al. [23] also showed that UV measurements obtained from chemical film dosimeters are susceptible to fluctuations in atmospheric ozone and also to seasonal changes in the solar zenith angle (SZA) and that this must be taken into account before beginning a series of measurements in the field.

Unlike polysulphone, the PPO dosimeter has yet to be tested in real world underwater environments. Therefore, the objective of this investigation was to deploy PPO dosimeters using a novel dosimeter submersible float (DSF) apparatus in three distinct underwater locales, each with their own particular characteristic constituents. These locales being a moderately turbid creek located within the confines of a public garden, an abandoned agricultural engineering dam site holding extremely turbid stagnant water and a large rust proofed water tank filled with clean sea water sourced from a coastal location. From this the applicability of PPO dosimeters to measure high UVB exposures at a range of different depths, alignments and geographical directions in these aquatic environments was evaluated. This was undertaken in each season throughout a single year and the data obtained was employed to calculate attenuation coefficients (K_d) for each water type. As a final test, these dosimetric K_d values were directly compared to K_d values calculated using a standard calibrated spectrometer.

MATERIALS AND METHODS

PPO Dosimeter Calibration and Immersion Effect Corrections

The fabrication, preparation and measurement technique for the PPO dosimeter has been previously described in Lester et al. and Schouten et al. [20, 21, 22]. To ensure maximum accuracy, the PPO dosimeters used in this research were calibrated over the waveband running from 298 nm to 320 nm for both in-air and underwater use against

an immersion effect corrected EPP2000 spectrometer (StellarNet EPP2000 C-UV-VIS, Tampa, Florida). Calibrations were performed over each season at the University of Southern Queensland Toowoomba campus, Australia ($27^{\circ} 33' S$, $151^{\circ} 57' E$, 691 m elevation) for each water type under analysis in this research from early 2007 through to early 2008 in order to factor in every possible SZA and a range of varying atmospheric parameters. The lower limit of 298 nm was chosen as it was the cut-off wavelength at which the EPP2000 spectrometer could obtain reliable underwater data. The upper limit of 320 nm was chosen as it has been used by photobiologists to denote the end of the UVB waveband and is more applicable to this research. The immersion effect is known to occur whenever any optical meter is submerged underwater to take a light measurement. A larger amount of electromagnetic radiation is backscattered out of the meter during a water-based measurement in comparison to an air-based measurement. This is due to the discrepancies between the refractive indices for air and water at the collector interface. The methodology employed to calculate immersion factors for optical instrumentation has been detailed in previous studies [24, 25, 26] with the actual immersion factors for the EPP2000 spectrometer provided in [22].

Dosimeter Submersible Float Specifications

The DSF employed for the field measurement campaign was fabricated by combining an aluminium frame and a PVC ballast cylinder with a total height of 64 cm, a width of 26 cm and a cross-sectional length of 67 cm. The PVC ballast cylinder had a volume of approximately 13 litres. This cylinder was filled with either small stones or gravel in order to ensure that the float would remain in its required upright stationary position throughout the duration of the given series of measurements. Four steel hook

anchors were also inserted through holes in the floor of the DSF and straight into the ground in order to increase its stability in the water during windy conditions.

The DSF had a column of four dosimeter attachment sites resting on each of its four sides. Each side of the DSF was positioned around the PVC ballast cylinder in 90° increments so that measurements for each geographical direction (north, south, east and west) could be made. In each of the four sides each attachment site was separated by a distance of 15 cm. The top attachment site was designed to remain above the water level at all times throughout each measurement series, while the three lower attachment sites were to receive UVB exposures underwater. These three underwater attachment sites received UVB exposures at depths of 5 cm ($Z_{5\text{CM}}$), 20 cm ($Z_{20\text{CM}}$) and 35 cm ($Z_{35\text{CM}}$) respectively.

All the attachment sites were able to hold up to three dosimeters at a time without obstruction, with each dosimeter set to different angular inclinations which were 0° to the horizontal (horizontally aligned), 45° to the horizontal (diagonally aligned) and 90° to the horizontal (vertically aligned). In all of the different water types, each of the dosimeters were checked regularly for any mud, moss or organic matter residue build up on their surfaces. Figure 1 (A) displays the north side of the DSF with a full payload of PPO dosimeters ready for deployment. Figure 1 (B) shows the top-down view of the DSF. Due to the geometry of the DSF, some minor shading of the $Z_{20\text{CM}}$ and the $Z_{35\text{CM}}$ dosimeters was found to occur during the measurements carried out in each underwater environment, influencing the amount of diffuse irradiance scattered upon the dosimeters. This shading took place most generally during high SZA conditions, such as in the early morning and in the late afternoon, where solar UV was

incident predominantly on the sides of the DSF in comparison to low SZA conditions in which solar UV was incident towards the top of the DSF.

To calculate K_d values only UVB exposure data measured at the 0° angular inclination was used. The calibrated UVB exposure data gathered at each of the three depths was used in conjunction with the modified Beer Lambert Bouguer Law which is of the form:

$$\ln\left(\frac{UVB^z_{EXPOSURE}}{UVB^{z=0}_{EXPOSURE}}\right) = -K_d z$$

where $UVB^z_{EXPOSURE}$ is the calibrated UVB exposure as measured by the PPO dosimeter at depth z in units of kJ m^{-2} and $UVB^{z=0}_{EXPOSURE}$ is the calibrated UVB exposure as measured by the PPO dosimeters at the first attachment site just below the water surface in units of kJ m^{-2} . Linear regression analysis was performed with the modified Beer Lambert Bouguer Law in order to extract the value for K_d . A final K_d estimate was determined by averaging together the particular K_d values calculated for each geographical direction.

Attenuation Coefficient Calculation for the Calibrated EPP2000 Spectrometer

Evaluation of K_d values for each of the three different water types were made using underwater UVB spectral irradiance data collected with the EPP2000 spectrometer during a measurement campaign over two cloud free days in early autumn (low SZA conditions ranging from 20° to 61°) and two additional cloud free days in mid winter (high SZA conditions ranging from 39° to 75°). Over the range of SZA encountered throughout the measurements made each day, for each water type at each depth, a

UVB irradiance value was calculated by integrating the spectral UVB irradiance across the UVB waveband specified previously. This integrated UVB value was then included in a series of depth profiles. The modified Beer-Lambert-Bouguer Law was again used together with the depth profiles to find the necessary K_d values in a similar way to how it was used with the dosimetric measurements, except irradiance data was used in the linear regression process instead of exposure data.

Underwater UV Exposures at Different Aquatic Locales

Japanese Gardens Creek

A creek situated in a Japanese Garden located on the boundary of the University of Southern Queensland Toowoomba campus was used as the first field site in which to test the PPO dosimeter with the DSF. The creek had a measured length of 95 metres, width of 65 metres and an approximated depth of 4 metres. Measurements were carried out using the DSF in the creek in each season from early July 2007 to early April 2008. The number of days that the DSF was deployed in the environment was determined by the visible deterioration state of the dosimeters located at the top attachment site. If it could be seen that these dosimeters were becoming optically saturated (distinguished by a change in appearance of the film from clear to orange) the measurement series was brought to an end. This protocol was employed not only for the creek water measurements, but also for the agricultural dam water measurements and the sea water measurements. The length of time it took for the top attachment site dosimeters to degrade changed slightly for each particular season across the year-long measurement series. Winter measurements ran over the space of 12 days inclusive from 16 July to 27 July 2007. Spring measurements ran over the space of 9 days inclusive from 1 October to 9 October 2007. Summer measurements

ran over the space of 10 days inclusive from 18 February to 28 February 2008. Autumn measurements ran over the space of 10 days inclusive from 31 March to 9 April 2008. During the deployments, the DSF was placed in a position located far enough away from the shoreline of the creek so that shading from nearby plants and trees was minimal.

Simulated Sea Water Environment

As the nearest coastline to Toowoomba is over 120 km away, it was decided that the 2nd site for the PPO dosimeter field trials would be carried out in a large field simulated sea water environment instead of in the ocean itself. This negated the complexities that come into play during oceanic measurement campaigns such as high winds, turbulence, tidal changes and possible vandalism. The simulated sea water environment consisted of a circular steel water tank which had a circumference of 10 metres and a depth of 1 ¼ metres. The sea water used in the tank was sourced from a coastal location near the city of Brisbane, Australia (27° 28' 04" S, 153° 01' 40" E, 38 m elevation). The DSF was positioned exactly in the centre of the tank so that it would receive only a minimal amount of shading during the early morning and the late afternoon. In order to eliminate any leakage from the tank and the seepage of rust into the sea water, the tank was covered with three layers of extra strength pond liner. Measurements were carried out using the DSF in the sea water tank in each season from June 2007 to December 2008. Spring measurements ran over the space of 9 days inclusive from 14 November to 22 November 2007. Autumn measurements ran over the space of 10 days inclusive from 31 March to 9 April 2008. Winter measurements ran over the space of 12 days inclusive from 30 June to 11 July 2008. Summer

measurements were carried out over a period of 6 days inclusive from 1 December to 6 December 2008.

University of Southern Queensland Research Dam

The 3rd site selected for the PPO dosimeter field trials was an abandoned agricultural engineering research dam again located on site at the University of Southern Queensland, Toowoomba campus. The agricultural dam had a measured length of 21 metres, width of 19 metres and an estimated depth of 3 metres. UVB exposure measurements were carried out using the DSF in the agricultural dam in four seasons from July 2007 to December 2008. Winter measurements ran over the space of 12 days inclusive from 2 July to 13 July 2007. Spring measurements ran over the space of 9 days inclusive from 15 October to 23 October 2007. Autumn measurements ran over the space of 8 days from 16 April to 23 April 2008. The autumn measurement series was initially planned to run for 10 days in total but flooding of the dam after overnight torrential rain brought the trial to a halt. Summer measurements ran for 6 days inclusive from 1 December 2008 to 6 December 2008. A comparison between the transmission and absorption spectra at an arbitrary wavelength of 315 nm for each of the water types found in the agricultural dam, the sea water tank and the Japanese Gardens creek is displayed in Figure 2.

RESULTS

Creek Water

Measurement data collected with the DSF in the creek in autumn, winter, spring and summer can be seen in Figure 3 (A), (B), (C) and (D) respectively. The first 12 data blocks on the x-axis represent the daily averaged UVB exposures measured at the

water surface running in order from the north, east, south and west cycling over the 0°, 90°, 45° orientations for each particular direction. This order continues for each following set of 12 data blocks along the x-axis for all the depths from 5 cm to 20 cm to 35 cm. The UVB exposure error was approximated as an accumulative $\pm 18\%$ uncertainty that results from errors generated during measurement and analysis procedures. This $\pm 18\%$ error threshold and the data presentation scheme remained the same for both the dam water and sea water measurements. At the water surface for each season it can be clearly seen from the figures that relatively high levels of UVB exposure were received by the dosimeters, which was to be expected as they were not submerged. Throughout each season at the water surface the largest exposures were generally recorded at either the north or west alignments usually at an inclination of 45°. The horizontally aligned dosimeters commonly intercepted UVB dosages comparable if not slightly less than those received at the 45° inclination, with the vertically aligned dosimeters measuring the lowest amounts of solar UVB.

In the creek, measurements were able to be obtained at a depth of 5 cm across each particular measurement position. The general distribution of the exposures at this depth was extremely similar to what was seen with the exposures measured at the surface of the water. The highest exposures were again usually seen at either the north or west alignments at the 45° inclination, except for the data collected in spring where the dosimeter aligned to the horizontal directed to the west received the most UVB. However, in each season the magnitude of the UVB exposures at the 5 cm depth was considerably reduced in comparison to the measurements made at the surface across every single position. For example, in autumn the maximum daily averaged exposure received at the surface was $57 \text{ kJ m}^{-2} \text{ day}^{-1}$ recorded at the north 45° position. In

comparison, at the same position 5 cm underwater the measurement recorded was 7.8 kJ m⁻² day⁻¹, a sizeable 86% reduction with respect to the surface UVB exposure. Again, in spring the maximum exposure was received at the north 45° position with a value of 55 kJ m⁻² day⁻¹. The measurement made at the same position 5 cm underwater was far less at 8 kJ m⁻² day⁻¹, which represented another reduction in UVB exposure of approximately 86%. As the DSF was anchored at a location in the creek so that it was not influenced by any shade produced by shoreline plants and trees, the most plausible explanation for the drastic reduction in UVB exposure would be due to the large clusters of organic matter produced by local wildlife such as ducks and birds and decaying plant matter that was observed to be floating through the water at regular intervals. This organic matter could have blocked the incoming UVB effectively shading the dosimeters positioned below it. Throughout the measurement campaign very few reliable UVB exposures were measured during any season at the 20 cm and the 35 cm depths in the creek. Even in summer where solar output is at its highest levels, it appears that the UVB wavelengths failed to penetrate the creek water any further than 5 cm. This result meant that no depth profiles could be obtained for the creek water.

Sea Water

UVB exposure data measured using the DSF in the simulated sea water environment averaged over each day in autumn, winter, spring and summer can be seen in Figure 3 (A), (B), (C) and (D) respectively. As was shown in the creek water, it is seen from the figures that across every position UVB exposures received by the dosimeters at the water surface were far greater than those intercepted underwater. Over the seasons the highest exposures on the surface of the sea water were generally measured at

either the west or north directions at the 45° or horizontal alignments. Again, due to the fact they were not exposed to the same amount of sky view as the 45° or horizontal dosimeters, the vertically aligned dosimeters measured UVB levels usually no more than half that measured by their 45° and horizontal counterparts oriented towards the same direction. As an example, in the spring measurement campaign, along the eastern orientation at the surface, the vertically aligned dosimeter measured an average daily UVB exposure of 28 kJ m⁻² day⁻¹, while comparatively the dosimeter at the horizontal alignment measured 73 kJ m⁻² day⁻¹ and the dosimeter at the 45° alignment measured 65 kJ m⁻² day⁻¹.

Unlike the underwater measurements made in both the creek and the agricultural dam, significant UVB measurements were able to be made at each depth from 5 cm down to 35 cm across the entirety of the measurement campaign. As was seen in the creek series of measurements, data obtained at the first depth underwater was significantly less in magnitude in comparison to measurements made at the water surface. For instance, in winter the value for UVB exposure obtained along the east direction at the horizontal inclination was measured to be 24 kJ m⁻² day⁻¹ in comparison to 15 kJ m⁻² day⁻¹ which was measured at the same position 5 cm underwater. This represented a decrease of roughly 38% in total UVB exposure.

From 5 cm deep to 20 cm deep and then again from 20 cm deep to 35 cm deep further considerable attenuation of the incoming UVB exposure was found to occur for every measurement series in the sea water. A good example of this can be seen in the spring measurement set, from the 5 cm depth to the 20 cm depth where a drop in UVB exposure of approximately 46% occurs at the horizontally aligned position facing

south. Once more, at this same position, from the 20 cm depth to the 35 cm depth, a reduction of around 41% in the UVB exposure was measured to exist between the two. Another example of high UVB attenuation is seen at the 45° alignment along the east direction in the autumn data set, where a reduction in UVB exposure of 37% was recorded between the 5 cm and 20 cm depths with a further 50% reduction in UVB exposure occurring between the 20 cm and 35 cm depths.

Unlike the creek water and the agricultural dam, it was found that the decrease in UVB exposure with increasing depth could be modelled with a good level of accuracy by using power law functions fitted to all of the exposure depth profiles for the sea water at each azimuth in every season. These equations each have the form:

$$UVB_{EXPOSURE} = \psi z^{-\omega}$$

where $UVB_{EXPOSURE}$ is the UVB dosage measured by the dosimeter during the exposure time in units of kJ m^{-2} and z is the depth in units of cm. Averaged UVB exposure depth profiles at 5 cm, 20 cm and 35 cm produced from the horizontally aligned sea water exposure distribution data can be viewed in Figure 4 for each season. The y-axis errors bars represent a calculated $\pm 18\%$ range of uncertainty inherent within each data point. From Figure 4 it can be seen that the UVB data obtained in the sea water in summer are smaller overall in magnitude in comparison to the measurements made in autumn and spring and only slightly greater than the UVB measurements made in winter. This was due to a substantial amount of cloud coverage and rain being prevalent for roughly three days out of the six day summer measurement campaign greatly reducing incident amounts of solar UVB.

Agricultural dam

Daily averaged UVB exposure measurement data recorded with the DSF in the agricultural dam in autumn, winter, spring and summer can be seen in Figure 3 (A), (B), (C) and (D) respectively. As was the case with the creek water and the sea water, the levels of UVB exposure recorded just above the water surface were the highest. Due to the very high level of UVB absorption present in the agricultural dam, no reliable data could be measured by the dosimeters underwater, except for some relatively small values found in each campaign. However, it is unclear if these measurements are reliable, as there were high amounts of soil discharge in the water that mildly stained the PPO dosimeter film. It is possible that this staining could have led to incorrect absorption values being measured by the spectrophotometer. Therefore, similarly to the creek water, no depth profiles could be provided for the agricultural dam water.

Comparison of the Attenuation Coefficients Calculated in the Sea Water with the EPP2000 Spectrometer and the Dosimeters

Figure 5 compares the K_d values calculated from the sea water UVB exposure depth regimes compared to the averaged sea water K_d value calculated using the EPP2000 spectrometer. The percentage variation calculated directly as $\frac{\sigma}{\mu} \cdot 100\%$ for each K_d estimation applicable to both the dosimeters and the EPP2000 spectrometer is represented in the figure by the y-axis error bars. Using the dosimeters, the K_d value in the sea water was estimated to be 0.045 cm^{-1} in summer, 0.073 cm^{-1} in winter, 0.043 cm^{-1} in autumn and 0.039 cm^{-1} in spring. The average value of these four measurements was found to be 0.049 with a standard deviation of ± 0.017 . The averaged K_d values determined with the EPP2000 spectrometer from the solar spectral

UVB data sets obtained in early autumn and mid winter were found to be 0.028 cm^{-1} with a standard deviation of ± 0.025 and 0.036 with a standard deviation of ± 0.014 respectively.

Almost all of the K_d values were found to be in relatively close agreement with each other in accordance to the estimated error margins. However, the winter K_d estimation calculated with the dosimeters was found to be substantially greater in value in comparison with all the other K_d approximations. This could have occurred due to the shading of the lower sections of the DSF in the sea water tank during high SZA conditions that are prevalent during winter especially in the early to mid morning and early to late afternoon. The dosimeters positioned primarily at the depths of 20 cm and 35 cm in the tank would have received a lower amount of UVB exposure during these intervals each day in comparison to their counterparts in the autumn, spring and summer measurement campaigns. By inspection of the modified Beer-Lambert-Law used to calculate the K_d values for the dosimeters, it can be clearly seen that any reduction in measured UVB leads to an inevitable increase in the K_d estimate. The agreement between the K_d measurements measured by the dosimeters over the autumn, spring and summer seasons and the K_d measurements made with the EPP2000 spectrometer in early autumn and mid winter was to be expected as it is known that the K_d for any given water type is not influenced by changes in the incident solar spectrum brought on by annual changes in the Sun's position [27].

DISCUSSION

The results produced in this research show that the PPO dosimeter provides comparable UVB exposure data compared to the spectrometric alternative within a

good level of accuracy in types of water with little amounts of DOM and particulate matter, such as the sea water. The PPO dosimeter is useful in water with increased turbidity and DOM content for depths up to approximately 5 cm. However, the usefulness of the PPO dosimeter at any depths greater than approximately 5 cm may be reduced in water with increased levels of water turbidity and DOM content, which both in turn reduce the overall UVB transmission and enhance the UVB absorption capabilities of the water leading to a reduction in the penetrative ability of the UVB. This was the case with the creek water and the agricultural dam water. In addition, in order to achieve accurate results with the PPO dosimeter, a rigid calibration regime such as the one carried out for this research must be applied in order to allow for variations in the solar UVB spectrum brought on by changes in the sun's position from season to season and to take into account any influence of column ozone fluctuations which may occur throughout the year.

It was seen from the measurements made with dosimeters in the creek water and in the agricultural engineering dam water that only small amounts of UVB exposure could be reliably recorded at the shallow depth of 5 cm in close to ideal conditions, with no UV recorded beneath that depth, even in high solar UVB conditions through summer, early autumn and late spring. This suggests that there is a characteristic limit to the depth at which the PPO dosimeter can be used underwater in water types with relatively high amounts of turbidity DOM content. In this research it appears that this limit is reached just below the 5 cm depth in water types having less than or equal to 75% UV transmission at a wavelength of 315 nm, which was the value obtained for the creek water. However it can be used up to at least 35 cm in sea water.

Not only do these water types like that found in the creek and the agricultural dam inhibit and attenuate the penetration of the solar UVB, but these water types are more likely to have free floating particulates and suspended masses of organic matter that could possibly condense on the dosimeter film and block out the UVB which would lead to distorted outcomes. Also, in creek, dam and estuary water type environments there is the possibility of the dosimeters being shaded by falling branches, leaves and other types of assorted plant matter which would further add to measurement uncertainty. One way to overcome these types of issues that occur at natural water locales such as dams, creeks and estuaries would be to check on and clean the dosimeters at regular intervals. However, this would be time consuming for the researcher and defeats the main purpose of the dosimeter, which is being able to leave it unattended underwater for extensive periods.

At this point in time it is recommended that this dosimeter only be used in 'cleaner' underwater locations distanced from influencing natural environmental factors like wildlife, shoreline trees and plants that have the potential to deposit various types of organic matter into the water. One such example of a 'cleaner' water locale would be in the ocean itself, preferably near or on a reef where frequent subsurface mixing takes place which would keep the water fresh and clear of any major contaminants. Fjords, such as those found in the Arctic regions and similar water bodies in Antarctica may also be an ideal location for PPO dosimeter measurements as the water found in them is sourced from glaciers or ice bergs, which is generally clear with an extremely high UV transmission capability. The PPO dosimeter could also be deployed in free flowing creeks, as the water in these locations is kept relatively clean due to its constant movement.

ACKNOWLEDGEMENTS

The authors would like to thank both Graham Holmes and Oliver Kinder from the Faculty of Sciences, University of Southern Queensland for their technical assistance throughout this project.

REFERENCES

- [1] A.T. Banaszak, P.J. Neale. *Limnol. Oceanogr.* 46 (2001) 592- 603.
- [2] B.E. Brown, R.P. Dunn, M.S. Goodson, A.E. Douglas, *Nature* 404 (2000) 142-143.
- [3] D.F. Gleason, G.M. Wellington, *Nature* 365 (1993) 836-838.
- [4] S. Johnsen, E.A. Widder, *Mar. Biol.* 138 (2001) 717-730.
- [5] M.P. Lesser, M.D. Lamare, M.F. Barker, *Limnol. Oceanogr.* 49(6) (2004) 1957-1963.
- [6] M. Tedetti, R. Sempéré, *Photochem. Photobiol.* 82(2) (2005) 389-397.
- [7] D-P. Hader, H.D. Kumar, R.C. Smith, R.C. Worrest, *Photochem. Photobiol. Sci.* 2 (2003) 39-50.
- [8] D-P. Hader, H.D. Kumar, R.C. Smith, R.C. Worrest, *J. Photoch. Photobio. B.* 46 (1998) 53-68.
- [9] H.W. Ducklow, C.A. Carlson, N.R. Bates, A.H. Knap, A.F. Michaels, *Phil. Trans. R. Soc. B.* 348 (1995) 161-167.
- [10] D. Hanelt, H. Tug, K. Bischof, C. Gross, H. Lippert, T. Sawall, C. Wiencke, *Mar. Biol.* 138 (2001) 649-658.
- [11] M.J. Dring, A. Wagner, L.A. Franklin, R. Kuhlenkamp, K. Luning, *Helgoland Mar. Res.*, 55 (2001) 3-11.
- [12] J. Frenette, M.T. Arts, J. Morin, *Aquat. Ecol.* 37 (2003) 77-85.
- [13] A. Reinart, H. Arst, D.C. Pierson, *Hydrobiologia*, 547 (2005) 41-49.
- [14] H. Schubert, S. Sagert, R.M Forster, *Helgoland Mar. Res.*, 55 (2001) 12-22.
- [15] R.P. Dunne, *Mar. Ecol. Prog. Ser.* 189 (1999) 53-63.
- [16] P.C. Frost, A. Mack, J.H. Larson, S.D. Bridgham, G.A. Lamberti, *Photochem. Photobiol.* 82(3) (2006) 781-786.

- [17] R.A. Lester, A.V. Parisi, M.G. Kimlin, J. Sabburg, *Phys. Med. Biol.* 48 (2003) 3685-3698.
- [18] A. Davis, G.W.H Deane, D. Gordon, G.V. Howell, K.J. Ledbury, *J. Appl. Polym. Sci.* 20 (1976) 1165-1174.
- [19] A. Davis, B.L. Diffey, B.K. Tate, *Photochem. Photobiol.* 34 (1981) 283-286.
- [20] B. Berre, D. Lala, *Sol. Energy.* 42(5) (1989) 405-416.
- [21] P. Schouten, A. Parisi, D.J. Turnbull, *Photochem. Photobiol.* 83(4) (2007) 931-937.
- [22] P.W Schouten, A.V. Parisi, D.J. Turnbull, *J. Photoch. Photobio. B.* 91(2-3) (2008) 108-116.
- [23] G.R Casale, M. Borra, A. Colosimo, M. Colucci, A. Militello, A.M. Siani, R. Sisto, *Phys. Med. Biol.* 51 (2006) 4413-4427.
- [24] G. Zibordi, *J. Atmos. Ocean. Tech.* 23 (2005) 302-313.
- [25] S.B. Hooker, G. Zibordi, *J. Atmos. Ocean. Tech.* 22 (2005) 757-770.
- [26] G. Zibordi, S.B. Hooker, J. Mueller, G. Lazin, *J. Atmos. Ocean. Tech.* 21 (2004) 501-514.
- [27] J.T.O Kirk, *Light and photosynthesis in aquatic ecosystems*, Cambridge University Press, Cambridge, 1994.

FIGURE AND TABLE LEGENDS

Figure 1 – (A) North side view of the DSF and (B) the top-down view of the DSF.

Figure 2 – Transmission (A) and absorption (B) spectrophotometry data at 315 nm for the clear, creek, dam and sea water.

Figure 3 – UVB exposure distributions in the creek, sea and dam water in autumn (A), winter (B), spring (C) and summer (D).

Figure 4 – Averaged UVB exposure depth regimes as extracted from horizontally aligned sea water exposure distribution data for each season of the year.

Figure 5 – K_d values calculated from the sea water UVB exposure depth regimes compared to the K_d value calculated using the EPP2000 spectrometer for sea water.

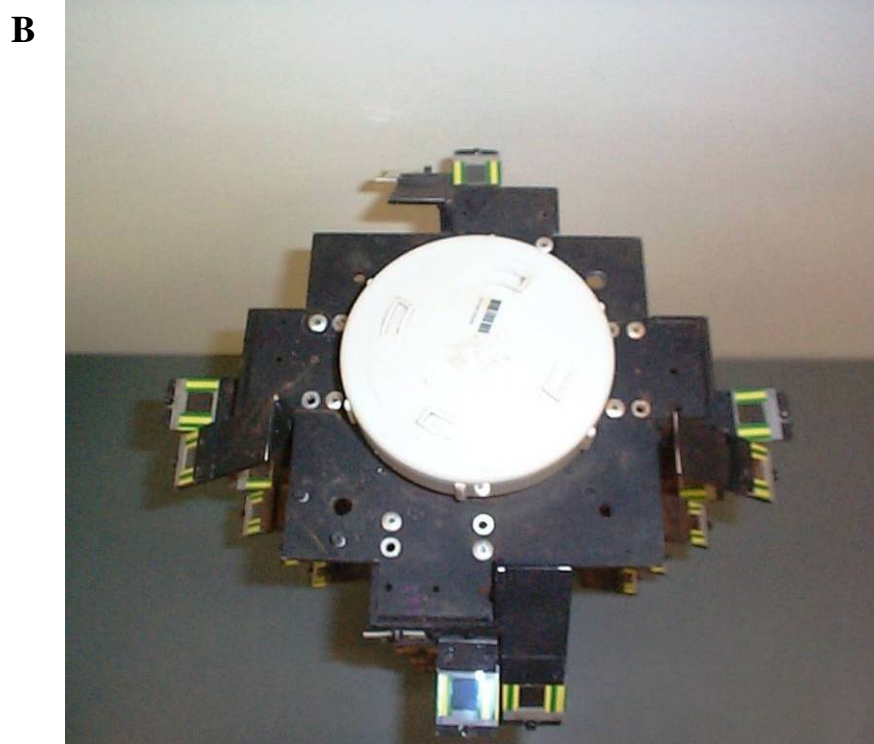
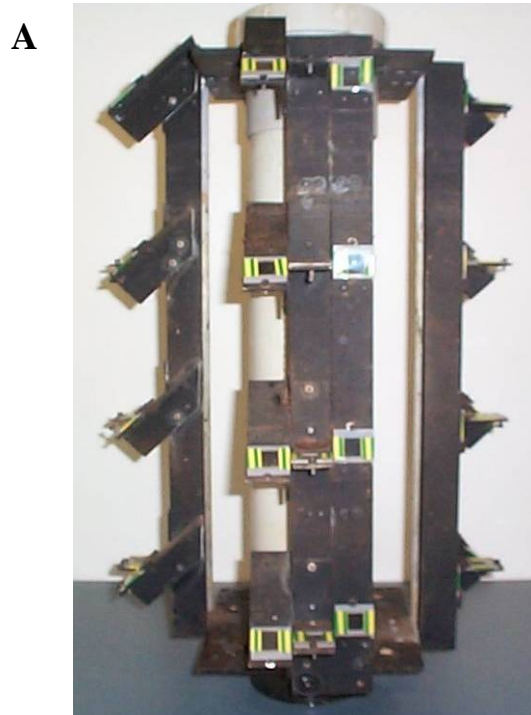


Figure 1 – (A) North side view of the DSF and (B) the top-down view of the DSF.

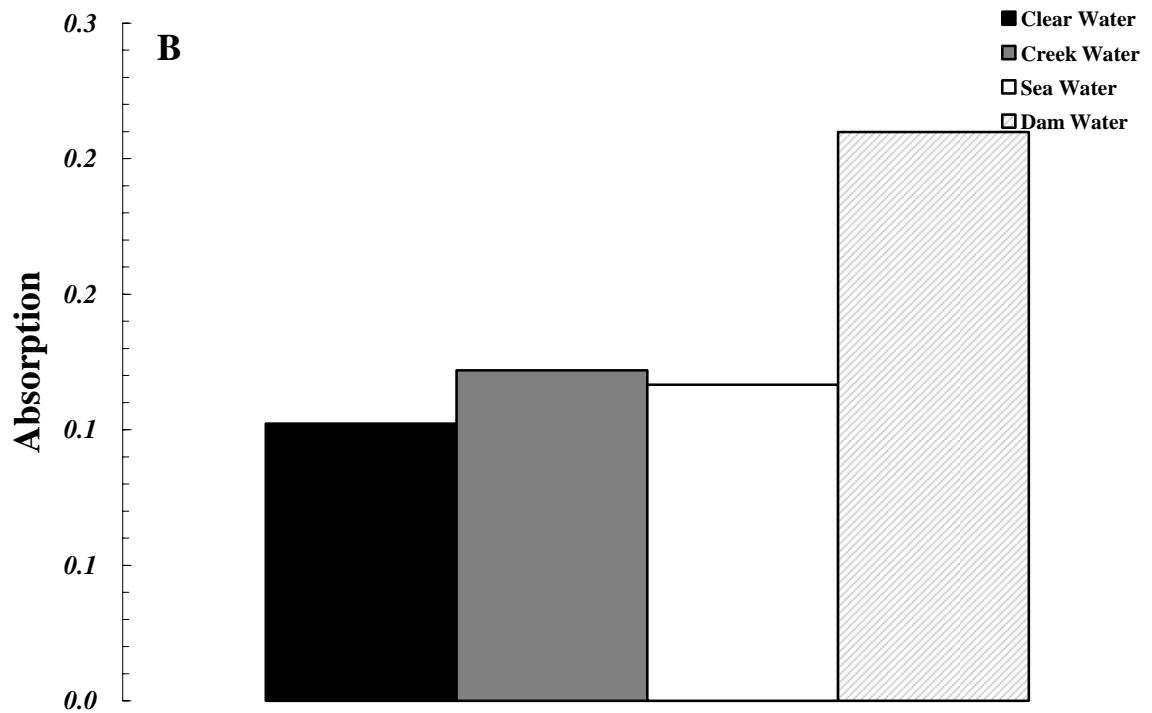
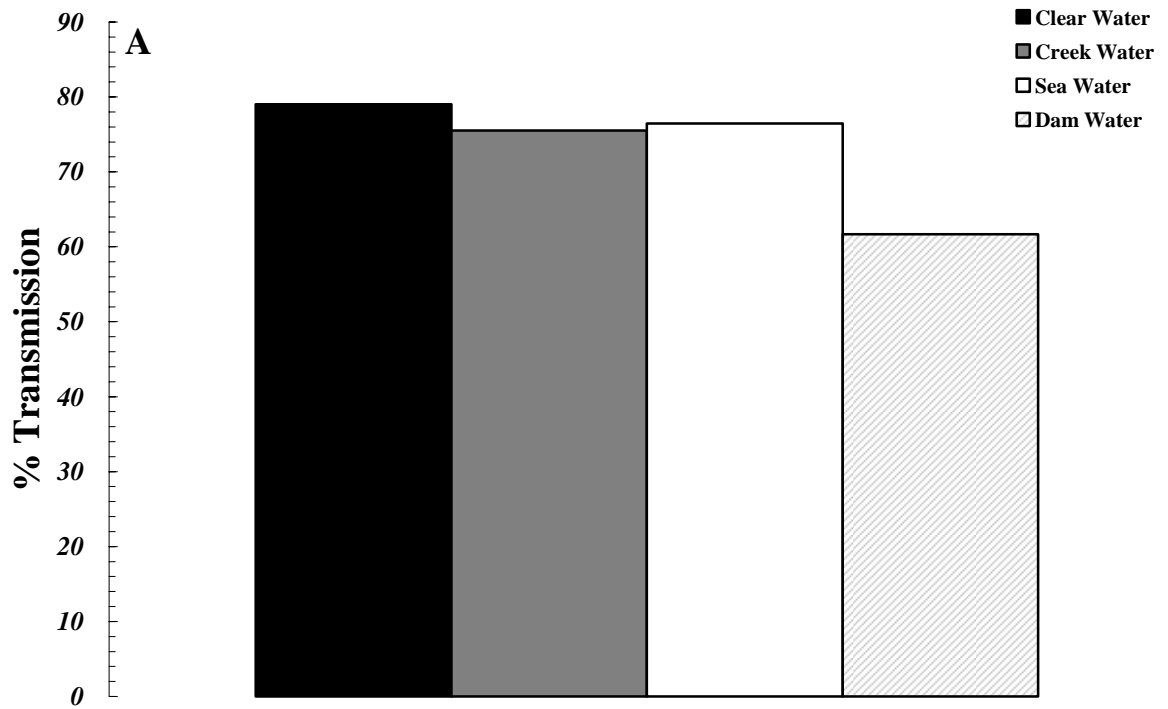
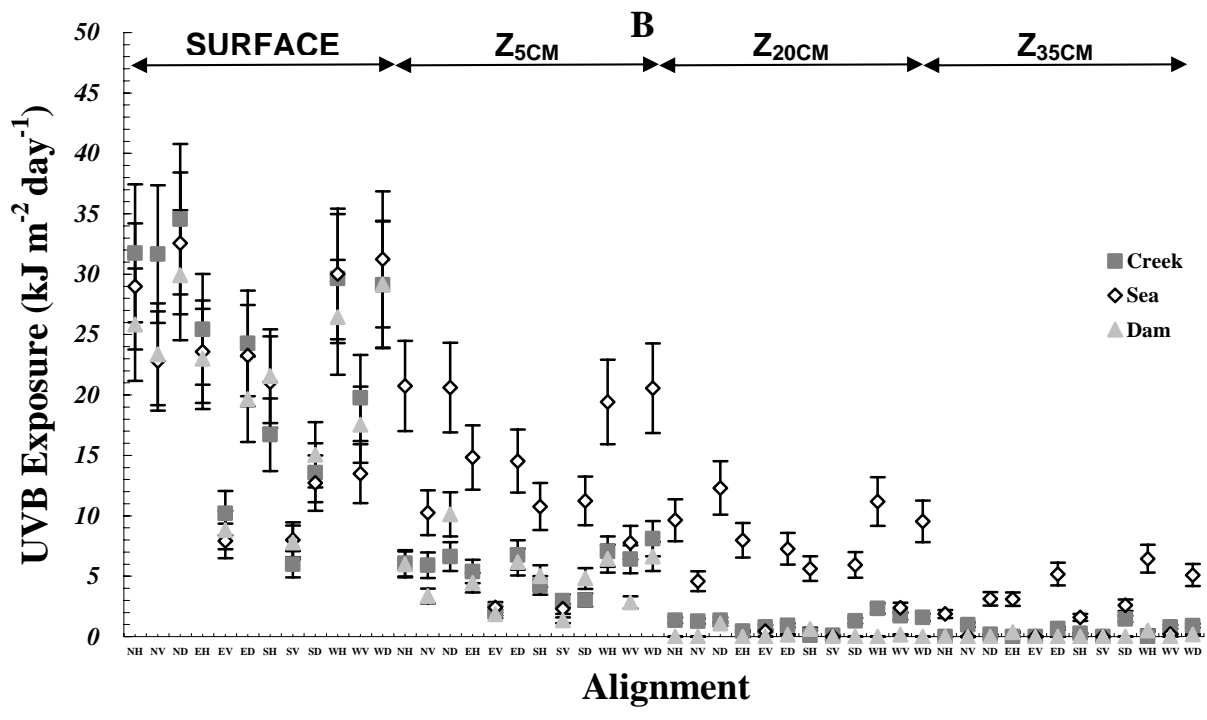
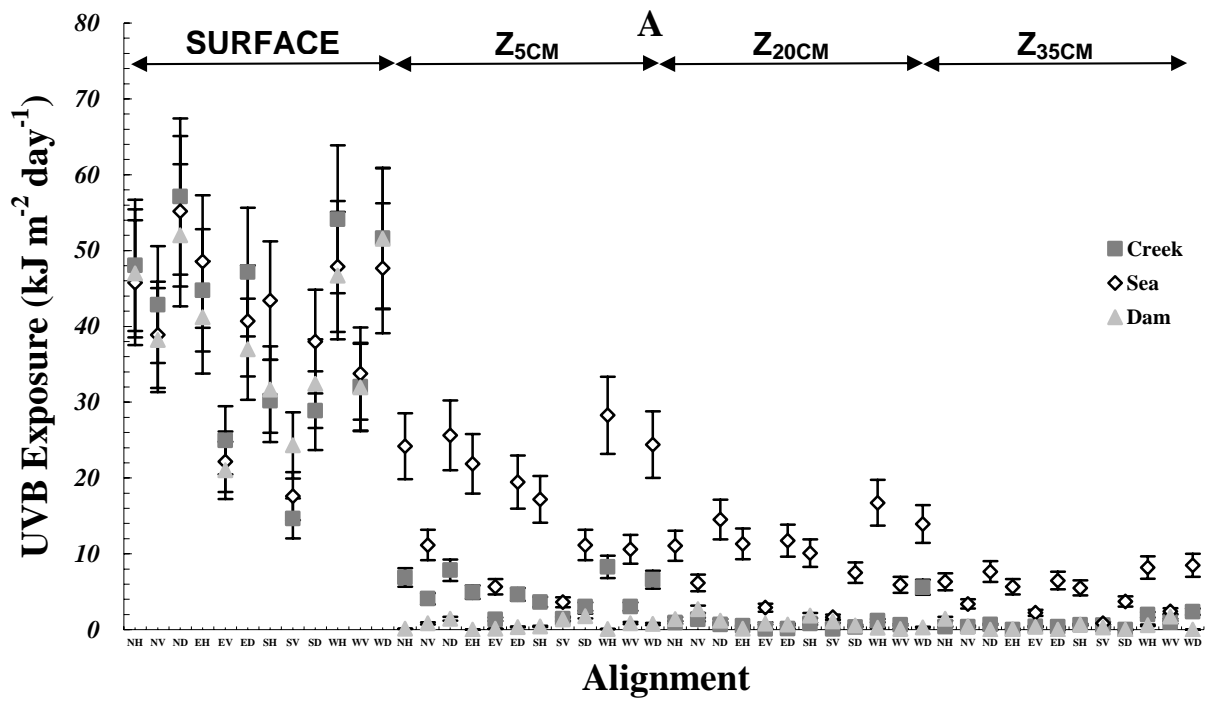


Figure 2 – Transmission (A) and absorption (B) spectrophotometry data at 315 nm for the clear, creek, dam and sea water.



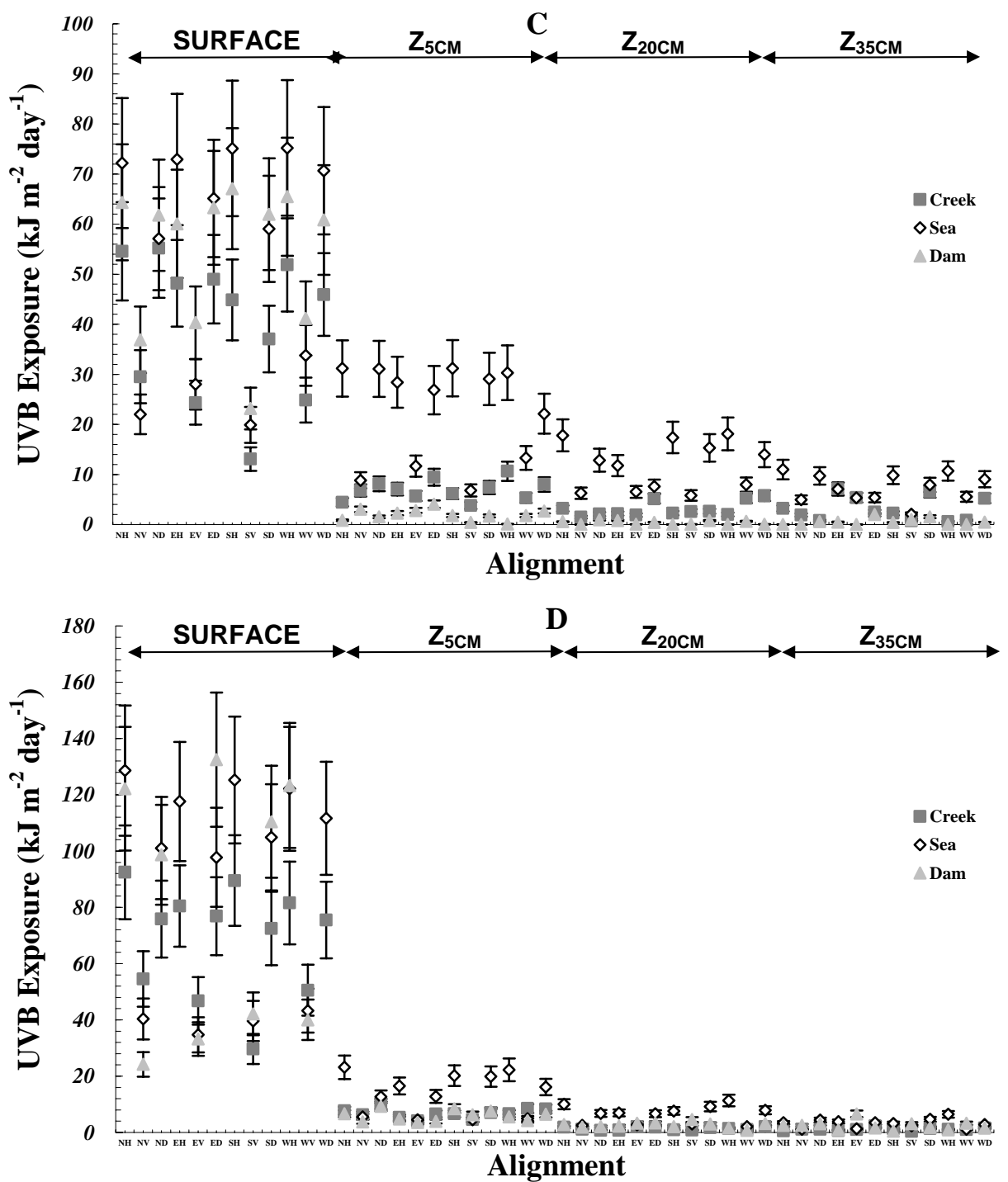


Figure 3 – UVB exposure distributions in the creek, sea and dam water in autumn (A), winter (B), spring (C) and summer (D).

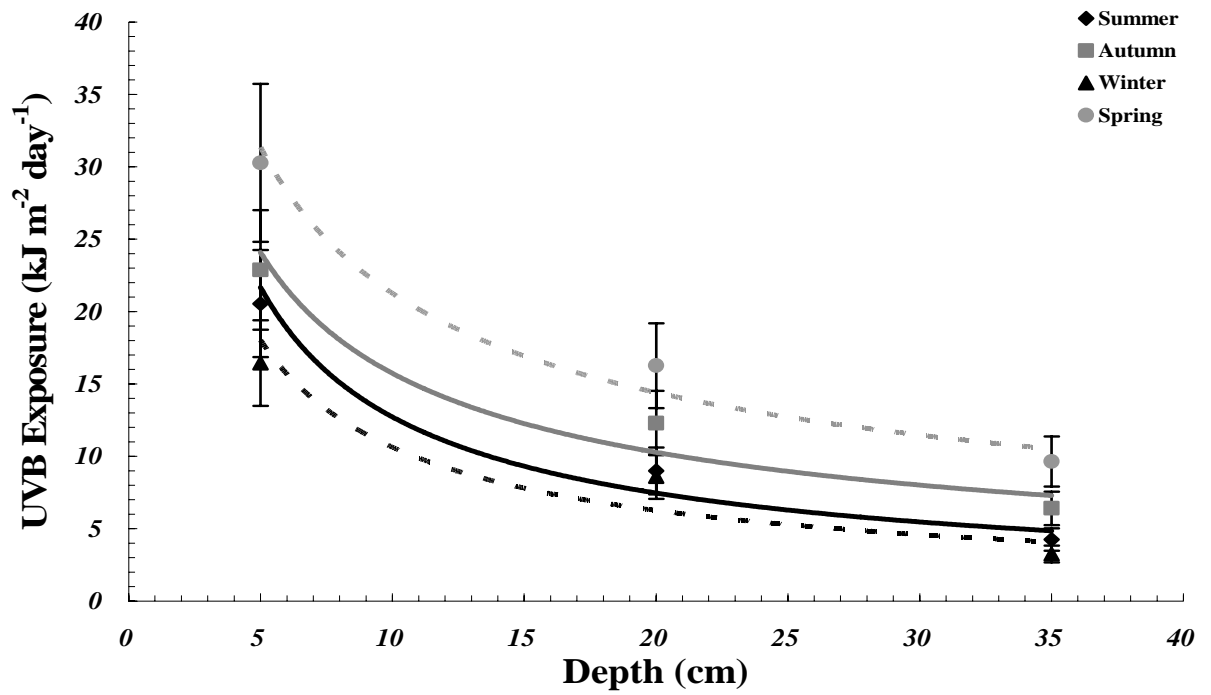


Figure 4 – Averaged UVB exposure depth regimes as extracted from horizontally aligned sea water exposure distribution data for each season of the year.

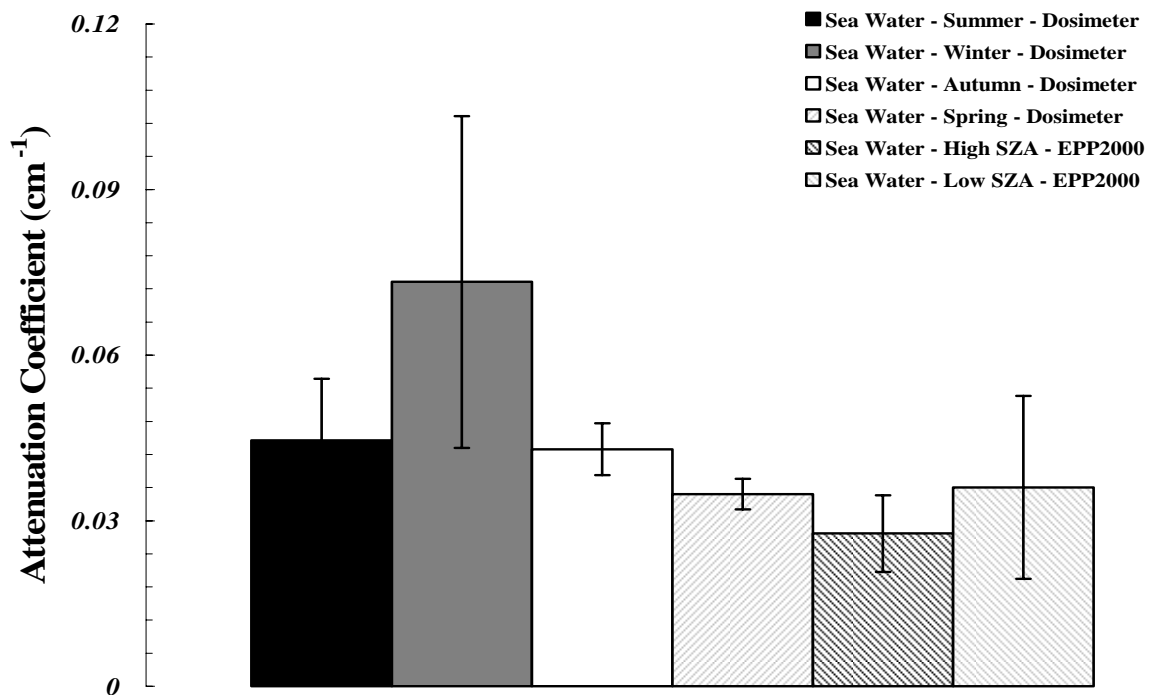


Figure 5 – K_d values calculated from the sea water UVB exposure depth regimes compared to the K_d value calculated using the EPP2000 spectrometer for sea water.